POLYMERS AND POLYMER-CONJUGATES FOR CANCER IMMUNOTHERAPY: FOREIGN CYTOTOXIC T LYMPHOCYTE EPITOPE DELIVERY, CYTOTOXIC T LYMPHOCYTE ACTIVATION, AND NK92 CELL SURFACE ENGINEERING

By

Shuyao Lang

A DISSERTATION

Submitted to
Michigan State University
in partial fulfillment of the requirements
for the degree of

Chemistry—Doctor of Philosophy

2021

ABSTRACT

POLYMERS AND POLYMER-CONJUGATES FOR CANCER IMMUNOTHERAPY: FOREIGN CYTOTOXIC T LYMPHOCYTE EPITOPE DELIVERY, CYTOTOXIC T LYMPHOCYTE ACTIVATION, AND NK92 CELL SURFACE ENGINEERING

By

Shuyao Lang

Cancer immunotherapy is considered as the fourth pillar of anti-cancer treatment, along with the traditional three pillars: surgery, radiotherapy, and chemotherapy. Polymers and polymer conjugates have been widely investigated as cancer immunotherapy carriers. The polymeric materials can not only prolong the circulation time of their small molecular cargoes, but also enhance immune activation *via* multiple mechanisms such as passively or actively targeting immune cells and specific tissue environment. With their great flexibility of monomer selection and post-polymerization modification, polymers and polymer conjugates can satisfy the various needs for immunotherapy. In this dissertation, three different polymer/polymer conjugates have been investigated for facilitating different immunotherapy strategies.

pH responsive acetalated dextran microparticles were (Ac-Dex MPs) investigated for the delivery of a high affinity foreign cytotoxic T lymphocyte (CTL) epitope, ovalbumin peptide (OVA), to tumor tissues. Successful OVA delivery to tumor tissue was observed. Both intratumorally and systematically administration of OVA encapsulated Ac-Dex MPs protected mice from pre-established “antigen-loss variant” tumor models.

Ultra-pH sensitive nanoparticles (NPs) based on methoxy poly(ethylene glycol)-b-[poly(diisopropylamino)ethyl methacrylate] have been synthesized as a platform for anti-cancer vaccine delivery. Representative CTL antigen OVA and adjuvant imiquimod (IMQ), were covalently conjugated to the polymer backbone through an acid responsive carboxy-dimethylmaleic amide linker (CDM) resulting in polymer P-CDM-OVA and P-CDM-IMQ, respectively. The P-CDM-OVA NPs greatly enhanced CTL responses *in vivo* compared to the free peptide or the previously reported Ac-Dex MPs encapsulating OVA. Co-administration of P-CDM-OVA NPs with P-CDM-IMQ NPs further improved CTL responses *in vivo* and effectively reduced tumor growth in mice.

Besides serving as delivery carriers, polymers can also be used for surface engineering of immune cells. NK92 cells are a natural killer cell line which is highly cytotoxic, but lack of inherent selectivity toward cancer. We investigated the surface engineering of NK92 with two different strategies: metabolic glycoengineering, and hydrophobic insertion of a polymer grafted with multiple copies of trisaccharide CD22 ligands and a cholesterol terminal. Both methods can successfully modify the surface of NK92 with CD22 ligand and enhance the specific lysis of $CD22^+$ cell lines *in vitro*. Further investigation of metabolic glycoengineering method showed significant protection against $CD22^+$ tumor *in vivo*.

ACKNOWLEDGEMENTS

First and foremost, I would like to say thank you to my advisor Dr. Xuefei Huang, for his great patience during my seven-year's PhD journey. I appreciate for his professional guidance in science and his kind support in life, which helped me getting through all difficulties during my graduate study. He was always patient and encouraging, which allowed me to finally catch up and qualify for graduation.

I would like to thank all my doctoral guidance committee members, Dr. Babak Borhan, Dr. Heedeok Hong an Dr. Milton R. Smith, for reviewing this thesis and providing thoughtful suggestions. I also thank all support staff in department of chemistry and institute of quantitative health science and engineering, for their assists during my study. Dr. Dan Holmes has trained me for NMR usage; Dr. Dan Jones and Anthony Schilmiller have trained me for high resolution mass spectrometer; Anthony helped me on collecting mass spectra data during the COVID-19 pandemic; Dr. Louis King trained me for flow cytometry usage.

I especially appreciate Dr. Herbert Kavunja and Dr. Xianwu Wang for our collaboration projects. They have made essential contributions to these works. I enjoy the time working with the Huang lab, and I thank all my coworkers for their assistants. Dr. Zhaojun Yin provided me helpful guidance when I started working with animals. Xuanjun Wu, Qian Qin, Suttipun Sungsuwan, Tianlu Li, Yuetao Zhao, Hui Li, Zibin Tan, Zahra Rashidijahanabad, Seyedmehdi Hossaini Nasr, Jia Gao, Hunter McFall-Boegeman, provided excellent suggestions during our biological subgroup

meeting. And all other members in Huang lab: Weizhun Yang, Jicheng Zhang, Changxin Huo, Peng Wang, Sherif Ramadan, Kedar Baryal, Mengxia Sun, Kunli Liu, Shivangi Chugh, Chia-wei Yang, Po-han Lin.

I would like to thank my husband Zibin Tan for his support all the time. I am proud and happy to have him accompany every day in my life. He has been taking care of most of the housework and trying his best to make me healthy and happy. I thank my family for the chance of viewing this world. And finally, to a secret person who may or may not listening: Life was perfect at 16-years old. Life is still wonderful after that.

TABLE OF CONTENTS

LIST OF TABLES

LIST OF FIGURES

LIST OF SCHEMES

KEY TO ABBREVIATIONS

7-AAD	7-Aminoactinomycin D
AC	Alginate-calcium
ACC	Alginate-calcium-chitosan
Ac-Dex	Acetalated dextran
ADA	Adipic acid
ADCC	Antibody dependent cell-mediated cytotoxicity
ALV	Antigen-loss variant
AMA	2-Aminoethyl methacrylate HCl salt
APC	Antigen presenting cell
aPD-1	Anti-PD-1 antibody
APN	Aminopeptidase N
B. Anthracis	Bacillus Anthracis
BMA	n-Butyl methacrylate
BMDC	Bone marrow dendritic cells
Boc	tert-Butyloxycarbonyl
Boc-AMA	Boc protected 2-aminoethylmethacylate monomer
BSA	Bovine serum albumin
CAC	Cyclic acetal coverage

CDC	Complement-dependent cytotoxicity
CDM	Carboxy-dimethylmaleic anhydride
CDN	Cyclic dinucleotide
CFA	Complete Freund's adjuvant
CFSE	Carboxyfluorescein succinimidyl ester
CPRG	Chlorophenol red-β-d-galactopyranoside
CPS 4	S. Pneumoniae serotype 4 capsular polysaccharides
CTL	Cytotoxic T lymphocyte
CTLp	CTL peptide epitope
CTP	Cytidine-5'-triphosphate
CuAAC	Copper catalyzed azido-alkyne coupling
DC	Dendritic cell
DCM	Dichloromethane
DIPEA	Diisopropylethylamine
DLS	Dynamic light scattering
DMAP	4-Dimethylaminopyridine
DMEM	Dulbecco’s modified Eagle’s medium
DMEM/F12	Dulbecco's modified Eagle medium nutrient mixture F-12 Ham
DMF	*N*,*N*-Dimethylformamide
DMSO	Dimethyl sulfoxide

DPAMA	Diisopropylaminoethyl methacrylate
EDC•HCl	1-Ethyl-3-(3-dimethylaminopropyl)carbodiimide hydrochloride
ELISA	Enzyme-linked immuno-sorbent assay
ELISpot	Enzyme-linked immune absorbent spot
EM	Emulsion
ES	Electrospray
FACS	Fluorescence activated cell sorting
FBS	Fetal bovine serum
FDA	Food and Drug Administration
FITC-MAL I	FITC-labeled α2,3-sialic acid binding plant lectin Maackia Amurensis Lectin I
FITC-SNA	FITC-labeled α2,6-sialic acid binding plant lectin Sambucus Nigra Lectin
Fmoc	Fluorenylmethyloxycarbonyl
GDR	Galactosyl-dextran-retinal
GPC	Gel-permeation chromatography
GPs	β-Glucan particles
HA	Hemagglutinin
HBSS	Hank's balanced salt solution
HBTU	O-(Benzotriazol-1-yl)-N,N,N',N'-tetramethyluronium hexafluorophosphate

HoBt	Hydroxybenzotriazole
HPLC	High performance liquid chromatography
IFA	Incomplete Freund's adjuvant
IMQ	Imiquimod
iNKT	Invariant natural killer T
KLH	Keyhole limpet hemocyanin
LPS	Lipopolysaccharide
M2e	Ectodomain of matrix protein 2
mAb	Monoclonal antibody
MDP	Muramyl dipeptide
MFI	Mean fluorescence intensities
MGlu	Methyl glutaric acid
MGlu-Dex	3-Methyl glutaryl dextran
MGlu-Man	3-Methyl glutaryl mannan
MHC I	Major histocompatibility complex class I
MHC II	Major histocompatibility complex class II
MP	Microparticle
MPB	m-Phenoxybenzoic acid
mPEG	Methoxy polyethylene glycol

mPEG-PDPAMA	Methoxy polyethyleneglycol-poly(diisopropylaminoethyl methacrylate)
mPEG-PDPAMA-PAMA	Methoxy polyethyleneglycol-poly(diisopropylaminoethyl methacrylate)-poly(aminoethyl methacrylate)
mPEG-PDPAMA-PBMA	Methoxy polyethyleneglycol-poly(diisopropylaminoethyl methacrylate)-poly(n-butyl methacrylate)
MPLA	Mannan and monophosphoryl lipid A
mTOR	Mammalian target of rapamycin
MUC1	Mucin 1
MWCO	Molecular weight cut-off
NHS	N-hydroxysuccinimide
NLRs	NOD-like receptors
NmCss	Neisseria meningitides
OVA	Ovalbumin
OVA peptide	Ovalbumin amino acid 257-264 antigen peptide
ox-Man	Oxidized mannan
ox-M-FP	Oxidative mannan-MUC1 fusion protein conjugate
PA	Protective Antigen
PBMCs	Peripheral blood mononuclear cells
PBS	Phosphate-buffered saline
Pd2,6ST	Photobacterium damselae α2−6-sialyltransferase

PE	Phycoerythrin
PLGA	Poly(lactic-co-glycolic acid)
PLL	Poly-L-lysine
PM	P. Pratense pollen-non-oxidized mannan conjugate
PMDETA	*N*,*N*,*N*′,*N*″,*N*″-Pentamethyldiethylenetriamine
PVA	Polyvinyl alcohol
R848	Resiquimod
red-Man	Reduced mannan
red-M-FP	Reductive mannan-MUC1 fusion protein conjugate
ROS	Reactive oxygen species
RPMI	Roswell Park Memorial Institute
SAS	Sigma adjuvant system
SEM	Scanning electron microscopy
Siglecs	Sialic acid-binding immunoglobulin-type lectins
SLP	Synthetic long peptide
SPAAC	Strain-promoted alkyne-azide cycloaddition
SPG	Schizophyllan
STING	Stimulator of interferon genes
STn	Sialyl-Tn
TACAs	Tumor-associated carbohydrate antigens

TAP	Transporter to be associated with antigen processing
tBA	α-Bromoisobutyryl bromide, t-butylacrylate
TCR	T cell receptor
TD	T dependent
TEA	Triethylamine
TF	Thomsen-Friedenreich
TFA	Trifluoroacetic acid
Th1	T helper cell type 1
Th2	T helper cell type 2
THF	Tetrahydrofuran
THPTA	Tris(3-hydroxypropyltriazolylmethyl)amine
TIPS	Triisopropylsilane
TLRs	Toll-like receptors
TMG	TiterMax Gold
TT	Tetanus toxoid
VC-PAB	Valine-citrulline-p-amino-benzyl
ZPSs	Zwitterionic polysaccharides

CHAPTER 1 Carbohydrate and Carbohydrate Conjugates in Vaccine Developments[1]

1.1 Introduction

Carbohydrates are common surface molecules in the living system. With their rich structural diversities, carbohydrate molecules play important roles in cellular recognition and signaling, including immune recognition and activation.[2-4]Most of the cell surface immune receptors, such as toll-like receptors (TLRs), NOD-like receptors (NLRs) and major histocompatibility complex class I and class II (MHC I and MHC II), are glycoproteins. Several essential receptors for immune cell activation, for example, TLRs, NLRs, C-type lectins and sialic acid-binding immunoglobulin-type lectins (Siglecs), can recognize glycan containing ligands including those expressed on the surface of many pathogenic microbes and cancer cells.[3]

Carbohydrates have been widely applied in vaccine development[5]. Vaccines containing bacterial polysaccharides have been commercialized as anti-bacterial vaccines,[6-7] and many anti-cancer vaccines have been studied to target tumor-associated carbohydrate antigens (TACAs).[6, 8-10] Carbohydrates are also attractive immune adjuvant candidates. Various carbohydrates such as β-glucan, mannan and monophosphoryl lipid A (MPLA) can activate the immune system and induce T helper cell type 1 (Th1) immune responses.[11-14] They may complement Alum, the Food and Drug Administration (FDA) approved adjuvant in humans, which only induces T helper cell type 2 (Th2) immune responses. Carbohydrates can be readily metabolized or degraded *in vivo* and are less likely to generate long-term toxicity.[13, 15-16] With their biocompatibility, low toxicity

and ease of modification, carbohydrates have been studied as carriers for antigen delivery,[17-21] which can often induce immune cell targeting and provide self-adjuvanting activities for a successful vaccination.

Although natural carbohydrates can be applied as vaccine components directly,[22-24] in many cases chemical modification of carbohydrates is necessary for enhanced efficacy. One of the commonly used strategies in vaccine design is to prepare conjugates of antigens and/or adjuvants with the delivery carrier.[25] This can be beneficial in multiple ways, such as prolonged circulation and controlled release, size-induced lymph node targeting, better immune recognition through multivalency, enhanced cell uptake and immune activation. In this chapter, we would review recent vaccine designs applying carbohydrates as vaccine delivery carriers and adjuvants. We will discuss examples involving chemical modifications of the carbohydrates, especially the covalent conjugates of antigens and carbohydrate-based delivery carrier or adjuvants. Vaccines that contain carbohydrates and derivatives only as antigen components, or natural carbohydrates encapsulated/admixed with other vaccine components, have been reviewed comprehensively,[26-31] and are not discussed here.

1.2 Zwitterionic polysaccharides (ZPSs)

Many types of bacteria can produce high molecular weight polysaccharides as their capsules. Polysaccharides have been traditionally considered as T cell independent antigens unless conjugated to proteins or lipids.[30, 32] Polysaccharides usually interact with polysaccharide-specific

B cells generating low-affinity IgM with little detectable IgG antibodies and little induction of T cell responses or immune memory.[33] However, a special group of polysaccharides, referred to as ZPSs, has been found to have the ability to induce MHC II mediated T cell response specifically.[34-35] At least eight different ZPSs have been isolated from Bacteroides Fragilis, Staphylococcus Aureus and Streptococcus Pneumoniae type 1, of which the PS A1 (isolated from Bacteroides Fragilis) is the most studied ZPS so far (**Scheme 1.1a**).[35-38]

TACAs are saccharides aberrantly expressed on surfaces of multiple types of cancer cells.[39] Like most types of carbohydrate antigens, TACAs induce only weak IgM responses when administered alone. For successful TACA vaccines, TACAs are commonly conjugated with strong immunogenic proteins, such as bovine serum albumin (BSA), tetanus toxoid (TT), keyhole limpet hemocyanin (KLH), and virus like particles, in order to generate high levels of IgG responses.[39-42] However, these carrier proteins can result in carrier induced suppression of antibody responses to the desired TACA due to high antibody responses to the carrier itself.[43] Furthermore, some of the protein carriers tend to aggregate or suffer from stability issues.[44] ZPSs as novel non-protein T cell-activating carriers have been applied to cancer vaccine design by the Andreana group.[45] They first reported an "entirely carbohydrate vaccine" by conjugating a model TACA, Tn, and the most studied type of ZPS, PS A1. PS A1 was isolated from B. Fragilis in a large scale, then subjected to selective oxidation leading to aldehyde functioned PS A1 that reacted with aminooxy functionalized Tn by oxime formation (**Scheme 1.1b**).

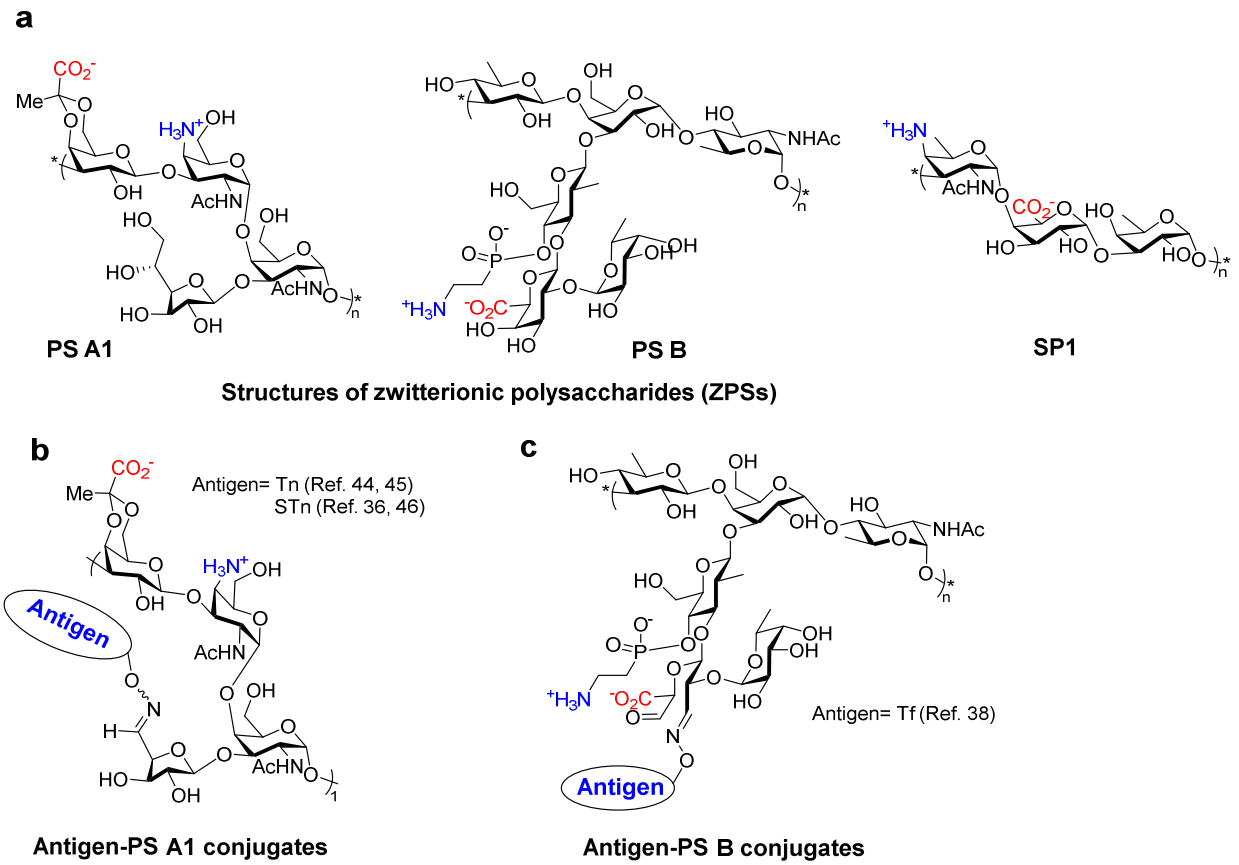

Scheme 1.1 a. Structures of several ZPSs. **b**. Examples of antigen-PS A1 conjugates. **c**. Examples of antigen-PS B conjugates.

Immunization of mice with Tn-PS A1 resulted in a 200-fold increase of total antibody titer against Tn compared to the pre-immunized sera, while the antibody titers against the PS A1 backbone were modest. IgM and IgG3 were the major subtypes of antibodies generated.[45] Anti-sera of Tn-PS A1 immunized mice were found to react with a range of Tn expressing cancer cell lines (MCF-7, MDA-231, Jurkat, JurkatTAg, Panc-1),[46] while binding little to human peripheral blood mononuclear cells and human bone marrow cells as the negative control. The anti-PS A1 and anti-Tn-PS A1 sera showed completely different cytokine profiles. A high level of IL-17A, a

pro-inflammatory factor promoting $CD4^+$ T cell proliferation, was detected in anti-Tn-PS A1 sera but not in anti-PS A1 sera. Besides Tn antigen, other TACAs such as sialyl-Tn (STn)[37, 47] and Thomsen-Friedenreich (Tf)[48] have been conjugated with PS A1 (Scheme 1b) and another ZPS, i.e., PS B (**Scheme 1.1c**).[48] The conjugates were able to induce moderate levels of both IgM and IgG antibodies against the target TACAs. Co-administration of an exogenous adjuvant such as Sigma adjuvant system (SAS) and TiterMax Gold (TMG) could enhance the levels of IgG antibodies. Post-immune sera bound with multiple types of cancer cells and were able to kill tumor cells via complement-dependent cytotoxicities while sparing normal cells. Furthermore, the STn-PS A1+SAS vaccine generated cellular immunity besides humoral antibody response. The enzyme-linked immune absorbent spot (ELISpot) assay of splenocytes from mice immunized with STn-PS A1+SAS pulsed with STn-PS A1 or BSM showed secretion of INF-γ, clearly indicating a Th1-dominant cellular immune response.

These studies indicated that ZPSs are promising vaccine carrier/adjuvant to elicit a selective immune response against TACAs. However, to date, the efficacy of protection in mouse tumor models by these entirely carbohydrate vaccines have not been reported. Further studies are needed to demonstrate the full potential of ZPS in anti-cancer vaccine development.

1.3 MPLA

MPLA is a derivative of lipopolysaccharide (LPS), a fraction isolated from cell walls of gram-negative bacteria such as Salmonella Minnesota.[49] Through a hydrolytic process reported by Edgar

Ribi, LPS can be converted into an acylated di-glucosamine mixture widely known as monophosphoryl lipid.[49-51] The majority of these species contains six acyl side chains, no polysaccharide chains and one phosphoryl group (**Scheme 1.2a**).[49, 52] Compared to LPS, MPLA is about 0.1% as toxic as the parent LPS compound in rabbit pyrogenicity assays while maintaining its immune-stimulating activities.[50, 52] MPLA interacts with the immune system through TLR-4 and usually induces Th1 or a blended Th1 and Th2 type immune response. With its low toxicity, MPLA has been applied as the adjuvant in several vaccines successfully in clinical trials.[52-54] Vaccines containing MPLA such as FENDrix (HBV vaccine), Cervarix (HPV vaccine), Melacine (melanoma vaccine), Pollinex Quattro (allergy vaccine) and Mosquirix (malaria vaccine for young children) have been registered for use in many countries.[53] MPLA can also serve as a vaccine carrier and a built-in adjuvant when conjugated with antigens covalently. Herein we discuss examples of fully synthetic vaccines containing MPLA as the carrier.[55-59]

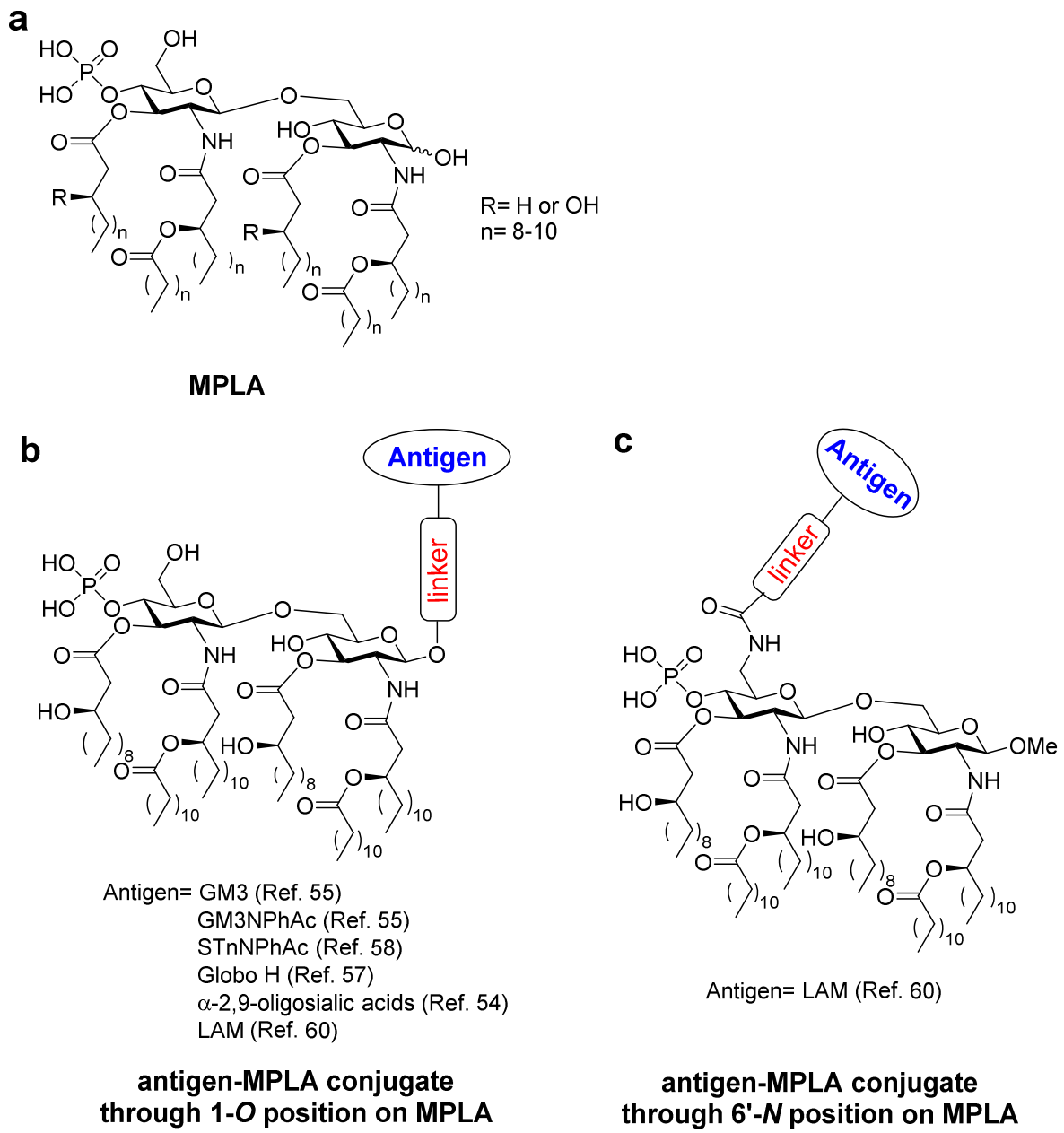

Scheme 1.2 a. Structure of MPLA. **b**. Examples of antigen-MPLA conjugate through 1-*O* position. **c**. Example of antigen-MPLA conjugate through 6'-*N* position on MPLA.

In 2011, the Guo lab first reported the covalent conjugation of a TACA, i.e., GM3, with MPLA as an anti-cancer vaccine.[56] The liposomal vaccine was formed by sonication of a mixture of the

GM3-MPLA conjugate, 1,2-distearoyl-sn-glycero-3-phosphocholine, and cholesterol. The resulting vaccine was injected to C57BL/6 mice subcutaneously for 4 weekly injections. A strong GM3-specific antibody response was observed by enzyme-linked immuno-sorbent assay (ELISA) in antisera on day 38, which included high levels of both IgM and IgG3 antibodies. When a GM3 derivative, GM3NPhAc,[60] was conjugated with MPLA using a similar strategy, a 3.8 times higher total antibody titer with a significant increase of IgG3 and IgG1 titers was observed in day 38 antisera compared to the GM3-MPLA group. The antisera from GM3NPhAc-MPLA immunized mice showed strong binding towards cancer cell SKMEL-28 by fluorescence activated cell sorting (FACS) analysis. The free phosphate and free hydroxyl groups on MPLA are important for immunostimulation, as the conjugates with benzyl protected phosphate and hydroxyl groups showed no significant immune responses. The linker between MPLA and GM3/GM3NPhAc did not significantly influence the immunological properties of the resulting conjugates. Interestingly, addition of an external adjuvant such as TiterMax Gold to the vaccine formulation led to lower antibody titers relative to GM3/GM3NPhAc-MPLA conjugates alone. This work indicated that the fully synthetic conjugation of MPLA-TACA can serve as a possible "self-adjuvanting" cancer vaccine candidate.

The generality of the MPLA platform has been demonstrated in later studies. Three more MPLA analogs with different lipid chain lengths and linkages were synthesized and conjugated to another TACA derivative, STnNPhAc,[57, 59] and formulated into a liposomal vaccine. All

STnNPhAc-MPLA conjugates successfully generated immune responses toward STnNPhAc in mice and the conjugate with an 8-carbon lipid chain length and free -OH groups induced the highest antibody titers. Similar to the GM3-MPLA conjugate, when the exogenous adjuvant TiterMax Gold was added to the formulation, the antibody titers decreased.

The optimized MPLA structure was used to conjugate with another TACA, globo H, and the immunological properties were compared with the globo H conjugate with KLH, a gold standard carrier commonly utilized in vaccine studies.[58] Significantly higher total antibody titers as well as IgG titers were observed in anti-sera from MPLA-globo H immunized mice compared to those immunized with KLH-globo H, suggesting the advantage of MPLA as the carrier. Both conjugates induced higher levels of pro-inflammatory cytokines including IL-4, IL-12, IFN-γ, and TNF-α in mice compared to the non-immunized group. Although the KLH-globo H group showed a higher level of cytokine secretion compared to MPLA-globo H, antisera from MPLA-globo H immunized mice showed a stronger binding toward both MCF-7 and SKMEL-28 tumor cells by FACS analysis and induced more cell lysis of human breast cancer cell MCF-7. The enhanced cytokine secretion in KLH conjugate group might come from the immune response against the protein carrier instead of the globo H antigen. This study indicated that the MPLA may serve as a good alternative to KLH protein vaccine carrier.

In addition to the aforementioned cancer vaccines, a Group C meningitis vaccine has been reported by conjugating MPLA and α-2,9-oligosialic acid containing di-, tri-, tetra- and penta-

sialic acid.[55] The resulting liposomal vaccines with various MPLA-oligosialic acid conjugates induced strong immune responses as revealed by high total antibody titers. The major antibody subtype generated was IgG2b indicating a T cell-dependent immunity. Both oligosialic acid chain length and MPLA structure influenced the immune responses. The shorter sialic acid chains (di- and tri-sialic acid) were overall better immunogens than longer ones (tetra- and penta-sialic acid). However, the antibody induced by the short sialic acid were more restricted to short sialic acid chains. Conjugates containing tri-, tetra- or penta-sialic acid showed stronger binding toward Group C meningitides capsule polysaccharide than the conjugate containing di-sialic acid. Consistent with cancer vaccine studies, addition of external adjuvants such as CFA, alum and TiterMax Gold did not lead to higher antibody responses. All conjugates showed protective effects against Group C meningitides bacterial challenges in mice, which suggested the possibility of applying the MPLA platform to anti-microbial vaccine development.

In the aforementioned MPLA based vaccine designs, the antigens were all conjugated with MPLA through 1-*O*-position instead of 6'-*O*-position where the polysaccharide chain is attached to LPS in nature.[61] Guo and Gu further studied the influence of different antigen linkage positions on immunological properties (**Schemes 1.2b and 1.2c**), by linking a tetrasaccharide antigen from lipoarabinomannan (LAM), a Mycobacterium tuberculosis cell surface lipopolysaccharide, to either 1 or 6' position of MPLA. As the ester linkage on 6' position was not stable, the 6'-*O* was first substituted with an amino group linker in order to form a more stable amide bond. The

resulting conjugates were evaluated *in vivo*. Both conjugates showed significantly enhanced antibody titers against LAM compared to the simple mixture of tetrasaccharide and MPLA, which indicated the importance of covalent conjugation between the antigen and MPLA. As revealed by ELISA, the antigen conjugated to MPLA through 6'-*N* position induced significantly higher IgG titers than the corresponding conjugate through the 1-*O* position. The method of vaccine administration also influenced the immune response outcome. Vaccine given through intraperitoneal injection induced a 4-5 times higher antibody titer compared to the subcutaneous route. This study suggested the conjugation through 6' position of MPLA could be a more superior strategy for MPLA based vaccine design.

As a low toxicity TLR4 stimulator, MPLA has been widely applied in many vaccines as an add-in adjuvant.[53] Guo's work demonstrated the potential of MPLA as a good "self-adjuvating" vaccine carrier. MPLA-antigen conjugates containing liposomal vaccines can induce strong immune responses comparable to KLH protein. The MPLA platform showed good generality for several carbohydrate antigens including TACAs and bacterial glycans. This platform is not compatible with many external adjuvants and the antigen conjugation site can significantly influence the outcome of vaccination.

1.4 Mannan

Mannan, a polysaccharide derived from the yeast cell wall, contains mostly β-1,4-linked mannose backbone with a small number of α-1,6- linked glucose and galactose side chain

residues[62]. In addition, around 5% proteins were contained in mannan (**Scheme 1.3a**).[63-64] As an important component of fungal cell wall, mannan has been widely targeted as carbohydrate based vaccines for Candidiasis.[65-67] It was noticed from patients suffering from Candidiasis that the mannan has immunomodulatory functions.[68-69] Mannan can be recognized through binding with mannose recognition lectins presented on macrophages and other immune cells, which activates the host immune system via a non-self-recognition mechanism.[70-71] The recognition initiates a set of signal transduction events leading to cytokine secretion, complement activation and $CD8^+$ T cell activation.[72-74] In this section, we focus on vaccines based on mannan carrier-antigen complex/conjugations, including mannan-mucin 1 (MUC1) fusion protein conjugation for tumor therapy, mannan-DNA vaccine and mannan-allergy vaccines.

The investigation of mannan's potential as a vaccine carrier started in 1990s. The Steward group conjugated mannan and dextran to hepatitis B virus (HBV) 139-147 peptide and studied the immune response in mice towards these two constructs.[75] The mannan carrier successfully induced high IgG titers against HBV 139-147 peptide without additional adjuvants, while the corresponding dextran conjugate failed to elicit an immune response. Although some previous studies showed that mannan could suppress immunity,[72, 76] this study opened the door for using mannan as a "self-adjuvanting" vaccine carrier to enhance antibody production.

1.4.1 Mannan-MUC1 fusion protein conjugation (M-FP)

Mucins are heavily glycosylated proteins expressed on cell surface. MUC1 is a prototypical mucin, which has been found to be over-expressed on a wide range of tumor cells. Furthermore, tumor associated MUC1 has drastically shorter *O*-glycans in the tandem repeat region of MUC1 made of 20-amino acid residues (APDTRPAPGSTAPPAHGVTS),[77] which leads to the exposure of the protein core, rendering it a highly attractive antigen for anti-cancer immune-therapy.[78-79]

MUC1 by itself is only weakly immunogenic in humans partly due to its self-antigen nature. Immunization of mice with MUC1 fusion protein containing 5 of the tandem repeats induced antibodies but with little measurable cytotoxic T lymphocyte (CTL) responses and poor tumor protection[80]. To enhance anti-MUC1 immunity, MUC1 has been conjugated with mannan.[81]

Two strategies (oxidative or reductive, **Scheme 1.3b**) for linking mannan to MUC1 have been investigated, which induced drastically different types of immune responses.[82] Human MUC1 FP was conjugated to mannan oxidized with sodium periodate to provide the oxidative mannan-MUC1 fusion protein conjugate (ox-M-FP). The reductive mannan-MUC1 fusion protein conjugate (red-M-FP) was obtained by treating ox-M-FP with sodium borohydride. BALB/c mice were immunized with either ox- or red- M-FP then challenged with $MUC1^+$ 3T3 tumor cells. The red-M-FP generated Th2 type immune responses and induced antibody secretion. However, it had little tumor protective effects. In contrast, the ox-M-FP generated Th1 type responses and induced a high tumor specific CTL precursor frequency providing protection in a mouse tumor model. The

CTL response elicited by ox-M-FP was MHC I restricted[83], and the CTL precursor frequency could be further enhanced by a combination with a chemotherapeutic drug, i.e., cyclophosphamide.[84] The detailed mechanism of the entry of ox-M-FP into MHC I pathway had also been studied.[85] While both aldehyde and Schiff base groups were presented on ox-M-FP, the aldehyde groups but not the Schiff base groups were found to be important for antigen presentation through the MHC I pathway.

The ox-M-FP had been evaluated in human clinical trials. In phase I studies, no significant toxicities or autoimmunities were noted among >100 patients with advanced melanoma. However, in contrast to preclinical mouse studies, the patients generated mainly antibodies rather than cellular immunity against MUC1.[86-88] The route of ox-M-FP administration influenced antibody generation in patients. Intraperitoneal injections were significantly more effective compared to intramuscular injections.[88] Pilot phase III study of ox-M-FP was performed in early-stage breast cancer.[89] Although vaccine-induced antibody and weak cellular immunity responses showed little benefits in advanced disease stage, ox-M-FP significantly improved survival time compared to the placebo control group in early-stage cancer patients.[89] In a 12-15 year follow-up study, the recurrence rate of ox-M-FP group was much lower than that of the placebo group (12.5% vs. 60%).[90] The mean time of recurrence in the ox-M-FP group was 52.2 months longer compared to placebo group (118 vs. 65.8 months).[90] In another study, autologous dendritic cells were chosen as the vaccine carrier to maximize the cellular immunity in patients.[91] The phase I/II clinical trial

showed ox-M-FP loaded monocyte derived dendritic cells were well tolerated for immunotherapy, and vaccine-specific IFN-γ secreting $CD4^+$ and $CD8^+$ T cells were successfully induced in all patients.[91]

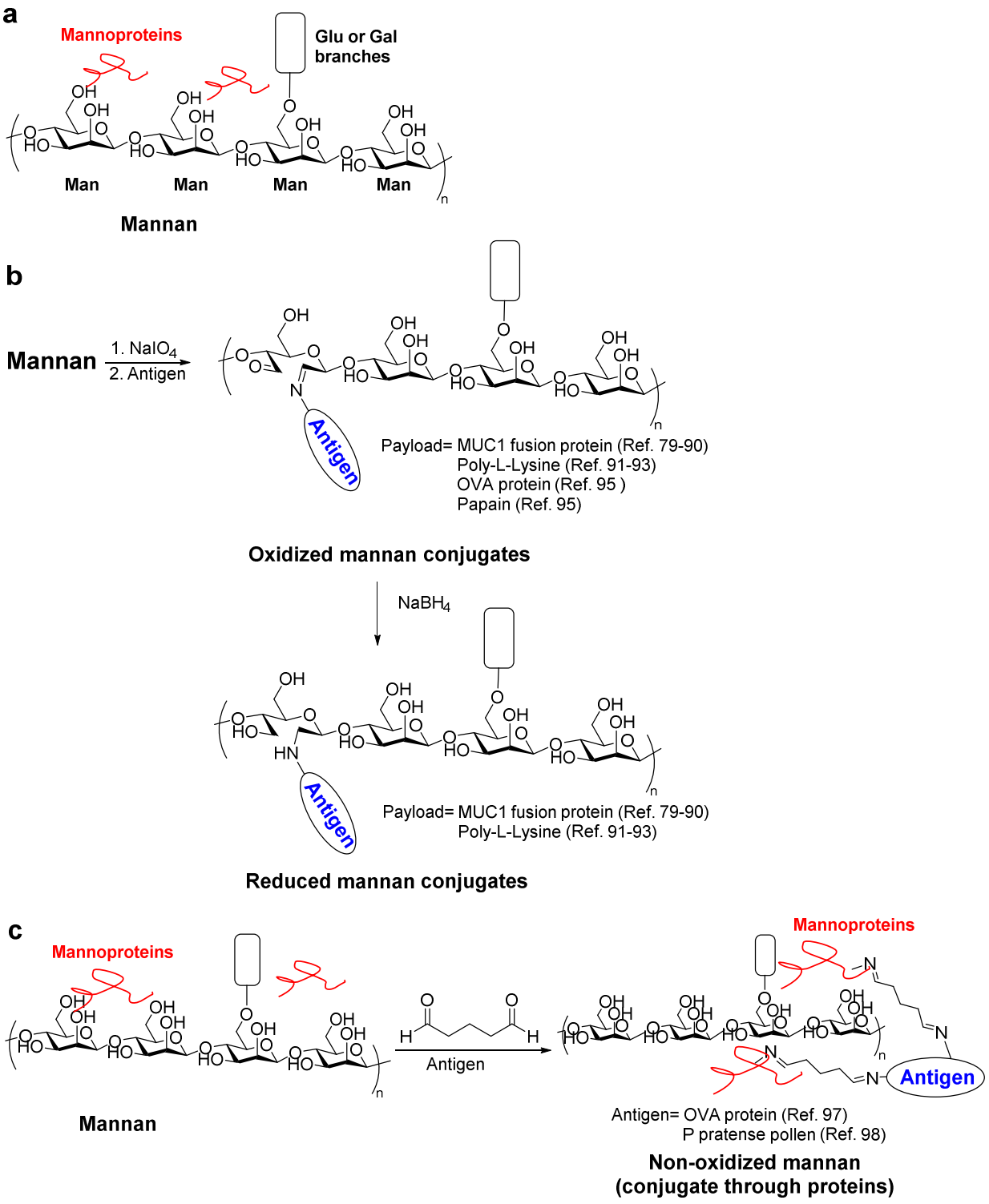

Scheme 1.3 a. Structure of Mannan. **b**. Examples of oxidized and reduced mannan conjugates. **c**. Examples of non-oxidized mannan conjugated with antigens through proteins.

1.4.2 Mannan as a carrier for DNA vaccines

Oxidized and reduced mannan (ox-Man and red-Man respectively) have been studied as DNA vaccine carriers. Apostolopoulos and Pietersz groups conjugated ox-Man and red-Man with polycationic linker poly-L-lysine (PLL) and then complexed them with DNA corresponding to the protein ovalbumin (OVA).[92] The conjugation with mannan reduced cytotoxicity of PLL, and the Man-PLL-OVA DNA complex successfully induced immune responses against OVA. At a lower dose (10 μg), red-Man-PLL-OVA DNA mainly induced $CD4^+$ T cell responses, while ox-Man-PLL-OVA DNA induced $CD8^+$ T cell responses. Meanwhile, at a higher immunization dose (50 μg), both red-Man and ox-Man-PLL-OVA DNA complex generated $CD4^+$ and $CD8^+$ T cell responses. Both complexes induced good tumor protection against OVA expressing EG.7 tumor using either low (10 μg) or high (50 μg) immunization doses.

With the success of OVA DNA vaccine, Apostolopoulos and coworkers further studied MUC1 DNA vaccine, by preparing the Man-PLL-DNA complex.[93] The resulting ox-Man-PLL-MUC1 DNA generated immune responses in C57BL/6 mice and protected mice in tumor challenge with a low immunization dose. In addition, the vaccines generated strong immune responses in MUC1 transgenic mice, which are tolerant towards human MUC1 as in humans. Similar to previous reports, the ox-Man-PLL-MUC1 DNA mainly generated a Th1 response while red-Man-PLL-MUC1 DNA generated a Th2 dominant response. A more detailed study showed the differences between DNA alone and Man-PLL-DNA complex upon immunization.[94] Man-PLL

protected cargo DNA against the DNase digestion. Ox-Man and red-Man induced different cytokine secreting profiles. Compared to DNA alone, ox-Man induced higher levels of IL-2, IL-12, IFN-γ and TNF-α while red-Man induced only IL-2. The Man-PLL-DNA complex was able to stimulate dendritic cell (DC) maturation through a TLR2 but not a TLR4 dependent pathway.

1.4.3 Mannan as the carrier for allergy vaccine

Allergen-specific immunotherapy has attracted researchers' attention as it may provide a long-lasting relief from allergy for the patients. Mannan-allergen conjugates have been studied as potential anti-allergy vaccines.[95]

The Weiss lab studied the conjugation between oxidized mannan and model allergens, OVA protein and papain, for vaccination targeting dendritic cells.[96] The mannan backbone here served as not only a targeting molecule towards the C-type lectin receptor (a receptor expressing on DCs), but also a platform to induce cross-linking for multimerization of allergen proteins for immunogenicity enhancement.[97] Sodium periodate was used for generating aldehyde groups on mannan backbone for allergen conjugation by oxidative cleavage between C2 and C3. The conjugation efficiency depended on antigen properties as well as the degree of oxidation. The C-lectin binding property of mannan was not disturbed after conjugation with antigen proteins when the oxidation degree was careful controlled. The mannan-antigen conjugate significantly increased the number of antigen-presenting DCs in lymph nodes *in vivo*. Immunization successfully reduced the enzymatic activity or IgE binding capacity of antigen proteins in vaccinated mice. Antibody

class-switching from allergy-promoting IgE subtype to non-allergic IgG1 subtype was noticed indicating an anti-allergy therapeutic effect.

Palomares et. al. used another strategy to conjugate allergen proteins to non-oxidized mannan by a simple treatment of glutaraldehyde (**Scheme 1.3c**).[98] The conjugate took advantage of the trace amount of mannan protein on mannan backbone. Allergens were polymerized and linked to mannan protein through glutaryl diimine linker and the resulting conjugate significantly reduced IgE binding activity against the allergens. Later Palomares et. al. applied this conjugation method for preparing P pratense pollen-non-oxidized mannan conjugate (PM).[99] The PM was hypoallergenic with low IgE binding *in vitro* and induced fewer mast cells under the skin in an *in vivo* skin-prick test. Immunization of rabbit with PM induced blocking antibodies against IgE binding. Compared to the free allergen or the polymerized allergen, the PM can be captured more effectively by human DCs. More anti-inflammatory cytokines IL-6 and IL-10 secretion in human DCs were induced by PM, and $Foxp3^+$ Treg generation through PD-L1 in human subjects was also promoted, which indicated a down-regulation of immune responses toward the allergen.

A drawback in using oxidized mannan is that the mannose ring in the mannan backbone is partially opened, which may impair the capture of PM by DCs in mice and human subjects.[99] This can be overcome with non-oxidized mannan.

Another important consideration in mannan based vaccine is the combination of external adjuvant. In a recent study, the Palomares lab reported the PM induced anti-allergy $Foxp3^+$ Treg

generation can be inhibited when co-administrated with Alum.[100] This was because Alum suppressed the increasing production of lactate and consumption of glucose induced by PM in human DCs by altering the glucose metabolic fate in mitochondria and inhibiting mammalian target of rapamycin (mTOR).

1.5 α-Galactosylceramide (α-GalCer)

The presentation of antigen fragments on antigen presenting cell (APC) surface is an important step for activating the adaptive immune system. Besides the commonly known MHC I and MHC II, CD1 family is a third subset of antigen presenting molecules.[101] There are 4 types of CD1 (CD1a-CD1d) capable of binding and presenting glycolipids to CD1-restricted T cells. A subtype of T cells, invariant natural killer T (iNKT) cells, is defined as a T cell lineage expressing NK cell receptors and an additional invariant CD1d restricted αβ-T cell receptor (TCR).[102] After activation through its TCR binding with glycolipid presenting CD1d on APCs, iNKT cells can secret various cytokines, which build a bridge between the innate and the adaptive immune system. iNKT cells can initiate "T dependent (TD) type II response", which needs no participation of $CD4^+$ T cells. It has been reported that iNKT cells play a role in protection against pathogens as well as cancer.[103-105] The first iNKT activator, α-GalCer (KRN7000, **Scheme 1.4a**) was a synthetic compound discovered from a class of glycolipids originally isolated from marine sponges.[106-108] Since then, hundreds of analogs were synthesized by varying the amide side chain length and functional groups, substitutions at galactose-6 position and galactose-ceramide linker etc. α-GalCer is by far

the most explored structure and the *C*-glycoside analog 7DW8-5 with an aryl side chain were also attractive structures for immune studies. Many excellent reviews about α-GalCer and its analogs have been published.[28, 109-111]

α-GalCer has been applied as an adjuvant in many studies,[53, 111-117] including vaccines against cancer, influenza, and malaria. To improve the delivery efficiency of α-GalCer and therefore enhancing the activation of iNKT cells, various delivery systems have been designed, such as liposomes, poly(lactic-co-glycolic acid) (PLGA) particles and bacteriophage particles.[118-122] By delivering covalently conjugated antigen and α-GalCer, the immune response could be stronger due to the simultaneous delivery of the antigen and the adjuvant to the same immune cell, and we focus on examples of covalent conjugate vaccines of α-GalCer.

The first examples of covalent conjugation of the antigen and α-GalCer were reported in 2014 .[123-124] The Painter and Herman's labs developed self-adjuvanting vaccines that suppressed allergy by conjugating the antigen peptide to α-GalCer through a cleavable linker (**Scheme 1.4b**).[123] Starting from α-GalCer, an N to O acyl migration occurred under acidic conditions, which produced an α-GalCer prodrug with a free amino group for further functionalization. The amino group was then capped with an esterase-labile acyloxymethyl carbamate group. The resulting ketone group could be functionalized with an aminooxy peptide containing the protease cleavable FFRK sequence following the desired antigen peptide. Under the physiological condition, the FFRK linker would be cleaved to release the desired antigen while the acyloxymethyl carbamate

group would be degraded by an esterase to release the α-GalCer prodrug. After a reversed *O* to *N* acyl migration, the active adjuvant α-GalCer would be formed *in situ*. In this study, two model antigen peptides, SIINFEKL and KAVYNFATM, were selected. Both peptide-GalCer conjugates stimulated greater $CD8^+$ T cell proliferation compared to non-conjugated mixtures containing the same amount of peptide and α-GalCer. By intracellular staining, large amounts of IFN-γ and TNF-α were detected, while allergy related IL-4 cytokine was not detectable. The conjugates induced antigen-specific cytotoxic responses in immunized animals, while the admixture of peptide and α-GalCer failed to do so. This strong activity was $CD4^+$ T cell independent and the covalent conjugation was shown to be critical. The SIINFEKL-α-GalCer conjugate strongly reduced inflammatory responses in an allergy animal model, sensitized by the OVA protein. In contrast, the mixture of peptide and α-GalCer did not reduce the allergic response.

About the same time, the De Libero' lab developed a semisynthetic vaccine against S. pneumoniae by conjugating S. pneumoniae serotype 4 capsular polysaccharides (CPS 4) to 6 position of α-GalCer through a cleavable linker (**Scheme 1.4c**).[124] Different from Painter and Herman's strategy, the immunogenic lipid tail was kept intact. Instead, an amino moiety was connected to 6-OH of α-GalCer then conjugated with CPS 4 via cyanogen bromide chemistry. The conjugates were usually a mixture of isoureas, *N*-substituted imidocarbonates and *N*-substituted carbamates, which could release the original CPS 4 under acidic condition when taken up by APCs. The CPS 4-GalCer conjugation generated polysaccharide-specific IgM, IgG1, IgG2a, IgG2b and

IgG3 antibody responses in mice, while the mixture of CPS 4 and α-GalCer and CPS 4 only generated weak IgM responses with no IgGs. The conjugation induced germinal centers and the resulting antibody induced S. pneumoniae opsonization. Animals vaccinated with the CPS 4-GalCer conjugate exhibited a significant survival advantage (89%) in bacterial challenge model compared to animals receiving CPS alone (25%). By FACS analysis of the splenocytes, CPS 4-GalCer, but not mixture of CPS 4 and α-GalCer or CPS4 alone, induced antibody isotype switching to IgG, generation of memory B cells and antigen secreting plasma cells. Experiments on CD1d-/- mice indicated that iNKT cells were required to establish effective protections against S. pneumoniae.

Both conjugation methods, i.e., conjugating antigen to lipid tail or to 6-OH on galactose through cleavable linker, were proven to be successful. The conjugated vaccines have been demonstrated to provide stronger immune stimulation compared to a simple mixture of antigen and adjuvant. Several more examples using either conjugation method have been published since then (**Schemes 1.4b** and **1.4c**).

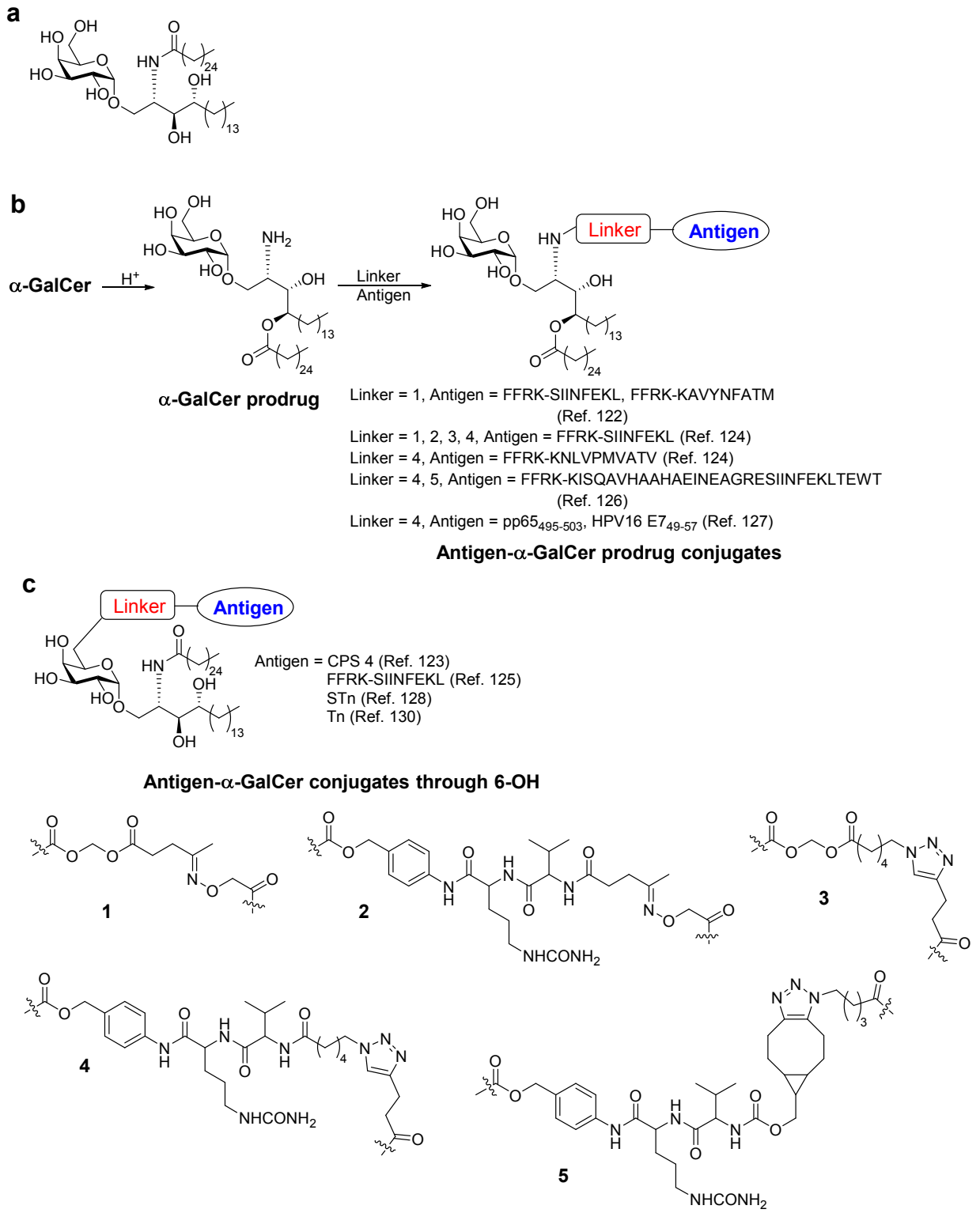

Scheme 1.4 a. Structure of α-GalCer. **b**. Examples of antigen-α-GalCer prodrug conjugates (conjugate through α-GalCer lipid chain). **c**. Examples of antigen-α-GalCer conjugate through 6-OH.

Painter and Herman continued the study on conjugation linkers and designed several possible linkage methods to covalently conjugate the antigen with α-GalCer (**Scheme 1.4c**).[125-126] They first investigated four different linkers to link short peptide antigens on GalCer lipid tail.[125] Similar to their previous work,[123] an N to O migration of the acyl group on α-GalCer was designed, resulting in an α-GalCer prodrug with a free amino group. The amino group was further capped with an esterase sensitive acyloxymethyl carbamate linker containing ketone (linker 1) or azido group (linker 3), or with protease sensitive valine-citrulline-*p*-amino-benzyl (VC-PAB) carbamate linkers containing ketone (linker 2) or azido group (linker 4). Short peptide antigens with a protease cleavable FFRK sequence were conjugated to the 4 different linkers through oxime formation (for linkers 1 and 2) or copper catalyzed azido-alkyne coupling (CuAAC) (for linkers 3 and 4). All four conjugates showed similar levels of NKT cell activation in a melanoma challenge model. These conjugates showed improved protection compared to unconjugated mixtures. Among the four choices, linker 4 provided a better stability under physiological pH and eased the synthesis of peptide payload, and therefore was considered as a lead compound for further development.

Painter and Turner applied the aforementioned conjugation strategy for the development of an influenza vaccine. They linked a synthetic long peptide (SLP) containing an immunogenic sequence OVA_{257} (amino sequence: SIINFEKL), a known $CD4^+$ T cell epitope OVA_{323} (amino acid sequence: ISQAVHAAHAEINEAGR) and a protease cleavage sequence FFRK, with the α-GalCer prodrug with VC-PAB linker through CuAAC (linker 4) or strain-promoted alkyne-azide

cycloaddition (SPAAC) (linker 5).[127] Though the two conjugation methods introduced slightly different linker structures in the final α-GalCer prodrug-SLP conjugates, the two vaccines primed NKT cells similarly *in vivo*. As the SPAAC strategy provided a higher yield with fewer side-products, this form of vaccine was subjected to further studies. It has been noted that the α-GalCer prodrug-SLP conjugate vaccine induced $CD8^+$ T memory cell at a similar level as A/PR8-OVA challenged group, which was known to induce OVA specific memory response. The memory T cell response lasted for at least 60 days after immunization. The α-GalCer alone, SLP alone or α-GalCer + SLP mixture failed to induce such memory T cell response. *In vivo* challenge study using OVA modified influenza virus showed that mice vaccinated with the α-GalCer prodrug-SLP conjugates showed a faster viral clearance and body weight recovery compared to α-GalCer alone or α-GalCer + SLP mixture, suggesting the generation of protective immunity by vaccination.

Weinkove and Painter reported an α-GalCer prodrug conjugated with $pp65_{495\text{-}503}$, an HLA-A*02-restricted peptide from cytomegalovirus (CMV) pp65 protein, through the VC-PAB linker using CuAAC chemistry (linker 4).[128] The resulting conjugate activated human DCs and $CD8^+$ T cells besides NKT cells *in vitro*. After incubating human peripheral blood mononuclear cells (PBMCs) with α-GalCer or α-GalCer-$pp65_{495\text{-}503}$ conjugate, increased NKT proliferation and IFN-γ secretion were observed. Human DCs can be activated by α-GalCer or α-GalCer-$pp65_{495\text{-}503}$ conjugate only when co-cultured with NKT cells. The activation of NKT cells and DCs can be blocked by anti-CD1d antibodies, which suggested α-GalCer-$pp65_{495\text{-}503}$ activate human immune

cells through the CD1d dependent pathway. The activation of human $CD8^+$ T cells also required NKT cells. The conjugation between antigen peptide and α-GalCer is crucial for $CD8^+$ T cell activation, as the admixed components failed to induce the expression of T cell activation marker CD137. An oncogenic viral antigen HPV16 $E7_{49-57}$ was conjugated to α-GalCer prodrug through the same strategy and the resulting conjugate vaccine showed significant antitumor response against HPV16 E7 expressing tumor in mice model, which further suggested the effectiveness of α-GalCer prodrug-peptide antigen conjugate strategy.

Painter and Herman's labs also investigated the conjugation of antigen to 6-OH position of α-GalCer through a disulfide bond or a maleimido-linker.[126] 6''-Deoxy-6''-thiol-α-GalCer was first synthesized and was proven to have similar bioactivities as α-GalCer. The thiol group may be trapped with 2,2'-dithiodipyridine followed by reacting with Cys-peptide to form a disulfide bond or reacting with *N*-propargyl bromomaleimide followed by CuAAC for conjugation with the peptide. Both conjugates induced a stronger peptide-specific cytotoxic response *in vivo* relative to a mixture of α-GalCer and the peptide.

Liu and Guo designed a fully synthetic cancer vaccine candidate by linking tumor associated STn antigen to α-GalCer through a covalent linker at the 6-OH position.[129] Previous study showed that PEGylation on 6-OH position of α-GalCer through the amide linker retained the specificity of CD1d receptor and the ability to activate iNKT cells.[130] Therefore, the 6 position of α-GalCer was selected as the site of conjugation *via* an amide bond to a non-cleavable linker consisted of a non-

branched aliphatic chain to link with the STn antigen. STn-β-GalCer was also synthesized as a weak iNKT activator. The synthetic STn-α-GalCer and STn-β-GalCer were mixed with other lipids to form liposomal vaccines respectively. Based on ELISA results, though the two vaccines generated similar sera IgM titers against STn on BALb/c mice, STn-α-GalCer induced 23-fold higher IgG titers compared to STn-β-GalCer. Subtype analysis indicated the IgG antibodies were primarily IgG1 and IgG3, which were strong inducers of complement-dependent cytotoxicity (CDC) and antibody dependent cell-mediated cytotoxicity (ADCC). In this case, α-GalCer served as a liposomal carrier as well as an adjuvant for iNKT cell activation. In a later study from the Seeberger lab, the liposomal form of Tn-α-GalCer conjugates showed effective activation of anti-Tn immunity *in vivo*.[131] Compared to Tn-CRM_{197}, a protein carrier-based vaccine, the anti-Tn IgG response generated by the liposomal form of Tn-α-GalCer conjugate was more consistent and more specific. Furthermore, the liposomal form of Tn-α-GalCer conjugates also generated long-lasting memory response against Tn, while the Tn-CRM_{197} only induced memory response to the carrier protein in some of the mice but not to the glycan antigen. Liposomes formed by Tn-lipid conjugate without the α-Gal structure could also generate anti-Tn IgG, but with a lower magnitude of response compared to Tn-α-GalCer liposomes. The size of the liposomes was shown to be crucial in this case. While the ~400 nm sized liposomes promoted Th1-type IgG2a antibodies, the smaller particles (~120 nm) mainly induced the production of Th2-type IgG1 antibodies. This report indicated the multivalent display of antigens by the antigen-α-GalCer conjugated liposome can be

beneficial.

The aforementioned examples have shown the promises of antigen-α-GalCer conjugates as vaccines. The conjugates have been reported to have a stronger protective effect compared to the antigen and α-GalCer mixture. Short peptides and carbohydrates antigens can be used and multiple methods for conjugation were developed, which provided flexible ways for vaccine design. The liposomal form of antigen-α-GalCer covalent conjugates can further help inducing strong and tunable immune responses.

1.6 Modified dextran

Dextran is a branched natural polysaccharide containing α-1,6-linkage between glucoses as the backbone with α-1,3 linked branches. It is a biocompatible, biodegradable and FDA proved material. Dextran is water soluble and is easy to modify with other functional groups to achieve environment responsive properties. Though crystalized dextran particles can serve as vaccine delivery vehicle as reported,[132-133] most studies have focused on modified dextran as a candidate for vaccine design. In this section, we discuss only modified dextran.

1.6.1 Acetalated dextran

Acetalated dextran (Ac-Dex) is a pH responsive material first reported in 2008 by the Fréchet's group.[134] It can be synthesized easily from dextran through a single step acetal formation with 2-methoxypropene. In contrast of dextran, Ac-Dex is not soluble in water and can form microparticles using an emulsion procedure. Under acidic conditions, the acetals get hydrolyzed

to unmask the parent water soluble dextran structure and therefore breaking up the hydrophobic microparticles. In Fréchet group's study, a model hydrophobic payload, OVA, was encapsulated inside Ac-Dex particles via double emulsion with a loading rate of 3.6 wt%. At pH=7.4, the particles were stable, while in pH=5.5 buffers, the particles degraded within 24h. T cell activation assay showed that OVA loaded Ac-Dex particles significantly increased MHC I presentation of SIINFEKL on RAW macrophages compared to free OVA group. We applied Ac-Dex to deliver foreign antigens for anti-tumor therapy, and more details are presented in Chapter 2 of this thesis.[135]

A great advantage of Ac-Dex over traditional PLGA is the ease in tuning rate of degradation, providing the possibility to optimize the payload releasing rate for a specific application.[136-137] During the acetal modification, two types of acetal, cyclic acetal which hydrolyzes more slowly and acyclic acetal with faster degradation rates, would be formed on dextran (**Scheme 1.5**). As the kinetic product acyclic acetal forms first before the more stable cyclic acetals, the ratio of cyclic/acyclic acetal on the dextran backbone can be tuned by reaction time. The ratio of cyclic and acyclic acetal in the final product dictates the degradation behavior of the Ac-Dex particles. By controlling the reaction time from 2-1,500 minutes, a set of Ac-Dex with different ratios of cyclic/acyclic acetal was prepared.[136] The degradation half-life at pH=5.5 was tuned from minutes to days. The degradation rates at pH=7.4 were usually 230-280 times slower than those at pH=5.5, which was stable enough for delivery applications. Half-life of degradation correlated well with

cyclic acetal content, which indicated the hydrolysis of cyclic acetal may be the rate-limiting step in particle degradation. The molecular weight of dextran also influenced the degradation of particles.[137] With similar cyclic acetal coverage, the Ac-Dex with higher molecular weight degraded faster.

The degradation rate can be important for both MHC I and MHC II antigen presentation.[136] OVA loaded Ac-Dex particles with degradation half-lives from 0.27h to 16h were prepared and incubated with bone marrow dendritic cells (BMDCs) followed by T cell activation assays to determine MHC I and MHC II presentation of OVA derived epitopes. The particles with 1.7 h degradation half-life led to an optimal MHC I or MHC II presentation of OVA derived epitopes compared to particles with either longer or shorter degradation half-life. These optimal particles performed an order of magnitude better than traditional PLGA or iron oxide particles. Interestingly, the Ac-Dex particles with 1.7 h degradation half-life did not require the transporter to be associated with antigen processing (TAP), a protein involved in the most common MHC I antigen loading mechanism, for antigen presentation, while the particles with 16 h degradation half-life required TAP for antigen loading.[136] The difference might be attributed to the surface chemistry difference of the two materials due to the different degradation rate. A recent *in vivo* study[138] showed that OVA loaded Ac-Dex particles with 20% cyclic acetal coverage (CAC) generated stronger antibody response during the entire experiment period compared to particles with 40% and 60% CAC. Notably, when the particles were used for adjuvant delivery, the immune activating behavior was

different. The adjuvant loaded Ac-Dex particles with 20% CAC induced stronger antibody and cytokine response at early time points (day 14), while the 40% and 60% CAC induced greater antibody titers at later time points (days 28 and 42). This study suggested the importance of delivery of antigen and adjuvant separately in individually optimized Ac-Dex particles.

One possible limitation for Ac-Dex is that, one of the products released from degradation is methanol, which is known to be highly toxic. Therefore, 2-ethoxypropene was explored as an alternative to functionalize dextran instead of 2-methoxypropene.[139] No significant differences were observed in cell viability when cells were incubated with the acetalated dextran formed with 2-ethoxypropene or Ac-Dex at concentrations below 1mg/ml. Further toxicity study is needed to determine if the new acetalated dextran improved the biocompatibility at higher concentrations. To date, most studies have been using Ac-Dex as the carrier material.

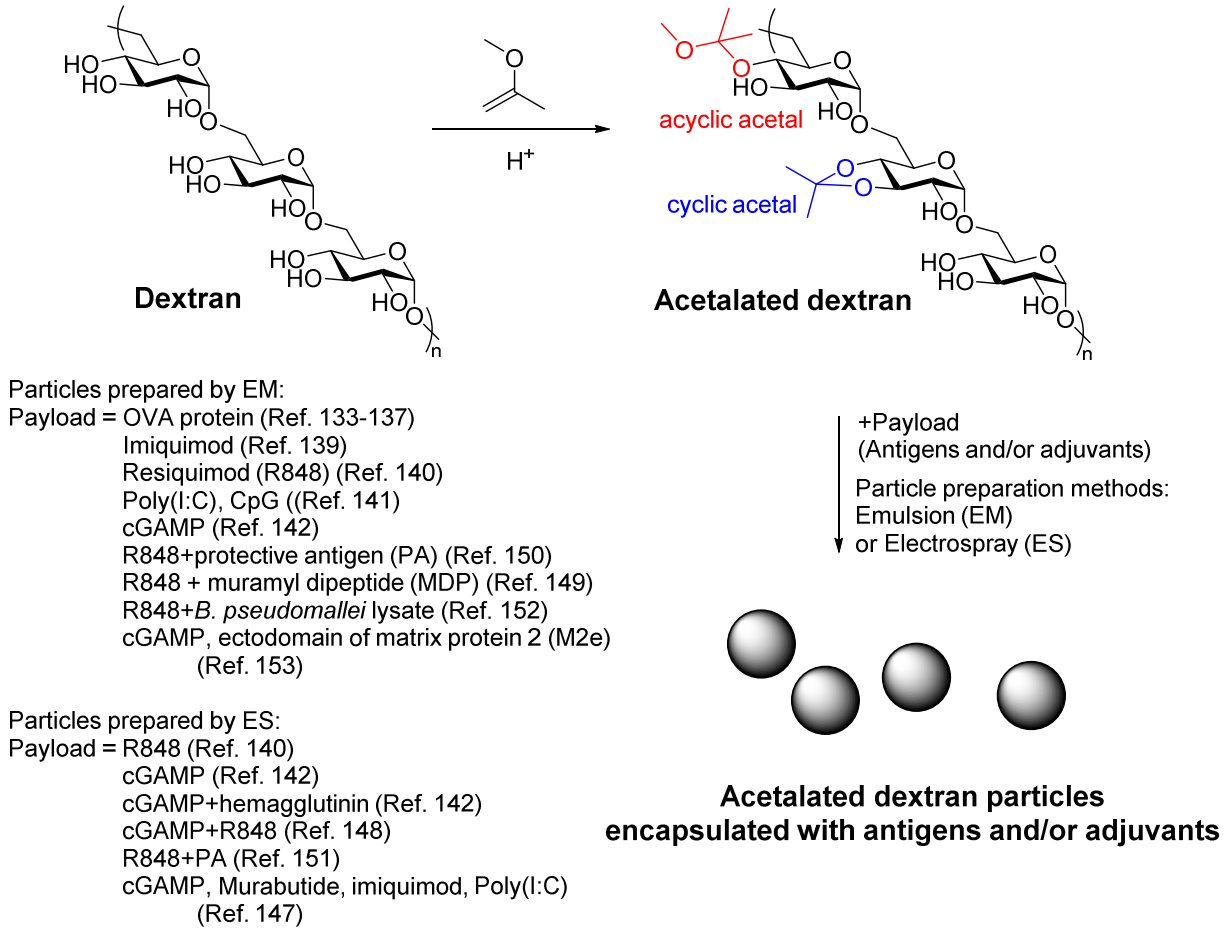

Scheme 1.5 Synthesis of antigen and/or adjuvant loaded acetalated dextran particles.

Ac-Dex has been introduced for vaccine adjuvant delivery since 2010[140] for several types of TLR agonists. Keane-Myers and co-workers first studied Ac-Dex microparticles as the delivery platform for imiquimod, a hydrophobic TLR7/8 agonist, as an adjuvant *in vitro*. Imiquimod loaded Ac-Dex microparticles were prepared with 4 wt% loading rate and 100% loading efficiency. After incubation with imiquimod loaded particles, the gene expression level, cytokine secretion level of inflammatory cytokines IL-1β, IL-6 and TNF-α, and the expression of two activation markers PD1-L1 and iNOS as well as the production of downstream product NO, were significantly

increased in two macrophage cell lines, MH-S and RAW 264.7. The particles also significantly increased the production of IL-1β, IL-6, IL-12p70 and MIP-1α in BMDCs. Compared to free imiquimod, the encapsulated imiquimod induced higher amounts of cytokine at lower concentrations of the particles. Empty Ac-Dex did not induce detectable inflammatory cytokine or activation marker increases. This *in vitro* study showed the promise of Ac-Dex as a vaccine adjuvant carrier to achieve a good immune stimulation effect.

Another method for Ac-Dex particle preparation, electrospray (ES), provided a better encapsulation efficiency (83%) toward a less hydrophobic TLR 7/8 agonist resiquimod compared to the standard emulsion encapsulation method (6%).[141] Particles made by electrospray were larger (1-5 μm) than those from the emulsion method (~300 nm) and had a collapsed morphology. More spherical particles could be obtained when blending with Tween 80 during electrospray process. The Tween 80-blended Ac-Dex particles stimulated macrophages *in vitro* to increase NO release and inflammatory cytokine secretion. The *in vivo* study showed that these particles reduced *L. donovani* amastigotes in heart and liver of mice relative to mice receiving empty nanoparticles or PBS.

The Ainslie's group applied Ac-Dex to deliver another two TLR agonists, i.e., poly I:C and CpG as vaccine adjuvants.[142] 71kDa Ac-Dex with 5 min acetalation reaction time (Ac-Dex (5min)) was found to be the best material for the delivery of both agonists. The encapsulation efficiencies of poly I:C and CpG in Ac-Dex (~55% and ~36% respectively) were significantly higher compared

to traditional PLGA particles (~33% and ~3% respectively). A significantly higher level of NO release and cytokine secretion including IL-6, IL-12p70, IL-1β, IL-2, TNF-α and IFN-γ was observed in RAW 264.7 macrophages with poly I:C encapsulated Ac-Dex (5min) particles compared to poly I:C encapsulated PLGA particles and another Ac-Dex, Ac-Dex (4h), which degraded slower. Due to the poor encapsulation of CpG in PLGA (~3%), only Ac-Dex (5min) was tested for delivering CpG to RAW 264.7. For both NO release and cytokine profile, CpG encapsulated in Ac-Dex was superior to free CpG.

Ting's lab applied Ac-Dex particles for the delivery of cyclic dinucleotide (CDN) 3'3'-cGAMP, a ligand of stimulator of interferon genes (STING), for immune cell activation[143]. The cGAMP is a water-soluble adjuvant, which has poor cell penetration abilities. Liposomes and hydrogel delivery carrier of cGAMP were associated with low encapsulation efficiency and poor long-term stability.[144-147] With the electrospray method, the Ac-Dex particles (ES Ac-Dex) loaded up to 0.52%wt of cGAMP with 89.7% encapsulation efficiency, which is significantly higher compared to Ac-Dex particles prepared through the emulsion method (EM Ac-Dex), PLGA particles or liposomes. The cGAMP loaded ES Ac-Dex remained intact in pH neutral media at 37□ for at least 28 days without losing the bioactivity of cGAMP. Strong immune activation was observed both *in vitro* and *in vivo* without significant toxicities. When ES Ac-Dex was co-administrated with a model antigen OVA, the level of antibody against OVA generated *in vivo* was enhanced by 104 to 106 folds compared to OVA alone. Analysis of antibody subtype indicated

the cGAMP encapsulated ES Ac-Dex particles induced balanced Th1 and Th2 associated immune responses, while the Alum adjuvant produced mainly Th2 polarized responses. Besides humoral responses, the cGAMP encapsulated ES Ac-Dex also induced cellular responses against the model antigen OVA. On a B16F10 melanoma model, the cGAMP Ac-Dex showed a better anti-tumor effect compared to three other Ac-Dex particles encapsulating different adjuvants, Murabutide, imiquimod and Poly I:C.[148] The successful anti-cancer immunotherapy by cGAMP Ac-Dex particles was also observed on a triple negative breast cancer cell line E0771. Systematic administration of cGAMP Ac-Dex through intravenously injection slowed down tumor growth as efficient as local administration through intratumoral injection. Interestingly, in the B16F10 model, the NK cells, instead of T cells, were the major type of cells for tumor lysis. However, for E0771 tumor, both NK and T cells were important for the anti-tumor responses. These results indicated the importance of activating both the innate immune cells (NKs) and adaptive immune cells (T cells) for tumor immunotherapy, as the T cells may not always be the major anti-tumor responders.

Co-delivering more than one adjuvant within one Ac-Dex particle can improve the immune activation compared to single adjuvant loaded Ac-Dex particles. For example, cGAMP ES Ac-Dex successfully induced high levels of IFN-β, IL-6 and TNF. With the co-encapsulation of resiquimod (R848) in the same particle, the cGAMP/R848 ES Ac-Dex elicited two more important cytokines for adaptive immune activation, IL-1β and IL-12p_{70}.[149] Co-administration of separate cGAMP ES Ac-Dex and R848 ES Ac-Dex particles was not as efficient as co-encapsulation of the

two adjuvants within the same particle based on *in vitro* cytokine release study. The combination of muramyl dipeptide (MDP), a NOD2 ligand, with R848, also showed superior additive effects.[150]

Besides serving as an adjuvant carrier, Ac-Dex particles can deliver both the antigen and the adjuvant as a full vaccine against various targets, such as anthrax, bacterial infection and influenza.

Anthrax caused by the infection of *Bacillus Anthracis* (*B. Anthracis*) can lead to death within 1 week, with the current vaccine Anthrax Vaccine Adsorbed requiring up to 6 doses and 18 months to achieve protection.[151] A vaccine that can generate fast immune protection against anthrax is urgently needed. The Ainslie' group designed an Ac-Dex based vaccine to generate a rapid immune response against anthrax, where Ac-Dex was used to encapsulate R848, and Protective Antigen (PA), the most important toxic component of anthrax antigen, in separate particles by emulsion.[151] Mice received both R848 Ac-Dex and PA Ac-Dex showed much stronger IgG responses on days 14, 28 and 42 after immunization compared to PA+Alum or free PA + R848 Ac-Dex particles. All mice immunized with PA Ac-Dex +R848 Ac-Dex vaccine survived 3 challenges on days 14, 28 and 42 with both low and high doses of *B. Anthracis*. This Ac-Dex based vaccine only required two injections at days 0 and 7, and effective protection against anthrax was observed as early as 14 days. The fast generation of protective immune response by Ac-Dex based vaccine provided a promising way fighting against fast progressing diseases. In a later study, electrospray method was used instead of emulsion to fabricate Ac-Dex particles with PA only or with both PA and R848.[152] Three vaccine formulations were used to immunize the mice: (i) PA

absorbed to resiquimod microparticles; (ii) PA and resiquimod encapsulated in separate particles; and (iii) PA and resiquimod encapsulated in same particle. Both (ii) and (iii) induced high IgG1 and IgG2a titers on day 42 after immunization similar to or higher than Anthrax Vaccine Adsorbed, the current anthrax vaccine. The *in vivo* study showed that (ii) was the best vaccine, which protected 50% mice from death during 28-day observation, while mice immunized with (iii) only had 10% survival. BioThrax group did not survive beyond 13 days. The *in vivo* study indicated that delivering PA and adjuvant in separate particles may provide a faster and stronger immune response towards anthrax. This finding supported the idea that adjuvant and antigen should be encapsulated in separate Ac-Dex particles optimized for each component with different CAC percentages.[138]

Ac-Dex was used as carrier for a *Burkholderia pseudomallei* subunit vaccine and showed the ability to generate immune responses within a short time period.[153] The antigen *B. pseudomallei* lysate and an adjuvant R848 were encapsulated in separate Ac-Dex particles. The rapid immunization schedule (two injections on day 0 and 7) slowed down the death progress during 26-day observation when mice were challenged on day 14 with a lethal dose *B. pseudomallei*. 12% of the immunized mice survived the challenge on day 26 while most mice in control groups died within 2 days of challenge and none survived beyond 20 days. The vaccinated group had higher antibody titers, stronger cytokine secretion (IL-4, IL-5, IL-17A, IL-12, IFN-γ, GM-CSF and TNF-α) and more cytotoxic T cells compared to the control group receiving PBS only.

The Ting lab applied the cGAMP encapsulated Ac-Dex with soluble hemagglutinin (HA) protein from H1N1 influenza virus for anti-influenza vaccination.[143] A strong Th1-biased antibody response was observed in cGAMP Ac-Dex + HA group, while Alum + HA only induced weak Th2-biased antibody response. The cGAMP Ac-Dex + HA protected 12 out of 13 mice from H1N1 influenza challenge, while >90% of untreated mice and >75% of mice immunized with free HA only were killed during the challenge. The neutralizing antibodies generated by cGAMP Ac-Dex + HA remained detectable in mouse sera for more than 4 months after immunization and protected the mice from a lethal dose of H1N1 influenza virus challenge 7 months after immunization. The Bachelder lab investigated the co-administration of cGAMP Ac-Dex and the ectodomain of matrix protein 2 (M2e) encapsulated Ac-Dex particles as an anti-influenza vaccine.[154] The M2e and cGAMP were encapsulated in separate Ac-Dex particles with different percentage of CAC. In contrast to the delivery of OVA antigen where a high antibody titer was observed in Ac-Dex particles with low CAC (20%),[138] it was observed that the M2e Ac-Dex with high CAC (60%) induced higher antibody titers compared to M2e Ac-Dex with lower CAC (40% and 20%). The cGAMP encapsulated Ac-Dex particles with different CAC (20%, 40% or 60%) did not significantly change the antibody titers. The M2e and cGAMP encapsulated in separate Ac-Dex particles (60% CAC) induced significantly higher antibody titers compared to the co-encapsulation of M2e and cGAMP in same Ac-Dex (60% CAC). Besides the antibody titer, significantly higher levels of IFN-γ, IL-2 and IL-6 secretion were detected in mice immunized with M2e Ac-Dex (40%

or 60% CAC) + cGAMP Ac-Dex (60% CAC), which suggested a successful generation of cellular immunity. Both vaccines, M2e Ac-Dex (40%) + cGAMP Ac-Dex (60%) and M2e Ac-Dex (60%) + cGAMP Ac-Dex (60%) showed significant improvement of survival during a lethal dose influenza challenge in mice.

The studies discussed so far relied on passive uptake of the Ac-Dex particles by immune cells. The Fréchet group studied mannosylated Ac-Dex particles for immunomodulation through mannose targeting.[155] "Click-able" Ac-Dex was obtained by partially modifying the hydroxyl groups on dextran backbone with an azido-triethylene glycol linker followed by acetalation. Microparticles were then prepared through the emulsion method with subsequent surface mannosylation using the CuAAC reaction. These particles (referred to as Man-Ac-Dex) with high density mannose on the surface (up to 106/particle) had high binding avidity to mannose receptors on DC surface. Man-Ac-Dex showed 1.5-2 fold increase of DC uptake and about 5 fold increase of MHC I presentation on DCs compared to Gal-Ac-Dex, azido-Ac-Dex or Ac-Dex particles, suggesting more potent immune activation. However, no *in vivo* study was performed with particles.

1.6.2 Reducible dextran nanogel

Besides acetalated dextran, reducible dextran nanogel is another type of modified dextran, which has been developed for antigen delivery to DCs.[156-157] A cationic dextran nanogel has been fabricated by inverse mini-emulsion photo-polymerization with methacrylated dextran, a

methacrylamide functionalized disulfide linker, and a positively charged methacrylate monomer. The nanogel was then covalently conjugated with a model antigen OVA through a disulfide linker (**Scheme 1.6**). The confocal microscopy indicated the OVA conjugated nanogel enhanced the uptake by D1 cells compared to non-covalently loaded OVA-nanogel, free OVA or empty nanogel. The OVA-conjugated nanogel combined with poly I:C significantly slowed down the growth of B16-OVA tumor expressing OVA antigen in a mouse tumor model compared to free OVA, non-covalent OVA-nanogel.[157] A preventive antitumor model was studied by immunizing C57BL/6 mice on days 0 and 14 with different vaccine formula followed by tumor challenge on day 28 with B16-OVA cells. All PBS or empty nanogel treated mice died within 20 days after tumor cell injection. Only 30% of the mice in non-covalent OVA-nanogel group were tumor-free on day 52, while 90% of mice immunized with OVA-conjugated nanogel+poly I:C remained tumor free. OVA-conjugated nanogel+poly I:C induced highest percentage of OVA specific $CD8^+$ T cell and OVA specific IgG titers. In addition to the preventive model, the efficacy of the vaccine was investigated in a therapeutic model. Mice were injected with B16-OVA on day 0, which was followed by two immunizations on days 6 and 16. While all other groups developed fast-growing tumor and died within 35 days, the OVA-conjugated nanogel+poly I:C significantly slowed the tumor growth and prolonged the survival.

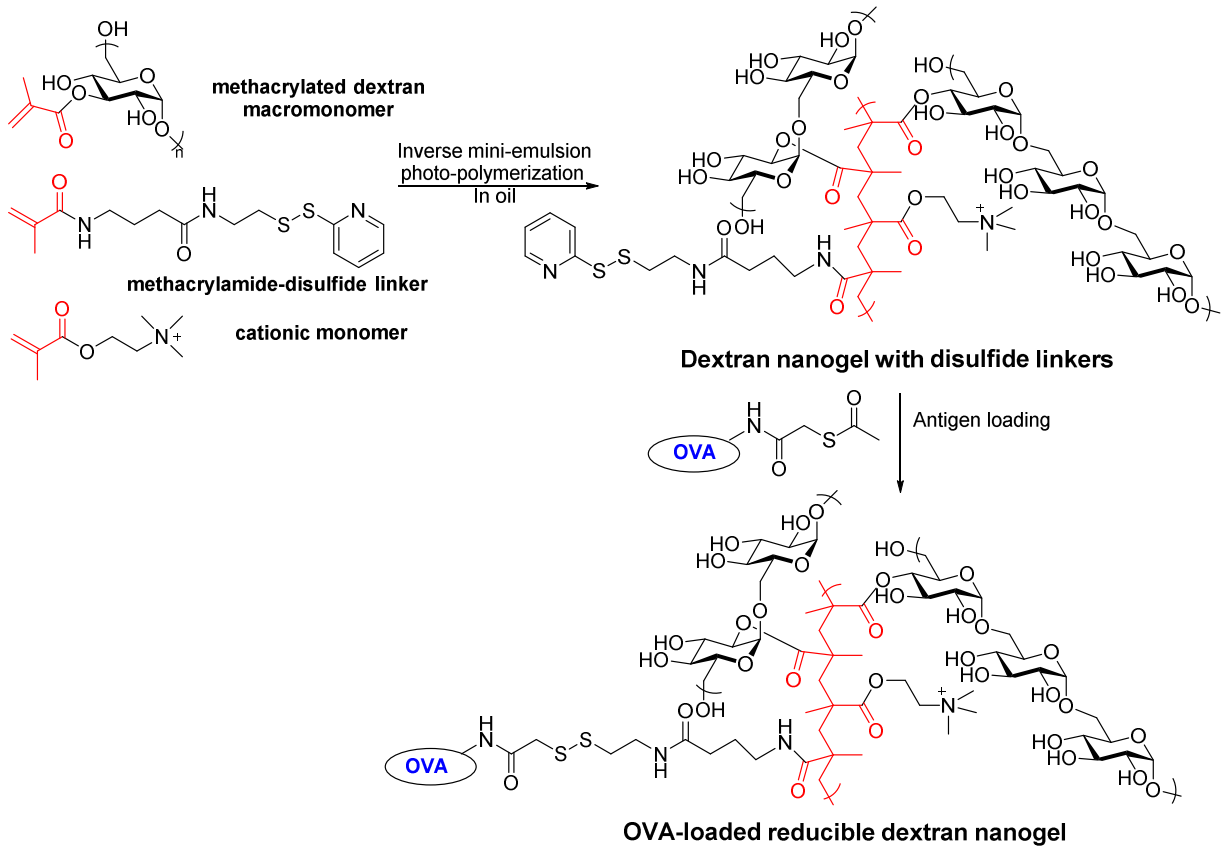

Scheme 1.6 Synthesis of OVA-loaded reducible dextran nanogel.

These two studies showed the reducible nanogel carrier can enhance DC activation *in vitro* and generate significant preventive and curative effects against tumor *in vivo*. It was found that the OVA-loaded nanogel exhibited cytotoxicity at high concentrations, which may require more chemical modifications to improve biocompatibility.[156] For example, the percentage of the cationic monomer may be lowered to reduce the level of positive surface potential to decrease cytotoxicity.

1.6.3 Oxidation sensitive dextran

Reactive oxygen species are heavily produced in the phagosomes of APCs, which are crucial for initiating immune responses.[158-159] It has been reported that the most effective APCs, DCs, may

have phagosomes with H_2O_2 concentration up to 1mM.[160] Therefore oxidation sensitive dextran was investigated as a vaccine carrier candidate.[161] Free hydroxyl groups on dextran were modified with arylboronic ester resulting in Oxi-Dex (**Scheme 1.7**). 100-200 nm sized particles were prepared *via* the standard emulsion method. The resulting particles were stable in PBS buffer but decomposed in 1 mM H_2O_2 with a half-life of 36 min. The OVA encapsulated Oxi-Dex induced a 27-fold increase of OVA presentation in DC 2.4 cells compared to OVA encapsulated PLGA particles, while free OVA did not get presented. However, this Oxi-Dex was not further studied after this report.

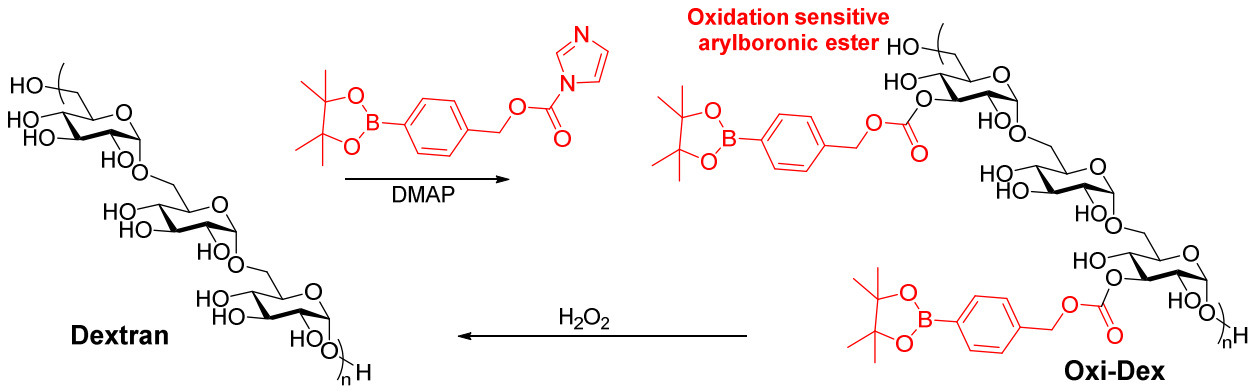

Scheme 1.7 Synthesis of oxidation sensitive dextran.

1.6.4 pH sensitive amphiphilic galactosyl-dextran-retinal conjugates (GDR)

The galactosyl-dextran-retinal (GDR) conjugates is a pH sensitive amphiphilic material reported by the Ma group.[162] All-trans retinal, the precursor of retinoic acid (active metabolite of Vitamin A), was first conjugated to dextran through a pH-responsive hydrazone bond then further

modified with ethylenediamine following reaction with NHS activated lactobionic acid to obtain the GDR conjugate. GDR was amphiphilic, which spontaneously self-assembled into nanogel with size around 115nm and zeta-potential around 27mV. At pH=7.4, the GDR was relatively stable with less than 10% of retinal release within 48h. However, the hydrazone bond in GDR conjugate could be rapidly cleaved at pH 5.0 resulting in over 50% retinal release within 24h, which could serve as an adjuvant. GDR nanogel induced BMDC maturation *in vitro* while free retinal failed to do so. OVA-loaded GDR nanogel enhanced both MHC I and MHC II antigen presentation on BMDCs. The release of retinal from GDR nanogel significantly elevated the reactive oxygen species (ROS) generation in BMDCs by 2-3 folds relative to free all-trans retinal within 4 h due to lysosomal disruption, and the resulting ROS significantly enhanced proteasome activity in BMDCs. In a B16-OVA tumor model, the OVA-GDR nanogel vaccine suppressed tumor growth and prolonged mouse survival compared to free OVA, free OVA+retinal and PBS groups. OVA-GDR nanogel induced robust $CD8^+$ T cell proliferation as well as high levels of IFN-γ production and lysis of tumor cells.

1.7 β-Glucans

β-Glucans are β-1,3-linked glucose polymers with β-1,6 branches. β-Glucans can be isolated from fungal cell wall, bacteria, seaweed, cereal, etc. Depending on the source, the polysaccharides may have varied primary, secondary or tertiary structures, or physical properties. Though heterogeneous, these polysaccharides can induce similar immune responses and therefore usually

termed as a common name "β-glucans".[163] The major β-glucan receptors in mammals are dectin-1, and complement receptor 3 (CR3, CD11b/CD18).[164] It has been reported that the stimulation *via* dectin-1 primes Th1, Th17 and cytotoxic T lymphocyte responses.[164-166] With their immune stimulating properties, β-glucans have been studied in vaccine design with an established record of safety in both preclinical and human trials.[163, 167-168] As a major component of fungal cell wall, β-glucans has been widely used as antigens for generating anti-glucan antibodies against fungal infections.[169-171] In this section, we focus on examples applying β-glucans as vaccine carriers and built-in adjuvants.

1.7.1 β-Glucan particles

β-Glucan particles (GPs) are the most studied vaccine carriers in the β-glucan family. They were developed in 1980s but only widely used as vaccine carriers in recent years.[24, 172-173] GPs are highly purified, hollow porous cell wall shells with 2-4 μm sizes. GPs can be derived from baker's yeast through a series of hot alkali and organic extractions.[174-175] It contains primarily 1,3-β-glucans along with small amounts of β-1,6-glucans and chitin.[164] GPs can be recognized by dectin-1 and upregulate cell surface presentation of MHC molecules and co-stimulation molecules as well as inducing the production of inflammatory cytokines.[176-178] The hollow GPs have been studied as carriers for proteins, DNA, siRNA and other small molecules.[179-184]

Antigens can be non-covalently trapped inside GPs with the addition of polymers such as yeast tRNA, alginate-calcium or alginate-calcium-chitosan mixture. The Levitz group used tRNA to trap

OVA protein inside GPs.[181] These GPs were efficiently taken up and proteolyzed by DCs to induce DC maturation. Significant T cell proliferation was observed when incubated with GP-OVA at concentrations starting from 0.03 μg OVA /ml, while the free OVA protein needed 100 times higher concentration to reach similar stimulation levels. The $CD4^+$ T cells isolated from GP-OVA immunized mice secreted significantly higher amounts of pro-inflammatory cytokines such as IL-4, IL-17 and IFN-γ compared to Alum/OVA immunized mice. For antibody responses, the GP-OVA vaccine successfully induced Th1 skewing antibody subtype IgG2c, while the Alum/OVA induced only IgG1 responses. The long-term immune responses were monitored 18-20 months after the last immunization.[185] The $CD4^+$ T cells isolated from immunized mice resumed cytokine secretion upon *ex vivo* OVA stimulation, and the serum antibody titer remained detectable. Notably, the encapsulation of OVA in GPs was found important, as the admixture of OVA and GPs was not as effective in inducing $CD4^+$ T cell cytokine secretion and antibody responses.[185] The Levitz group also studied polymers such as alginate-calcium (AC) or alginate-calcium-chitosan (ACC) mixture for trapping antigens in GPs.[185] The AC and ACC trapped GP-OVA showed comparable capacities to induce antigen-specific T cell responses and antibody responses in mice as the tRNA trapped GP-OVA. Other antigens such as BSA,[186] FedF,[187] could also be trapped inside GPs as vaccine candidates.

Antigens can be loaded into GPs through covalent coupling. The Hunter group covalently conjugated antigen BSA to GPs through amide bonds.[188] The BSA-GP conjugates were

phagocytized by macrophages and both intradermal and oral administration of BSA-GP vaccine induced immune responses against BSA. OVA-GP conjugates were synthesized similarly, which induced strong BMDC, $CD4^+$ and $CD8^+$ T cells activation *in vitro*.[189] The Hong group prepared OVA loaded GPs in organic phase, which reduced GP aggregation compared to aqueous phase conjugation, and provided more homogenous OVA-GPs.[190] With this novel conjugation method, the GPs were first dispersed in cyclohexane/Igepal CO-520 (85:15) solution followed by the addition of aqueous solution containing the OVA antigen and glutaraldehyde cross-linker sequentially. The hydrophilic antigen and cross-linker would be slowly soaked into GP cavity due to the hydrophilic environment of the glucans and the conjugation primarily took place inside the GP cores rather than on the exterior of the GPs, which may cause cross-linking between particles and lead to aggregation. The resulting OVA-GPs successfully induced BMDC maturation and T cell proliferation *in vitro* and stimulated B cell activation and germinal center formation *in vivo*. High anti-OVA IgG2c titers were detected after only one immunization with the OVA-GP vaccine, which indicated a strong Th1 biased immune response. The OVA-GPs successfully induced antigen-specific $CD8^+$ T cell response *in vivo* and provided significant protection against tumor development to EG.7-OVA tumor bearing mice.

An interesting property of GPs is that they can be administered orally. GPs can be taken up by human intestinal epithelial cells and induce the secretion of chemokines and the expression of pattern recognition receptors and costimulatory molecules.[186] The GP-OVA complex can be

delivered by M cells to mucosal lymphoid tissues and induce the proliferation of OVA specific $CD4^+$ T cells when given orally to mice. Surface functionalization of an immunoglobulin-binding protein G followed by the anti-aminopeptidase N (APN, an intestinal epithelial receptor) antibody on GPs can further enhance the passage of particles through the epithelial barrier.[191] Compared to isotype antibody conjugated GPs, the anti-APN GPs were internalized 10 times more by intestinal epithelial cell line IPEC-J2 at a 16-fold lower concentration. *In vivo* study showed that orally administrated anti-APN-coated, FedF-loaded GPs induced significantly higher titers of antibodies compared to non-targeting FedF loaded GPs.

1.7.2 β-Glucan-antigen complex

A β-glucan member, schizophyllan (SPG), contains a β-1,3-glucan main chain with β-1,6-glycosyl side chain every three glucose residues. It can form stoichiometric complexes with specific homonucleiotides such as poly(C) or poly (dA) *via* a combination of hydrogen bonding and hydrophobic interactions (**Scheme 1.8**).[192-194] Unlike β-glucan particles, these SPG complexes are nano-rod shaped with diameters around 10-20 nm.[195] The complex includes two SPG chains and one polynucleiotide chain forming a triple helix through interactions between two main-chain glucoses and one base, and the stability of complex depends on the length of polynucleotide.[193-194] The complex can be recognized by dectin-1 receptor inducing immune responses,[196-197] and therefore have been studied as vaccine adjuvants.

A complex of SPG with CpG-dA40, a short single stranded DNA fragment with CpG motif and a 40-mer poly(dA) tail, has shown strong immune activating effects due to the combination delivery of immunocytes targeting SPG and immuno-stimulative CpG.[195, 198-199] This complex can induce antigen-presenting cell activation as well as Th1 and $CD8^+$ T cell responses.[195, 200-201] Intravenous injection of CpG-SPG complex suppressed tumor growth more efficiently than SPG, CpG or mixture of SPG and CpG on several tumor models.[202] The CpG-SPG complex could be cross-linked to form nanogels with a larger size (~150 nm) by mixing CpG-SPG and its complementary sequence,[195, 203] which may further improve the delivery efficiency toward immune cells due to the size effect.[204] Compared to CpG-SPG complex, the cross-linked CpG-SPG nanogel induced significantly higher IL-6 secretion in mice splenocytes *in vitro*.[195] The fluorescence microscopy imaging indicated a 10 times higher uptake of the cross-linked CpG-SPG nanogel than CpG-SPG complex by macrophages.[203] The CpG-SPG nanogel induced more antigen specific $CD8^+$ T cells *in vivo* compared to CpG-SPG complex when co-administrated with OVA antigen. The nanogel immunization significantly slowed down EG7 tumor growth and prolonged survival in mice compared to free CpG or CpG-SPG complex.[203]

Besides CpG, peptide antigens can be conjugated with poly(dA) for preparing SPG-antigen complexes. The Sakurai group reported an OVA-SPG complex prepared with OVA peptide-poly(dA) conjugate and SPG.[205-206] It was observed that the conjugation strategy could influence the immune cell processing of the OVA-SPA complex.[206] OVA-poly(dA) conjugated through a

glutathione cleavable disulfide linker can induce significantly higher levels of OVA antigen presentation on macrophages compared to the OVA-poly(dA) conjugated through a triazole. The conjugation of poly(dA) at the N terminal of OVA peptide, instead of at the C terminal, showed a higher OVA presentation by macrophages.[206] The OVA-SPG induced peptide specific $CD8^+$ T cell responses both *in vitro* and *in vivo* when co-administrated with CpG-SPG complex. OVA-SPG/CpG-SPG vaccine immunized mice showed significantly more effective *in vivo* lysis of OVA-pulsed target cells compared to free OVA peptide, free OVA + free CpG and free OVA + CpG-SPG group as indicated by *in vivo* CTL assays.[205] The strong CTL activation was observed with a very low dose of OVA peptide (100 ng/mouse).[206] The OVA-SPG/CpG-SPG vaccine also successfully suppressed the growth of EG7 tumor and prolonged survival time in mice.[205]

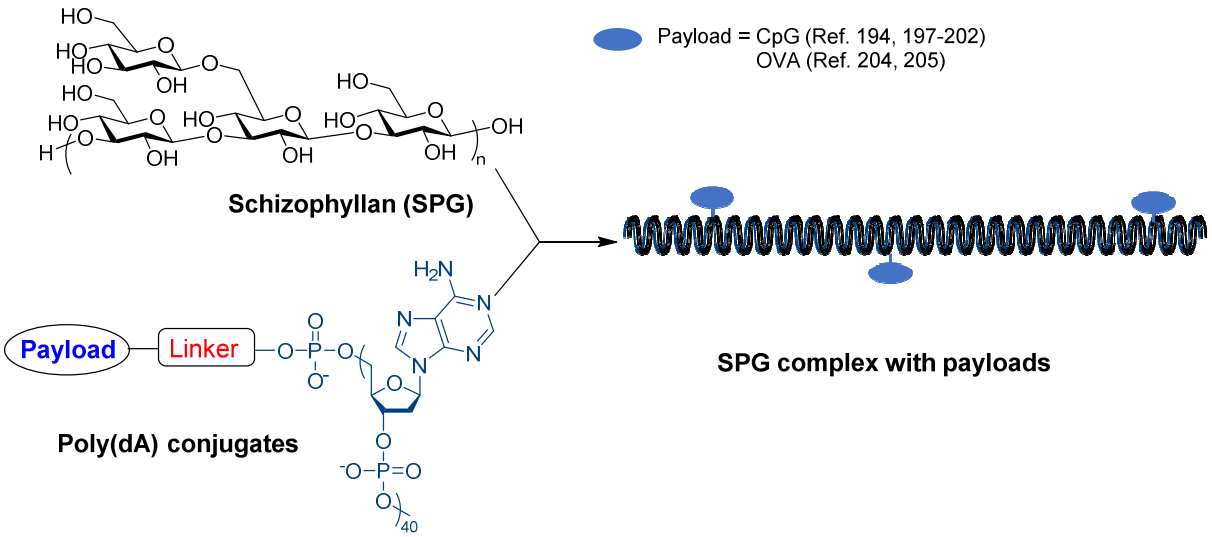

Scheme 1.8 Structure of SPG, Poly(dA) and SPG complex.

1.7.3 β-Glucan based nanoparticles for vaccine delivery

Beside the large-sized GPs and rod-shaped SPG complexes, β-glucan nanoparticles were investigated for vaccine delivery. The Dong group developed a synthetic MUC1 vaccine by conjugating MUC1 peptide with a β-glucan chain.[207] The resulting MUC1-β-glucan material formed homogenous nanoparticles sized 150 nm due to hydrophobic interactions. This MUC1-β-glucan nanoparticle induced significantly higher serum antibody titers and IFN-γ and IL-6 cytokines. The Zhang lab prepared β-glucan nanoparticles based vaccines by mixing positively charged aminated β-glucan with negatively charged CpG adjuvant and OVA protein antigen.[208] The combination of dectin-1 activating β-glucan and TLR-9 activating CpG in one nanoparticle showed synergistic effects in inducing both strong humoral and cellular immune responses.

The Kono lab reported a set of β-glucan based pH sensitive materials for cytoplasmic delivery of antigen.[209] Curdlan, a kind of β-glucan, was modified with methyl glutaric acid (MGlu) to generate a pH responsive polysaccharide MGlu-Curd. Using a similar strategy, pH responsive 3-methyl glutaryl mannan (MGlu-Man) and 3-methyl glutaryl dextran (MGlu-Dex) were prepared. 1-Aminodecane was then conjugated to these polysaccharides to anchor these pH responsive polysaccharide chains onto membranes of OVA-loaded liposomes. All three types of liposomes with different polysaccharides induced the release of cargo from liposome at around pH 5. The polysaccharide backbone played an important role for obtaining liposomes with high affinity to DC cells. Compared to MGlu-Man and MGlu-Dex coated liposomes, the liposome containing

MGlu-Curd with 59 MGlu groups per chain ($MGlu_{59}$-Curd), induced the highest DC uptake of the liposomes. The percentage of MGlu modification also influenced the immune activation. In general, curdlan with higher percentage of MGlu content ($MGlu_{71}$-Curd and $MGlu_{59}$-Curd) induced higher pro-inflammatory cytokines such as TNF-α and IL-12 in DC2.4 cells compared to those with lower MGlu content ($MGlu_{41}$-Curd and $MGlu_{21}$-Curd). Compared to MGlu-Man and MGlu-Dex, $MGlu_{59}$-Curd elicited more IFN-γ and higher cell-mediated cytotoxicity in splenocytes isolated from OVA-immunized mice *in vitro*. The tumor challenge study showed that mice immunized with $MGlu_{59}$-Curd had the smallest tumor size and longest survival time highlighting the advantage of the curdlan backbone.

1.8 Conclusions and future outlooks

In summary, we have reviewed recent advances in vaccine development applying carbohydrates as adjuvants and/or vaccine carriers. With their biocompatibility, ease for modification, and the ability to interact with the immune system through multiple mechanisms, carbohydrates provide a great variety of choices to meet the various needs for vaccine studies.

Carbohydrates can be modified through multiple methods such as amide or ester formation, CuAAC reaction, oxidation of sugar rings followed by imine or oxime formation, which make them flexible for various applications in vaccine designs. For example, the controlled release of the antigen and adjuvant from the vaccine carrier is important for immune activation. A desired carrier should not release their cargos before entering immune tissues, and should not release too

slow after encountering immune cells, which may fail to produce enough immune stimulation resulting in tolerance.[210-211]

The optimal deliveries of antigens and adjuvants can be different, and the carriers may need to be optimized separately.[138, 154] By controlling the reaction time during the acetalation of dextran, a carbohydrate-based vaccine carrier with fine-tuned releasing profile can be achieved, which can serve as a great platform for vaccine optimization. Antigen-MPLA and antigen-α-GalCer conjugates can be easily combined with other well-studied lipid molecules to form liposomal vaccines. Taking advantage of the well-developed strategies for liposome preparation,[212-213] carriers with controlled size and surface charges, another two important factors for immune targeting,[214-215] can be obtained.

Notably, although there are many examples showing that successful carbohydrate conjugate-based vaccines can be achieved through multiple chemistry reactions and linker structures, the small structure alteration of carbohydrate backbones due to the conjugation may significantly influence the final immune outcomes. The carbohydrates often contain more than one position available for chemical modification. When designing carbohydrate vaccines, the conjugation site should be carefully chosen in order to obtain optimal immune recognition. As an example, the antigen-MPLA conjugates through 6'-position, where the polysaccharide chain is attached to the natural LPS, were superior in generating IgG responses compared to the antigen-MPLA conjugates that using 1-*O*-position as the conjugation site,[61] while the blockade of the phosphate group on

MPLA completely suppressed the ability for immune activation.[56] The linkers between the payload and the carbohydrate backbones also played important roles in immune tuning. For example, the oxidative conjugation of mannan and MUC1 FP through imine linkers induced Th1 type immune response and successfully protected mice from tumor growth, while reductive conjugation through amines induced Th2 type immune response without successful tumor protection.[82] Interestingly, there are examples using the trace amount of mannoproteins (~5% in mannan) for allergen conjugation as allergic vaccines.[98-99] This strategy, taking advantage of other components in polysaccharide mixtures for chemical conjugation, can maintain the intact carbohydrate structure, which may reduce the chance of disturbing the immune activation function. However, the disadvantage of this strategy might be the difficulty in quality control. The protein components may vary batch-to-batch, which may influence the conjugation efficiency, the physical and biological properties of the final materials. A recent review has summarized chemistry methods for site-selective glycoconjugate synthesis, which provided multiple options for glycoconjugate vaccine development.[216]

An attractive strategy for future vaccine design can be the combination of different adjuvants that activates the immune system through different receptors. Adjuvants are playing crucial roles in vaccine design, and there have been examples indicating that combining adjuvants with different immune activating mechanisms can trigger additive effects and enhance the vaccine efficacy.[149-150] However, cautions need to be taken in combining other adjuvants with the "self-adjuvating"

carbohydrates. There are examples indicating the additional adjuvants have negative effects in MPLA and mannan based vaccine conjugates.[55-59, 99-100] Therefore, the external adjuvant needs to be carefully selected. Understanding the detailed mechanism of how multiple adjuvants collaborate with each other can guide future vaccine designs

REFERENCES

REFERENCES

1. Lang, S.; Huang, X., Carbohydrate Conjugates in Vaccine Developments. *Frontiers in Chemistry* **2020,** *8*, 284.

2. Mahla, R.; Reddy, C.; Prasad, D.; Kumar, H., Sweeten PAMPs: Role of Sugar Complexed PAMPs in Innate Immunity and Vaccine Biology. *Front. Immunol.* **2013,** *4*, 248.

3. Rabinovich, G. A.; Kooyk, Y. v.; Cobb, B. A., Glycobiology of Immune Responses. *Ann. N. Y. Acad. Sci.* **2012,** *1253*, 1-15.

4. Varki, A., Biological Roles of Glycans. *Glycobiology* **2016,** *27*, 3-49.

5. Lesinski, G. B.; Westerink, J., Vaccines Against Polysaccharide Antigens. *Curr. Drug Targets Infect. Disord.* **2001,** *1*, 325-334.

6. Astronomo, R. D.; Burton, D. R., Carbohydrate Vaccines: Developing Sweet Solutions to Sticky Situations? *Nature Reviews Drug Discovery* **2010,** *9*, 308-324.

7. Roy, R., New Trends in Carbohydrate-based Vaccines. *Drug Discovery Today: Technol.* **2004,** *1*, 327-336.

8. Feng, D.; Shaikh, A. S.; Wang, F., Recent Advance in Tumor-associated Carbohydrate Antigens (TACAs)-based Antitumor Vaccines. *ACS Chem. Biol.* **2016,** *11*, 850-863.

9. Guo, Z.; Wang, Q., Recent Development in Carbohydrate-based Cancer Vaccines. *Curr. Opin. Chem. Biol.* **2009,** *13*, 608-617.

10. Yin, Z.; Huang, X., Recent Development in Carbohydrate Based Anticancer Vaccines. *J. Carbohydr. Chem.* **2012,** *31*, 143-186.

11. Hu, X.; Liu, R.; Zhu, N., Enhancement of Humoral and Cellular Immune Responses by Monophosphoryl Lipid A (MPLA) as an Adjuvant to the Rabies Vaccine in BALB/c Mice. *Immunobiology* **2013,** *218*, 1524-1528.

12. Suzuki, Y.; Adachi, Y.; Ohno, N.; Yadomae, T., Th1/Th2-balancing Immunomodulating Activity of Gel-forming (1→ 3)-β-Glucans from Fungi. *Biol. Pharm. Bull.* **2001,** *24*, 811-819.

13. Petrovsky, N.; Cooper, P. D., Carbohydrate-based Immune Adjuvants. *Expert Rev. Vaccines* **2011,** *10*, 523-537.

14. Stambas, J.; Pietersz, G.; McKenzie, I.; Nagabhushanam, V.; Cheers, C., Oxidised Mannan-listeriolysin *O* Conjugates Induce Th1/Th2 Cytokine Responses After Intranasal Immunisation. *Vaccine* **2002,** *20*, 1877-1886.

15. Hu, J.; Qiu, L.; Wang, X.; Zou, X.; Lu, M.; Yin, J., Carbohydrate-based Vaccine Adjuvants – Discovery and Development. *Expert Opin. Drug Discovery* **2015,** *10*, 1133-1144.

16. Li, P.; Wang, F., Polysaccharides: Candidates of Promising Vaccine Adjuvants. *Drug Discoveries Ther.* **2015,** *9*, 88-93.

17. Cordeiro, A. S.; Alonso, M. J.; de la Fuente, M., Nanoengineering of Vaccines Using Natural Polysaccharides. *Biotechnol. Adv.* **2015,** *33*, 1279-1293.

18. Correia-Pinto, J. F.; Csaba, N.; Alonso, M. J., Vaccine Delivery Carriers: Insights and Future Perspectives. *Int. J. Pharm.* **2013,** *440*, 27-38.

19. Liu, Z.; Jiao, Y.; Wang, Y.; Zhou, C.; Zhang, Z., Polysaccharides-based Nanoparticles as Drug Delivery Systems. *Adv. Drug Delivery Rev.* **2008,** *60*, 1650-1662.

20. Pushpamalar, J.; Veeramachineni, A. K.; Owh, C.; Loh, X. J., Biodegradable Polysaccharides for Controlled Drug Delivery. *ChemPlusChem* **2016,** *81*, 504-514.

21. Zhang, N.; Wardwell, P.; Bader, R., Polysaccharide-based Micelles for Drug Delivery. *Pharmaceutics* **2013,** *5*, 329-352.

22. Arca, H. Ç.; Günbeyaz, M.; Şenel, S., Chitosan-based Systems for the Delivery of Vaccine Antigens. *Expert Rev. Vaccines* **2009,** *8*, 937-953.

23. Mata-Haro, V.; Cekic, C.; Martin, M.; Chilton, P. M.; Casella, C. R.; Mitchell, T. C., The Vaccine Adjuvant Monophosphoryl Lipid A as a TRIF-biased Agonist of TLR4. *Science* **2007,** *316*, 1628-1632.

24. Mirza, Z.; Soto, E. R.; Dikengil, F.; Levitz, S. M.; Ostroff, G. R., Beta-Glucan Particles as Vaccine Adjuvant Carriers. In *Vaccines for Invasive Fungal Infections*, Springer: 2017; pp 143-157.

25. Liu, H.; Irvine, D. J., Guiding Principles in the Design of Molecular Bioconjugates for Vaccine Applications. *Bioconjugate Chem.* **2015,** *26*, 791-801.

26. Colombo, C.; Pitirollo, O.; Lay, L., Recent Advances in the Synthesis of Glycoconjugates for Vaccine Development. *Molecules* **2018,** *23*, 1712.

27. Jin, K.-T.; Lan, H.-R.; Chen, X.-Y.; Wang, S.-B.; Ying, X.-J.; Lin, Y.; Mou, X.-Z., Recent Advances in Carbohydrate-based Cancer Vaccines. *Biotechnol. Lett.* **2019,** *41*, 641-650.

28. Marzabadi, C. H.; Franck, R. W., Small-Molecule Carbohydrate-Based Immunostimulants. *Chem. Eur. J.* **2017,** *23*, 1728-1742.

29. Micoli, F.; Del Bino, L.; Alfini, R.; Carboni, F.; Romano, M. R.; Adamo, R., Glycoconjugate Vaccines: Current Approaches Towards Faster Vaccine Design. *Expert Rev. Vaccines* **2019,** *18*, 881-895.

30. Wei, M.-M.; Wang, Y.-S.; Ye, X.-S., Carbohydrate-based Vaccines for Oncotherapy. *Med. Res. Rev.* **2018,** *38*, 1003-1026.

31. Weyant, K. B.; Mills, D. C.; DeLisa, M. P., Engineering a New Generation of Carbohydrate-Based Vaccines. *Curr. Opin. Chem. Eng.* **2018,** *19*, 77-85.

32. Stein, K. E., Thymus-Independent and Thymus-Dependent Responses to Polysaccharide Antigens. *J. Infect. Dis.* **1992,** *165*, S49-S52.

33. Abbas, A. K.; Lichtman, A.; Pober, J., Congenital and Acquired Immunodeficiencies. In *Clin. Exp. Immunol.*, 2000; pp 463-488.

34. Kalka-Moll, W. M.; Tzianabos, A. O.; Bryant, P. W.; Niemeyer, M.; Ploegh, H. L.; Kasper, D. L., Zwitterionic Polysaccharides Stimulate T Cells by MHC Class II-Dependent Interactions. *J. Immunol.* **2002,** *169*, 6149-6153.

35. Mazmanian, S. K.; Kasper, D. L., The Love–hate Relationship Between Bacterial Polysaccharides and the Host Immune System. *Nat. Rev. Immunol.* **2006,** *6*, 849-858.

36. Cobb, B. A.; Kasper, D. L., Microreview: Zwitterionic Capsular Polysaccharides: the New MHCII-dependent Antigens. *Cell. Microbiol.* **2005,** *7*, 1398-1403.

37. Nishat, S.; Andreana, P. R., Entirely Carbohydrate-Based Vaccines: An Emerging Field for Specific and Selective Immune Responses. *Vaccines (Basel)* **2016,** *4*, 19.

38. Surana, N. K.; Kasper, D. L., The Yin Yang of Bacterial Polysaccharides: Lessons Learned from B. fragilis PSA. *Immunol Rev* **2012,** *245*, 13-26.

39. Heimburg-Molinaro, J.; Lum, M.; Vijay, G.; Jain, M.; Almogren, A.; Rittenhouse-Olson, K., Cancer Vaccines and Carbohydrate Epitopes. *Vaccine* **2011,** *29*, 8802-8826.

40. Kaltgrad, E.; Sen Gupta, S.; Punna, S.; Huang, C.-Y.; Chang, A.; Wong, C.-H.; Finn, M. G.; Blixt, O., Anti-Carbohydrate Antibodies Elicited by Polyvalent Display on a Viral Scaffold. *ChemBioChem* **2007,** *8*, 1455-1462.

41. Wu, X.; McKay, C.; Pett, C.; Yu, J.; Schorlemer, M.; Ramadan, S.; Lang, S.; Behren, S.; Westerlind, U.; Finn, M. G.; Huang, X., Synthesis and Immunological Evaluation of Disaccharide Bearing MUC-1 Glycopeptide Conjugates with Virus-like Particles. *ACS Chem. Biol.* **2019,** *14*, 2176-2184.

42. Wu, X.; Yin, Z.; McKay, C.; Pett, C.; Yu, J.; Schorlemer, M.; Gohl, T.; Sungsuwan, S.; Ramadan, S.; Baniel, C.; Allmon, A.; Das, R.; Westerlind, U.; Finn, M. G.; Huang, X., Protective Epitope Discovery and Design of MUC1-based Vaccine for Effective Tumor Protections in Immunotolerant Mice. *J. Am. Chem. Soc.* **2018,** *140*, 16596-16609.

43. Leclerc, C.; Schutze, M. P.; Deriaud, E.; Przewlocki, G., The *in vivo* Elimination of $CD4^+$ T cells Prevents the Induction but not the Expression of Carrier-induced Epitopic Suppression. *J. Immunol.* **1990,** *145*, 1343-1349.

44. Dasgupta, S.; Erturk-Hasdemir, D.; Ochoa-Reparaz, J.; Reinecker, H.-C.; Kasper, D. L., Plasmacytoid Dendritic Cells Mediate Anti-inflammatory Responses to a Gut Commensal Molecule via Both Innate and Adaptive Mechanisms. *Cell Host Microbe* **2014,** *15*, 413-423.

45. De Silva, R. A.; Wang, Q.; Chidley, T.; Appulage, D. K.; Andreana, P. R., Immunological Response from an Entirely Carbohydrate Antigen: Design of Synthetic Vaccines Based on Tn−PS A1 Conjugates. *J. Am. Chem. Soc.* **2009,** *131*, 9622-9623.

46. De Silva, R. A.; Appulage, D. K.; Pietraszkiewicz, H.; Bobbitt, K. R.; Media, J.; Shaw, J.; Valeriote, F. A.; Andreana, P. R., The Entirely Carbohydrate Immunogen Tn-PS A1 Induces a Cancer Cell Selective Immune Response and Cytokine IL-17. *Cancer Immunol. Immunother.* **2012,** *61*, 581-585.

47. Shi, M.; Kleski, K. A.; Trabbic, K. R.; Bourgault, J.-P.; Andreana, P. R., Sialyl-Tn Polysaccharide A1 as an Entirely Carbohydrate Immunogen: Synthesis and Immunological Evaluation. *J. Am. Chem. Soc.* **2016,** *138*, 14264-14272.

48. Trabbic, K. R.; Bourgault, J.-P.; Shi, M.; Clark, M.; Andreana, P. R., Immunological Evaluation of the Entirely Carbohydrate-based Thomsen-Friedenreich – PS B Conjugate. *Org. Biomol. Chem.* **2016,** *14*, 3350-3355.

49. Casella, C. R.; Mitchell, T. C., Putting Endotoxin to Work for Us: Monophosphoryl Lipid A as a Safe and Effective Vaccine Adjuvant. *Cell. Mol. Life. Sci.* **2008,** *65*, 3231-3240.

50. Qureshi, N.; Takayama, K.; Ribi, E., Purification and Structural Determination of Nontoxic Lipid A Obtained from the Lipopolysaccharide of Salmonella Typhimurium. *J. Biol. Chem.* **1982,** *257*, 11808-11815.

51. Ribi, E.; Parker, R.; Strain, S. M.; Mizuno, Y.; Nowotny, A.; Von Eschen, K. B.; Cantrell, J. L.; McLaughlin, C. A.; Hwang, K. M.; Goren, M. B., Peptides as Requirement for Immunotherapy of the Guinea-pig Line-10 Tumor with Endotoxins. *Cancer Immunol. Immunother.* **1979,** *7*, 43-58.

52. Evans, J. T.; Cluff, C. W.; Johnson, D. A.; Lacy, M. J.; Persing, D. H.; Baldridge, J. R., Enhancement of Antigen-specific Immunity via the TLR4 Ligands MPL™ Adjuvant and Ribi.529. *Expert Rev. Vaccines* **2003,** *2*, 219-229.

53. Artiaga, B. L.; Yang, G.; Hackmann, T. J.; Liu, Q.; Richt, J. A.; Salek-Ardakani, S.; Castleman, W. L.; Lednicky, J. A.; Driver, J. P., α-Galactosylceramide Protects Swine Against Influenza Infection when Administered as a Vaccine Adjuvant. *Sci Rep* **2016,** *6*, 23593.

54. Cluff, C. W., Monophosphoryl Lipid A (MPL) as an Adjuvant for Anti-cancer Vaccines: Clinical Results. In *Lipid A in Cancer Therapy*, Springer: 2009; pp 111-123.

55. Liao, G.; Zhou, Z.; Suryawanshi, S.; Mondal, M. A.; Guo, Z., Fully Synthetic Self-adjuvanting α-2, 9-Oligosialic Acid Based Conjugate Vaccines Against Group C Meningitis. *ACS Cent. Sci.* **2016,** *2*, 210-218.

56. Wang, Q.; Zhou, Z.; Tang, S.; Guo, Z., Carbohydrate-Monophosphoryl Lipid A Conjugates are Fully Synthetic Self-adjuvanting Cancer Vaccines Eliciting Robust Immune Responses in the Mouse. *ACS Chem. Biol.* **2011,** *7*, 235-240.

57. Wu, J.; Guo, Z., Improving the Antigenicity of STn Antigen by Modification of Its Sialic Acid Residue for Development of Glycoconjugate Cancer Vaccines. *Bioconjugate Chem.* **2006,** *17*, 1537-1544.

58. Zhou, Z.; Liao, G.; Mandal, S. S.; Suryawanshi, S.; Guo, Z., A Fully Synthetic Self-Adjuvanting Globo H-Based Vaccine Elicited Strong T cell-Mediated Antitumor Immunity. *Chem. Sci.* **2015,** *6*, 7112-7121.

59. Zhou, Z.; Mondal, M.; Liao, G.; Guo, Z., Synthesis and Evaluation of Monophosphoryl Lipid A Derivatives as Fully Synthetic Self-adjuvanting Glycoconjugate Cancer Vaccine Carriers. *Org. Biomol. Chem.* **2014,** *12*, 3238-3245.

60. Pan, Y.; Chefalo, P.; Nagy, N.; Harding, C.; Guo, Z., Synthesis and Immunological Properties of N-modified GM3 Antigens as Therapeutic Cancer Vaccines. *J. Med. Chem.* **2005,** *48*, 875-883.

61. Wang, L.; Feng, S.; Wang, S.; Li, H.; Guo, Z.; Gu, G., Synthesis and Immunological Comparison of Differently Linked Lipoarabinomannan Oligosaccharide–Monophosphoryl Lipid A Conjugates as Antituberculosis Vaccines. *J. Org. Chem.* **2017,** *82*, 12085-12096.

62. Moreira, L. R. S.; Filho, E. X. F., An Overview of Mannan Structure and Mannan-degrading Enzyme Systems. *Appl. Microbiol. Biotechnol.* **2008,** *79*, 165-178.

63. Nelson, R. D.; Shibata, N.; Podzorski, R. P.; Herron, M. J., Candida Mannan: Chemistry, Suppression of Cell-mediated Immunity, and Possible Mechanisms of Action. *Clin. Microbiol. Rev.* **1991,** *4*, 1-19.

64. Tzianabos, A. O., Polysaccharide Immunomodulators as Therapeutic Agents: Structural Aspects and Biologic Function. *Clin. Microbiol. Rev.* **2000,** *13*, 523-533.

65. Cassone, A., Development of Vaccines for Candida albicans: Fighting a Skilled Transformer. *Nat. Rev. Microbiol.* **2013,** *11*, 884-891.

66. Han, Y.; Rhew, K. Y., Comparison of Two Candida Mannan Vaccines: The Role of Complement in Protection Against Disseminated Candidiasis. *Arch. Pharmacal Res.* **2012,** *35*, 2021-2027.

67. Johnson, M. A.; Bundle, D. R., Designing a New Antifungal Glycoconjugate Vaccine. *Chem. Soc. Rev.* **2013,** *42*, 4327-4344.

68. Domer, J. E.; Elkins, K.; Prescott, B.; Caldes, G.; Baker, P. J., Separation of Immunomodulatory Effects of Mannan from Candida albicans into Stimulatory and Suppressive Components. *Cell. Immunol.* **1986,** *101*, 403-414.

69. Wang, Y.; Li, S. P.; Moser, S. A.; Bost, K. L.; Domer, J. E., Cytokine Involvement in Immunomodulatory Activity Affected by Candida albicans Mannan. *Infect. Immun.* **1998,** *66*, 1384-1391.

70. Gadjeva, M.; Takahashi, K.; Thiel, S., Mannan-binding Lectin—A Soluble Pattern Recognition Molecule. *Mol. Immunol.* **2004,** *41*, 113-121.

71. Vasta, G. R.; Quesenberry, M.; Ahmed, H.; O'Leary, N., C-type Lectins and Galectins Mediate Innate and Adaptive Immune Functions: Their Roles in the Complement Activation Pathway. *Dev. Comp. Immunol.* **1999,** *23*, 401-420.

72. Garner, R. E.; Childress, A. M.; Human, L. G.; Domer, J. E., Characterization of Candida Albicans Mannan-induced, Mannan-Specific Delayed Hypersensitivity Suppressor Cells. *Infect. Immun.* **1990,** *58*, 2613-2620.

73. Garner, R. E.; Hudson, J. A., Intravenous Injection of Candida-derived Mannan Results in Elevated Tumor Necrosis Factor alpha Levels in Serum. *Infect. Immun.* **1996,** *64*, 4561-4566.

74. Tzianabos, A. O.; Finberg, R. W.; Wang, Y.; Chan, M.; Onderdonk, A. B.; Jennings, H. J.; Kasper, D. L., T Cells Activated by Zwitterionic Molecules Prevent Abscesses Induced by Pathogenic Bacteria. *J. Biol. Chem.* **2000,** *275*, 6733-6740.

75. Okawa, Y.; Howard, C. R.; Steward, M. W., Production of Anti-peptide Specific Antibody in Mice Following Immunization with Peptides Conjugated to Mannan. *J. Immunol. Methods* **1992,** *149*, 127-131.

76. Podzorski, R. P.; Gray, G. R.; Nelson, R. D., Different Effects of Native Candida albicans Mannan and Mannan-derived Oligosaccharides on Antigen-stimulated Lymphoproliferation *in vitro*. *J. Immunol.* **1990,** *144*, 707-716.

77. Gendler, S. J.; Lancaster, C. A.; Taylor-Papadimitriou, J.; Duhig, T.; Peat, N.; Burchell, J.; Pemberton, L.; Lalani, E. N.; Wilson, D., Molecular Cloning and Expression of Human Tumor-associated Polymorphic Epithelial Mucin. *J. Biol. Chem.* **1990,** *265*, 15286-15293.

78. Gendler, S.; Taylor-Papadimitriou, J.; Duhig, T.; Rothbard, J.; Burchell, J., A Highly Immunogenic Region of a Human Polymorphic Epithelial Mucin Expressed by Carcinomas is Made up of Tandem Repeats. *J. Biol. Chem.* **1988,** *263*, 12820-12823.

79. Hanisch, F.-G.; Uhlenbruck, G.; Peter-Katalinic, J.; Egge, H.; Dabrowski, J.; Dabrowski, U., Structures of Neutral O-linked Polylactosaminoglycans on Human Skim Milk Mucins. A Novel Type of Linearly Extended Poly-N-acetyllactosamine Backbones with Gal beta (1-4) GlcNAc beta (1-6) Repeating Units. *J. Biol. Chem.* **1989,** *264*, 872-883.

80. Apostolopoulos, V.; Xing, P.-X.; McKenzie, I. F. C., Murine Immune Response to Cells Transfected with Human MUC1: Immunization with Cellular and Synthetic Antigens. *Cancer Res.* **1994,** *54*, 5186-5193.

81. Apostolopoulos, V.; Pietersz, G. A.; McKenzie, I. F. C., Cell-mediated Immune Responses to MUC1 Fusion Protein Coupled to Mannan. *Vaccine* **1996,** *14*, 930-938.

82. Apostolopoulos, V.; Pietersz, G. A.; Loveland, B. E.; Sandrin, M. S.; McKenzie, I. F., Oxidative/Reductive Conjugation of Mannan to Antigen Selects for T1 or T2 Immune Responses. *Proc. Natl. Acad. Sci. U. S. A.* **1995,** *92*, 10128-10132.

83. Apostolopoulos, V.; Loveland, B. E.; Pietersz, G. A.; McKenzie, I. F., CTL in Mice Immunized with Human Mucin 1 are MHC-Restricted. *J. Immunol.* **1995,** *155*, 5089-5094.

84. Apostolopoulos, V.; Popovski, V.; McKenzie, I. F., Cyclophosphamide Enhances the CTL Precursor Frequency in Mice Immunized with MUC1-mannan Fusion Protein (M-FP). *J. Immunother.* **1998,** *21*, 109-113.

85. Apostolopoulos, V.; Pietersz, G. A.; Gordon, S.; Martinez□Pomares, L.; McKenzie, I. F. C., Aldehyde□Mannan Antigen Complexes Target the MHC Class I Antigen□Presentation Pathway. *Eur. J. Immunol.* **2000,** *30*, 1714-1723.

86. Karanikas, V.; Hwang, L.-A.; Pearson, J.; Ong, C.-S.; Apostolopoulos, V.; Vaughan, H.; Xing, P.-X.; Jamieson, G.; Pietersz, G.; Tait, B., Antibody and T Cell Responses of Patients with Adenocarcinoma Immunized with Mannan-MUC1 Fusion Protein. *J. Clin. Invest.* **1997,** *100*, 2783-2792.

87. Karanikas, V.; Lodding, J.; Maino, V. C.; McKenzie, I. F. C., Flow Cytometric Measurement of Intracellular Cytokines Detects Immune Responses in MUC1 Immunotherapy. *Clin. Cancer Res.* **2000,** *6*, 829-837.

88. Karanikas, V.; Thynne, G.; Mitchell, P.; Ong, C.-S.; Gunawardana, D.; Blum, R.; Pearson, J.; Lodding, J.; Pietersz, G.; Broadbent, R., Mannan Mucin-1 Peptide Immunization: Influence of Cyclophosphamide and the Route of Injection. *J. Immunother.* **2001,** *24*, 172-183.

89. Apostolopoulos, V.; Pietersz, G. A.; Tsibanis, A.; Tsikkinis, A.; Drakaki, H.; Loveland, B. E.; Piddlesden, S. J.; Plebanski, M.; Pouniotis, D. S.; Alexis, M. N., Pilot Phase III Immunotherapy Study in Early-stage Breast Cancer Patients Using Oxidized Mannan-MUC1 [ISRCTN71711835]. *Breast Cancer Res.* **2006,** *8*, R27.

90. Vassilaros, S.; Tsibanis, A.; Tsikkinis, A.; Pietersz, G. A.; McKenzie, I. F. C.; Apostolopoulos, V., Up to 15-Year Clinical Follow-up of a Pilot Phase III Immunotherapy Study in Stage II Breast Cancer Patients Using Oxidized Mannan–MUC1. *Immunotherapy* **2013,** *5*, 1177-1182.

91. Loveland, B. E.; Zhao, A.; White, S.; Gan, H.; Hamilton, K.; Xing, P.-X.; Pietersz, G. A.; Apostolopoulos, V.; Vaughan, H.; Karanikas, V., Mannan-MUC1–pulsed Dendritic Cell Immunotherapy: A Phase I Trial in Patients with Adenocarcinoma. *Clin. Cancer Res.* **2006,** *12*, 869-877.

92. Tang, C. K.; Lodding, J.; Minigo, G.; Pouniotis, D. S.; Plebanski, M.; Scholzen, A.; McKenzie, I. F. C.; Pietersz, G. A.; Apostolopoulos, V., Mannan-mediated Gene Delivery for Cancer Immunotherapy. *Immunology* **2007,** *120*, 325-335.

93. Tang, C. K.; Sheng, K.-C.; Pouniotis, D.; Esparon, S.; Son, H.-Y.; Kim, C.-W.; Pietersz, G. A.; Apostolopoulos, V., Oxidized and Reduced Mannan Mediated MUC1 DNA Immunization Induce Effective Anti-tumor Responses. *Vaccine* **2008,** *26*, 3827-3834.

94. Tang, C. K.; Sheng, K.-C.; Esparon, S. E.; Proudfoot, O.; Apostolopoulos, V.; Pietersz, G. A., Molecular Basis of Improved Immunogenicity in DNA Vaccination Mediated by a Mannan Based Carrier. *Biomaterials* **2009,** *30*, 1389-1400.

95. Benito-Villalvilla, C.; Soria, I.; Subiza, J. L.; Palomares, O., Novel Vaccines Targeting Dendritic Cells by Coupling Allergoids to Mannan. *Allergo J. Int.* **2018,** *27*, 256-262.

96. Weinberger, E. E.; Himly, M.; Myschik, J.; Hauser, M.; Altmann, F.; Isakovic, A.; Scheiblhofer, S.; Thalhamer, J.; Weiss, R., Generation of Hypoallergenic Neoglycoconjugates for Dendritic Cell Targeted Vaccination: A Novel Tool for Specific Immunotherapy. *J. Controlled Release* **2013,** *165*, 101-109.

97. Chackerian, B.; Lenz, P.; Lowy, D. R.; Schiller, J. T., Determinants of Autoantibody Induction by Conjugated Papillomavirus Virus-like Particles. *J. Immunol.* **2002,** *169*, 6120-6126.

98. Manzano, A. I.; Cases, B.; Sirvent, S.; Soria, I.; Palomares, O.; Fernández-Caldas, E.; Casanovas, M.; Jiménez-Barbero, J.; Subiza, J. L., Structural Studies of Novel Glycoconjugates from Polymerized Allergens (Allergoids) and Mannans as Allergy Vaccines. *Glycoconjugate J.* **2016,** *33*, 93-101.

99. Sirvent, S.; Soria, I.; Cirauqui, C.; Cases, B.; Manzano, A. I.; Diez-Rivero, C. M.; Reche, P. A.; López-Relaño, J.; Martínez-Naves, E.; Cañada, F. J., Novel Vaccines Targeting Dendritic Cells by Coupling Allergoids to Nonoxidized Mannan Enhance Allergen Uptake and Induce Functional Regulatory T Cells through Programmed Death Ligand 1. *J. Allergy Clin. Immunol.* **2016,** *138*, 558-567.

100. Benito□Villalvilla, C.; Soria, I.; Pérez□Diego, M.; Fernández□Caldas, E.; Subiza, J. L.; Palomares, O., Alum Impairs Tolerogenic Properties Induced by Allergoid□mannan Conjugates Inhibiting mTOR and Metabolic Reprogramming in Human DCs. *Allergy* **2019,** *75*, 648-659.

101. Zajonc, D. M., The CD1 Family: Serving Lipid Antigens to T Cells Since the Mesozoic Era. *Immunogenetics* **2016,** *68*, 561-576.

102. Bendelac, A.; Savage, P. B.; Teyton, L., The Biology of NKT Cells. *Annu. Rev. Immunol.* **2007,** *25*, 297-336.

103. Kawano, T.; Cui, J.; Koezuka, Y.; Toura, I.; Kaneko, Y.; Motoki, K.; Ueno, H.; Nakagawa, R.; Sato, H.; Kondo, E.; Koseki, H.; Taniguchi, M., CD1d-Restricted and TCR-Mediated Activation of Vα14 NKT Cells by Glycosylceramides. *Science* **1997,** *278*, 1626-1629.

104. Merle, N. S.; Noe, R.; Halbwachs-Mecarelli, L.; Fremeaux-Bacchi, V.; Roumenina, L. T., Complement System Part II: Role in Immunity. *Front. Immunol.* **2015,** *6*, 257.

105. Metelitsa, L. S.; Naidenko, O. V.; Kant, A.; Wu, H.-W.; Loza, M. J.; Perussia, B.; Kronenberg, M.; Seeger, R. C., Human NKT Cells Mediate Antitumor Cytotoxicity Directly by Recognizing Target Cell CD1d with Bound Ligand or Indirectly by Producing IL-2 to Activate NK Cells. *J. Immunol.* **2001,** *167*, 3114-3122.

106. Morita, M.; Motoki, K.; Akimoto, K.; Natori, T.; Sakai, T.; Sawa, E.; Yamaji, K.; Koezuka, Y.; Kobayashi, E.; Fukushima, H., Structure-Activity Relationship of α-Galactosylceramides Against B16-Bearing Mice. *J. Med. Chem.* **1995,** *38*, 2176-2187.

107. Natori, T.; Koezuka, Y.; Higa, T., Agelasphins, Novel α-Galactosylceramides from the Narine Sponge Agelas Mauritianus. *Tetrahedron Lett.* **1993,** *34*, 5591-5592.

108. Shimosaka, A., Role of NKT Cells and α-Galactosyl Ceramide. *Int. J. Hematol.* **2002,** *76*, 277-279.

109. Carreño, L. J.; Kharkwal, S. S.; Porcelli, S. A., Optimizing NKT Cell Ligands as Vaccine Adjuvants. *Immunotherapy* **2014,** *6*, 309-320.

110. Waldowska, M.; Bojarska-Junak, A.; Roliński, J., A Brief Review of Clinical Trials Involving Manipulation of Invariant NKT Cells as a Promising Approach in Future Cancer Therapies. *Cent. Eur. J. Immunol.* **2017,** *42*, 181-195.

111. Zhang, Y.; Springfield, R.; Chen, S.; Li, X.; Feng, X.; Moshirian, R.; Yang, R.; Yuan, W., α-GalCer and iNKT Cell-based Cancer Immunotherapy: Realizing the Therapeutic Potentials. *Front. Immunol.* **2019,** *10*, 1126.

112. Faveeuw, C.; Trottein, F., Optimization of Natural Killer T Cell–Mediated Immunotherapy in Cancer Using Cell-Based and Nanovector Vaccines. *Cancer Res.* **2014,** *74*, 1632-1638.

113. Fujii, S.-i.; Yamasaki, S.; Sato, Y.; Shimizu, K., Vaccine Designs Utilizing Invariant NKT-Licensed Antigen-Presenting Cells Provide NKT or T Cell Help for B Cell Responses. *Front. Immunol.* **2018,** *9*, 1267.

114. Liu, Z.; Guo, J., NKT-Cell Glycolipid Agonist as Adjuvant in Synthetic Vaccine. *Carbohydr. Res.* **2017,** *452*, 78-90.

115. Mattarollo, S. R.; Smyth, M. J., NKT Cell Adjuvants in Therapeutic Vaccines Against Hematological Cancers. *Oncoimmunology* **2013,** *2*, e22615.

116. Sainz, V.; Moura, L. I. F.; Peres, C.; Matos, A. I.; Viana, A. S.; Wagner, A. M.; Vela Ramirez, J. E.; S Barata, T.; Gaspar, M.; Brocchini, S.; Zloh, M.; Peppas, N. A.; Satchi-Fainaro, R.; F Florindo, H., α-GalactosylCeramide and Peptide-based Nano-vaccine Synergistically Induced a Strong Tumor Suppressive Effect in Melanoma. *Acta Biomater.* **2018,** *76*, 193-207.

117. Yamashita, K.; Arimoto, A.; Nishi, M.; Tanaka, T.; Fujita, M.; Fukuoka, E.; Sugita, Y.; Nakagawa, A.; Hasegawa, H.; Suzuki, S.; Kakeji, Y., Application of iNKT Cell-targeted Active Immunotherapy in Cancer Treatment. *Anticancer Res.* **2018,** *38*, 4233-4239.

118. Dölen, Y.; Kreutz, M.; Gileadi, U.; Tel, J.; Vasaturo, A.; van Dinther, E. A. W.; van Hout-Kuijer, M. A.; Cerundolo, V.; Figdor, C. G., Co-delivery of PLGA Encapsulated Invariant NKT Cell Agonist with Antigenic Protein Induce Strong T Cell-mediated Antitumor Immune Responses. *Oncoimmunology* **2016,** *5*, e1068493.

119. Ghinnagow, R.; Cruz, L. J.; Macho-Fernandez, E.; Faveeuw, C.; Trottein, F., Enhancement of Adjuvant Functions of Natural Killer T Cells Using Nanovector Delivery Systems: Application in Anticancer Immune Therapy. *Front. Immunol.* **2017,** *8*, 879.

120. Ghinnagow, R.; De Meester, J.; Cruz, L. J.; Aspord, C.; Corgnac, S.; Macho-Fernandez, E.; Soulard, D.; Fontaine, J.; Chaperot, L.; Charles, J.; Soncin, F.; Mami-Chouaib, F.; Plumas, J.; Faveeuw, C.; Trottein, F., Co-delivery of the NKT Agonist α-Galactosylceramide and Tumor Antigens to Cross-priming Dendritic Cells Breaks Tolerance to Self-antigens and Promotes Antitumor Responses. *Oncoimmunology* **2017,** *6*, e1339855.

121. Macho-Fernandez, E.; Cruz, L. J.; Ghinnagow, R.; Fontaine, J.; Bialecki, E.; Frisch, B.; Trottein, F.; Faveeuw, C., Targeted Delivery of α-Galactosylceramide to CD8α+ Dendritic Cells Optimizes Type I NKT Cell–Based Antitumor Responses. *J. Immunol.* **2014,** *193*, 961-969.

122. Sartorius, R.; D'Apice, L.; Barba, P.; Cipria, D.; Grauso, L.; Cutignano, A.; De Berardinis, P., Vectorized Delivery of Alpha-GalactosylCeramide and Tumor Antigen on Filamentous Bacteriophage fd Induces Protective Immunity by Enhancing Tumor-Specific T Cell Response. *Front. Immunol.* **2018,** *9*, 1496.

123. Anderson, R. J.; Tang, C.-W.; Daniels, N. J.; Compton, B. J.; Hayman, C. M.; Johnston, K. A.; Knight, D. A.; Gasser, O.; Poyntz, H. C.; Ferguson, P. M.; Larsen, D. S.; Ronchese, F.; Painter, G. F.; Hermans, I. F., A Self-adjuvanting Vaccine Induces Cytotoxic T Lymphocytes that Suppress Allergy. *Nat. Chem. Biol.* **2014,** *10*, 943-949.

124. Cavallari, M.; Stallforth, P.; Kalinichenko, A.; Rathwell, D. C. K.; Gronewold, T. M. A.; Adibekian, A.; Mori, L.; Landmann, R.; Seeberger, P. H.; De Libero, G., A Semisynthetic Carbohydrate-Lipid Vaccine that Protects Against S. Pneumoniae in Mice. *Nat. Chem. Biol.* **2014,** *10*, 950-956.

125. Anderson, R. J.; Compton, B. J.; Tang, C.-W.; Authier-Hall, A.; Hayman, C. M.; Swinerd, G. W.; Kowalczyk, R.; Harris, P.; Brimble, M. A.; Larsen, D. S., NKT Cell-dependent Glycolipid–peptide Vaccines with Potent Anti-Tumour Activity. *Chem. Sci.* **2015,** *6*, 5120-5127.

126. Compton, B. J.; Tang, C.-w.; Johnston, K. A.; Osmond, T. L.; Hayman, C. M.; Larsen, D. S.; Hermans, I. F.; Painter, G. F., Synthesis and Activity of 6 ″-Deoxy-6 ″-thio-α-GalCer and Peptide Conjugates. *Org. Lett.* **2015,** *17*, 5954-5957.

127. Anderson, R. J.; Li, J.; Kedzierski, L.; Compton, B. J.; Hayman, C. M.; Osmond, T. L.; Tang, C.-w.; Farrand, K. J.; Koay, H.-F.; Almeida, C. F. D. S. S. E., Augmenting Influenza-Specific T Cell Memory Generation with a Natural Killer T Cell-Dependent Glycolipid–Peptide Vaccine. *ACS Chem. Biol.* **2017,** *12*, 2898-2905.

128. Speir, M.; Authier-Hall, A.; Brooks, C. R.; Farrand, K. J.; Compton, B. J.; Anderson, R. J.; Heiser, A.; Osmond, T. L.; Tang, C. W.; Berzofsky, J. A.; Terabe, M.; Painter, G. F.; Hermans, I. F.; Weinkove, R., Glycolipid-Peptide Conjugate Vaccines Enhance CD8(+) T Cell Responses Against Human Viral Proteins. *Sci Rep* **2017,** *7*, 14273.

129. Yin, X.-G.; Chen, X.-Z.; Sun, W.-M.; Geng, X.-S.; Zhang, X.-K.; Wang, J.; Ji, P.-P.; Zhou, Z.-Y.; Baek, D. J.; Yang, G.-F.; Liu, Z.; Guo, J., IgG Antibody Response Elicited by a Fully Synthetic Two-Component Carbohydrate-Based Cancer Vaccine Candidate with α-Galactosylceramide as Built-in Adjuvant. *Org. Lett.* **2017,** *19*, 456-459.

130. Ebensen, T.; Link, C.; Riese, P.; Schulze, K.; Morr, M.; Guzmán, C. A., A Pegylated Derivative of α-Galactosylceramide Exhibits Improved Biological Properties. *J. Immunol.* **2007,** *179*, 2065-2073.

131. Broecker, F.; Götze, S.; Hudon, J.; Rathwell, D. C. K.; Pereira, C. L.; Stallforth, P.; Anish, C.; Seeberger, P. H., Synthesis, Liposomal Formulation, and Immunological Evaluation of a Minimalistic Carbohydrate-α-GalCer Vaccine Candidate. *J. Med. Chem.* **2018,** *61*, 4918-4927.

132. Schröder, U.; Ståhl, A., Crystallized Dextran Nanospheres with Entrapped Antigen and Their Use as Adjuvants. *J. Immunol. Methods* **1984,** *70*, 127-132.

133. Shen, L.; Higuchi, T.; Tubbe, I.; Voltz, N.; Krummen, M.; Pektor, S.; Montermann, E.; Rausch, K.; Schmidt, M.; Schild, H.; Grabbe, S.; Bros, M., A Trifunctional Dextran-based Nanovaccine Targets and Activates Murine Dendritic Cells, and Induces Potent Cellular and Humoral Immune Responses in Vivo. *PLoS One* **2013,** *8*, e80904.

134. Bachelder, E. M.; Beaudette, T. T.; Broaders, K. E.; Dashe, J.; Fréchet, J. M. J., Acetal-derivatized Dextran: An Acid-responsive Biodegradable Material for Therapeutic Applications. *J. Am. Chem. Soc.* **2008,** *130*, 10494-10495.

135. Kavunja, H. W.; Lang, S.; Sungsuwan, S.; Yin, Z.; Huang, X., Delivery of Foreign Cytotoxic T Lymphocyte Epitopes to Tumor Tissues for Effective Antitumor Immunotherapy Against Pre-established Solid Tumors in Mice. *Cancer Immunol. Immunother.* **2017,** *66*, 451-460.

136. Broaders, K. E.; Cohen, J. A.; Beaudette, T. T.; Bachelder, E. M.; Fréchet, J. M. J., Acetalated Dextran is a Chemically and Biologically Tunable Material for Particulate Immunotherapy. *Proc. Natl. Acad. Sci. U. S. A.* **2009,** *106*, 5497-5502.

137. Chen, N.; Collier, M. A.; Gallovic, M. D.; Collins, G. C.; Sanchez, C. C.; Fernandes, E. Q.; Bachelder, E. M.; Ainslie, K. M., Degradation of Acetalated Dextran can be Broadly Tuned Based on Cyclic Acetal Coverage and Molecular Weight. *Int. J. Pharm.* **2016,** *512*, 147-157.

138. Chen, N.; Johnson, M. M.; Collier, M. A.; Gallovic, M. D.; Bachelder, E. M.; Ainslie, K. M., Tunable Degradation of Acetalated Dextran Microparticles Enables Controlled Vaccine Adjuvant and Antigen Delivery to Modulate Adaptive Immune Responses. *J. Controlled Release* **2018,** *273*, 147-159.

139. Kauffman, K. J.; Do, C.; Sharma, S.; Gallovic, M. D.; Bachelder, E. M.; Ainslie, K. M., Synthesis and Characterization of Acetalated Dextran Polymer and Microparticles with Ethanol as a Degradation Product. *ACS Appl. Mater. Interfaces* **2012,** *4*, 4149-4155.

140. Bachelder, E. M.; Beaudette, T. T.; Broaders, K. E.; Fréchet, J. M. J.; Albrecht, M. T.; Mateczun, A. J.; Ainslie, K. M.; Pesce, J. T.; Keane-Myers, A. M., *In vitro* Analysis of Acetalated Dextran Microparticles as a Potent Delivery Platform for Vaccine Adjuvants. *Mol. Pharmaceutics* **2010,** *7*, 826-835.

141. Duong, A. D.; Sharma, S.; Peine, K. J.; Gupta, G.; Satoskar, A. R.; Bachelder, E. M.; Wyslouzil, B. E.; Ainslie, K. M., Electrospray Encapsulation of Toll-like Receptor Agonist Resiquimod in Polymer Microparticles for the Treatment of Visceral Leishmaniasis. *Mol. Pharmaceutics* **2013,** *10*, 1045-1055.

142. Peine, K. J.; Bachelder, E. M.; Vangundy, Z.; Papenfuss, T.; Brackman, D. J.; Gallovic, M. D.; Schully, K.; Pesce, J.; Keane-Myers, A.; Ainslie, K. M., Efficient Delivery of the Toll-like Receptor Agonists Polyinosinic: Polycytidylic Acid and CpG to Macrophages by Acetalated Dextran Microparticles. *Mol. Pharmaceutics* **2013,** *10*, 2849-2857.

143. Junkins, R. D.; Gallovic, M. D.; Johnson, B. M.; Collier, M. A.; Watkins-Schulz, R.; Cheng, N.; David, C. N.; McGee, C. E.; Sempowski, G. D.; Shterev, I., A Robust Microparticle

Platform for a STING-targeted Adjuvant that Enhances Both Humoral and Cellular Immunity During Vaccination. *J. Controlled Release* **2018,** *270*, 1-13.

144. Hanson, M. C.; Crespo, M. P.; Abraham, W.; Moynihan, K. D.; Szeto, G. L.; Chen, S. H.; Melo, M. B.; Mueller, S.; Irvine, D. J., Nanoparticulate STING Agonists are Potent Lymph Node-Targeted Vaccine Adjuvants. *J. Clin. Invest.* **2015,** *125*, 2532-2546.

145. Irvine, D. J.; Hanson, M. C.; Rakhra, K.; Tokatlian, T., Synthetic Nanoparticles for Vaccines and Immunotherapy. *Chem. Rev.* **2015,** *115*, 11109-11146.

146. Koshy, S. T.; Cheung, A. S.; Gu, L.; Graveline, A. R.; Mooney, D. J., Liposomal Delivery Enhances Immune Activation by STING Agonists for Cancer Immunotherapy. *Adv. Biosyst.* **2017,** *1*, 1600013.

147. Lee, E.; Jang, H.-E.; Kang, Y. Y.; Kim, J.; Ahn, J.-H.; Mok, H., Submicron-sized Hydrogels Incorporating Cyclic Dinucleotides for Selective Delivery and Elevated Cytokine Release in Macrophages. *Acta Biomater.* **2016,** *29*, 271-281.

148. Watkins-Schulz, R.; Tiet, P.; Gallovic, M. D.; Junkins, R. D.; Batty, C.; Bachelder, E. M.; Ainslie, K. M.; Ting, J. P. Y., A Microparticle Platform for STING-targeted Immunotherapy Enhances Natural Killer Cell-and CD8+ T Cell-mediated Anti-tumor Immunity. *Biomaterials* **2019,** *205*, 94-105.

149. Collier, M. A.; Junkins, R. D.; Gallovic, M. D.; Johnson, B. M.; Johnson, M. M.; Macintyre, A. N.; Sempowski, G. D.; Bachelder, E. M.; Ting, J. P. Y.; Ainslie, K. M., Acetalated Dextran Microparticles for Codelivery of STING and TLR7/8 Agonists. *Mol. Pharmaceutics* **2018,** *15*, 4933-4946.

150. Paßlick, D.; Piradashvili, K.; Bamberger, D.; Li, M.; Jiang, S.; Strand, D.; Wich, P. R.; Landfester, K.; Bros, M.; Grabbe, S., Delivering All in One: Antigen-Nanocapsule Loaded with Dual Adjuvant Yields Superadditive Effects by DC-Directed T Cell Stimulation. *J. Controlled Release* **2018,** *289*, 23-34.

151. Schully, K. L.; Sharma, S.; Peine, K. J.; Pesce, J.; Elberson, M. A.; Fonseca, M. E.; Prouty, A. M.; Bell, M. G.; Borteh, H.; Gallovic, M., Rapid Vaccination Using an Acetalated Dextran Microparticulate Subunit Vaccine Confers Protection Against Triplicate Challenge by Bacillus Anthracis. *Pharm. Res.* **2013,** *30*, 1349-1361.

152. Gallovic, M. D.; Schully, K. L.; Bell, M. G.; Elberson, M. A.; Palmer, J. R.; Darko, C. A.; Bachelder, E. M.; Wyslouzil, B. E.; Keane□Myers, A. M.; Ainslie, K. M., Acetalated Dextran Microparticulate Vaccine Formulated via Coaxial Electrospray Preserves Toxin Neutralization and Enhances Murine Survival Following Inhalational Bacillus Anthracis Exposure. *Adv. Healthcare Mater.* **2016,** *5*, 2617-2627.

153. Schully, K. L.; Bell, M. G.; Prouty, A. M.; Gallovic, M. D.; Gautam, S.; Peine, K. J.; Sharma, S.; Bachelder, E. M.; Pesce, J. T.; Elberson, M. A., Evaluation of a Biodegradable Microparticulate Polymer as a Carrier for Burkholderia pseudomallei Subunit Vaccines in a Mouse Model of Melioidosis. *Int. J. Pharm.* **2015,** *495*, 849-861.

154. Chen, N.; Gallovic, M. D.; Tiet, P.; Ting, J. P. Y.; Ainslie, K. M.; Bachelder, E. M., Investigation of Tunable Acetalated Dextran Microparticle Platform to Optimize M2e-based Influenza Vaccine Efficacy. *J. Controlled Release* **2018,** *289*, 114-124.

155. Cui, L.; Cohen, J. A.; Broaders, K. E.; Beaudette, T. T.; Fréchet, J. M. J., Mannosylated Dextran Nanoparticles: A pH-Sensitive System Engineered for Immunomodulation through Mannose Targeting. *Bioconjugate Chem.* **2011,** *22*, 949-957.

156. Li, D.; Kordalivand, N.; Fransen, M. F.; Ossendorp, F.; Raemdonck, K.; Vermonden, T.; Hennink, W. E.; Van Nostrum, C. F., Reduction□sensitive Dextran Nanogels Aimed for Intracellular Delivery of Antigens. *Adv. Funct. Mater.* **2015,** *25*, 2993-3003.

157. Li, D.; Sun, F.; Bourajjaj, M.; Chen, Y.; Pieters, E. H.; Chen, J.; Van Den Dikkenberg, J. B.; Lou, B.; Camps, M. G. M.; Ossendorp, F., Strong *in vivo* Antitumor Responses Induced by An Antigen Immobilized in Nanogels via Reducible Bonds. *Nanoscale* **2016,** *8*, 19592-19604.

158. Jones, D. P., Radical-free Biology of Oxidative Stress. *Am. J. Physiol. Cell Physiol.* **2008,** *295*, C849-C868.

159. Winterbourn, C. C., Reconciling the Chemistry and Biology of Reactive Oxygen Species. *Nat. Chem. Biol.* **2008,** *4*, 278-286.

160. Savina, A.; Peres, A.; Cebrian, I.; Carmo, N.; Moita, C.; Hacohen, N.; Moita, L. F.; Amigorena, S., The Small GTPase Rac2 Controls Phagosomal Alkalinization and Antigen Crosspresentation Selectively in CD8+ Dendritic Cells. *Immunity* **2009,** *30*, 544-555.

161. Broaders, K. E.; Grandhe, S.; Fréchet, J. M. J., A Biocompatible Oxidation-Triggered Carrier Polymer with Potential in Therapeutics. *J. Am. Chem. Soc.* **2011,** *133*, 756-758.

162. Wang, C.; Li, P.; Liu, L.; Pan, H.; Li, H.; Cai, L.; Ma, Y., Self-adjuvanted Nanovaccine for Cancer Immunotherapy: Role of Lysosomal Rupture-induced ROS in MHC Class I Antigen Presentation. *Biomaterials* **2016,** *79*, 88-100.

163. Novak, M.; Vetvicka, V., β-Glucans, History, and the Present: Immunomodulatory Aspects and Mechanisms of Action. *J. Immunotoxicol.* **2008,** *5*, 47-57.

164. Levitz, S. M.; Huang, H.; Ostroff, G. R.; Specht, C. A., Exploiting Fungal Cell Wall Components in Vaccines. *Semin. Immunopathol.* **2015,** *37*, 199-207.

165. Geijtenbeek, T. B. H.; Gringhuis, S. I., Signalling through C-type Lectin Receptors: Shaping Immune Responses. *Nat. Rev. Immunol.* **2009,** *9*, 465-479.

166. LeibundGut-Landmann, S.; Osorio, F.; Brown, G. D.; e Sousa, C. R., Stimulation of Dendritic Cells via the Dectin-1/Syk Pathway Allows Priming of Cytotoxic T-cell Responses. *Blood* **2008,** *112*, 4971-4980.

167. Weitberg, A. B., A Phase I/II Trial of Beta-(1,3)/(1,6) D-glucan in the Treatment of Patients with Advanced Malignancies Receiving Chemotherapy. *J. Exp. Clin. Cancer Res.* **2008,** *27*, 40.

168. Williams, D. L.; Sherwood, E. R.; Browder, I. W.; McNamee, R. B.; Jones, E. L.; Di Luzio, N. R., Pre-clinical Safety Evaluation of Soluble Glucan. *Int. J. Immunopharmacol.* **1988,** *10*, 405-414.

169. Bromuro, C.; Romano, M.; Chiani, P.; Berti, F.; Tontini, M.; Proietti, D.; Mori, E.; Torosantucci, A.; Costantino, P.; Rappuoli, R., Beta-Glucan-CRM197 Conjugates as Candidates Antifungal Vaccines. *Vaccine* **2010,** *28*, 2615-2623.

170. Cassone, A.; Casadevall, A., Recent Progress in Vaccines Against Fungal Diseases. *Curr. Opin. Microbiol.* **2012,** *15*, 427-433.

171. Liao, G.; Zhou, Z.; Burgula, S.; Liao, J.; Yuan, C.; Wu, Q.; Guo, Z., Synthesis and Immunological Studies of Linear Oligosaccharides of β-Glucan as Antigens for Antifungal Vaccine Development. *Bioconjugate Chem.* **2015,** *26*, 466-476.

172. Abraham, A.; Ostroff, G.; Levitz, S. M.; Oyston, P. C. F., A Novel Vaccine Platform Using Glucan Particles for Induction of Protective Responses Against Francisella tularensis and Other Pathogens. *Clinical & Experimental Immunology* **2019,** *198*, 143-152.

173. Hunter Jr, K. W.; Gault, R. A.; Berner, M. D., Preparation of Microparticulate β-Glucan from Saccharomyces cerevisiae for Use in Immune Potentiation. *Lett. Appl. Microbiol.* **2002,** *35*, 267-271.

174. Di Luzio, N. R.; Williams, D. L.; McNamee, R. B.; Edwards, B. F.; Kitahama, A., Comparative Tumor□inhibitory and Anti□bacterial Activity of Soluble and Particulate Glucan. *Int. J. Cancer* **1979,** *24*, 773-779.

175. Williams, D. L.; Yaeger, R. G.; Pretus, H. A.; Browder, I. W.; McNamee, R. B.; Jones, E. L., Immunization Against Trypanosoma cruzi: Adjuvant Effect of Glucan. *Int. J. Immunopharmacol.* **1989,** *11*, 403-410.

176. Berner, M. D.; Sura, M. E.; Alves, B. N.; Hunter Jr, K. W., IFN-γ Primes Macrophages for Enhanced TNF-α Expression in Response to Stimulatory and Non-stimulatory Amounts of Microparticulate β-Glucan. *Immunol. Lett.* **2005,** *98*, 115-122.

177. Huang, H.; Ostroff, G. R.; Lee, C. K.; Wang, J. P.; Specht, C. A.; Levitz, S. M., Distinct Patterns of Dendritic Cell Cytokine Release Stimulated by Fungal β-Glucans and Toll-like Receptor Agonists. *Infect. Immun.* **2009,** *77*, 1774-1781.

178. Hunter Jr, K. W.; Redelman, D., Microparticulate β-Glucan Upregulates the Expression of B7. 1, B7. 2, B7-H1, but not B7-DC on Cultured Murine Peritoneal Macrophages. *Immunol. Lett.* **2004,** *93*, 71-78.

179. Aouadi, M.; Tesz, G. J.; Nicoloro, S. M.; Wang, M.; Chouinard, M.; Soto, E.; Ostroff, G. R.; Czech, M. P., Orally Delivered siRNA Targeting Macrophage Map4k4 Suppresses Systemic Inflammation. *Nature* **2009,** *458*, 1180-1184.

180. Huang, H.; Ostroff, G. R.; Lee, C. K.; Agarwal, S.; Ram, S.; Rice, P. A.; Specht, C. A.; Levitz, S. M., Relative Contributions of Dectin-1 and Complement to Immune Responses to Particulate β-Glucans. *J. Immunol.* **2012,** *189*, 312-317.

181. Huang, H.; Ostroff, G. R.; Lee, C. K.; Specht, C. A.; Levitz, S. M., Robust Stimulation of Humoral and Cellular Immune Responses following Vaccination with Antigen-loaded β-Glucan Particles. *MBio* **2010,** *1*, e00164-10.

182. Soto, E. R.; Caras, A. C.; Kut, L. C.; Castle, M. K.; Ostroff, G. R., Glucan Particles for Macrophage Targeted Delivery of Nanoparticles. *J. Drug. Deliv.* **2012,** *2012*, Article ID 143524.

183. Soto, E. R.; Ostroff, G. R., Characterization of Multilayered Nanoparticles Encapsulated in Yeast Cell Wall Particles for DNA Delivery. *Bioconjugate Chem.* **2008,** *19*, 840-848.

184. Tesz, G. J.; Aouadi, M.; Prot, M.; Nicoloro, S. M.; Boutet, E.; Amano, S. U.; Goller, A.; Wang, M.; Guo, C.-A.; Salomon, W. E., Glucan Particles for Selective Delivery of siRNA to Phagocytic Cells in Mice. *Biochem. J.* **2011,** *436*, 351-362.

185. Huang, H.; Ostroff, G. R.; Lee, C. K.; Specht, C. A.; Levitz, S. M., Characterization and Optimization of the Glucan Particle-based Vaccine Platform. *Clin. Vaccine Immunol.* **2013,** *20*, 1585-1591.

186. De Smet, R.; Demoor, T.; Verschuere, S.; Dullaers, M.; Ostroff, G. R.; Leclercq, G.; Allais, L.; Pilette, C.; Dierendonck, M.; De Geest, B. G., β-Glucan Microparticles are Good Candidates for Mucosal Antigen Delivery in Oral Vaccination. *J. Controlled Release* **2013,** *172*, 671-678.

187. Baert, K.; De Geest, B. G.; De Greve, H.; Cox, E.; Devriendt, B., Duality of β-Glucan Microparticles: Antigen Carrier and Immunostimulants. *Int. J. Nanomed.* **2016,** *11*, 2463-2469.

188. Berner, V. K.; Sura, M. E.; Hunter, K. W., Conjugation of Protein Antigen to Microparticulate β-Glucan from Saccharomyces cerevisiae: A New Adjuvant for Intradermal and Oral Immunizations. *Appl. Microbiol. Biotechnol.* **2008,** *80*, 1053-1061.

189. Berner, V. K.; Redelman, D.; Hunter, K. W., Microparticulate β-Glucan Vaccine Conjugates Phagocytized by Dendritic Cells Activate Both Naive CD4 and CD8 T Cells *in vitro*. *Cell. Immunol.* **2015,** *298*, 104-114.

190. Yang, Z.; Xu, M.; Jia, Z.; Zhang, Y.; Wang, L.; Zhang, H.; Wang, J.; Song, M.; Zhao, Y.; Wu, Z., A Novel Antigen Delivery System Induces Strong Humoral and CTL Immune Responses. *Biomaterials* **2017,** *134*, 51-63.

191. Baert, K.; De Geest, B. G.; De Rycke, R.; da Fonseca Antunes, A. B.; De Greve, H.; Cox, E.; Devriendt, B., β-Glucan Microparticles Targeted to Epithelial APN as Oral Antigen Delivery System. *J. Controlled Release* **2015,** *220*, 149-159.

192. Numata, M.; Matsumoto, T.; Umeda, M.; Koumoto, K.; Sakurai, K.; Shinkai, S., Polysaccharide–polynucleotide Complexes (15): Thermal Stability of Schizophyllan (SPG)/poly(C) Triple Strands is Controllable by α-Amino Acid Modification. *Bioorg. Chem.* **2003,** *31*, 163-171.

193. Sakurai, K.; Mizu, M.; Shinkai, S., Polysaccharide− Polynucleotide Complexes. 2. Complementary Polynucleotide Mimic Behavior of the Natural Polysaccharide Schizophyllan in the Macromolecular Complex with Single-stranded RNA and DNA. *Biomacromolecules* **2001,** *2*, 641-650.

194. Sakurai, K.; Shinkai, S., Molecular Recognition of Adenine, Cytosine, and Uracil in a Single-stranded RNA by a Natural Polysaccharide: Schizophyllan. *J. Am. Chem. Soc.* **2000,** *122*, 4520-4521.

195. Kobiyama, K.; Aoshi, T.; Narita, H.; Kuroda, E.; Hayashi, M.; Tetsutani, K.; Koyama, S.; Mochizuki, S.; Sakurai, K.; Katakai, Y., Nonagonistic Dectin-1 Ligand Transforms CpG into a Multitask Nanoparticulate TLR9 Agonist. *Proc. Natl. Acad. Sci. U. S. A.* **2014,** *111*, 3086-3091.

196. Minari, J.; Mochizuki, S.; Matsuzaki, T.; Adachi, Y.; Ohno, N.; Sakurai, K., Enhanced Cytokine Secretion from Primary Macrophages due to Dectin-1 Mediated Uptake of CpG DNA/β-1, 3-Glucan Complex. *Bioconjugate Chem.* **2010,** *22*, 9-15.

197. Mochizuki, S.; Sakurai, K., Dectin-1 Targeting Delivery of TNF-α Antisense ODNs Complexed with β-1, 3-Glucan Protects Mice from LPS-induced Hepatitis. *J. Controlled Release* **2011,** *151*, 155-161.

198. Miyamoto, N.; Mochizuki, S.; Sakurai, K., Enhanced Immunostimulation with Crosslinked CpG-DNA/β-1, 3-Glucan Nanoparticle through Hybridization. *Chem. Lett.* **2014,** *43*, 991-993.

199. Miyamoto, N.; Mochizuki, S.; Sakurai, K., Designing an Immunocyte-targeting Delivery System by Use of Beta-Glucan. *Vaccine* **2018,** *36*, 186-189.

200. Ito, H.; Ando, T.; Nakamura, M.; Ishida, H.; Kanbe, A.; Kobiyama, K.; Yamamoto, T.; Ishii, K. J.; Hara, A.; Seishima, M., Induction of Humoral and Cellular Immune Response to Hepatitis B Virus (HBV) Vaccine can be Upregulated by CpG Oligonucleotides Complexed with Dectin□1 Ligand. *J. Viral Hepatitis* **2017,** *24*, 155-162.

201. Kobiyama, K.; Temizoz, B.; Kanuma, T.; Ozasa, K.; Momota, M.; Yamamoto, T.; Aoshi, T.; Kuroda, E.; Ishii, K. J., Species□dependent Role of Type I IFNs and IL□12 in the CTL Response Induced by Humanized CpG Complexed with β□Glucan. *Eur. J. Immunol.* **2016,** *46*, 1142-1151.

202. Kitahata, Y.; Kanuma, T.; Hayashi, M.; Kobayashi, N.; Ozasa, K.; Kusakabe, T.; Temizoz, B.; Kuroda, E.; Yamaue, H.; Coban, C., Circulating Nano-particulate TLR9 Agonist Scouts out Tumor Microenvironment to Release Immunogenic Dead Tumor Cells. *Oncotarget* **2016,** *7*, 48860.

203. Miyamoto, N.; Mochizuki, S.; Fujii, S.; Yoshida, K.; Sakurai, K., Adjuvant Activity Enhanced by Cross-Linked CpG-Oligonucleotides in β-Glucan Nanogel and Its Antitumor Effect. *Bioconjugate Chem.* **2017,** *28*, 565-573.

204. Manolova, V.; Flace, A.; Bauer, M.; Schwarz, K.; Saudan, P.; Bachmann, M. F., Nanoparticles Target Distinct Dendritic Cell Populations According to Their Size. *Eur. J. Immunol.* **2008,** *38*, 1404-1413.

205. Mochizuki, S.; Morishita, H.; Kobiyama, K.; Aoshi, T.; Ishii, K. J.; Sakurai, K., Immunization with Antigenic Peptides Complexed with β-Glucan Induces Potent Cytotoxic T-Lymphocyte Activity in Combination with CpG-ODNs. *J. Controlled Release* **2015,** *220*, 495-502.

206. Mochizuki, S.; Morishita, H.; Sakurai, K., Complex Consisting of β-Glucan and Antigenic Peptides with Cleavage Site for Glutathione and Aminopeptidases Induces Potent Cytotoxic T Lymphocytes. *Bioconjugate Chem.* **2017,** *28*, 2246-2253.

207. Wang, H.; Yang, B.; Wang, Y.; Liu, F.; Fernández-Tejada, A.; Dong, S., β-Glucan as an Immune Activator and a Carrier in the Construction of a Synthetic MUC1 Vaccine. *Chem. Commun.* **2019,** *55*, 253-256.

208. Jin, J. W.; Tang, S. Q.; Rong, M. Z.; Zhang, M. Q., Synergistic Effect of Dual Targeting Vaccine Adjuvant with Aminated β-Glucan and CpG-Oligodeoxynucleotides for Both Humoral and Cellular Immune Responses. *Acta Biomater.* **2018,** *78*, 211-223.

209. Yuba, E.; Yamaguchi, A.; Yoshizaki, Y.; Harada, A.; Kono, K., Bioactive Polysaccharide-based pH-Sensitive Polymers for Cytoplasmic Delivery of Antigen and Activation of Antigen-specific Immunity. *Biomaterials* **2017,** *120*, 32-45.

210. Lofthouse, S., Immunological Aspects of Controlled Antigen Delivery. *Adv. Drug Delivery Rev.* **2002,** *54*, 863-870.

211. Sivakumar, S. M.; Safhi, M. M.; Kannadasan, M.; Sukumaran, N., Vaccine Adjuvants – Current Status and Prospects on Controlled Release Adjuvancity. *Saudi Pharm. J.* **2011,** *19*, 197-206.

212. Abu Lila, A. S.; Ishida, T., Liposomal Delivery Systems: Design Optimization and Current Applications. *Biol. Pharm. Bull.* **2017,** *40*, 1-10.

213. Bulbake, U.; Doppalapudi, S.; Kommineni, N.; Khan, W., Liposomal Formulations in Clinical Use: An Updated Review. *Pharmaceutics* **2017,** *9*, 12.

214. Bachmann, M. F.; Jennings, G. T., Vaccine Delivery: A Matter of Size, Geometry, Kinetics and Molecular Patterns. *Nat. Rev. Immunol.* **2010,** *10*, 787-796.

215. Xiang, S. D.; Scholzen, A.; Minigo, G.; David, C.; Apostolopoulos, V.; Mottram, P. L.; Plebanski, M., Pathogen Recognition and Development of Particulate Vaccines: Does Size Matter? *Methods* **2006,** *40*, 1-9.

216. Lin, L.; Qiao, M.; Zhang, X.; Linhardt, R. J., Site-selective Reactions for the Synthesis of Glycoconjugates in Polysaccharide Vaccine Development. *Carbohydr. Polym.* **2020,** *230*, 115643.

CHAPTER 2 Delivery of Foreign Cytotoxic T Lymphocyte Epitopes to Tumor Tissues for Effective Antitumor Immunotherapy Against Pre□established Solid Tumors in Mice[1]

Adapted by permission from Springer Nature Customer Service Centre GmbH: Springer Cancer immunology, immunotherapy, Kavunja, H. W.; Lang, S.; Sungsuwan, S.; Yin, Z.; Huang, X., Delivery of Foreign Cytotoxic T Lymphocyte Epitopes to Tumor Tissues for Effective Antitumor Immunotherapy Against Pre-established Solid Tumors in Mice. *Cancer Immunol. Immunother.* **2017,** *66*, 451-460. COPYRIGHT (2017)

2.1 Introduction

Cytotoxic T lymphocytes (CTLs) are a key component of antitumor immunity. Anticancer immunotherapies invoking CTLs are being actively pursued.[2-3] However, clinical successes have been limited so far with multiple challenges to overcome. CTLs eliminate target cells through binding with specific peptide epitopes presented by the major histocompatibility complex class I (MHC-I) on the target cell surface. Since most of tumor antigens are self-antigens, it is often very difficult to generate highly active CTLs targeting tumor-associated antigens, as these CTLs are generally eliminated during development due to negative selection.[4] In addition, with high heterogeneities of tumor cells, subpopulations of the cells may not express the cognate tumor-associated antigen.[5] These antigen-loss variants (ALVs) are thus not subjected to the immune surveillance bestowed by the specific CTLs and can continue to grow, resulting in failure of the therapy. Moreover, due to the genetic instability, some tumor cells can downregulate their MHC-

I expression levels under the selection pressure,[6-7] a phenomenon termed immune-editing.[8] The low abundance of MHC-I/antigen complexes on the cell surface may lead to insufficient tumor recognition by CTLs and eventual tumor escape.[9] To address these challenges, we report a strategy to selectively deliver a CTL peptide epitope (CTLp) by pH-sensitive microparticles to tumor tissues not endogenously expressing such an epitope and to effectively protect mice from pre-established ALV solid tumor models in a therapeutic setting.

Compared to tumor-associated antigens, foreign CTLp can be advantageous as high-affinity CTLs recognizing these epitopes are not subjected to negative selection and may be more readily elicited via vaccination. If the high affinity CTLp can be delivered to tumor tissues in vaccinated hosts, they can potentially outcompete endogenous epitopes for binding with the limited number of MHC-I molecules, sensitizing tumor cells toward CTL killing. In addition, tumor stromal cells are known to provide the critical extracellular microenvironment supporting tumor growth.[10] As stromal cells are derived from the host, they are genetically more stable and less prone to mutation. CTLp delivered to tumor tissues can result in epitope presentation by stromal cells and their subsequent killing by CTLs.[11] The elimination of tumor stromal cells removes the favorable microenvironment supporting tumor growth and facilitates tumor death by the bystander effect.[12-13]

To achieve tumor selectivity in CTLp delivery, we resorted to pH-responsive "smart" particles[14] that are stable at neutral pH. Due to the hyperpermeability of blood vessels and the

defective lymphatic system in tumor tissues, nanoparticles/microparticles (MPs) can selectively accumulate in these tissues with slow clearance due to the enhanced permeability and retention effect.[15-16] The CTLp can be released in the acidic tumor microenvironment[17] or intracellularly for MHC-I presentation by both tumor and stromal cells sensitizing them toward CTL killing.

*The work in this chapter was in collaboration with Dr. Herbert Kavunja. For a clear demonstration of this work, Dr. Kavunja's data has been included.

2.2 Results and discussions

2.2.1 Synthesis and characterization of the CTLp□Ace□Dex□MPs

Acetalated dextran (Ac-Dex)[18] was utilized to construct the pH-responsive particles due to its high biocompatibility. The Ac-Dex was prepared by treating a mixture of dextran (MW: 9–11 kDa) and 2-methoxypropene in DMSO with pyridinium *p*-toluenesulfonate (**Figure 2.1**). Two CTL peptide epitopes, one from human mucin-1 with the sequence of PDTRPAP[19] and the other from ovalbumin with the sequence of SIINFEKL, were synthesized through solid-phase peptide synthesis using fluorenylmethyloxycarbonyl (Fmoc) chemistry (**Figure 2.2a**). Ac-Dex was treated with an emulsion evaporation method[20] to form MPs encapsulating the peptide. Of the two peptides, SIINFEKL was encapsulated at a much higher efficiency (40%) compared to mucin-1 (<5%) and was used in subsequent studies. The SIINFEKL is a well-known CTLp capable of binding strongly with MHC-I H-2Kb with a Kd value of 3 nM.[21] The higher encapsulation efficiency of SIINFEKL peptide is presumably due to its higher lipophilicity (The value of cLogP, a common measure of

lipophilicity of a compound, of SIINFEKL is calculated to be −2.2, while that for MUC1 PDTRPAP sequence is −5.1). The CTLp-Ac-Dex-MPs had average diameters of 597 nm by SEM (**Figure 2.1**) with a zeta potential of −5.3 mV.

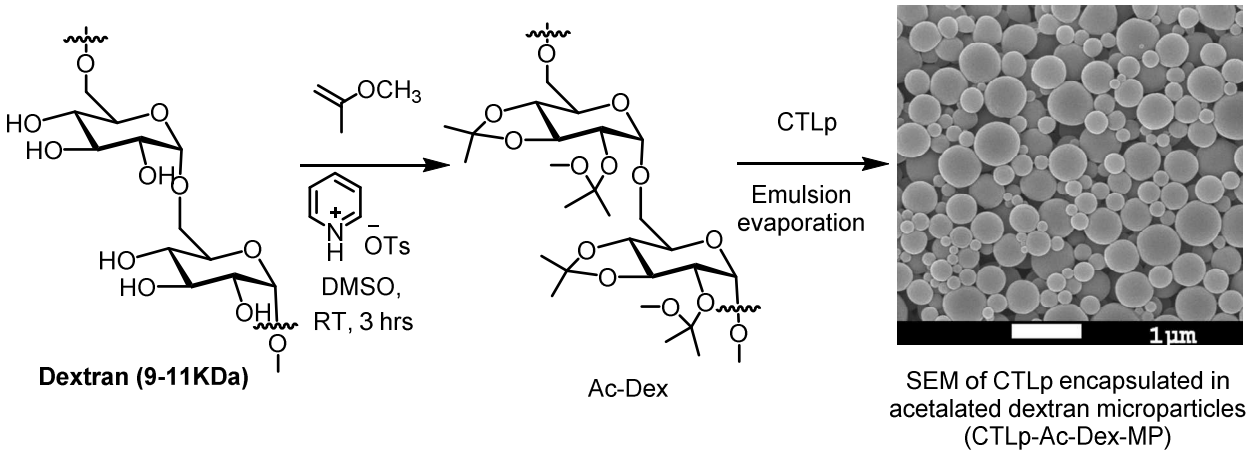

Figure 2.1. Synthesis of acetalated dextran and CTLp encapsulated acetalated dextran microparticles. (SEM image collected by Dr. Kavunja)

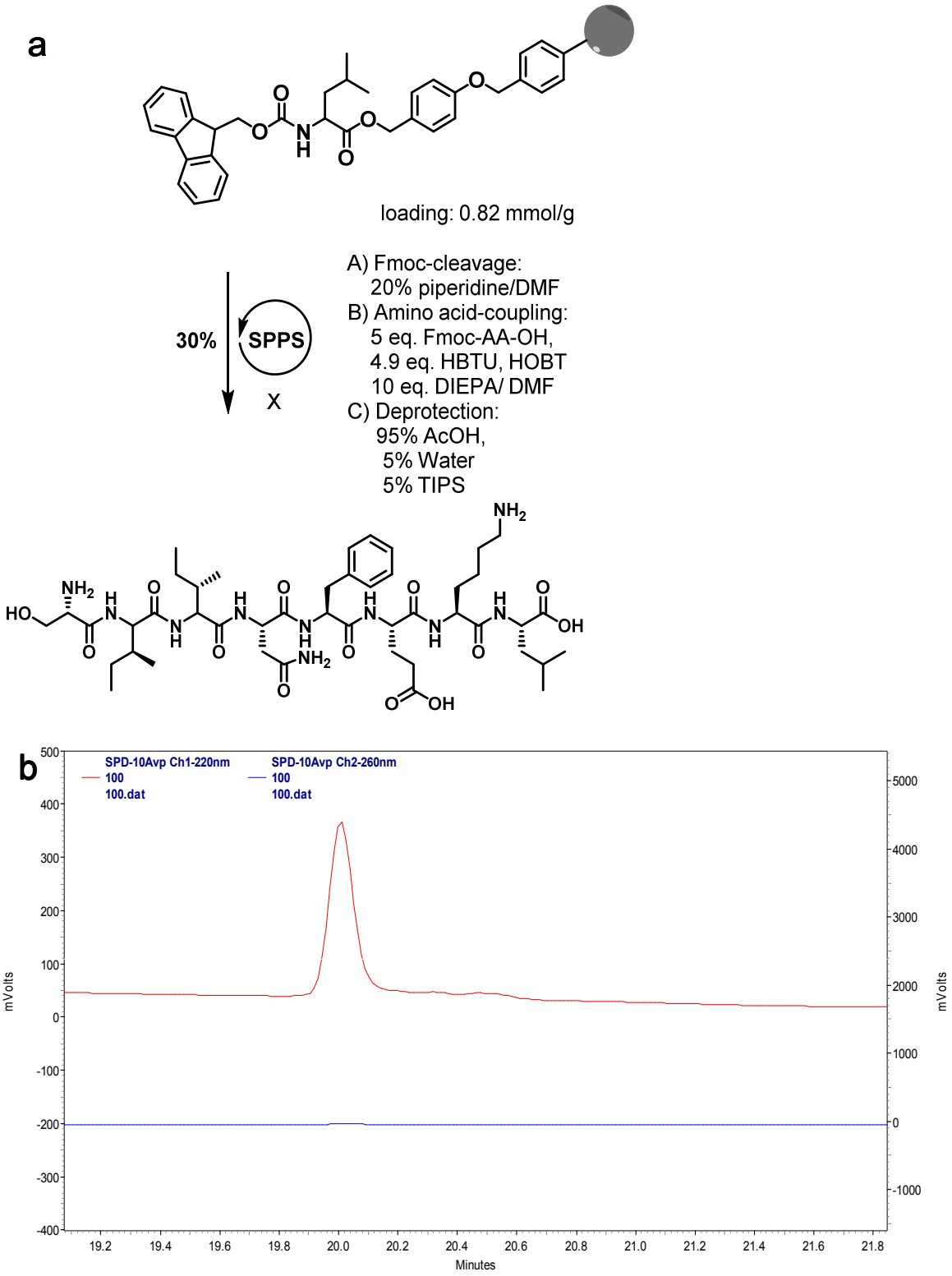

Figure 2.2 a. Synthesis scheme of CTLp SIINFEKL through solid phase peptide synthesis. **b**. HPLC chromatogram of purified CTLp SIINFEKL. (Data collected by Dr. Kavunja) **c**. ESI spectrum of purified CTLp SIINFEKL. (Data collected by Dr. Kavunja)

Figure 2.2 c (cont'd)

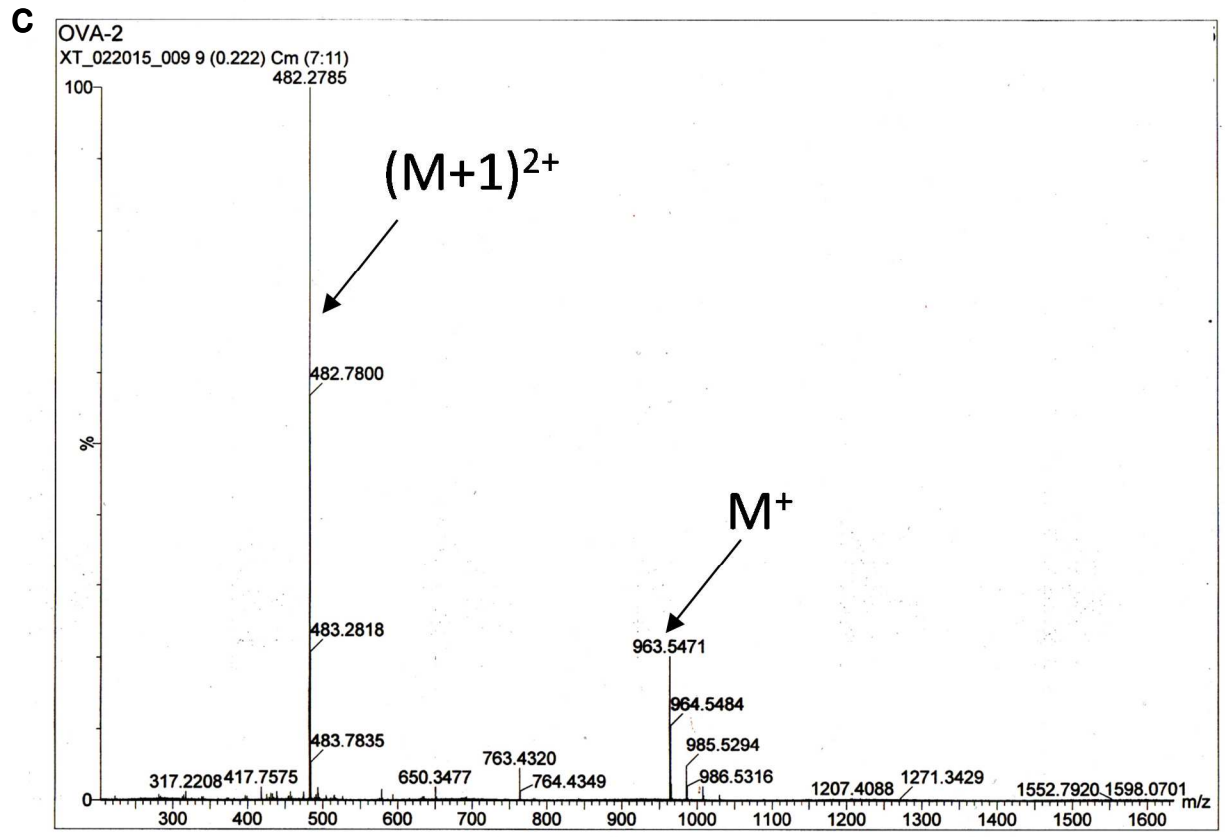

To test the pH responsiveness, the Ac-Dex-MPs were incubated in PBS buffers with pH values of 7.4, 6.5, 6.0 and 5.5 at room temperature and 37 °C, respectively. The scattering of light by the MP suspension was monitored by UV–Vis at 600 nm. At pH 7.4, 6.5 and 6.0, there were very little absorbance changes over 80 h at either room temperature or 37 °C (**Figure 2.3a**). At pH 5.5, the MPs gradually dissolved in solution over 40 h due to the cleavage of acetal linkages under the acidic condition. The rate of peptide release from the MPs was evaluated with the amounts of CTLp discharged to solution determined by HPLC analysis. At pH 7.4, the majority of CTLp remained within the MPs over 24 h, suggesting despite the small size of the CTLp, the spontaneous

release rate from the MPs was slow (**Figure 2.3b**). The release rate was significantly enhanced at pH 5.5 with a half-life of about 4 h. Based on HPLC quantification (Appendix **Figure 2.15**), the CTLp-Ace-Dex-MPs contained 20 µg CTLp/mg MP and 100% of the peptide could be released from the MPs at pH 5.5.

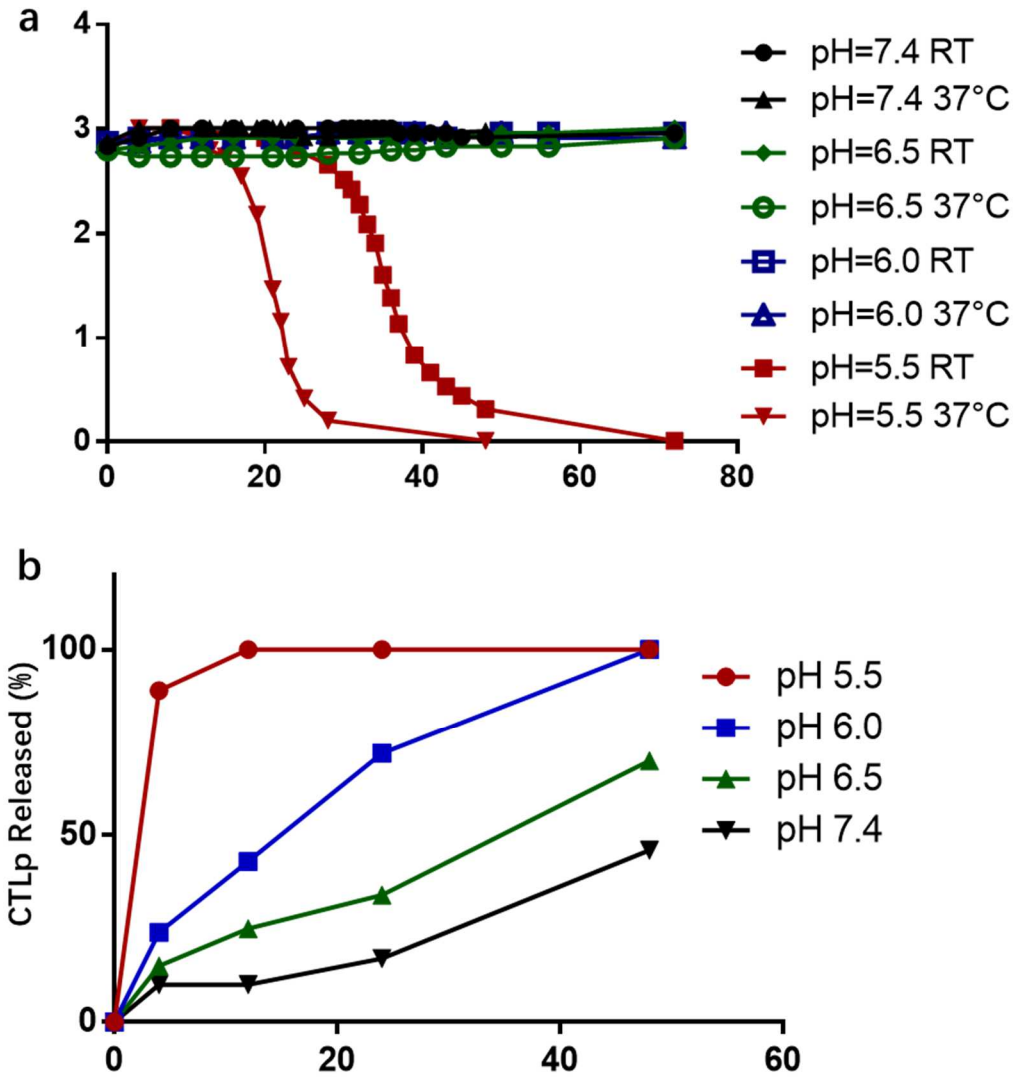

Figure 2.3 a. Hydrolysis of Ac-Dex-MP at pH values of 7.4, 6.5, 6.0 and 5.5 at room temperature and 37 °C, respectively, in PBS buffer as monitored by UV–Vis at 600 nm. **b.** CTLp release from CTLp-Ac-Dex-MPs at 37 °C in PBS buffer at pH 5.5, 6.0, 6.5 and 7.4

2.2.2 CTLp delivered by the MPs could be loaded on MHC□I of target cells and activate T cells *in vitro*

In order to elicit a CTL response, the CTLp needs to be presented on MHC-I molecules of target cells. Dr. Kavunja evaluated the abilities of the MPs to deliver CTLp to cells *in vitro* using EL4 cells. EL4 cells do not naturally express the CTLp SIINFEKL, thus serving as a model of ALV cells. CTLp-MPs were incubated with EL4 cells at 37 °C. To detect the presentation of SIINFEKL peptide by MHC-I through flow cytometry, fluorescently labeled monoclonal antibody (mAb) (clone 25-D1.16), which recognizes the complex formed by SIINFEKL with MHC-I but not the free peptide itself, was utilized. A dose-dependent increase of cellular fluorescence intensity was observed upon increasing the amounts of CTLp added (**Figure 2.4**). Even with a short incubation time of 15 min with the CTLp-MPs (containing 54 ng of CTLp), significant amounts of CTLp/MHC-I complexes were detected on cell surface (**Figure 2.5a**). The highest fluorescence intensity was observed after 6 h of incubation. These results suggest that the exogenous CTLp delivered by CTLp-MPs could compete with endogenous CTLp to be presented by MHC-I molecules on tumor cells.

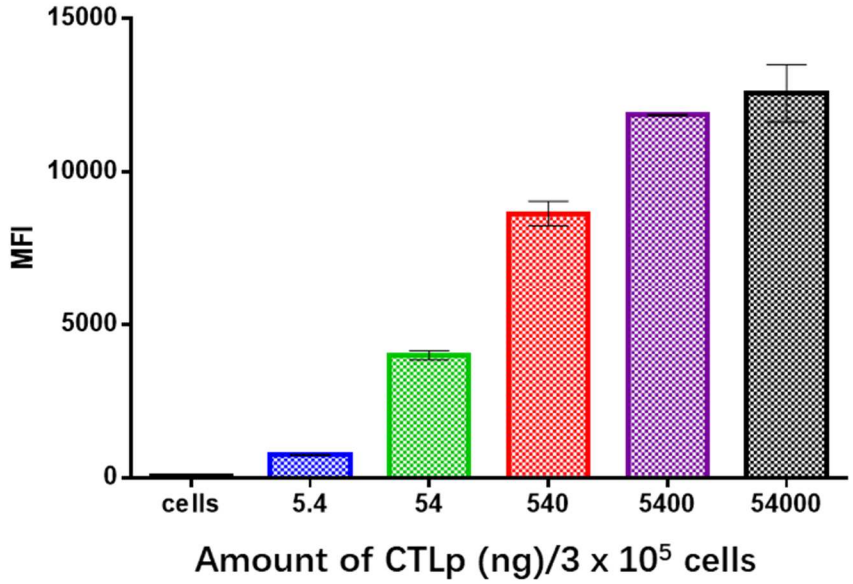

Figure 2.4 *In vitro* detection of CTLp presented by MHC-I of EL4 cancer cells upon incubation with CTLp-Ac-Dex-MPs. (Data collected by Dr. Kavunja)

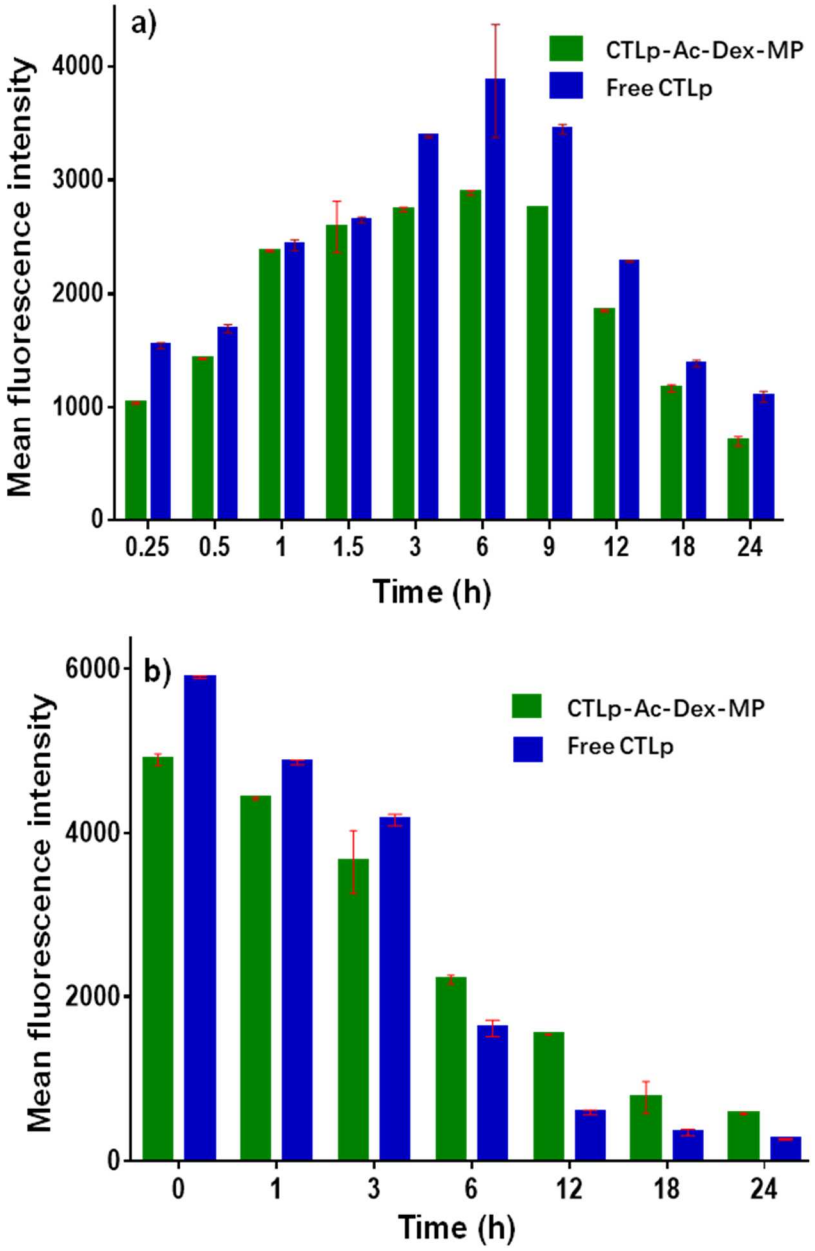

Figure 2.5 a. Effect of incubation time on the levels of CTLp presented by EL4 cells; **b**. Duration of CTLp presented on EL4 cells after incubation with either free CTLp or CTLp-Ac-Dex-MPs for one hour followed by removal of all unbound CTLp or MPs in the cell culture media. 54 ng of the CTLp was used for each study (Data collected by Dr. Kavunja)

Dr. Kavunja further evaluated the duration of CTLp SIINFEKL presented on tumor cells. After incubation of EL4 cells with CTLp-MP or free CTLp (54 ng) for 1 h, cells were centrifuged to remove the culture media containing the unbound MP and peptide. Fresh media was then added to the cells, and the amounts of CTLp/MHC-I complexes remained on cell surface were monitored. While free CTLp was presented on cell surface quicker than encapsulated CTLp (0–3 h) (**Figure 2.5b**), more CTLp/MHC-I complexes were observed 6 h after cells were pulsed with CTLp-MPs, hinting the gradual release of encapsulated CTLp inside the cells. After 24 h, there were about 15% of CTLp/MHC-I remaining on cell surface.

To assess whether the CTLp presented by EL4 tumor cells could be recognized by CTLs, *in vitro* CTL activation assay was carried out by Dr. Kavunja using B3Z $CD8^+$ T cells.[22] B3Z cells express T cell receptors (TCR) specific to the SIINFEKL epitope presented on H-2Kb MHC-I molecules and secret β-galactosidase upon TCR-CTLp/MHC I complex recognition, which cleaves its substrate CPRG to yield a colorimetric readout. Incubation of EL4 tumor cells with CTLp-MPs led to much higher activation of B3Z cells than the free peptide at the equivalent peptide concentrations (**Figure 2.6**). These results suggest CTLp-Ac-Dex-MPs can potentially be highly effective against tumors. This observation corroborated with the report from Frechet group that a protein encapsulated by MPs could activate CTLs *in vitro*.[18]

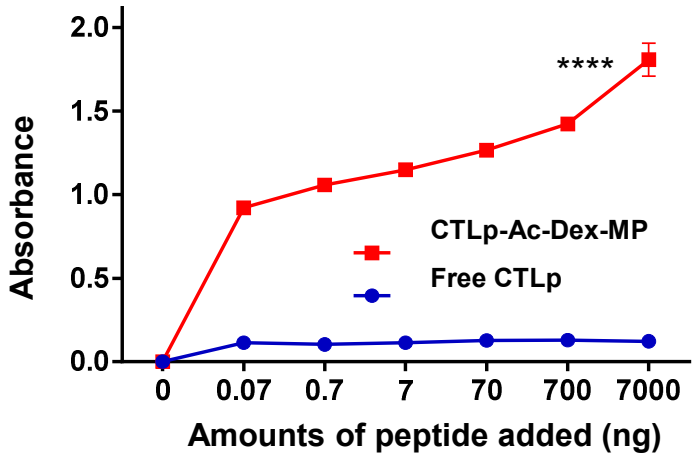

Figure 2.6 *In vitro* CTL activation assay of B3Z cells cultured with EL4 cells following incubation with either free CTLp or CTLp-Ac-Dex-MPs. The t-test was used for analysis, ****p < 0.0001. Absorbance was measured at 595 nm (Data collected by Dr. Kavunja)

2.2.3 CTLp□Ac□Dex□MPs protected mice from tumor□induced death under a therapeutic setting

With the abilities of MPs delivering CTLp to cells and activating CTLs established *in vitro*, tests were carried out to determine if CTLp-MPs can offer protection against tumor growth *in vivo*. To expand CTLs against the SIINFEKL epitope, C57BL/6 mice were immunized subcutaneously under the scruff on day 0 with 50 μg of ovalbumin protein containing the SIINFEKL sequence as an emulsion in complete Freund's adjuvant.[23] Booster injections were given on days 14 and 28 with ovalbumin and incomplete Freund's adjuvant. To confirm the generation of SIINFEKL-specific CTLs, an *in vivo* CTL assay based on carboxyfluorescein succinimidyl ester (CFSE) labeling was carried out by injecting $CFSE^{hi}$-labeled cells loaded with the CTLp along with $CFSE^{lo}$-labeled control cells to ovalbumin-immunized mice.[24] Mice were euthanized 24 h after CFSE labeled cell injection, and spleens and lymph nodes were collected for the analysis of the

viability of CTLp loaded cells. The viabilities of cells pulsed with the CTLp were significantly reduced compared to those not incubated with the epitope based on the ratio change of $CFSE^{lo}$:$CFSE^{hi}$ before and after injection (**Figure 2.7**), suggesting the successful production of SIINFEKL-specific CTLs in mice through immunization.

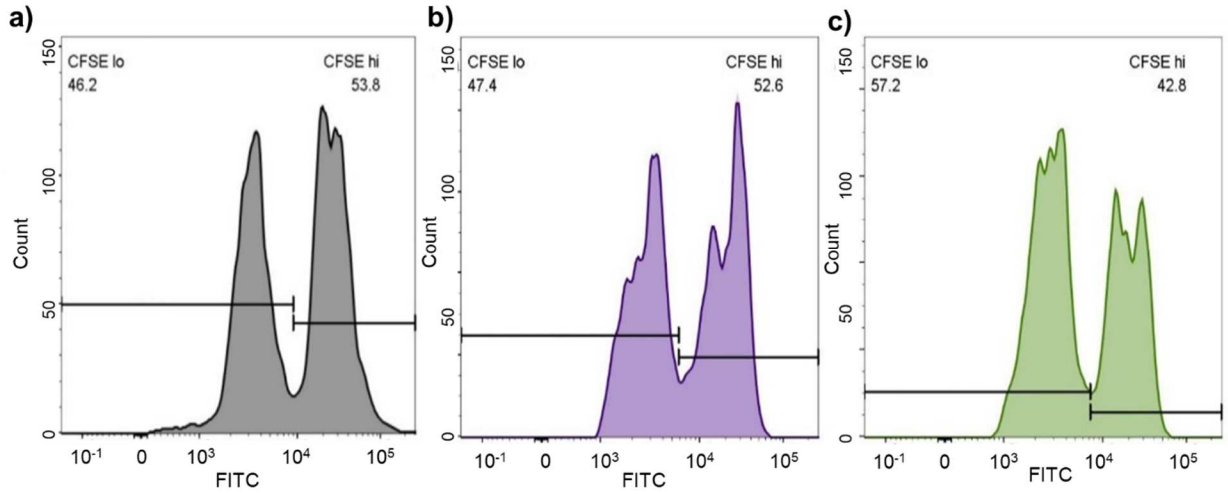

Figure 2.7 *In vivo* CTL activity assay results based on the analysis of the relative viabilities of CFSE labeled cells by FACS. **a**. The "before injection" sample showing a mixture of CTLp pulsed $CFSE^{hi}$ and $CFSE^{lo}$ splenic cells (the ratio of $CFSE^{hi}$ to $CFSE^{lo}$ cells was 53.8 : 46.2); **b**. Cells isolated from a naïve mouse 7 days after injection of the mixture of CFSEhi and CFSElo cells (the ratio of $CFSE^{hi}$ to $CFSE^{lo}$ cells obtained from this mouse was 52.6 : 47.4); **c**. Cells isolated from an ovalbumin immunized mouse 7 days after injection of the mixture of $CFSE^{hi}$ and $CFSE^{lo}$ cells (the ratio of $CFSE^{hi}$ to $CFSE^{lo}$ cells obtained from this mouse was 42.8 : 57.2) showing reduced viabilities of CTLp pulsed $CFSE^{hi}$ cells relative to $CFSE^{lo}$ cells without the CTLp. This suggests the activation of CTLp specific CTLs in the immunized mice.

Dr. Kavunja evaluated the protection of EL4 tumor-bearing mice with the administration of CTLp-Ac-Dex-MPs. EL4 cells (2×10^5 cells) were injected subcutaneously into the left flank of ovalbumin-immunized mice (day 0).[25] When the tumor sizes reached 90 mm^3, mice were injected intratumorally with free SIINFEKL CTLp (7 μg), CTLp-Ac-Dex-MPs (equivalent to 7 μg of

peptide), empty Ac-Dex-MPs or PBS, respectively, every other day for a total of three injections. Tumor in the group receiving PBS only grew rapidly and all mice died from tumor on day 20 (**Figure 2.8a**, **b**). The group administered with empty Ac-Dex-MPs showed similar tumor growth and mortality rates as the PBS group, suggesting empty Ac-Dex-MPs did not bestow any protections. The injection of free peptide slowed down the growth of tumor and protected 20% of the mice from tumor-induced death. In contrast, the group receiving CTLp-Ac-Dex-MPs showed 100% survival and the sizes of the tumor were significantly smaller (**Figure 2.8a, b**). The superiority of CTLp-Ac-Dex-MPs compared to free peptide in tumor protection may be partially due to the more efficient CTL activation by tumor cells incubated with the CTLp-MPs compared to those with the free peptide (**Figure 2.6**).

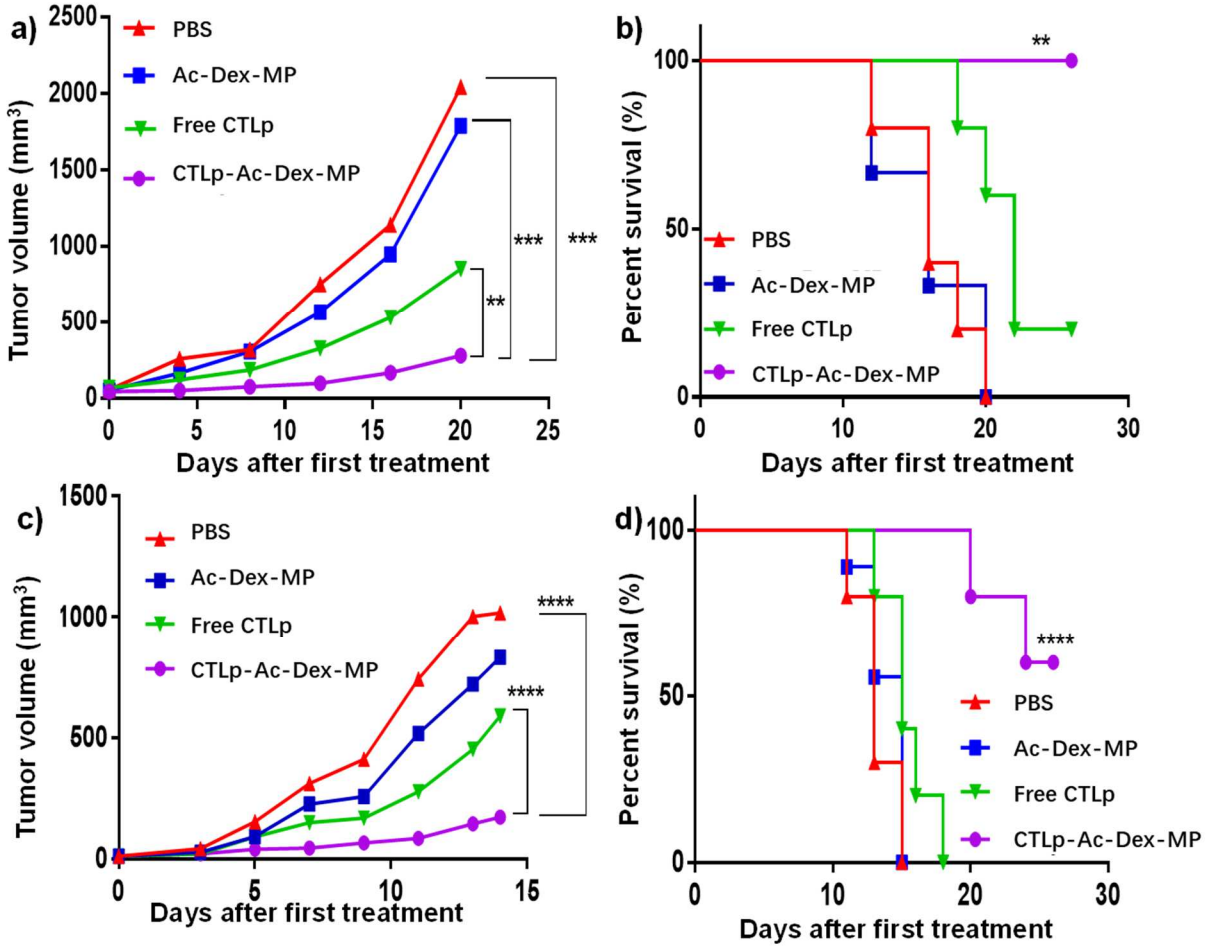

Figure 2.8 Protection efficacy of mice bearing established subcutaneous EL4 tumors through **a**–**b** intratumoral and **c**–**d** intravenous administration of PBS, Ac-Dex-MP, free CTLp or CTLp-Ac-Dex-MPs. Compounds were administered on days 3, 5 and 7. **a**, **c** Changesof tumor volume over time; **b**, **d** Kaplan–Meier survival curve. **p < 0.005; ****p < 0.0001 compared to the group receiving free CTLp. The log-rank and the t-test methods were used for analysis. (Data collected by Dr. Kavunja)

With the efficacy of local intratumoral delivery of CTLp-MPs established, systemic administration was tested next by Dr. Kavunja. The subcutaneous EL4 tumor-bearing ovalbumin immunized mice were injected intravenously via tail vein with CTLp-Ac-Dex-MPs (equivalent to 20 µg of CTLp), free CTLp (20 µg), empty Ac-Dex-MPs or PBS, respectively, on days 3, 5 and 7

as in the intratumoral study. All mice in the PBS and empty Ac-Dex-MP study groups died within 15 days (**Figures 2.8c**, **d**). The free CTLp had little protection as all mice died by day 18. The CTLp-Ac-Dex-MPs, however, provided significant protection with 60% of the mice surviving the tumor challenge (**Figure 2.8d**). No adverse autoimmunity complications were observed in all mice.

To test the generality of the approach, I examined another subcutaneous tumor model using MC38 colon adenocarcinoma cells. The subcutaneous MC38 tumor-bearing ovalbumin-immunized mice were treated with PBS, free CTLp, empty Ac-Dex-MPs or CTLp-Ac-Dex-MPs following a similar schedule as that for the EL4 model. The tumor sizes of CTLp-Ac-Dex-MPs-treated groups were significantly smaller than other groups (**Figure 2.9**).

The analysis of EL4 and MC38 tumors from untreated mice indicated there were significant amounts of $CD8^+$ T cells (9.4% and 7.2% respectively) presented in the tumor tissue (**Figure 2.10**). However, the pre-existing CTLs did not protect mice from tumor growth, probably due to the difficulty of tumor antigen recognition. The OVA specific CTLs induced by previous ovalbumin immunization may not have much direct tumor killing ability, as both EL4 and MC38 cells do not endogenously express the SIINFEKL epitope. Still, treatment of mice with SIINFEKL containing MPs either intratumorally or systematically significantly reduced tumor growth (**Figure 2.8** and **Figure 2.9**). This suggests epitope delivery by MPs can be an effective approach to combat ALVs. The MPs could release the free CTLp in the tumor microenvironment for loading onto MHC-I of tumor and stromal cells, rendering it possible to remove both tumor cells and the cells supporting

tumor growth by anti-SIINFEKL CTLs. In addition, we noticed the CTLp-Ac-Dex MPs reduced tumor growth without pre-existing anti-OVA immunity. A group of non-immunized mice was grafted with MC38 cells and treated with CTLp-Ac-Dex-MPs under the same schedule. Interestingly, even without prior ovalbumin immunization, these mice exhibited reduced tumor growth rates as preimmunized mice (**Figure 2.9**). Possibly, immune cells in tumor tissues including macrophages can uptake the MPs into acidic organelles such as lysosomes, which can cleave MPs and release the encapsulated CTLp for cross-presentation on MHC-I and activation of anti-SIINFEKL CTLs. However, the exact mechanism for such a fast CTL activation by CTLp-Ac-Dex-MPs is not known and needs further study.

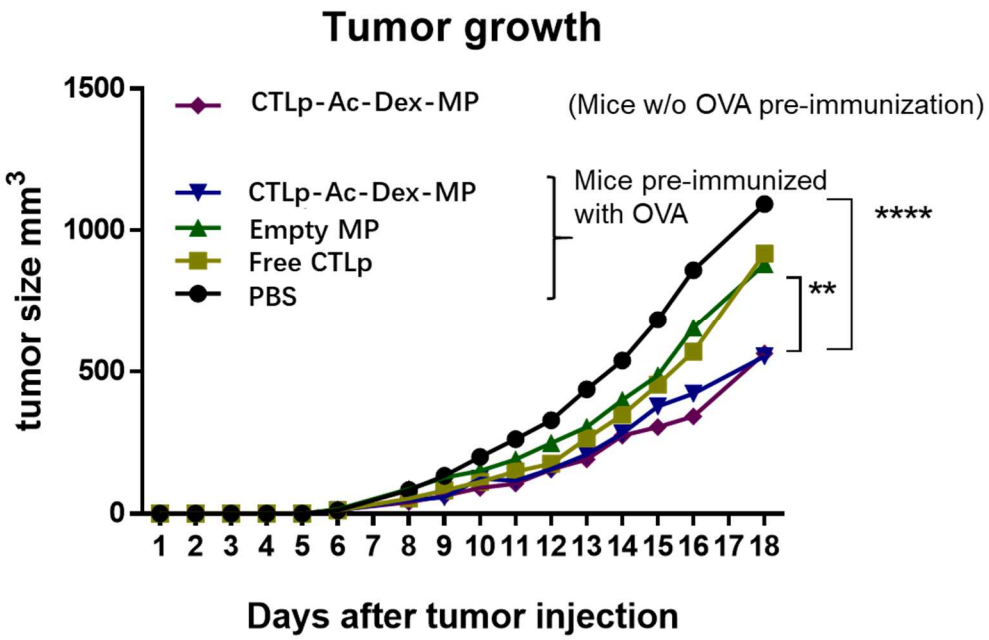

Figure 2.9 Protection efficacy of mice bearing MC38 tumor. Tumor growth in ovalbumin pre-immunized mice bearing established subcutaneous MC38 tumors following intravenous administration of PBS, free CTLp, empty Ac-Dex-MP, or CTLp-Ac-Dex-MPs. Administration of CTLp-Ac-Dex-MPs significantly reduced tumor growth. Another group of mice were inoculated with MC38 tumor without prior immunization with ovalbumin. These mice were administered

Figure 2.9 (cont'd) with CTLp-Ac-Dex-MPs, which also significantly slowed down tumor growth. **, $p < 0.005$; ****, $p < 0.0001$. The Log-rank and the t-test methods were used for analysis. The results suggest that CTLp-Ac-Dex-MPs could reduce the rates of tumor growth with or without prior immunization with ovalbumin

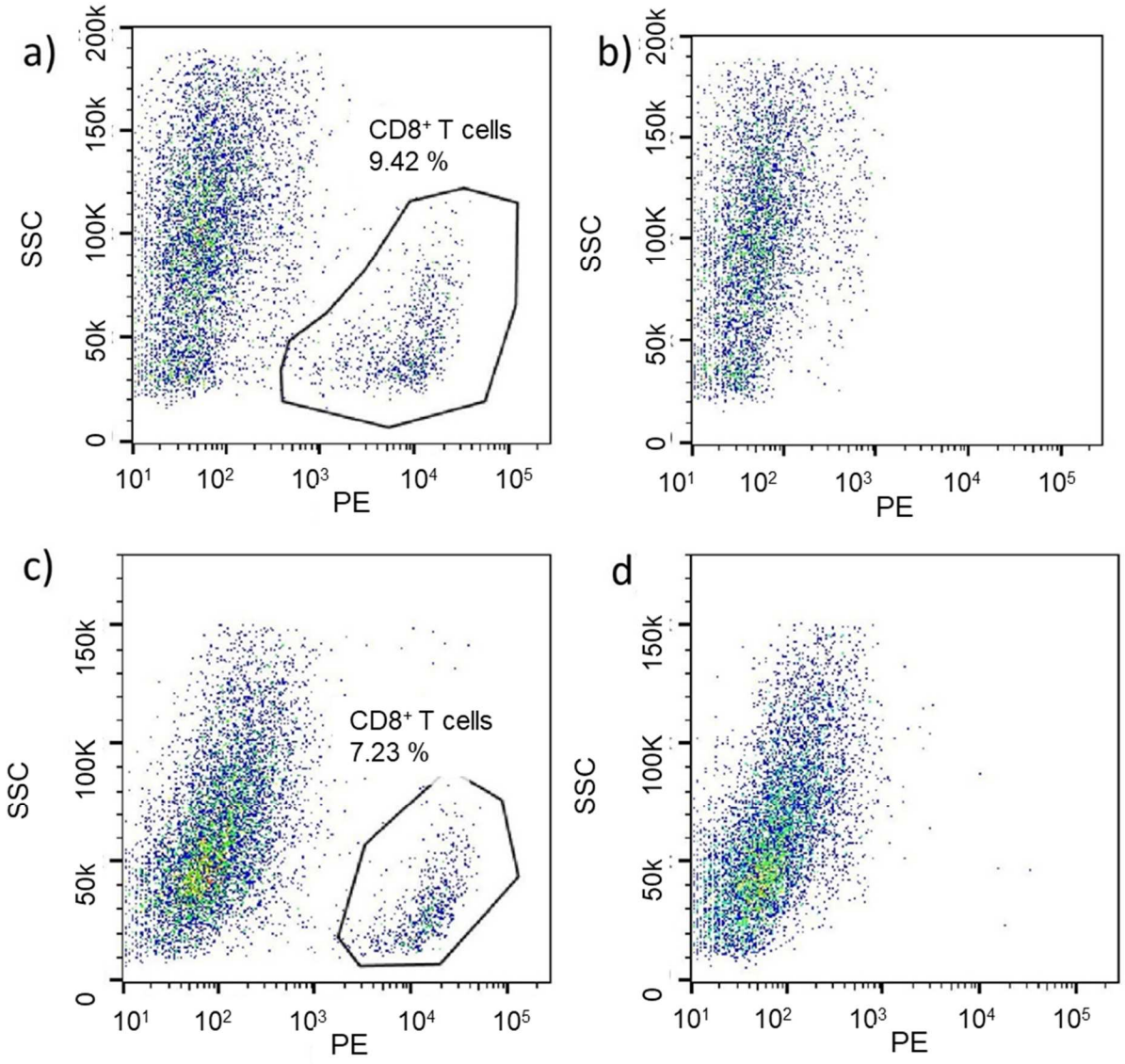

Figure 2.10 Determination of percentage of $CD8^+$ T cells present in **a)**, **b)** subcutaneous EL4 tumor , and **c)**, **d)** subcutaneous MC38 tumor by FACS. The tumor tissues were removed from mice and single cell suspensions were generated. The cells were then stained with PE labeled anti CD8 mAb (**a** and **c**), and PE labeled isotype control (**b** and **d**). In EL4 cells, 9.42% of tumor associated cells are $CD8^+$, while 7.23% of cells isolated from MC38 tumor are $CD8^+$. These indicate that there were large numbers of $CD8^+$ T cells in tumor tissues.

2.2.4 CTLp□Ac□Dex□MPs delivered the CTLp into tumor tissues

To better understand the protective effects of CTLp-Ac-Dex-MPs *via* systemic administration, the delivery of CTLp to tumor environment was evaluated. Dr. Kavunja evaluated the presence of CTLps in tumor tissues. Naïve mice bearing 300 mm^3 EL4 tumor were administered intravenously with CTLp-Ac-Dex-MPs *via* tail vein. The mice were euthanized 9 h post-injection with the tumors harvested. Both FACS analysis of tumor cell suspension (**Figure 2.11**) and tumor tissue histopathology staining (**Figure 2.12a**) showed a significant enhancement in cellular fluorescence, suggesting the successful epitope delivery and MHC-I presentation by cells in tumor tissues. The confocal images of tumor tissue histopathology staining also revealed the co-localization of the red (CTLp/MHC-I) and green (CD11b) colors (**Figure 2.12c**) indicating that CTLp was presented by tumor stromal cells as well. In contrast, tumor obtained from mice injected with free CTLp gave little staining by the mAb 25-D1.16 (**Figure 2.12d**), possibly due to unfavorable pharmacokinetics and limited half-life of the free peptide *in vivo*.[26]

I further analyzed the CTLp distribution in different organs with MC38-bearing mice (**Figure 2.13**). Naïve mice bearing 300 mm^3 sized MC38 tumor were injected with CTLp-Ac-Dex-MPs intravenously *via* tail vein. The mice were euthanized 9 h post-injection with the tumors, livers, spleens and lungs harvested. Single cell suspensions were prepared from these organs followed by staining with mAb25-D1.16 for detection of CTLp-MHC I complexes or an isotype control mAb and subjected to flow cytometry analysis. The presence of CTLp in different organs was examined

in PBS or CTLp-Ac-Dex-MP-treated mice by the mean fluorescence intensities (MFI) upon mAb25-D1.16 incubation *vs* those from isotype control. A significant enhancement of CTLp bounded MHC-I signal was observed in tumor tissue compared to PBS treated mice (**Figure 2.13**), which indicated MP enrichment in tumor tissue and a successful CTLp delivery. This result is consistant with the previous mentioned data collected from EL4 tumor (**Figure 2.11** and **Figure 2.12**). The favorable distribution of MPs in tumor tissues can be explained by the enhanced permeability and retention effect.[15-16] There were negligible changes of CTLp presented by MHC-I in spleens and lungs, while higher mean level of CTLp was found in livers compared to PBS-treated mice (**Figure 2.13**). The distribution of CTLps in liver but not lung and spleen indicates that a major pathway for MP clearance is through the liver, which is common for many particle-based systems.[27] No autoimmune responses or liver toxicities were observed during the current study.

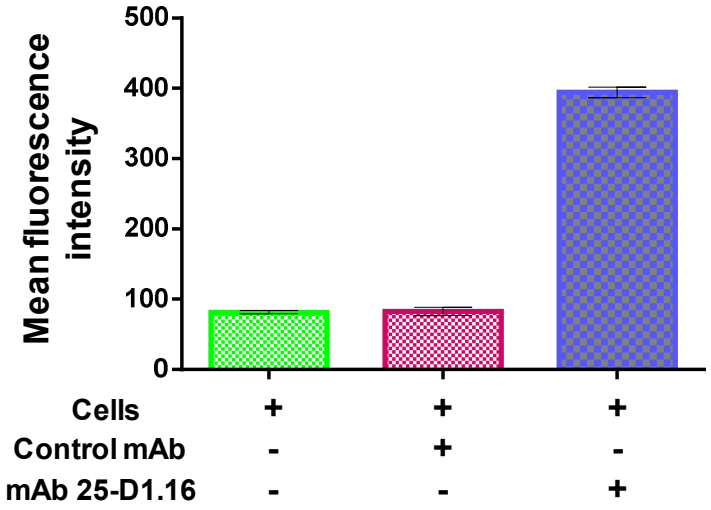

Figure 2.11 MHC I presentation of CTLp in tumor tissue. Flow cytometry analysis of cells from subcutaneous EL4 tumor tissues harvested from a representative mouse receiving intravenous injection of CTLp-Ac-Dex-MPs showed much higher fluorescence intensities when stained with

Figure 2.11 (cont'd) mAb25-D1.16 compared to those with an isotype control mAb. This suggested successful delivery and MHC-I cross-presentation of CTLp by cells in tumor tissues. (Data collected by Dr. Kavunja)

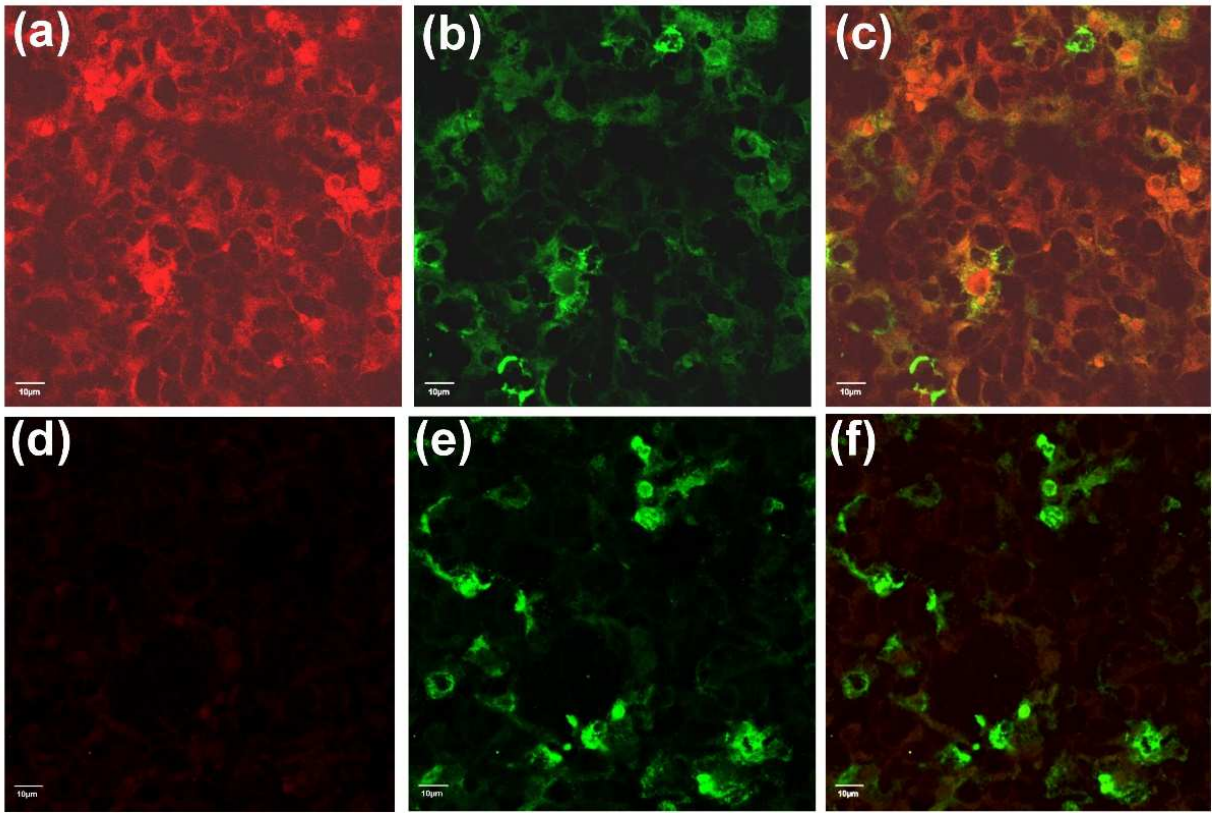

Figure 2.12 Confocal microscopy images of tumor tissues from mice receiving intravenous injection of **a**–**c** CTLp-Ac-Dex-MPs and **d**–**f** free CTLp. **a**, **d** Red channel showing PE-labeled mAb 25-D1.16 detecting CTLp/MHC-I H-2Kb complexes; **b**, **e** Green channel showing FITC-labeled anti-CD11b, a marker for stromal cells; **c** Overlay of panels **a** and **b**; **f** Overlay of panels **d** and **e**. The scale bar is 10 μm. The significantly higher intensities of red color in panel **a** *versus* **d** indicate higher amounts of CTLp/MHC-I complexes in tumor tissues of mice receiving CTLp-Ac-Dex-MPs (Data collected by Dr. Kavunja)

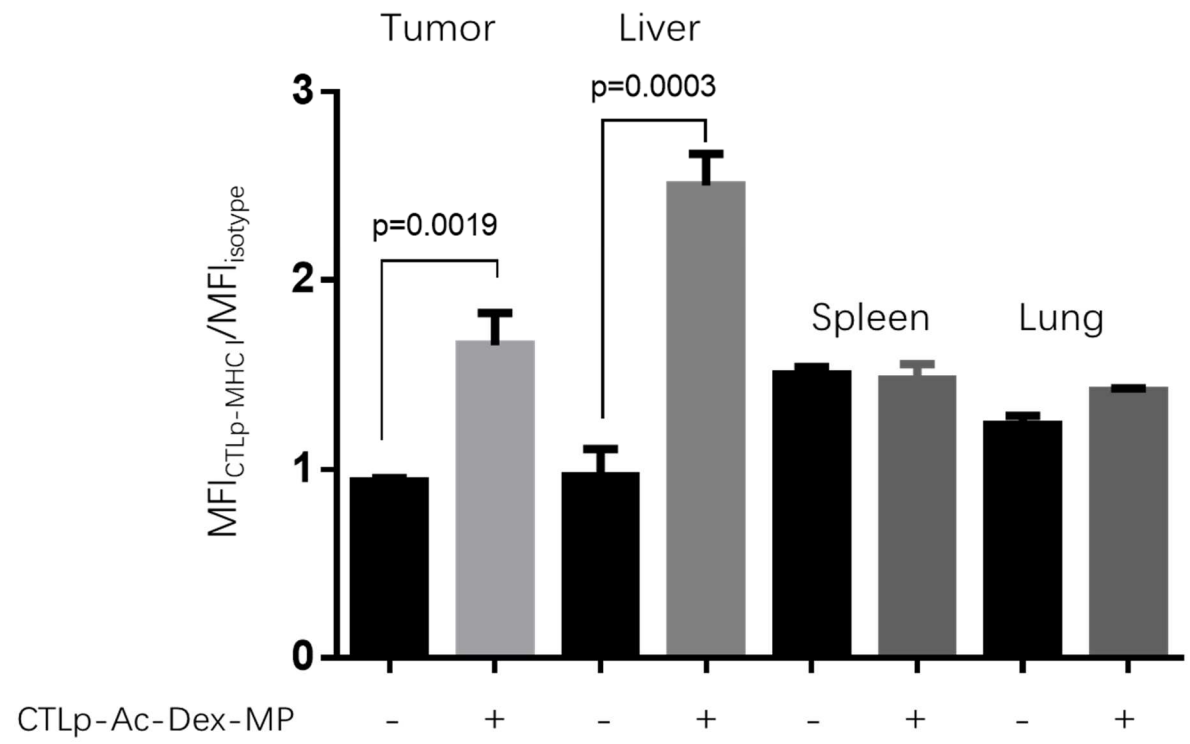

Figure 2.13 CTLp distribution in different organs. Two groups of mice were prepared bearing subcutaneous MC38 tumor. One group of these mice were administered CTLp-Ace-Dex-MPs intravenously and the other group received PBS injection. After 9 hours, mice were sacrificed. Their tumor, liver, spleen and lung were harvested and single cell suspensions were prepared from these organs. The cells were stained with mAb25-D1.16 for detection of CTLp-MHC I complexes or an isotype control mAb and subjected to flow cytometry analysis. The mean fluorescence intensities (MFI) upon mAb25-D1.16 incubation vs those from isotype control were plotted. Compared to mice receiving PBS only, the mice receiving CTLp-Ac-Dex-MPs gave much higher intensities of mAb25-D1.16 staining in tumor and liver, while spleen and lung did not show much change. T test was used for statistical analysis.

Besides delivery of CTLp to tumor tissues, the possibility that CTLp-MPs elicit CTL responses directly *in vivo* has been investigated. To test this possibility, CTLp-MPs, free CTLp, CTLp admixed with MPs were injected intravenously into naïve mice at equivalent amounts of 20 μg peptide. Mice immunized with ovalbumin were used as a positive control. CTL activities were

evaluated in these mice via the *in vivo* CFSE CTL assay. Interestingly, even without any exogenous adjuvant, CTLp-MPs were able to induce SIINFEKL-specific CTL responses 7 days after intravenous injection leading to reduced viabilities of CTLp-bearing cells to a similar extent as the positive control (**Figure 2.14**). By day 14, the CTL activities waned. In comparison, mice receiving free CTLp or empty MPs admixed with free CTLp without encapsulation did not elicit much CTLp-specific responses. These results suggest that empty Ac-Dex-MPs do not non-specifically boost immune responses. The superior protection bestowed by CTLp-Ac-Dex-MPs compared to free CTLp could be attributed to enhanced CTLp delivery to tumor tissues and/or the additional CTLp-specific CTLs generated by CTLp-Ac-Dex-MPs.

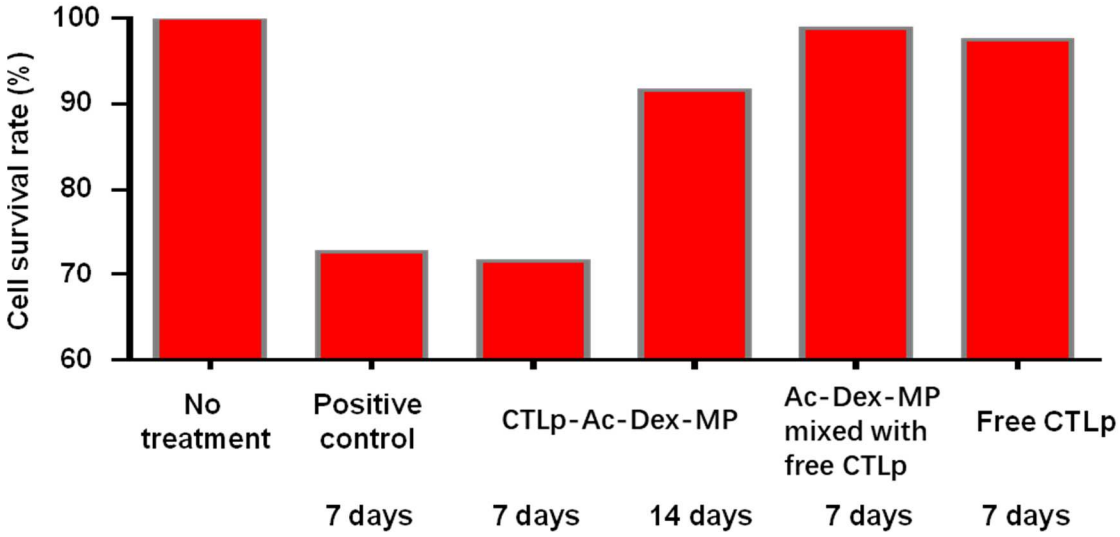

Figure 2.14 *In vivo* CTL activity assays. Mice were injected with CTLp-Ac-Dex-MP, Ac-Dex-MP mixed with CTLp or free CTLp (20 μg), respectively, every other day with a total of three injections. The positive control is ovalbumin-immunized mice. The time indicated is the number of days after the final injection. CFSE-labeled live CTLp pulsed cells were then injected into the mice and isolated from lymph nodes and spleens 24 h after injection. Mice with high CTL activities led to lower relative survival rates of CFSE-labeled live CTLp pulsed cells. Cells isolated from lymph nodes and spleens gave similar results that CTLp-Ac-Dex-MPs could induce SIINFEKL-specific CTLs, while Ac-Dex-MPs admixed with CTLp or free CTLp was ineffective.

2.2.5 Future outlooks

Development of novel constructs that can provide powerful immune protection against tumor development is of high current interests. While particle-based antitumor vaccine constructs have been investigated,[28] they have been primarily aimed at targeting professional antigen-presenting cells. At the same time, most of the studies on introducing foreign antigenic epitopes to tumor did not include a delivery system and therefore required administration of antigens locally to tumor.[29-31] Recently, a novel hyaluronic acid–OVA protein conjugate was shown to transport OVA epitopes to tumor cells upon systemic administration[32]. In comparison, our approach delivers foreign epitopes to tumor cells as well as stromal cells utilizing pH-responsive MPs.

Innovative studies have been performed using Ac-DEX MPs for cargo delivery.[18, 33-35] Our study is the first time that Ac-DEX-MPs were shown to be effective in delivering small peptides to tumor microenvironment to enhance antitumor immunotherapy. Compared to intratumoral injection, intravenous administration of CTLp-Ac-Dex-MPs did not provide complete protection of the mice from tumor-induced death. This may be due to lower concentration of CTLp reaching the tumor tissue upon systematic administration, which could be improved by increasing the frequency of injections and optimization of the injection protocol. Furthermore, tumor tissue targeting ligands can be installed onto MPs to enhance tumor selectivity and reduce the amounts of CTLp reaching other organs such as liver.

SIINFEKL epitope from ovalbumin was selected as the CTLp due to its high affinity with MHC-I H-2Kb and efficient MP encapsulation. For potential future translations to human patients, as many people have been immunized against diseases such as papillomavirus and hepatitis B infection, high-affinity lipophilic CTL epitopes can be selected from these viruses[36-37] to match MHC-I haplotypes of the subjects. Patients may already have memory CTLs[38] against these epitopes from prior immunizations enabling ready expansion of epitope-specific CTLs to combat tumor. In addition, antigen delivery to tumor tissues can be combined with other promising antitumor immunotherapy strategies to increase the protective efficiencies. For example, mAbs capable of blocking immune regulatory checkpoints[39] can enhance antitumor functions of CTLs. Combination of CTLp delivery and immune checkpoint inhibition can provide synergistic effects on tumor protection. These considerations suggest the potential for clinical translation using MPs for CTLp delivery.

2.3 Conclusion

In conclusion, we have demonstrated that acid-responsive MPs can deliver foreign high-affinity CTLp to tumor tissues and release CTLp for presentation by MHC-I on both tumor and stromal cells. CTLp delivery by MPs to two models of ALV solid tumor led to significant reduction of tumor growth. The simplicity and versatility of the MP system coupled with its antitumor efficacy suggest that it can be a promising new direction to enhance the efficacy of CTL therapy against established solid tumor.

2.4 Experimental methods

2.4.1 Materials and instrumentation

All chemicals were reagent grade and were used as received from the manufacturer unless otherwise indicated. Fetal bovine serum (FBS), phosphate buffered saline (PBS), high glucose Dulbecco's modified Eagle medium (DMEM), Dulbecco's modified Eagle medium nutrient mixture F-12 Ham (DMEM/F12), complete Freund's adjuvant (CFA), incomplete Freund's adjuvant (IFA), RPMI-1640, ovalbumin (OVA), chlorophenol red-β-D-galactopyranoside (CPRG), dimethyl sulfoxide cell culture grade, pyruvate, acetonitrile HPLC grade, pyridinium p-toluenesulfonate, triisopropylsilane (TIPS), dextran (Mw =9,000-11,000 g/mol), sodium azide (NaN_3), *N,N*-dimethylformamide (DMF), dichloromethane (DCM) were purchased from Sigma Aldrich. Methoxypropene, anhydrous DMSO and *N,N*-diisopropylethylamine were purchased from Acros. Hydroxybenzotriazole (HOBt), *O*-(benzotriazol-1-yl)-*N,N,N′,N′*-tetramethyluronium hexafluorophosphate (HBTU), Fmoc protected amino acids were was purchased from Chem Impex international. Piperidine, polyvinyl alcohol (PVA, Mw = 13,000 – 23,000 g/mol, 86-89% hydrolyzed) was purchased from Alfa Aesar. Regular and HPLC grade trifluoroacetic acid (TFA) was purchased from EMD millipore. L-glutamine, streptomycin, penicillin, collagenase type IV and Hank's balanced salt solution were purchased from Gibco.

Scanning electron microscopy (SEM) images were acquired on the 7500F ultra-high resolution scanning electron microscope. FACS data was acquired using LSR II flow cytometer

analyzer and analyzed by FlowJo_V10 software. Confocal microscopy images were acquired using an Olympus FluoView 1000 LSM confocal microscope. Dynamic light scattering (DLS) was performed on a Zetasizer Nano zs apparatus (Malvern, UK).

2.4.2 Procedure for CTLp synthesis

The CTLp was synthesized through solid phase peptide synthesis using Fmoc chemistry. The procedures for SIINFEKL are: the Fmoc protected leucine resin in a syringe was swollen overnight in DCM at room temperature. The DCM was discarded and Fmoc was removed by adding 20% piperidine in DMF and keep constant rotation (20 minutes, twice). At the end of the 40 minutes the solution was discarded, and the resin was washed with DMF 4 times followed by DCM 4 times. Lysine's free carboxylic acid was activated with HBTU, HOBt and DIPEA base in anhydrous DMF (10 mL) for 30 minutes. The activated lysine was added to the washed resin and the coupling reaction left to proceed for 10 h at room temperature. After the reaction, the solution in the syringe was discarded and the resin washed 3 times with DMF followed by 3 times with DCM. Fmoc was deprotected and the resin was washed as previous described. The next activated amino acid was added and the procedure was repeated until all the amino acids had been coupled. Fmoc on the final amino acid was removed as previous described. The peptide was cleaved from the resin by a solution containing 95% TFA, 2.5% MilliQ water, and 2.5% TIPS. At this acidic condition, all the protecting groups were cleaved. Excess TFA was removed by evaporation on a rotavap followed by precipitation in diethylether and centrifugation until the resultant diethylether

supernatant was clear. The peptide was air dried in the hood overnight, dissolved in minimum amount of DMSO and purified by HPLC using 0.1% TFA MilliQ water and acetonitrile over a C18 column (2% acetonitrile to 100% acetonitrile in 40 minutes). Successful coupling was confirmed by ESI mass spectrometry.

2.4.3 Preparation of CTLp-Ac-Dex-MPs

CTLp-Ac-Dex-MPs were prepared by an emulsion evaporation method.[20]

Ac-Dex was synthesized following a published procedure[18]. To a solution of dextran (MW = 9-11 kDa, 1.00 g, 0.1 mmol) in anhydrous DMSO (10 mL) under nitrogen pyridinium *p*-toluenesulfonate (16 mg, 0.06 mmol) was added followed by 2-methoxypropene (3 mL, 34 mmol). After 3 hours, the reaction was quenched with triethylamine (1 mL) and the modified dextran was precipitated from the reaction mixture with addition of water (100 mL). The mixture was centrifuged and the resulting pellet was washed thoroughly with water by vortexing and sonication followed by centrifugation and removal of the supernatant. The residual water was removed by lyophilization, yielding Ac-Dex (1.0 g) as a fine white powder.

Ac-Dex (200 mg) was dissolved in DCM (1 mL) and added to a solution of CTLp (10 mg) in DMSO (50 μL). This mixture was emulsified by sonicating for 30 seconds on ice using a probe sonicator (Branson Digital Sonifier 250) with a duty cycle of 20%. An aqueous solution of PVA (2 mL, 3% w/v in PBS) was added to the emulsion and sonicated for an additional 30 seconds on ice using the same setting except that the duty cycle was increased to 30%. The resulting emulsion

was immediately poured into a second PVA solution (10 ml, 0.3% w/v in PBS) and stirred for 4 h allowing the organic solvent to evaporate. The particles were isolated by centrifugation (10,000 RPM, 20 min) and washed with PBS (30 mL) and MilliQ-H_2O (2 x 30 mL, pH 8) by vortexing and sonication followed by centrifugation and removal of the supernatant. The washed particles were resuspended in MilliQ-H_2O (2 mL, pH 8) and lyophilized to yield a white fluffy solid of CTLp-Ac-Dex-MP. Empty particles without the peptide (Ac-Dex-MP) were prepared following the same procedures omitting the CTLp.

2.4.4 Hydrolysis of CTLp-Ac-Dex-MPs and CTLp release from CTLp-Ac-Dex-MPs

Solutions of CTLp-Ac-Dex-MPs (4 mg/ml) were prepared in pH = 7.4, 6.5, 6 or 5.5 PBS buffer respectively. These stock solutions were kept under room temperature or in 37 □ water bath. UV-vis absorption at 600nm were measured every 1 - 4 hours over 72 hours. In order to measure CTLp release rates, CTLp-Ac-Dex-MPs were dissolved in 4 ml of pH 7.4, 6.5, 6.0 and 5.5 PBS buffer or RPMI-1640 cell culture media respectively. Each stock solution was divided into 4 Eppendorf tubes (1 ml each) and incubated at 37 □. At each time point (6, 12, 24, 48 h), one Eppendorf tube from each group was taken out and centrifuged (10,000 rpm, 15 min). The pellets were collected and dissolved in 0.5 ml H2O/trifluoroacetic acid (pH = 1), which were followed by HPLC quantification using a standard curve (Appendix **Figure 2.15**).

2.4.5 Animals and Cell Lines

Pathogen free female C57BL/6 mice age 6 - 10 weeks were obtained from Charles River. EL4 cells were generously donated by Dr. Sandra Gendler (Mayo clinic). Cells were cultured in RPMI medium 1640 supplemented with 10 % FBS, 1% L-glutamine, and 1% streptomycin penicillin. B3Z cells was generously donated by Dr. Nilabh Shastri (University of California, Berkeley). These cells were cultured in RPMI-1640 supplemented with 10% FBS, 1 mM pyruvate, 50 μM 2-mercaptoethanol, 1% L-glutamine, and 1% streptomycin penicillin. MC38 cells were cultured in DMEM medium supplement with 10% FBS, 1% L-glutamine, 1mM sodium pyruvate, 0.1mM non-essential amino acid and 1% streptomycin penicillin. All cell lines were grown at 37 °C in a 5% CO_2/air incubator.

2.4.6 Detection of CTLp Presentation on MHC-I of EL4 cells by FACS

EL4 cells were pulsed with increasing concentrations of either free CTLp or CTLp-Ac-Dex-MPs and incubated at 37 °C in a 5% CO_2/air incubator for 1 hour. Cells were washed 3 times with FACS buffer (1 % FBS, 0.5 % NaN_3 in PBS), stained with either anti-mouse H-2Kb bound to SIINFEKL (Clone 25-D1.16) or anti-mouse IgG1K (isotype control) for 30 minutes in FACS buffer on ice then washed with FACS buffer three times followed by FACS analysis. Control mAb showed little cellular staining over background. In contrast, a dose dependent increase of cellular fluorescence intensity was observed with mAb 25-D1.16 (**Figure 2.4**).

2.4.7 B3Z T Cell Activation Assay

2 x 10^4 EL4 cells were cultured overnight in a 96 well plate and subsequently incubated with CTLp-Ac-Dex-MPs or free CTLp at increasing concentrations. After 6 hours, the cells were washed and 1x10^5 B3Z cells were added to the EL4 cells and co-cultured for an additional 16 hours. The culture media was removed and 100 μL of CPRG buffer (9.1 mg of CPRG, 0.1% triton-X and 90 mg MgCl2 in 100 mL of PBS) was added to each well. After 6 hours, the absorbance at 595 nm was measured using a microplate reader. The results were presented as a mean quadruplicate.

2.4.8 Tumor protection studies against EL4 and MC38 tumor

C57BL/6 wild-type mice were immunized subcutaneously under the scruff on day 0 with 0.1 mL of ovalbumin (50 μg) as an emulsion in complete Freund's adjuvant. Boosters were given on days 14 and 28 with emulsion in incomplete Freund's adjuvant. The mice were inoculated with subcutaneous tumor (2×10^5 EL4 or 5×10^5 MC38 cells were injected) on the left flank on day 35. When the tumor size was about 70–90 mm^3, intratumoral injection of either CTLp-Ac-Dex-MPs, free CTLp, empty Ac-Dex-MPs, or PBS was performed every other day for a total of three injections (10 mice per study group). For the groups where treatment was via intravenous injection, mice were treated when tumor size was about 20–30 mm^3 (usually on day 3 following tumor inoculation). The amounts of injected CTLp were normalized to 7 μg for intravenous injection and 20 μg for intravenous injection. Tumor volume was determined using the formula: volume $(cm)^3$

= 1/2(L ×W× H).[40] Tumor growth was monitored by measuring the tumor volume every other day. Mice were euthanized when the tumor volume was over 1.6 cm^3 or ulceration of tumor was observed.

2.4.9 *In vivo* CTL activity assay

To evaluate CTL activities induced by MP, naïve mice were injected intravenously through tail vein with 1 mg CTLp-Ac-Dex-MP (with 20 μg OVA peptide encapsulated), 1 mg MP (empty) + 20 μg CTLp, or 20 μg CTLp, respectively, every other day with a total of three injections. On day 7 after the final injection, a mixture of $CFSE^{lo}$- and CTLp pulsed $CFSE^{hi}$ splenic cells (0.2 ml, 2 million cells) was injected through tail vein to mice. The excess cell mixture was stored in culture media under 37 °C as a "before injection" sample. Mice were euthanized after 24 h. Spleen cells were collected and then suspended in 3 ml FACS buffer containing 30 μg/ml 7-aminoactinomycin D (7-AAD). Three to four lymph nodes were collected from each mouse. Lymph nodes were set in same Petri dish, smashed and filtered to create lymph node cell samples. Cells were washed twice with PBS buffer and suspended in 1 ml FACS buffer containing 10 μg/ml 7-AAD. The changes of ratio of $CFSE^{hi}$ to $CFSE^{lo}$ before and after injection were determined from FITC-SSC plot to calculate target cell viability.

2.4.10 CTLp distribution in organs and quantification of $CD8^+$ T cell infiltration in tumor

C57BL/6 mice with established subcutaneous MC38 tumor (~300 mm^3) were injected with CTLp-Ac-Dex-MPs (20 μg CTLp) or PBS. Animals were euthanized 9 h post-injection. Organs

(spleen, liver, lung and tumor) were collected from each mouse and digested into single-cell suspension with collagenase IV (1 mg/ml in DMEM-F12 media) followed by washing with PBS buffer twice. Cells were stained with anti-mouse H-2Kb bound to SIINFEKL (Clone 25-D1.16) or anti-mouse IgG1K (isotype control) for 30 min in FACS buffer on ice and then washed with FACS buffer three times followed by FACS analysis. Mean fluorescence intensity ratio of 25-D1.16 mAb-stained group versus isotype control group was recorded for each organ. In addition, single-cell suspension of tumor from PBS group was stained with PE–anti-mouse CD8a mAb or PE–anti-IgGa Ab (isotype control). FACS analysis was performed to determine the percentage of $CD8^+$ T cells in tumor.

2.4.11 $CD8^+$ T cell infiltration in tumor

EL4 ($2x10^5$) or MC38 ($5x10^5$) cells were injected to C57BL/6 mice subcutaneously. Tumor tissue was collected when tumor size reached ~$300mm^3$. Collagenase IV (1mg/ml) in DMEM-F12 media was used to digest tumor tissue for single cell suspension preparation. The resulting cell suspension was then washed with Hank's Balanced Salt Solution (HBSS) supplemented with 2% FBS twice and resuspended in FACS buffer. Cells were then stained with PE-Anti mouse CD8a mAb or PE-Anti IgG2a,κ mAb (Isotype control) on ice in dark for 30min followed by washing with FACS buffer twice. FACS analysis was done to determine percentage of $CD8^+$ T cell population.

APPENDIX

APPENDIX

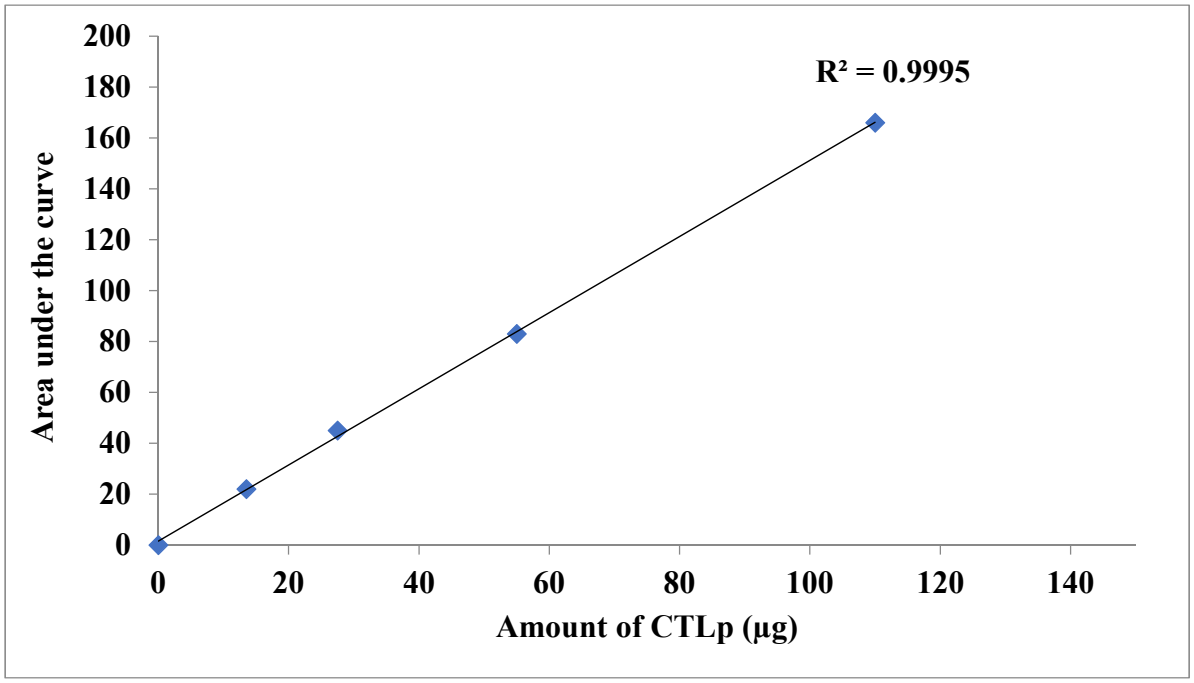

Figure 2.15 Calibration curve between the amounts of CTLp and areas of integration from HPLC chromatograms. (Data collected by Dr. Kavunja)

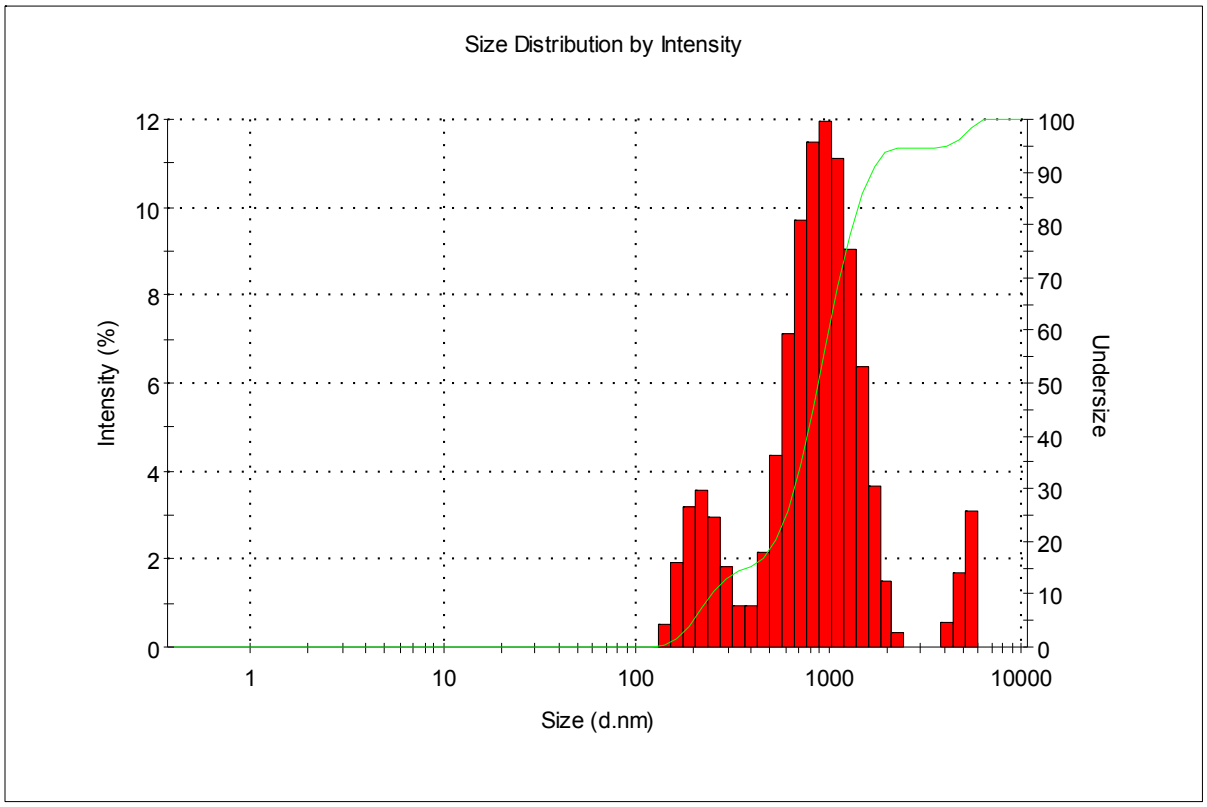

Figure 2.16 DLS analysis of Ac-Dex MPs.

REFERENCES

REFERENCES

1. Kavunja, H. W.; Lang, S.; Sungsuwan, S.; Yin, Z.; Huang, X., Delivery of Foreign Cytotoxic T Lymphocyte Epitopes to Tumor Tissues for Effective Antitumor Immunotherapy Against Pre-established Solid Tumors in Mice. *Cancer Immunol. Immunother.* **2017,** *66*, 451-460.

2. Melero, I.; Gaudernack, G.; Gerritsen, W.; Huber, C.; Parmiani, G.; Scholl, S.; Thatcher, N.; Wagstaff, J.; Zielinski, C.; Faulkner, I., Therapeutic Vaccines for Cancer: An Overview of Clinical Trials. *Nat. Rev. Clin. Oncol.* **2014,** *11*, 509-524.

3. June, C. H., Adoptive T Cell Therapy for Cancer in the Clinic. *J. Clin. Invest.* **2007,** *117*, 1466-1476.

4. Klein, L.; Kyewski, B.; Allen, P. M.; Hogquist, K. A., Positive and Negative Selection of the T cell Repertoire: What Thymocytes See (and don't see). *Nat. Rev. Immunol.* **2014,** *14*, 377-391.

5. Uyttenhove, C.; Maryanski, J.; Boon, T., Escape of Mouse Mastocytoma P815 After Nearly Complete Rejection is Due to Antigen-loss Variants Rather than Immunosuppression. *J. Exp. Med.* **1983,** *157*, 1040-1052.

6. Khong, H. T.; Restifo, N. P., Natural Selection of Tumor Variants in the Generation of "Tumor Escape" Phenotypes. *Nat. Immunol.* **2002,** *3*, 999-1005.

7. Lakshminarayanan, V.; Supekar, N. T.; Wei, J.; McCurry, D. B.; Dueck, A. C.; Kosiorek, H. E.; Trivedi, P. P.; Bradley, J. M.; Madsen, C. S.; Pathangey, L. B., MUC1 Vaccines, Comprised of Glycosylated or Non-glycosylated Peptides or Tumor-derived MUC1, Can Circumvent Immunoediting to Control Tumor Growth in MUC1 Transgenic Mice. *PLoS One* **2016,** *11*, e0145920.

8. Dunn, G. P.; Bruce, A. T.; Ikeda, H.; Old, L. J.; Schreiber, R. D., Cancer Immunoediting: From Immunosurveillance to Tumor Escape. *Nat. Immunol.* **2002,** *3*, 991-998.

9. Ward, P. L.; Koeppen, H. K.; Hurteau, T.; Rowley, D. A.; Schreiber, H., Major histocompatibility complex class I and unique antigen expression by murine tumors that escaped from CD8+ T-cell-dependent surveillance. *Cancer Res.* **1990,** *50*, 3851-3858.

10. Tlsty, T. D.; Coussens, L. M., Tumor Stroma and Regulation of Cancer Development. *Annu. Rev. Pathol. Mech. Dis.* **2006,** *1*, 119-150.

11. Spiotto, M. T.; Schreiber, H., Rapid Destruction of the Tumor Microenvironment by CTLs Recognizing Cancer-specific Antigens Cross-presented by Stromal Cells. *Cancer Immun.* **2005,** *5*, 8.

12. Schietinger, A.; Philip, M.; Liu, R. B.; Schreiber, K.; Schreiber, H., Bystander killing of Cancer Requires the Cooperation of $CD4^+$ and $CD8^+$ T cells During the Effector Phase. *J. Exp. Med.* **2010,** *207*, 2469-2477.

13. Spiotto, M. T.; Rowley, D. A.; Schreiber, H., Bystander Elimination of Antigen Loss Variants in Established Tumors. *Nat. Med.* **2004,** *10*, 294-298.

14. Gao, W.; Chan, J. M.; Farokhzad, O. C., pH-Responsive Nanoparticles for Drug Delivery. *Mol. Pharmaceutics* **2010,** *7*, 1913-1920.

15. Prabhakar, U.; Maeda, H.; Jain, R. K.; Sevick-Muraca, E. M.; Zamboni, W.; Farokhzad, O. C.; Barry, S. T.; Gabizon, A.; Grodzinski, P.; Blakey, D. C., Challenges and Key Considerations of the Enhanced Permeability and Retention Effect for Nanomedicine Drug Delivery in Oncology. *Cancer Res.* **2013,** *73*, 2412-2417.

16. Maeda, H.; Bharate, G. Y.; Daruwalla, J., Polymeric Drugs for Efficient Tumor-targeted Drug Delivery Based on EPR-effect. *Eur. J. Pharm. Biopharm.* **2009,** *71*, 409-419.

17. Tannock, I. F.; Rotin, D., Acid pH in Tumors and Its Potential for Therapeutic Exploitation. *Cancer Res.* **1989,** *49*, 4373-4384.

18. Bachelder, E. M.; Beaudette, T. T.; Broaders, K. E.; Dashe, J.; Fréchet, J. M. J., Acetal-derivatized Dextran: An Acid-responsive Biodegradable Material for Therapeutic Applications. *J. Am. Chem. Soc.* **2008,** *130*, 10494-10495.

19. Apostolopoulos, V.; Haurum, J. S.; McKenzie, I. F. C., MUC1 Peptide Epitopes Associated with Five Different H□2 Class I Molecules. *Eur. J. Immunol.* **1997,** *27*, 2579-2587.

20. Bilati, U.; Allémann, E.; Doelker, E., Sonication Parameters for the Preparation of Biodegradable Nanocapsulesof Controlled Size by the Double Emulsion Method. *Pharm. Dev. Technol.* **2003,** *8*, 1-9.

21. Eisen, H. N.; Hou, X. H.; Shen, C.; Wang, K.; Tanguturi, V. K.; Smith, C.; Kozyrytska, K.; Nambiar, L.; McKinley, C. A.; Chen, J., Promiscuous Binding of Extracellular Peptides to Cell Surface Class I MHC Protein. *Proc. Natl. Acad. Sci. U. S. A.* **2012,** *109*, 4580-4585.

22. Karttunen, J.; Shastri, N., Measurement of Ligand-induced Activation in Single Viable T Cells Using the lacZ Reporter Gene. *Proc. Natl. Acad. Sci. U. S. A.* **1991,** *88*, 3972-3976.

23. Ke, Y.; Li, Y.; Kapp, J. A., Ovalbumin Injected with Complete Freund's Adjuvant Stimulates Cytolytic Responses. *Eur. J. Immunol.* **1995,** *25*, 549-553.

24. Durward, M.; Harms, J.; Splitter, G., Antigen Specific *in vivo* Killing Assay using CFSE Labeled Target Cells. *J. Vis. Exp.* **2010**, e2250.

25. Breart, B.; Lemaître, F.; Celli, S.; Bousso, P., Two-photon Imaging of Intratumoral $CD8^+$ T Cell Cytotoxic Activity During Adoptive T Cell Therapy in Mice. *J. Clin. Invest.* **2008,** *118*, 1390-1397.

26. Fosgerau, K.; Hoffmann, T., Peptide Therapeutics: Current Status and Future Directions. *Drug Discovery Today* **2015,** *20*, 122-128.

27. Varna, M.; Ratajczak, P.; Ferreira, I.; Leboeuf, C.; Bousquet, G.; Janin, A., *In vivo* Distribution of Inorganic Nanoparticles in Preclinical Models. *J. Biomater. Nanobiotechnol.* **2012,** *3*, 269-279.

28. Shao, K.; Singha, S.; Clemente-Casares, X.; Tsai, S.; Yang, Y.; Santamaria, P., Nanoparticle-based Immunotherapy for Cancer. *ACS Nano* **2015,** *9*, 16-30.

29. Kang, T. H.; Knoff, J.; Yang, B.; Tsai, Y.-C.; He, L.; Hung, C.-F.; Wu, T. C., Control of Spontaneous Ovarian Tumors by $CD8^+$ T Cells Through NKG2D-targeted Delivery of Antigenic Peptide. *Cell Biosci.* **2013,** *3*, 48.

30. Song, L.; Yang, M.-C.; Knoff, J.; Sun, Z.-Y.; Wu, T. C.; Hung, C.-F., Cancer Immunotherapy Using a Potent Immunodominant CTL Epitope. *Vaccine* **2014,** *32*, 6039-6048.

31. Kanzaki, M.; Okamoto, T.; Mitsui, H.; Shibagaki, N.; Shimada, S., A Novel Immunotherapeutic Approach to Melanoma-bearing Hosts with Protein-transduction Domain-containing Immunogenic Foreign Antigens. *J. Dermatol. Sci.* **2010,** *60*, 84-94.

32. Lee, Y.-H.; Yoon, H. Y.; Shin, J. M.; Saravanakumar, G.; Noh, K. H.; Song, K.-H.; Jeon, J.-H.; Kim, D.-W.; Lee, K.-M.; Kim, K., A Polymeric Conjugate Foreignizing Tumor Cells for Targeted Immunotherapy *in vivo*. *J. Controlled Release* **2015,** *199*, 98-105.

33. Cohen, J. A.; Beaudette, T. T.; Cohen, J. L.; Broaders, K. E.; Bachelder, E. M.; Fréchet, J. M. J., Acetal□modified Dextran Microparticles with Controlled Degradation Kinetics and Surface

Functionality for Gene Delivery in Phagocytic and Non□phagocytic Cells. *Adv. Mater.* **2010,** *22*, 3593-3597.

34. Peine, K. J.; Guerau-de-Arellano, M.; Lee, P.; Kanthamneni, N.; Severin, M.; Probst, G. D.; Peng, H.; Yang, Y.; Vangundy, Z.; Papenfuss, T. L., Treatment of Experimental Autoimmune Encephalomyelitis by Codelivery of Disease Associated Peptide and Dexamethasone in Acetalated Dextran Microparticles. *Mol. Pharmaceutics* **2014,** *11*, 828-835.

35. Suarez, S.; Grover, G. N.; Braden, R. L.; Christman, K. L.; Almutairi, A., Tunable Protein Release from Acetalated Dextran Microparticles: A Platform for Delivery of Protein Therapeutics to the Heart Post-MI. *Biomacromolecules* **2013,** *14*, 3927-3935.

36. Feltkamp, M. C. W.; Smits, H. L.; Vierboom, M. P. M.; Minnaar, R. P.; De Jongh, B. M.; Drijfhout, J. W.; Schegget, J. T.; Melief, C. J. M.; Kast, W. M., Vaccination with Cytotoxic T lymphocyte Epitope□containing Peptide Protects Against a Tumor Induced by Human Papillomavirus Type 16□transformed Cells. *Eur. J. Immunol.* **1993,** *23*, 2242-2249.

37. Vitiello, A.; Ishioka, G.; Grey, H. M.; Rose, R.; Farness, P.; LaFond, R.; Yuan, L.; Chisari, F. V.; Furze, J.; Bartholomeuz, R., Development of a Lipopeptide-based Therapeutic Vaccine to Treat Chronic HBV Infection. I. Induction of a Primary Cytotoxic T Lymphocyte Response in Humans. *J. Clin. Invest.* **1995,** *95*, 341-349.

38. Wherry, E. J.; Ahmed, R., Memory CD8 T-cell Differentiation During Viral Infection. *J. Virol.* **2004,** *78*, 5535-5545.

39. Pardoll, D. M., The Blockade of Immune Checkpoints in Cancer Immunotherapy. *Nat. Rev. Cancer* **2012,** *12*, 252-264.

40. Tomayko, M. M.; Reynolds, C. P., Determination of Subcutaneous Tumor Size in Athymic (Nude) Mice. *Cancer Chemother. Pharmacol.* **1989,** *24*, 148-154.

CHAPTER 3 Synthesis of Carboxy-Dimethylmaleic Amide Linked Polymer Conjugates Based pH Ultrasensitive Nanoparticles for Enhanced T Cell Based Anti-Tumor Immunotherapy[1]

Adapted with permission from (Lang, S.; Tan, Z.; Wu, X.; Huang, X., Synthesis of Carboxy-Dimethylmaleic Amide Linked Polymer Conjugate Based Ultra-pH-sensitive Nanoparticles for Enhanced Antitumor Immunotherapy. *ACS Macro Letters* **2020,** *9*, 1693-1699, https://pubs.acs.org/doi/abs/10.1021/acsmacrolett.0c00755). Copyright (2020) American Chemical Society.)

3.1 Introduction

Anti-cancer vaccines are a promising new strategy for cancer prevention and treatment.[2-3] Cytotoxic T lymphocytes (CTLs) are an important component of the adaptive immune system to fight against cancer. CTLs recognize short peptide epitopes typically between 8 and 11 amino acids in length,[4] and cancer specific CTLs are capable of killing tumor cells and protecting against tumor development. However, direct administration of CTL peptides is often ineffective to induce strong CTL activation.

An appealing strategy in eliciting CTLs is utilizing macromolecular carriers to deliver peptide epitopes to immune cells or tumor tissues.[5-7] For such systems, it is desirable to build in stimuli responsive mechanisms to regenerate and release the free antigens once the vaccine reaches the targeted sites.[8-10] We hypothesize that new pH sensitive polymer-based particles capable of responding to pH values around 6.5 can be a powerful vaccine delivery system. We chose to focus

on pH 6.5 because 1) the pH values of the extracellular matrix of many tumor tissues are around 6.5.[11] The release of the cargo such as antigens and adjuvant in the tumor microenvironment can help activate the local antigen presenting cells (APCs) and CTLs for immune protection.[12-13] 2) MHC class I (MHC-I) molecules, found on the cell surface of all nucleated cells in vertebrates, are responsible for presenting the peptide antigens for CTL recognition and activation. The early endosomes with pH about 6.5 have been shown to play roles in MHC-I recycling aiding in antigen presentation and immune responses.[14-15]

In order to achieve responses around pH 6.5, we focused on a class of interesting pH sensitive polymers capable of undergoing sharp transitions within a narrow pH window.[16-19] This type of polymers has been primarily applied as innovative probes for pH sensing. [16-19] Recently, several such polymers have been utilized to non-covalently encapsulate peptides for immunotherapy against cancer.[20] Parallel to this pioneering work, herein, we describe new types of nanoparticles (NPs) based on acid sensitive methoxy poly(ethylene glycol)-b-[poly(diisopropylamino)ethyl methacrylate] (mPEG-PDPAMA) as an antigen delivery platform, which responds to pH around 6.5. mPEG-PDPAMA was designed to contain primary amine side chains, to which a CTL epitope was covalently conjugated through a carboxy-dimethylmaleic anhydride (CDM) linker. The new polymer is versatile, which could deliver not only CTL epitopes with high payload capacity, but also immune-stimulating adjuvants. The polymer conjugates were able to significantly enhance immune responses towards the CTL epitope, effectively reducing cancer development in mice.

3.2 Results and Discussions

3.2.1 Synthesis and characterization of mPEG-PDPAMA polymer

The synthesis of the mPEG-PDPAMA **3** polymer started from atom transfer radical polymerization (ATRP) of (diisopropylamino)ethyl methacrylate monomer (DPAMA) **2** with mPEG-Br initiator **1** (**Scheme 3.1a**). The resulting polymer has a number average molecular weight (Mn) of 20,500 calculated from the ratio of ^{1}H-NMR (**Scheme 3.1d**) integration values of the terminal methyl group (proton a) vs the methylene (proton e, f) and the methine (proton g) of the repeating units of the polymer, with a polydispersity index (PDI) below 1.2 (**Figure 3.1**). Titration of the polymer solution with base showed its pKa value of 6.46 (**Scheme 3.1e**). The mPEG-PDPAMA **3** formed NPs with average diameters of 109 nm when added into pH 7.4 PBS buffer under sonication (**Scheme 3.1f**). The dynamic light scattering (DLS) count rate of NP dispersion in pH 7.4 PBS buffer decreased rapidly when pH value of the solution was lowered to 6.5, reaching the background level at pH below 6.0 (**Scheme 3.1g**). The DLS results suggested the disassembly of NPs at pH between 6.0 and 6.6, consistent with the pKa value of 6.46 for the polymer.

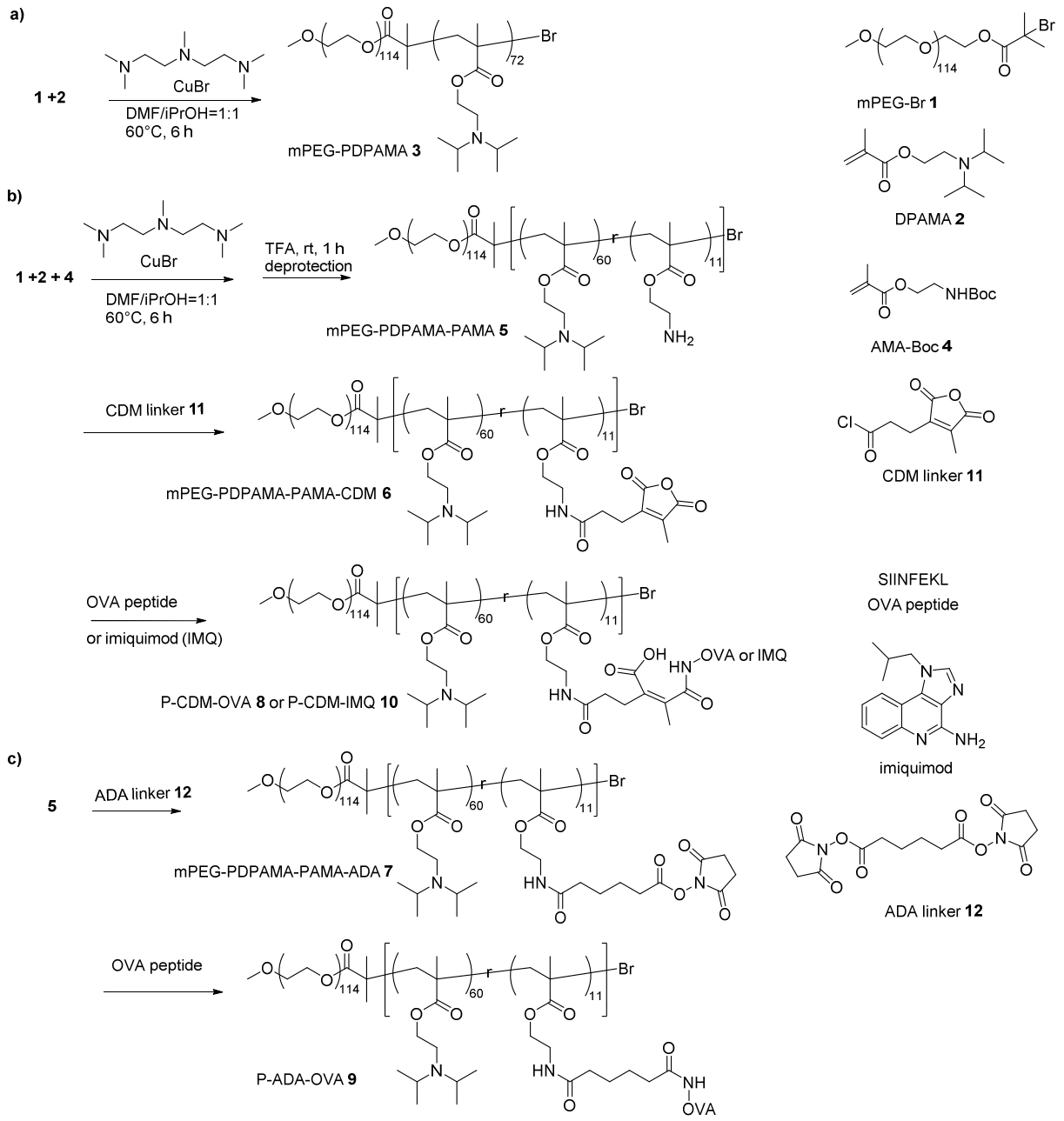

Scheme 3.1 Synthesis and characterization of the polymers. Synthesis of **(a)** polymer mPEG-PDPAMA **3**; **(b)** polymer-antigen and polymer-adjuvant conjugates through CDM linker (r in the structure drawn denotes the polymers are random polymers); and **(c)** polymer-antigen conjugate through ADA linker. **(d)** ^{1}H-NMR and **(e)** pKa titration curve for mPEG-PDPAMA **3**; **(f)** hydrodynamic diameters and **(g)** pH responsive behavior of mPEG-PDPAMA **3** NPs monitored by DLS.

Scheme 3.1 (cont'd)

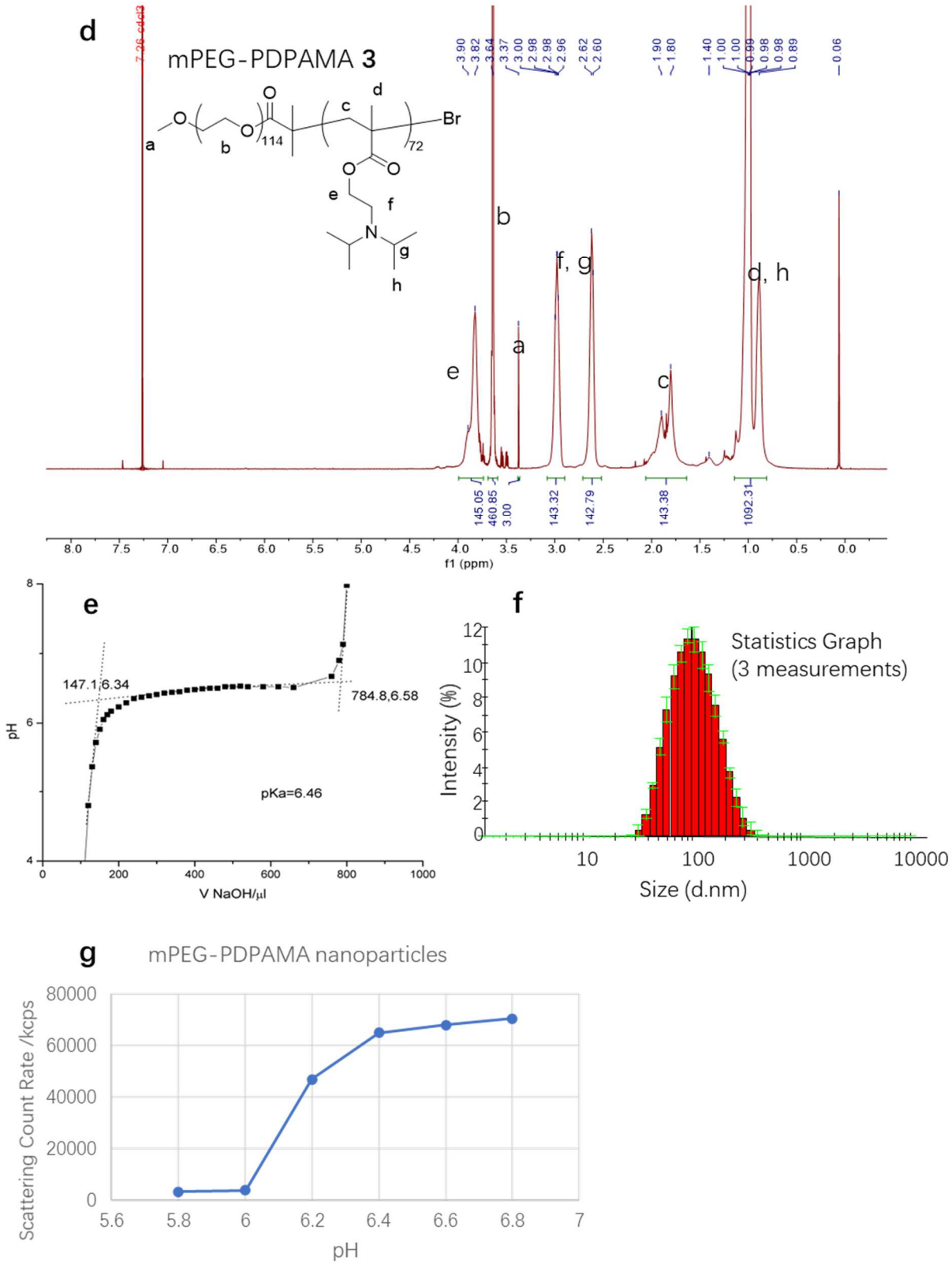

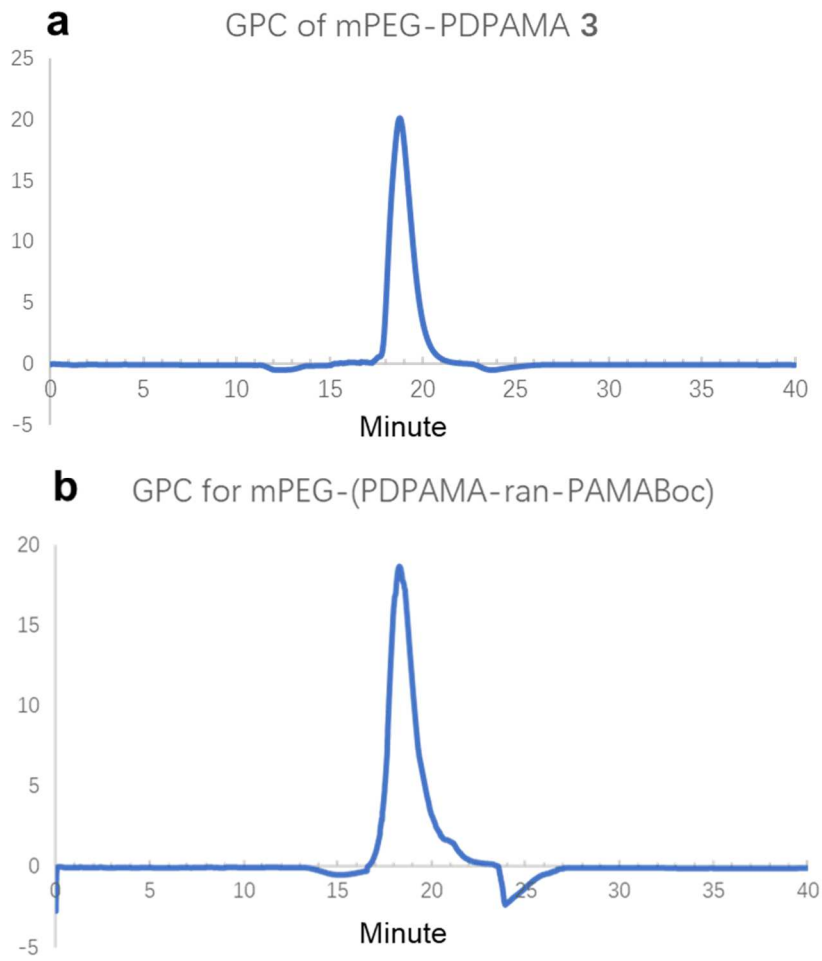

Figure 3.1 GPC data for synthetic polymers. **a**. mPEG-PDPAMA **3**, **b**. mPEG-(PDPAMA-ran-PAMA-Boc)

An important criterion for designing biomaterials is that they should be biocompatible without undesired side effects such as inflammation. The mPEG-PDPAMA polymer **3** was incubated with macrophages or dendritic cells, which did not activate these cells (**Figure 3.2**) indicating the polymer alone had little inflammatory activities.

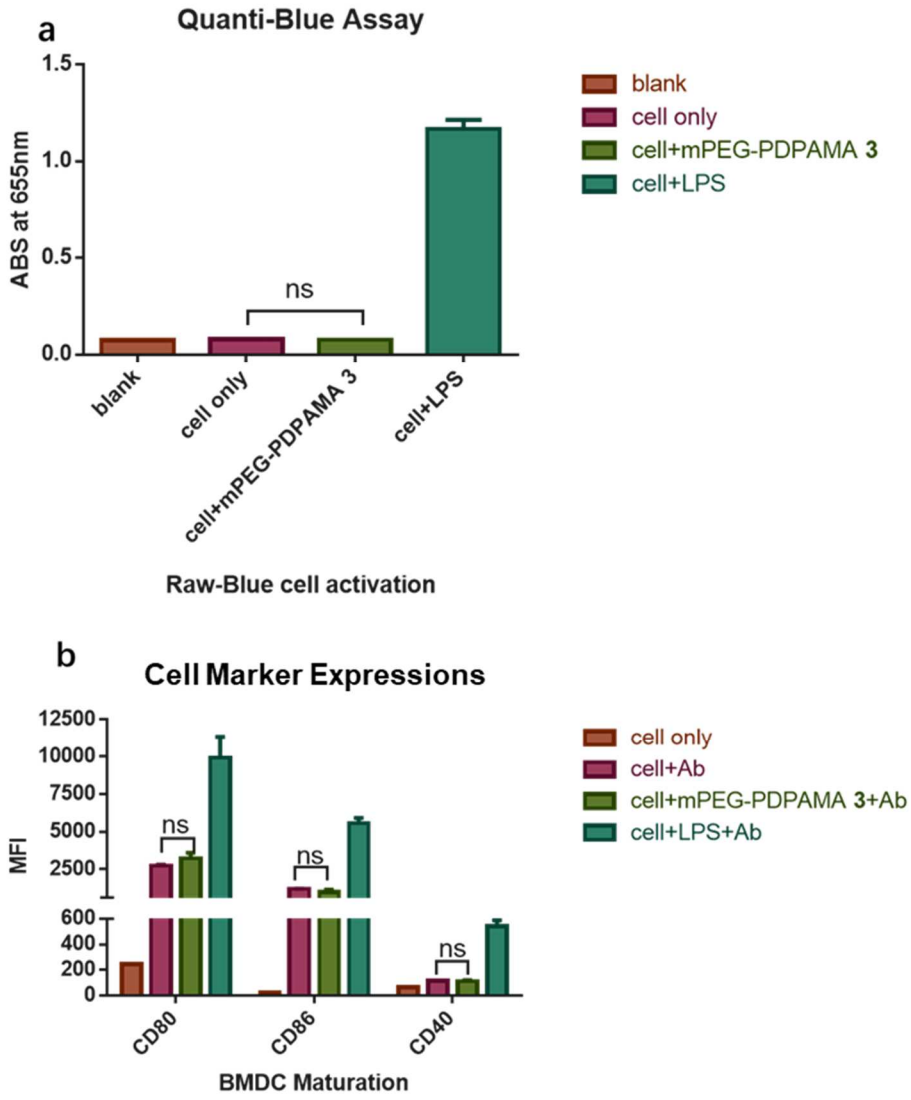

Figure 3.2 mPEG-PDPAMA **3** and immune cell interaction. **a**. Upon incubation of RAW-Blue cells with mPEG-PDPAMA **3** for 24h, little cellular activations were observed, while RAW-Blue cells responded well to LPS (100 ng/mL) as the positive control. **b.** Incubation of bone marrow dendritic cells (BMDCs) with mPEG-PDPAMA **3** (1 mg/mL) for 48h did not lead to maturation or activation of BMDCs, while LPS (100 ng/mL) readily led to maturation of the cells. Statistical significance was assessed using two-tailed unpaired t-test. ns: No significant differences.

3.2.2 Non-covalent OVA peptide encapsulation with mPEG-PDPAMA 3 particles

With the mPEG-PDPAMA **3** polymer in hand, the non-covalent encapsulation of a prototypical CTL antigen OVA peptide (SIINFEKL) was tested first. The OVA peptide was dissolved together with mPEG-PDPAMA in THF/dimethylsulfoxide (DMSO) (v/v = 10: 1) and added to pH 7.4 PBS buffer. The resulting particles (diameter ~110 nm) were passed through a G25 size exclusion column to remove any free peptides. The peptide loading level was 2 wt% based on HPLC quantification after dissembling the particles with 0.1% trifluoroacetic acid (TFA) in water. However, when the NPs were kept in pH 7.4 PBS buffer for 2 h, significant amounts (>80%) of the OVA peptide were found in solution, which suggested leakage of the peptide from the NPs. We surmised that the undesired leakage of the cargo was due to insufficient hydrophobicity in the NP interior. To overcome this, a new mPEG-PDPAMA polymer was synthesized with an additional monomer, i.e., ^{n}butyl methacrylate, either via random or block polymerization, to potentially enhance the hydrophobic interactions between the polymer carrier and OVA peptide. However, while the new copolymer formed NPs in pH 7.4 PBS buffer, it did not improve much the retention of OVA peptide inside the particles.

3.2.3 Synthesis of covalent OVA-polymer conjugate P-CDM-OVA 8 and OVA release profile

In order to reduce the undesired premature antigen release from non-covalent encapsulation, we decided to test the covalent attachment approach, which has not been reported before with the ultra pH sensitive NPs. We introduced protected primary amines into the polymer by co-

polymerizing DPAMA **2** with Boc-2-aminoethyl methacrylate (Boc-AMA) monomer **4** at 6 : 1 ratio (**Scheme 3.1b**). Analysis of the resulting polymer product by ^{1}H-NMR indicated the ratio of the repeating units from DPAMA **2** and Boc-AMA **4** was 60 : 11, suggesting similar polymerization rates of the two monomers. The Mn of the polymer was ~20,500 based on ^{1}H-NMR analysis and the GPC analysis suggested a narrow PDI (**Figure 3.1b**). Addition of TFA to the polymer removed the Boc moieties generating free primary amines in the mPEG-PDPAMA-PAMA polymer **5**. To conjugate the peptide to PDPAMA-PAMA **5**, the carboxy-dimethylmaleic anhydride (CDM) linker was used (**Scheme 3.1b**). CDM is known to readily react with a primary amine, and the resulting maleic amide is acid sensitive and cleavable at pH below 6.5 to release the free amine.[21] As a control, adipic acid (ADA) was used as the linker to form amides, which are not cleavable at pH around 6.5 (**Scheme 3.1c**). OVA peptides were conjugated with the polymer through either CDM or ADA, forming polymer-CDM-OVA peptide conjugate (P-CDM-OVA **8**) and polymer-ADA-OVA peptide conjugate (P-ADA-OVA **9**) respectively (**Schemes 3.1b**, **c**). The conjugation reactions were highly efficient with over 90% of the peptide added covalently linked with the polymer. The peptide loadings in both P-CDM-OVA **8** and P-ADA-OVA **9** were about 10 wt%, which were 5 times vs those achieved through the non-covalent encapsulation methods highlighting the advantage of covalent conjugation. P-CDM-OVA **8** and P-ADA-OVA **9** polymers both formed NPs in pH 7.4 PBS buffer with average hydrodynamic diameters of 170 nm as determined by DLS (**Figure 3.3a**, **b**).

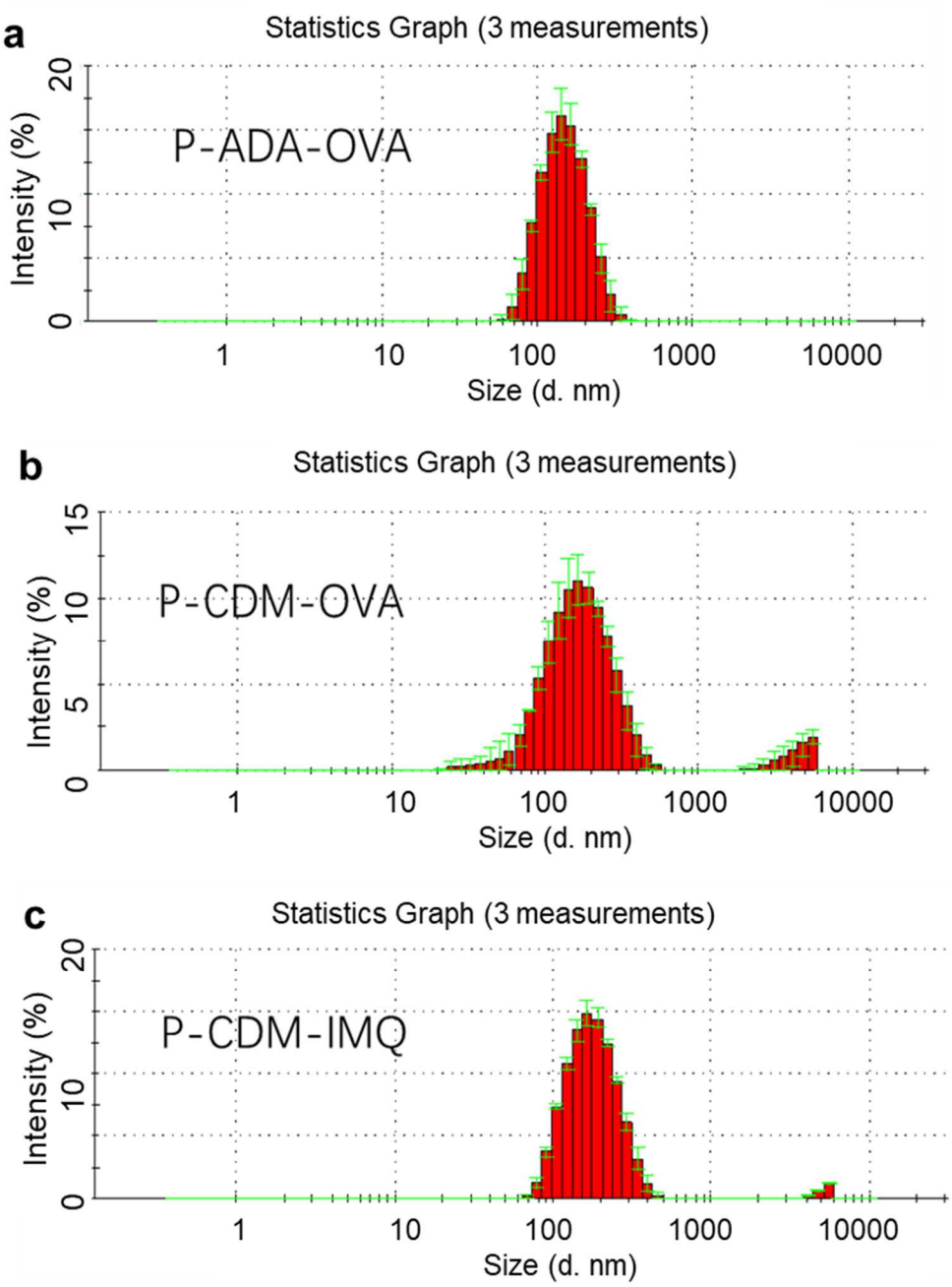

Figure 3.3 Hydrodynamic diameters of nanoparticles formed by various polymer-antigen or polymer-adjuvant conjugates. **a.** P-ADA-OVA particles at pH 7.4. **b.** P-CDM-OVA particles at pH 7.4. **c.** P-CDM-IMQ particles at pH 7.4. **d.** DLS scattering count rate for P-CDM-OVA particles at different pH values **e.** P-CDM-OVA/P-CDM-IMQ hybrid particles at pH 7.4.

Figure 3.3 (cont'd)

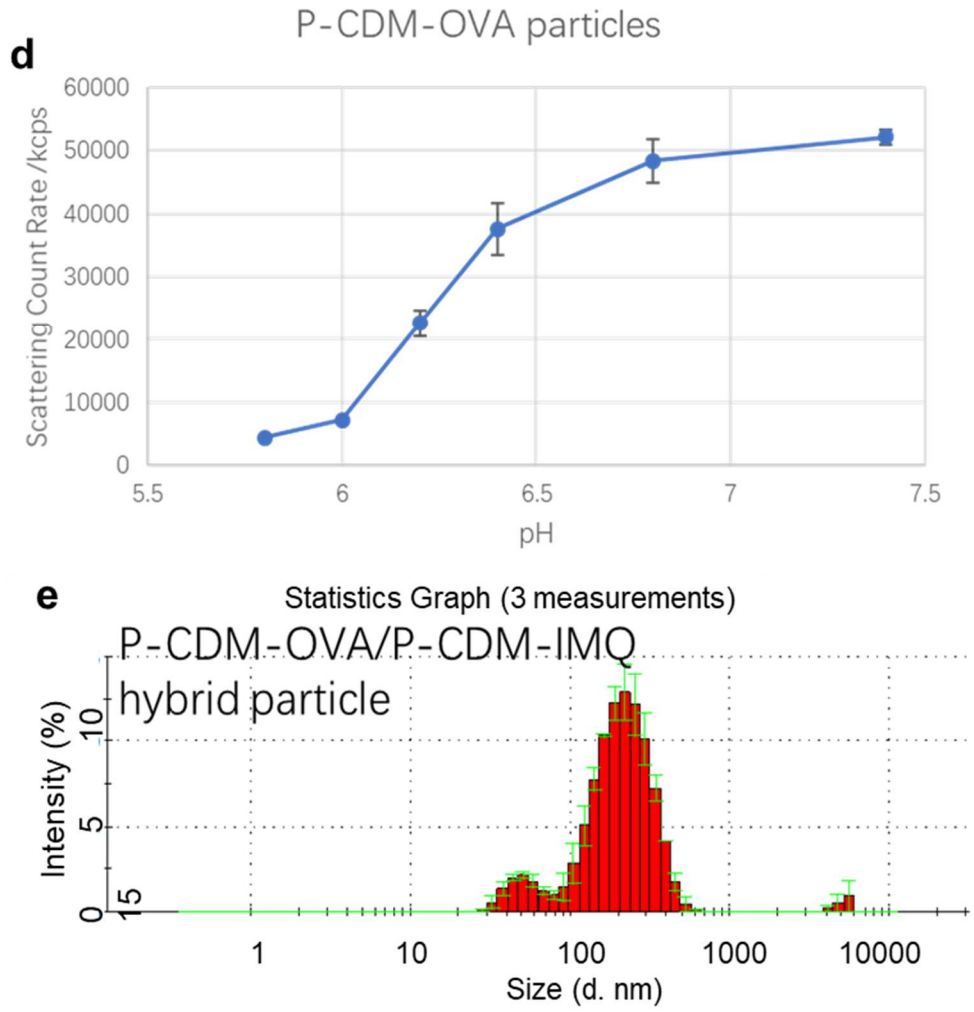

We next tested the stability of the P-CDM-OVA **8**. Interestingly, while the NPs dissembled readily at pH below 6.4 based on DLS scattering count rate measurement (**Figure 3.3d**), the release of OVA peptide was much slower. At pH 7.4, no releases were detected at all after one week. When incubation in pH 4.5 buffer, only 17.6% OVA peptide was released from the polymer after one week (**Figure 3.4a**). As a control experiment, we reacted dimethylmaleic anhydride with OVA peptide, and the resulting derivative was completely hydrolyzed to regenerate OVA peptide at pH

6.4 within 4 hours. The stability of the polymer peptide-conjugate was not limited to the OVA peptide. Another peptide, PADRE (aKFVAAWTLKAAa), was conjugated with the polymer through the CDM linker, which showed similar high stability to acid to that of P-CDM-OVA **8**. The slow acid hydrolysis of peptides linked to P-CDM polymer suggested the significant influence of polymer on the properties of the cargo, which may be due to the interactions of peptide with polymer stabilizing the complex and inhibiting the hydrolysis of amide bonds formed with the CDM linker.

Figure 3.4 OVA release from P-CDM-OVA by LC-MS detection. P-CDM-OVA (1 mg/ml) was incubated in pH 4.5, 6.0, 6.4 or 7.4 citric buffer with or without BSA (0.5 mg/ml) for different time periods followed by LC-MS detection. **a.** OVA release without BSA, **b.** OVA release with BSA. At pH 7.4, OVA release was not detectable in "no BSA" group at all time points.

To analyze whether P-CDM-OVA **8** could deliver the OVA peptide to cells, the polymer was incubated with EL4 lymphoma cells and probed with the monoclonal antibody (mAb) D1.16, which specifically recognizes the complex of OVA peptide with MHC-I on cell surface. The binding of OVA by MHC-I is required for activation of OVA specific T cells. Significant amounts of OVA bound MHC-I complexes were detected on EL4 cells by D1.16 mAb comparable to the levels when free OVA was added to EL4 cells up to 24 hours (**Figure 3.5**). P-CDM-OVA **8** could better sustain OVA release, as at 48 and 72 hours, cells incubated with P-CDM-OVA **8** presented much higher levels of OVA vs those treated with free OVA. This suggested the successful intracellular release, and cell surface display of OVA on MHC-I enabled by P-CDM-OVA **8**. In contrast, incubation of EL4 cells with P-ADA-OVA **9** led to little OVA displayed on cell surface after 24 hours (**Figure 3.5**). These results highlight the importance of the CDM linker in P-CDM-OVA **8** for antigen release and presentation by MHC-I.

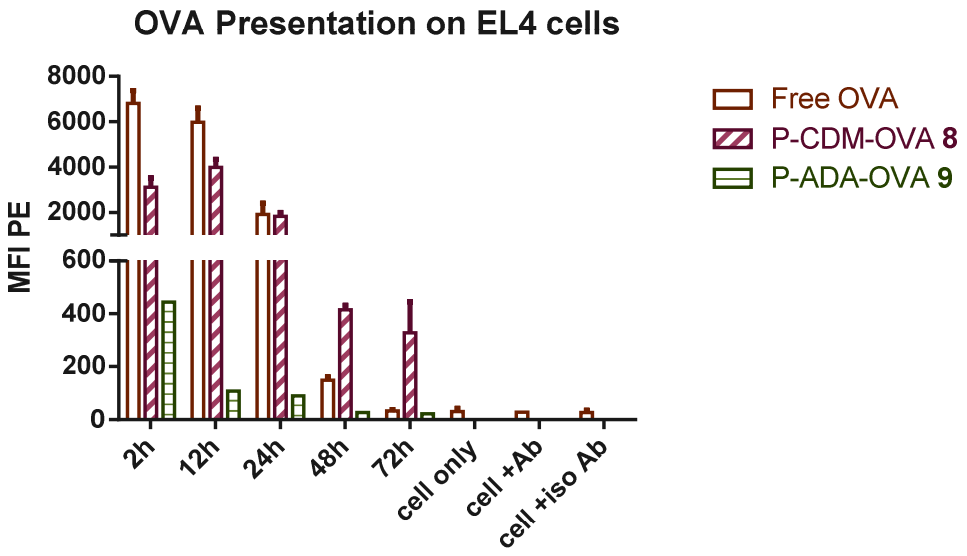

Figure 3.5 Presentation of OVA peptide on EL4 cells. Free OVA peptide (100 ng) or polymers containing 100 ng OVA peptide were incubated with EL4 cells for a certain time period. The cells were then washed and stained with PE labeled antibody D1.16 specific against anti-H2Kb bound to SIINFEKL or anti-mouse IgG1K (isotype control) followed by fluorescence-activated cell sorter (FACS) analysis.

It is interesting that while the OVA peptide was released slowly from P-CDM-OVA **8** in buffer, significant cellular presentation of OVA peptide could be observed after only 2 hour co-incubation of P-CDM-OVA **8** and EL4 cells (**Figure 3.5**). To gain a better understanding of the acceleration of OVA cleavage upon cellular incubation, we incubated P-CDM-OVA **8** in pH 4.5, 6.0 and 6.4 citrate acid buffers with bovine serum albumin (BSA) protein (P-CDM-OVA **8** : BSA = 2 : 1, w/w) to mimic proteins NPs may encounter in the biological system. Surprisingly, in the presence of BSA, the release of OVA peptide from P-CDM-OVA **8** was much accelerated. After 1-week incubation with BSA, 59% of the OVA peptide was released in pH 6.4, compared to 14.4% OVA

release after 1-week incubation without BSA at the same pH value (**Figure 3.4b**). Significant amounts of the free peptide were observed at 4 hours at pH values 6.4 or lower, providing an explanation of the significant peptide presentation by EL4 cells after a short period. The OVA release remained low at pH 7.4 (9.6%) after one week even with the addition of BSA, which indicated the OVA release was facilitated by both slightly acidic pH and the presence of a protein. Thus, a possible mechanism for the acceleration of cellular OVA release from P-CDM-OVA **8** is that proteins present in cells culture such as BSA in the medium, or MHC-I molecules on the surface of EL4 cells may interact with the OVA peptide. These proteins can compete with the polymer for OVA interactions. This may reduce the interaction of the polymer with OVA, sensitizing the maleic amide towards acid mediated cleavage and enabling the loading of OVA onto MHC-I for cell surface presentation.

3.2.4 CTL activation by P-CDM-OVA 8 *in vitro* and *in vivo*

With its ability to deliver CTL epitopes established, P-CDM-OVA **8** was analyzed for CTL activation. P-CDM-OVA **8**, free OVA or a mixture of empty NP with OVA was incubated with bone marrow derived dendritic cells (BMDCs) for 12 hours. BMDCs were then extensively washed to remove unbound peptide or NPs. B3Z T cells, which can specifically recognize and be activated by OVA peptide presented on MHC-I molecules, were then added and co-cultured for another 24 hours. BMDCs pulsed with free OVA activated B3Z cells, and the addition of empty mPEG-PDPAMA **3** NP with free OVA did not interfere with B3Z activation (**Figure 3.6a**). P-

CDM-OVA **8** could deliver OVA to BMDCs to activate B3Z cells in a dose dependent manner similar to free OVA, while the empty NPs showed low B3Z activation even at 10 times the concentration of the corresponding NP (**Figure 3.6a**).

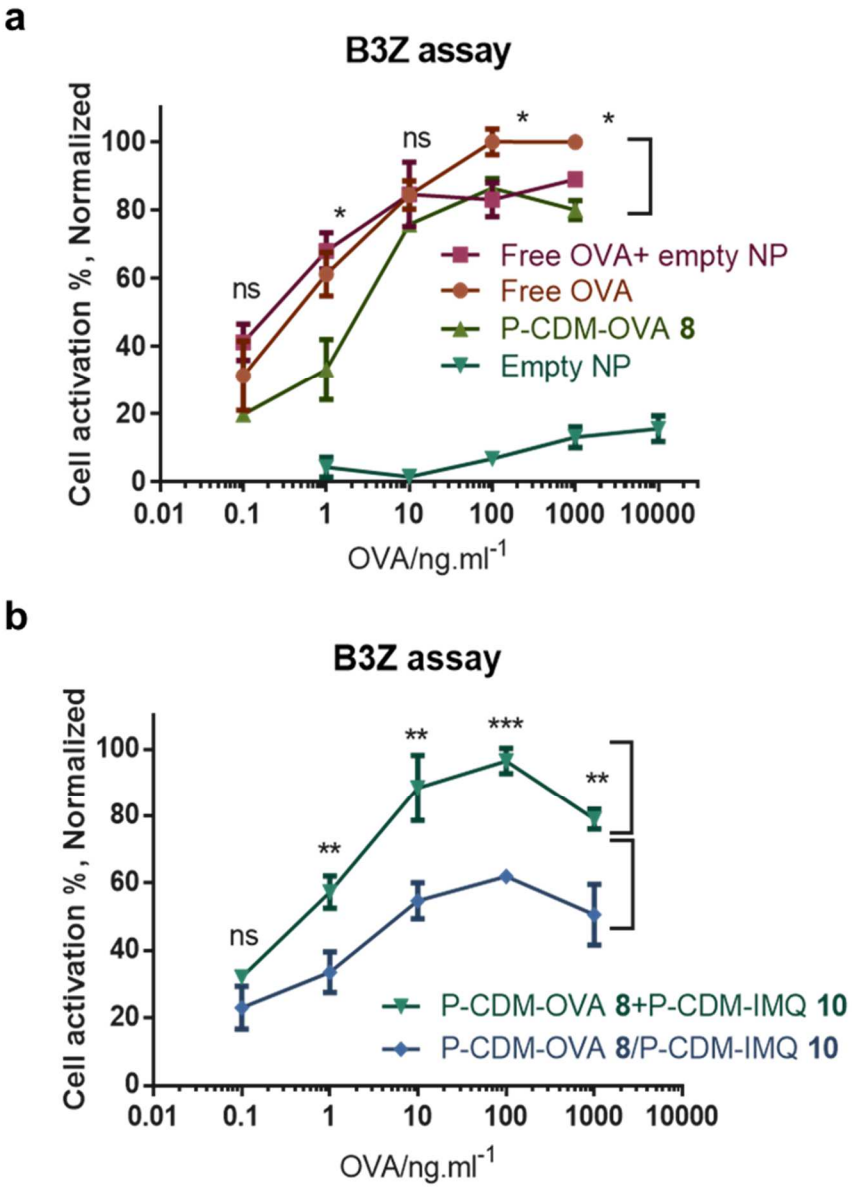

Figure 3.6 B3Z assay for detecting *in vitro* CTL activation. **a.** $2x10^4$ BMDCs were co-cultured with empty NPs or various formulations of OVA (at 0.1-1,000 ng total amounts of OVA peptide), in 96-well plate for 12 hours. The cells were then washed and $1x10^5$ B3Z cells were added to the plate and co-cultured for another 24h. **b.** To evaluate the effects of different combinations of

Figure 3.6 (cont'd) antigen and adjuvant, $2x10^4$ BMDCs were co-cultured with the mixture of separate particles P-CDM-OVA **8** +P-CDM-IMQ **10** (0.1-1,000 ng OVA peptide and 0.1-1000 ng IMQ), or the hybrid particles P-CDM-OVA **8**/P-CDM-IMQ **10** (0.1-1,000 ng OVA peptide and 0.1-1000 ng IMQ). Cells were incubated for 12 hours followed by washing and the addition of $1x10^5$ B3Z cells for another 24 hours co-incubation. Absorbance values at 595 nm were measured and normalized against the value at maximum B3Z cell activation. Statistical significance was assessed using two-tailed unpaired t-test. ns: No significant difference; *$p<0.05$; **$p<0.01$; ***$p<0.001$.

CTL activation by P-CDM-OVA **8** *in vivo* was evaluated next. Mice were vaccinated with P-CDM-OVA **8** by three weekly injections. To establish the best route for vaccination, P-CDM-OVA **8** was administered either subcutaneously or intravenously, with the resulting CTL activities of immunized animals determined by the *in vivo* CTL assay.[22] As shown in **Figure 3.7**, P-CDM-OVA **8** vaccination induced OVA specific CTL responses, as shown by specific lysis of OVA containing target cells in both spleens and lymph nodes. Subcutaneous (SC) administration of P-CDM-OVA **8** elicited stronger CTL activation compared to intravenous (IV) injection. Thus, the SC route was used in further studies. While free OVA peptide could activate B3Z cells i*n vitro*, administration of free OVA peptide *in vivo* failed to generate much CTL response (*vide infra*). The significant *in vivo* CTL activation induced by P-CDM-OVA **8** highlights the importance of using pH responsive polymers for delivery.

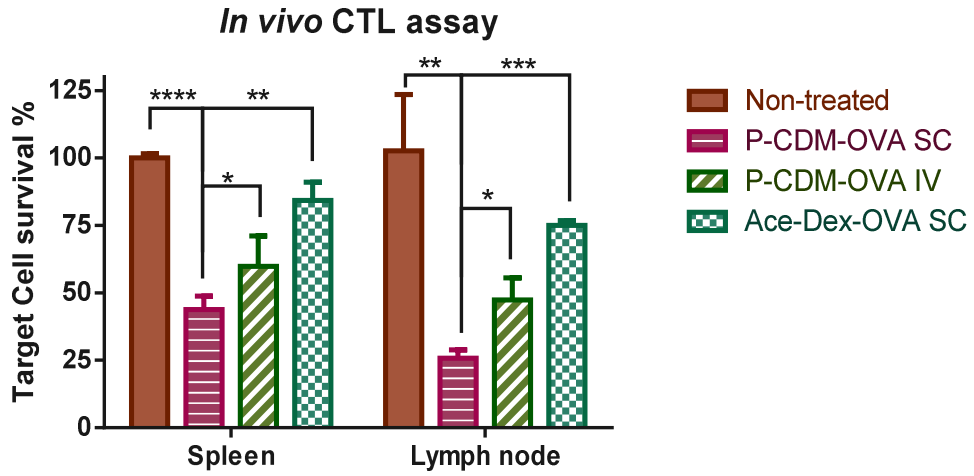

Figure 3.7 *In vivo* CTL activation assay. Mice (3 per group) were first immunized with P-CDM-OVA subcutaneously (SC) and intravenously (IV), or Ace-Dex-OVA subcutaneously (SC). $CFSE^{hi}$ labeled OVA peptide pulsed target cells were injected together with $CFSE^{lo}$ labeled control cells 3 days after the last immunization. Mice were euthanized 24 hours after cell injection and spleen and lymph nodes were collected for FACS analysis. Target cell survival was calculated by the target: control cell ratio changes before and after injection. Statistical significance was assessed using the two-tailed unpaired t-test. * $p<0.05$, ** $p<0.01$, *** $p<0.001$

As a comparison to P-CDM-OVA **8**, we prepared another pH responsive polymer, i.e., acetalated dextran polymer, following the previously established procedure, which formed microparticles (Ace-Dex MPs).[23] The Ace-Dex MPs could encapsulate peptide non-covalently, with a modest loading (~ 2% w/w). The peptide could be released rapidly at pH lower than 5.5 and taken up by antigen presenting cells (APCs) and tumor cells leading to potent CTL activation. Mice were immunized with the Ace-Dex-OVA MPs following the same immunization protocol as P-CDM-OVA **8**. CTL assay showed that mice immunized with P-CDM-OVA **8** exhibited significantly higher killing activities than those administered with Ace-Dex-OVA MPs (**Figure**

3.7). This demonstrates P-CDM-OVA **8** is superior to Ace-Dex-OVA in activation of OVA specific CTLs.

3.2.5 Combining P-CDM-OVA 8 with an adjuvant-polymer conjugate P-CDM-IMQ 10 for optimized immune activation

The addition of a co-stimulatory signal to the immune system together with the vaccine can potentially enhance CTL responses. We investigated next the possibility of incorporating a small molecule adjuvant imiquimod (IMQ) to the vaccine formulation using the same pH responsive polymer platform. IMQ is an agonist of Toll like receptor-7 (TLR-7) for immune potentiation. We conjugated IMQ to mPEG-PDPAMA-AMA **5** through the CDM linker producing P-CDM-IMQ **10** with 10wt% loading of IMQ (**Scheme 3.1b**). Interestingly, the P-CDM-IMQ **10** pH release profile was different from that of P-CDM-OVA **8**. Within 2 h, 100% and 50% IMQ releases were observed when P-CDM-IMQ **10** was incubated in buffers at pH=4.5 and 6.0 respectively (**Figure 3.8**). The more rapid release of IMQ from P-CDM-IMQ **10** supports the aforementioned idea that the slow rate of OVA release from P-CDM-OVA **8** in buffer in the absence of BSA was due to polymer/peptide interaction.

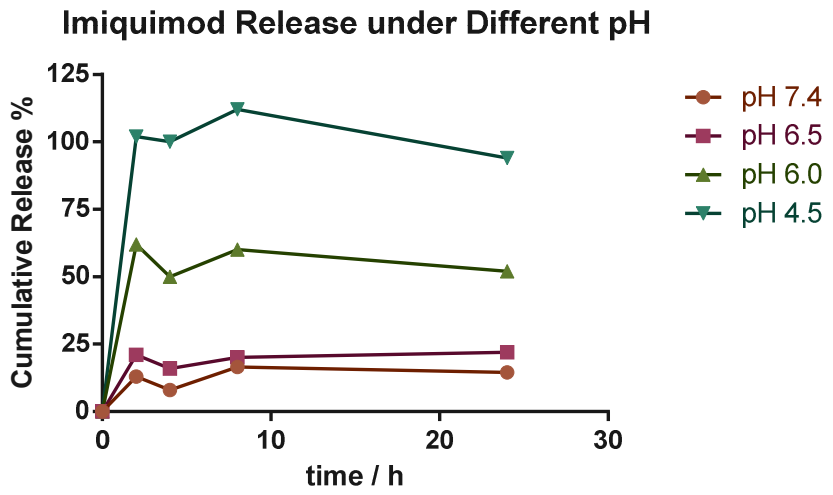

Figure 3.8 Cumulative release rates of imiquimod from P-CDM-IMQ **10** under different pH. P-CDM-IMQ **10** was diluted in buffer with different pH values. At each time point, an aliquot of solution was collected followed by centrifuge filtration. The amounts of released IMQ in flow-through were calculated from the values of UV-Vis absorbance at 318nm.

To test the impact of polymer conjugation on adjuvant activities, macrophage Raw-Blue cells were incubated with free IMQ and P-CDM-IMQ **10**. Stronger Raw-Blue cell activations by P-CDM-IMQ **10** were observed compared to that by free IMQ at IMQ concentration higher than 0.1 μg (**Figure 3.9**) suggesting the advantage of polymer aided adjuvant delivery. The loading levels of IMQ on polymer did not significantly impact cellular activation when the same total amounts of IMQ were added (**Figure 3.10**), and the loading level of P-CDM-IMQ **10** was controlled at 10 wt% for subsequent studies.

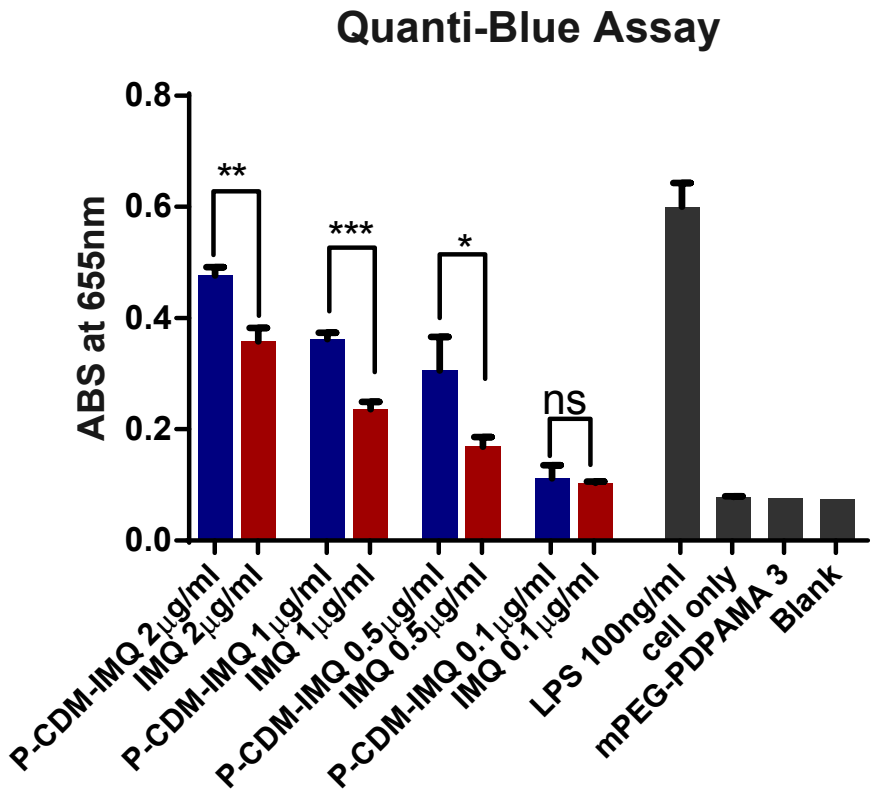

Figure 3.9 Macrophage cells activation by free IMQ and P-CDM-IMQ. $1x10^5$ Raw-Blue cells were incubated with different concentration of free IMQ and P-CDM-IMQ **10**, 100ng LPS (positive control) or mPEG-PDPAMA **3** for 24 h. 20 μL cell culture supernatant was collected and added to Quanti-Blue™ solution and incubated for another 2 h. Absorbance at 655nm was measured. Statistical significance was assessed using two-tailed unpaired t-test. ns: no significant difference; *p<0.05; **p<0.01; ***p<0.001

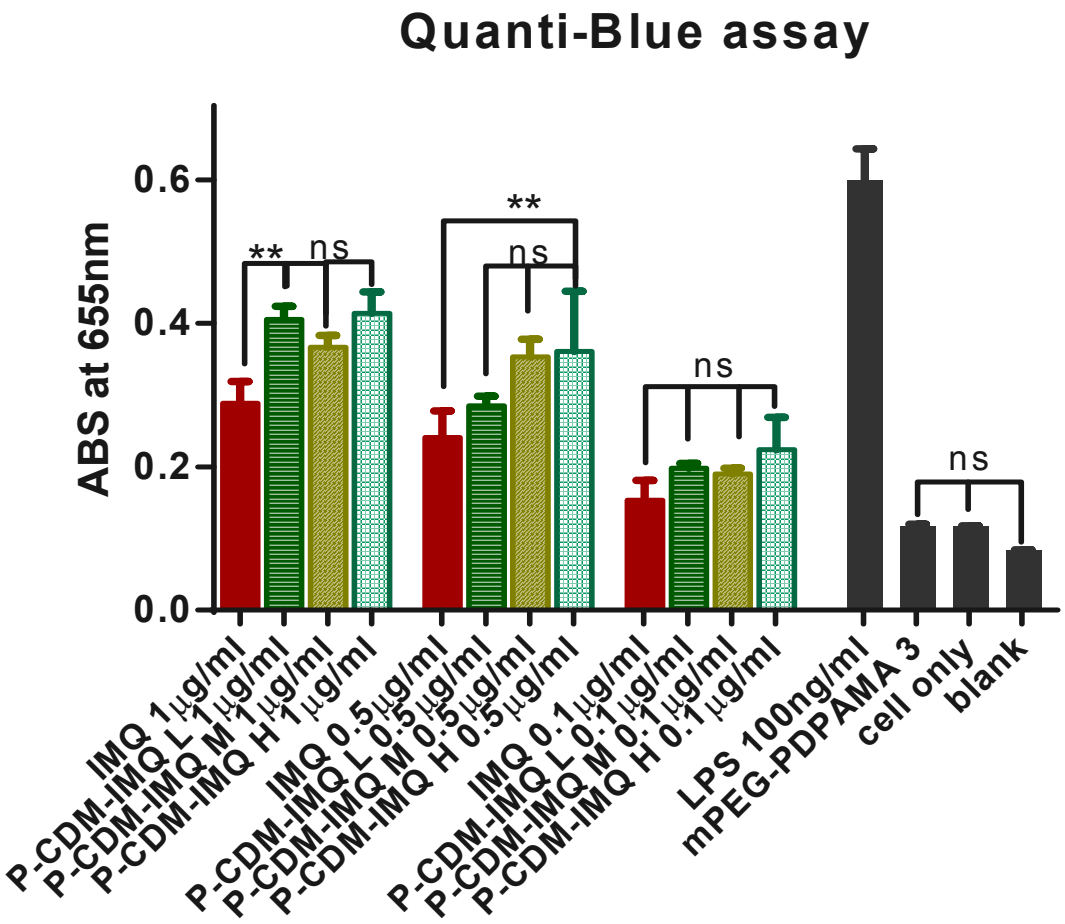

Figure 3.10 Macrophage activation by P-CDM-IMQ with different IMQ loading indicating the IMQ loading level per polymer did not have a significant impact on cellular activation. $1x10^5$ Raw-Blue cells were incubated with various concentrations of free IMQ, P-CDM-IMQ L (2% IMQ), P-CDM-IMQ M (5% IMQ), P-CDM-IMQ H (10% IMQ), 100ng LPS (positive control) or mPEG-PDPAMA **3** for 24 h. 20 µL cell culture supernatants were collected and added to Quanti-Blue™ solution and incubated for another 2 h. Absorbance at 655nm was measured. Statistical significance was assessed using two-tailed unpaired t-test. ns: no significant difference; **$p<0.01$; ***$p<0.001$

Seymour and Seder synthesized IMQ polymer to potentiate the immune system.[24] In their study, the density of IMQ on polymer backbone significantly influenced the assembly of the NPs as well as the interactions of the polymer with the immune system. In our system, the amphiphilic

P-CDM-IMQ **10** polymer formed particles (hydrodynamic diameter 170 nm, **Figure 3.3c**) regardless of the loading level of IMQ. Our polymer can load varying amounts of IMQ as needed without significantly impacting particle sizes or adjuvant activities.

How antigen is formulated with the adjuvant can greatly impact immune responses.[25] To establish the best combination of antigen and IMQ, we investigated various methods for incorporating IMQ. Besides free IMQ and the P-CDM-IMQ **8** particles, which could be directly mixed with P-CDM-OVA **8** or free OVA for vaccination, we prepared a hybrid particle combining P-CDM-OVA **8** and P-CDM-IMQ **10** within one particle (~190 nm diameter, **Figure 3.3e**). We first performed B3Z assays with the mixture of P-CDM-OVA **8** particles and P-CDM-IMQ **10** particles (P-CDM-OVA **8** + P-CDM-IMQ **10**) or P-CDM-OVA **8**/P-CDM-IMQ **10** hybrid particles (**Figure 3.6b**). The P-CDM-OVA **8** + P-CDM-IMQ **10** group showed significantly higher activation of B3Z cells compared to the P-CDM-OVA **8**/P-CDM-IMQ **10** hybrid particles at OVA concentrations above 1 ng/ml.

In vivo CTL assays were performed to analyze the impacts of various forms of IMQ on P-CDM-OVA **8** mediated CTL activation. While free OVA peptide did not activate CTL much, the administration of P-CDM-OVA **8** induced significant CTL activities in both spleen and lymph node analysis (**Figure 3.11**). This confirms the important roles of the polymer in potentiating OVA specific CTL activities. The addition of IMQ adjuvant to P-CDM-OVA **8** enhanced cell killing, as survival rate of OVA bearing target cells in the group treated with P-CDM-OVA **8** + IMQ (42%

in spleen and 28% in lymph node) was lower than that receiving P-CDM-OVA **8** only (63% in spleen and 50% in lymph node). Lower cell survival (27% in spleen and 20% in lymph node) was observed when P-CDM-OVA **8** and P-CDM-IMQ **10** were co-administrated in separate particles (P-CDM-OVA **8**+P-CDM-IMQ **10**). Hybrid particles containing both P-CDM-OVA **8** and P-CDM-IMQ **10** (P-CDM-OVA **8**/P-CDM-IMQ **10**) were not as effective in target cell killing (62% cell survival in spleen and 31% in lymph node) compared to the mixture of two separate particles. This trend was consistent with the B3Z assay results (**Figure 3.6b**).

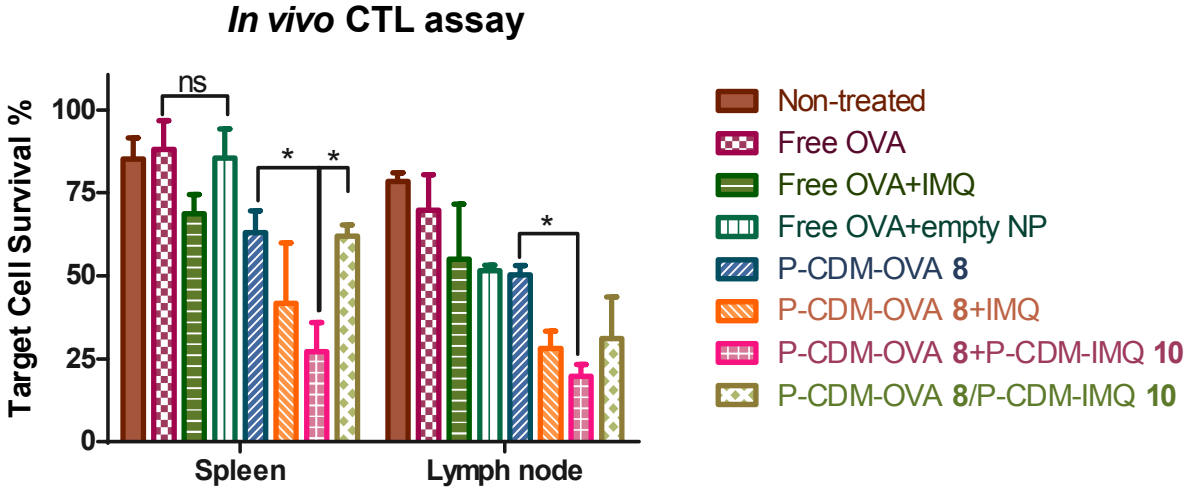

Figure 3.11 *In vivo* CTL assay. Mice (2 per group) were first immunized with free OVA, free OVA+IMQ, free OVA+empty NP, P-CDM-OVA **8**, P-CDM-OVA **8**+IMQ, P-CDM-OVA **8** and P-CDM-IMQ **10** in separate particles (P-CDM-OVA **8**+P-CDM-IMQ **10**), or P-CDM-OVA **8** and P-CDM-IMQ **10** in hybrid particle (P-CDM-OVA **8**/P-CDM-IMQ **10**). $CFSE^{hi}$ labeled OVA peptide pulsed target cells were injected together with $CFSE^{lo}$ labeled control cells 3 days after the last immunization. Mice were euthanized 24 hours after cell injection and the spleens and lymph nodes were collected for FACS analysis. Target cell survival were calculated by the target: control cell ratio changes before and after injection. Statistical significance was assessed using two-tailed unpaired t-test. ns: No significant differences; *$p<0.05$.

Whether the co-localization of antigen and adjuvant in same delivery vehicles is important for generating strong immune response remains unclear so far. It is believed hybrid particles are better in stimulating the immune system, as these particles can simultaneously deliver both antigen and adjuvant to the same APC.[26-29] However, there are also reports showing that administration of antigen and adjuvant in separate particles induce stronger immune responses.[30-33] In the current study, the separate particle strategy performed better, possibly due to the drastically different cargo release rates associated with P-CDM-OVA **8** and P-CDM-IMQ **10**. It has been reported that the releases of antigens and adjuvants may need to be optimized individually.[34] The hybrid particles may not have the optimal releasing rates for the antigen and the adjuvant. In addition to better CTL stimulation, another advantage for co-administration of P-CDM-OVA **8** and P-CDM-IMQ **10** in separate particles is that it provides a convenient "mix-and-inject" method for vaccine formulation. The relative ratio of antigen and adjuvant can be easily tuned by mixing different amounts of two particles. Furthermore, several antigens may be readily co-administrated with adjuvant particles as a multivalent vaccine without the need to produce multiple hybrid particles.

3.2.6 P-CDM-OVA 8 + P-CDM-IMQ 10 protected mice from EG7 tumor

With the superior CTL activation by P-CDM-OVA **8**+P-CDM-IMQ **10**, we evaluated their abilities to provide tumor protection *in vivo*. It is known that a significant challenge in combating cancer is the suppression of the immune system by tumor.[35-37] Recently, programmed cell death 1 (PD-1) and its ligand (PD-L1) have been shown to be important inhibitory checkpoint molecules,

aiding the escape of tumors from immune surveillance.[38-40] As anti-PD-1 mAbs can block the functions of PD-1, we tested the combination of anti-PD-1 mAb with vaccination for tumor protection. Mice were implanted subcutaneously with EG7 tumor cells, which express OVA on cell surface. Five days after EG7 tumor injection, mice were injected with various vaccine formulations every other day for a total 5 injections and the growth of tumor was monitored. As shown in **Figure 3.12**, anti-PD1 antibody alone or free OVA + IMQ + empty NPs were ineffective in slowing down tumor growth compared to the mock group receiving PBS injection. In contrast, treatment with P-CDM-OVA **8**+P-CDM-IMQ **10** at the same total dose of OVA and IMQ led to a significant reduction in tumor sizes indicating the superiority of the polymer system. The addition of anti-PD1 to P-CDM-OVA **8**+ P-CDM-IMQ **10** slightly improved the tumor protection effect.

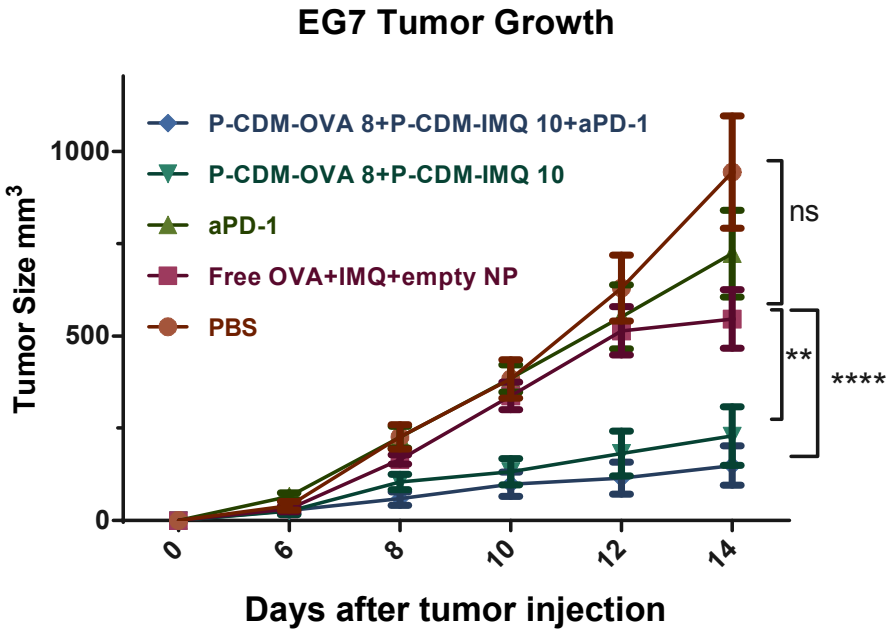

Figure 3.12 EG7 tumor growth under a variety of treatment conditions. C57BL/6 female mice were injected with $1x10^6$ EG7 tumor cells. Starting from day 5, a total of 5 injections with PBS, mixture of free OVA, IMQ and empty NPs (Free OVA+IMQ+empty NP), or P-CDM-OVA **8**

Figure 3.12 (cont'd) combining with P-CDM-IMQ **10** were given intratumorally every other day with a dose of 25 μg OVA and 25 μg IMQ. On days 6, 9, and 12, aPD-1 and P-CDM-OVA **8**+P-CDM-IMQ **10**+aPD-1 group received 100 μg anti-PD-1 antibody intraperitoneally. Tumor size were measured every other day until the first animal reached the end point. Statistical significance was assessed using two-tailed unpaired t-test. ns: no significant difference, **p<0.01, ****p<0.0001

To evaluate the potential risk of harmful cytokine release *in vivo* due to vaccination, serum TNF-α levels were monitored for mice immunized with free IMQ, empty NPs, or P-CDM-OVA **8** +P-CDM-IMQ **10** after 24 hours and 1 week (3 injections on days 0, 3, and 6) (**Figure 3.13**). No significant increases of serum TNF-α levels were detected compared to mice receiving only PBS injections, suggesting that the polymer-antigen/adjuvant conjugates can induce strong anti-tumor immune responses but not likely to generate harmful cytokine storm.

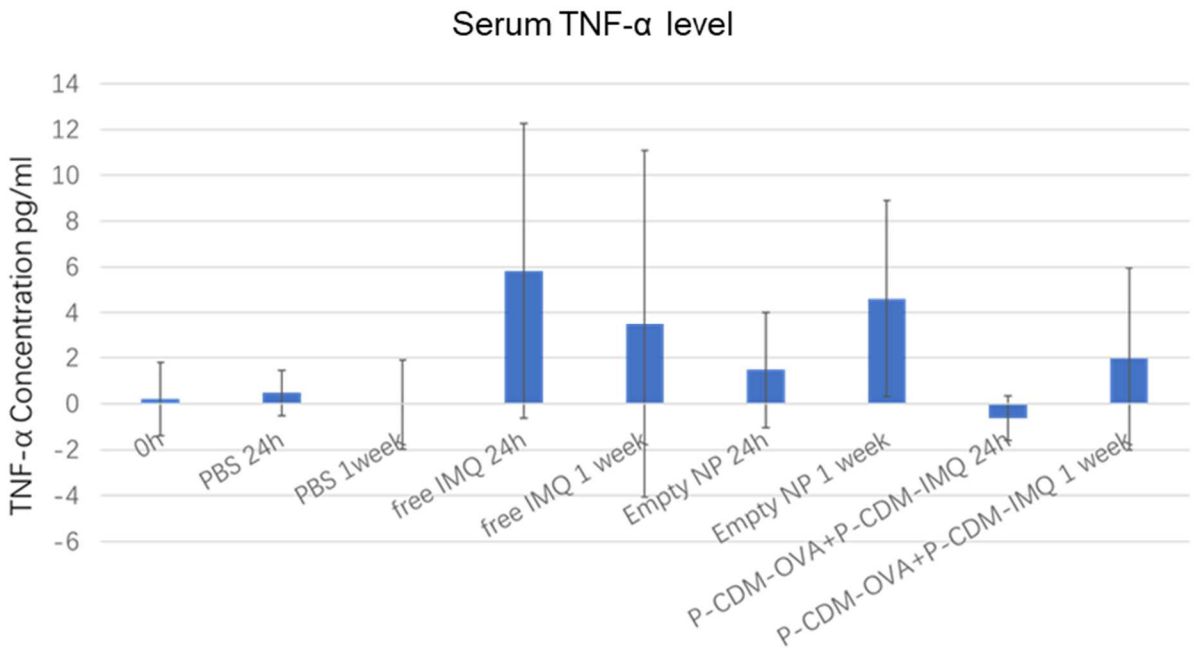

Figure 3.13 Mouse sera TNF-α level after immunization. Mice were injected with PBS, free IMQ (20 μg/dose), empty NPs (200 μg/dose) or P-CDM-OVA **8** +P-CDM-IMQ **10** (20 μg OVA+20 μg

Figure 3.13 (cont'd) IMQ/dose) and euthanized after 24 h (1 injection) or 1 week (3 injections on day 0, 3 and 6). Sera was collected and analyzed by TNF-α ELISA kit.

3.3 Conclusion

Anti-cancer immunotherapy is gaining increasing prominence for cancer treatment. As an important type of immune cells, CTLs can kill tumor cells and protect against tumor development. However, direct administration of CTL peptide epitope often fails to potently activate CTLs. To enhance the efficacy of CTL based therapy, we have developed a new ultra pH sensitive NP system, to which CTL epitope such as OVA can be conjugated with high efficiency and high loading through a CDM linker. Interestingly, the polymer conjugation greatly enhanced the stability of CDM with little cleavage of the incorporated OVA antigen observed in pH 6.4 buffer. On the other hand, the presence of a protein such as BSA significantly increased the polymer cleavage rate. The P-CDM-OVA polymer released the OVA antigen to cells under physiological conditions, enabling sustained presentation of OVA by MHC-I on cell surface and stronger CTL activation than free OVA underlying the advantage of the polymer assisted delivery. The polymer platform is flexible, which was also utilized to deliver a small molecule adjuvant IMQ. The combination of P-CDM-OVA with P-CDM-IMQ provided significant protection to tumor development, highlighting the power of the judiciously designed polymer system.

3.4 Experimental methods

3.4.1 Materials and equipment

Methoxy polyethylene glycol (mPEG, average Mn=5,000), diisopropylaminoethyl methacrylate (DPAMA) 99%, n-butyl methacrylate (BMA) 99%, *N,N',N',N''*-pentamethyldiethylenetriamine (PMDETA), CuBr, NaH 60%, chlorophenol red-β-D-galactopyranoside (CPRG), *N*-hydroxysuccimide (NHS), adipic acid were purchased from Milipore-Sigma-Aldrich. 2-Aminoethyl methacrylate HCl salt (AMA), 95% without inhibitor, was purchased from Polyscience Inc. Triethyl phosphoryl propionate 98%, di-tert-butyl dicarbonate 99%, were purchased from Acros. Diethyl ketoglutarate 95% was purchased from TCI. Carboxyfluorescein succinimidyl ester (CFSE), triethylamine (TEA), *N*,*N*-dimethylformamide (DMF), dimethylsulfoxide (DMSO), tetrahydrofuran (THF), dichloromethane (DCM) were purchased from Fisher Scientific. Ovalbumin$_{257-264}$ antigen peptide (OVA peptide, SIINFEKL) 95% purity was purchased from Genscript. Imiquimod (95% purity) was purchased from AK Scientific. All antibodies were purchased from Biolegend. Quanti-blueTM and TNF-α ELISA kit were purchased from Invivogen.

Scanning electron microscopy (SEM) images were acquired on the 7500F ultra-high resolution scanning electron microscope. Fluorescence-activated cell sorting (FACS) data was acquired using LSR II flow cytometer analyzer and analyzed by FlowJo_V10 software. Dynamic light scattering (DLS) was performed on a Zetasizer Nano zs apparatus (Malvern, UK) with laser

set at 137° and attenuation at 7 for all samples. NMR spectrum were acquired on the Agilent DDR2 500 MHz NMR spectrometers

3.4.2 Animals and cell lines

Pathogen free female C57BL/6 mice age 6 - 10 weeks were utilized for experiments. All animal experiments were performed in accordance with the guidelines of the Institutional Animal Care and Use Committee (IACUC) of Michigan State University. EL4 cells were generously donated by Dr. Sandra Gendler (Mayo clinic). Cells were cultured in RPMI medium 1640 supplemented with 10 % Fetal Bovine Serum (FBS), 1% L-glutamine, and 1% streptomycin penicillin. B3Z cells was generously donated by Dr. Nilabh Shastri (University of California, Berkeley). These cells were cultured in RPMI-1640 supplemented with 10% FBS, 1 mM pyruvate, 50 μM 2-mercaptoethanol, 1% L-glutamine, and 1% streptomycin penicillin. EG.7 OVA cells were purchased from ATCC and cultured in RPMI-1640 supplemented with 10% FBS, 1% glutamine, 10 mM HEPES, 1.0 mM sodium pyruvate, 50 μM 2-mercaptoethanol, 0.4 mg/L G418 and 1% streptomycin penicillin. Bone marrow dendritic cells (BMDCs) were collected from C57BL/6 mice femur and cultured in RPMI-1640 supplemented with 10% FBS, 1% Streptomycin Penicillin and 20 ng/mL GM-CSF. Equal amounts of culture media were added to the dishes seeded with cells on day 3. The non-adherent cells were collected on day 6 and re-seeded in new dishes and cultured for another 2 days. The non-adherent cells were collected on day 9 with >90%

of the population $CD11c^+$ as determined by fluorescence-activated cell sorting (FACS) analysis. All cell lines were grown at 37 °C in a 5% CO2/air incubator.

3.4.3 Synthesis of mPEG-Br macroinitiator 1

mPEG (average MW=5,000, 10 g, 2 mmol) and pyridine (316 mg, 4 mmol) were dissolved in $CHCl_3$ (100 mL) and cooled on ice in dark. 2-Bromoisobutyryl bromide (0.92 g, 4 mmol) was added to the solution and the reaction was first incubated on ice in dark for 1 h followed by stirring at room temperature in dark for 24 h. When reaction was completed, the solution was concentrated to a small volume then precipitated from diethylether three times to obtain product **1** (9.92 g, yield= 96%). ^{1}H-NMR (500MHz, $CDCl_3$, ppm) δ 4.33-4.30 (m, 2H), 3.64 (s, 454H), 3.37 (s, 3H), 1.93 (s, 6H).

3.4.4 Synthesis of methoxy polyethyleneglycol-poly(diisopropylaminoethyl methacrylate) (mPEG-PDPAMA) 3

Initiator mPEG-Br **1** (100 mg, 20 μmol) and monomer DPAMA **2** (365 mg, 1.7 mmol) were dissolved in DMF: isopropanol (1: 1, 10 mL). PMDETA (3.5 mg, 20 μmol) was added to the solution. Then three cycles of freeze-pump-thaw were performed to remove oxygen. CuBr (2.9 mg, 20 μmol) was added under N_2 and the reaction mixture was kept under 60□ for 6 h. The reaction was quenched by diluting with equal volume of THF (10 mL) and the mixture was passed through a short basic Al_2O_3 column. The solution was collected then concentrated under vacuum followed by dialysis (MWCO 3,500 Da) against pure water for 48 h. The solution in the dialysis tubing was collected and lyophilized to give a white solid compound (370 mg). A typical monomer

conversion rate is 85% based on ^{1}H-NMR analysis of the crude reaction mixture. ^{1}H NMR (500 MHz, CDCl3, ppm) δ 3.99 – 3.74 (m, 145H), 3.64 (s, 454H), 3.37 (s, 3H), 3.00 (s, 145H), 2.64 (s, 145H), 2.06 – 1.64 (m, 145H), 1.14 – 0.81 (m, 1087H).

3.4.5 Synthesis of Boc protected 2-aminoethylmethacylate monomer (Boc-AMA) 4

2-Aminoethylmethacylate HCl salt (1.0 g, 6 mmol) was dissolved in DCM (20 mL) and cooled to 0°C. TEA (0.92 mL, 6.6 mmol) was added to the solution on ice and stirred for 20 min. Then, Boc_2O (1.44 g, 6.6 mmol) in DCM (5 mL) was added to the flask. The reaction mixture was allowed to reach room temperature and stirred for 24 h. The organic phase was then washed with water, 1M HCl, saturated $NaHCO_3$ solution and saturated NaCl solution followed by drying over Na_2SO_4. The solvent was then removed under vacuum to give a white solid product, which was used without further purification. ^{1}H NMR (500 MHz, $CDCl_3$, ppm) δ 6.15 – 6.11 (m, 1H), 5.61 – 5.57 (m, 1H), 4.78 (s, 1H), 4.21 (t, J = 5.4 Hz, 2H), 3.45 (t, J = 5.4 Hz, 2H), 1.98 – 1.93 (m, 3H), 1.45 (s, 9H). ^{13}C NMR (126 MHz, CDCl3, ppm) δ 167.30, 155.98, 136.01, 125.95, 79.60, 63.98, 39.68, 28.35, 18.31. MS: (ESI^+): $C_{11}H_{19}NO_4[M+Na]^+$ calculated mass: 252.1206, observed mass: 252.1208.

3.4.6 Synthesis of methoxy polyethyleneglycol-poly(diisopropylaminoethyl methacrylate)-poly(n-butyl methacrylate) (mPEG-PDPAMA-PBMA)

The polymerization procedure was similar to that for mPEG-PDPAMA **3**. For random polymer (mPEG-PDPAMA-r-PBMA), DPAMA **2** (213 mg, 1.0 mmol) and BMA (142 mg, 1.0 mmol) were dissolved together with mPEG-Br **1** (100 mg, 20 μmol) and PMDETA (3.5 mg, 20

μmol) in DMF: isopropanol (1: 1, 10 mL). CuBr (2.9 mg, 20 μmol) was added to the flask after three cycles of freeze-pump-thaw. The polymerization was performed under 60□ for 6 h. The purification of resulting product was the same as that for mPEG-PDPAMA **3**. ^{1}H-NMR (500 MHz, $CDCl_3$, ppm) δ 3.94 (s, 100H), 3.82 (s, 60H), 3.64 (s, 454H), 3.38 (s, 3H), 2.99 (s, 60H), 2.62 (s, 60H), 1.97 – 1.75 (m, 160H), 1.40 (s, 100H), 1.09 – 0.80 (m, 850H).

For block polymer (mPEG-PDPAMA-b-PBMA), mPEG-PDPAMA **3** (200 mg, ~10 μmol), BMA (142 mg, 1.0 mmol) and PMDETA (1.7 mg, 10 μmol) were dissolved in mixed solvent of DMF: isopropanol (5 mL, 1: 1). CuBr (1.5 mg, 10 μmol) was added to the flask after three cycles of freeze-pump-thaw. The polymerization was performed under 60 °C for 6 h. The purification of resulting product was the same as that for mPEG-PDPAMA **3**. ^{1}H NMR (500 MHz, $CDCl_3$, ppm) δ 4.03 – 3.75 (m, 290H), 3.64 (s, 454H), 3.38 (s, 3H), 2.99 (s, 134H), 2.62 (s, 134H), 2.07 – 1.71 (m, 290H), 1.47 – 1.34 (m, 156H), 1.28 – 0.79 (m, 1630H).

3.4.7 Quantification of free OVA peptide and imiquimod

High performance liquid chromatography (HPLC) was used for the quantification of OVA peptide. A standard curve between the amounts of OVA peptide and the area integration of HPLC chromatograms were acquired first. OVA peptide standard samples (0.5 mL, containing 2 μg, 12.5 μg, 25 μg, 50 μg, 100 μg peptide) were analyzed by HPLC using 0.1% TFA MilliQ water and acetonitrile over a C18 column (2% acetonitrile to 55% acetonitrile in 47 minutes, 220 nm UV detector). The elution time of OVA peptide under this condition was 33 min. The standard curve

between the amounts of OVA peptide and the areas of integration from HPLC were plotted (Appendix **Figure 3.15a**). The amount of OVA peptide in other samples were quantified based on the standard curve.

The amount of imiquimod was quantified by UV absorption at 318 nm. The UV absorption at 318 nm of imiquimod standard samples (1 mL, containing 0.78 μg, 1.56 μg, 3.13 μg, 6.25 μg, 12.5 μg, 25 μg, 50 μg imiquimod) were acquired and the standard curve between the concentration of imiquimod and the UV absorption were created (Appendix **Figure 3.15b**). The amount of imiquimod in other samples were quantified based on the standard curve.

3.4.8 Encapsulation and release of OVA peptide in mPEG-PDPAMA 3 or mPEG-PDPAMA-b/r-PBMA nanoparticles

The polymer (10 mg) was dissolved in THF (100 μL). OVA peptide (0.5 mg) was dissolved in DMSO (10 μL) and added to the polymer solution. The resulting organic solution was dropped slowly into PBS buffer (1 mL) under sonication. The mixture was then purified by passing through a G25 column to remove free OVA peptide. The amount of OVA encapsulated was determined by treating the nanoparticle solution with 0.1% TFA followed by HPLC quantification of free OVA in the solution. To determine the kinetics of OVA release, the OVA encapsulated nanoparticles were incubated in PBS buffer at room temperature for various time periods. The mixture was then centrifuged through a membrane filter (MWCO 100 KDa) and the flow through was analyzed by HPLC for the level of free OVA peptide.

3.4.9 Synthesis of methoxy polyethyleneglycol-poly(diisopropylaminoethyl methacrylate)-poly(aminoethyl methacrylate) (mPEG-PDPAMA-PAMA) 5

Initiator mPEG-Br **1** (100 mg, 20 μmol), DPAMA **2** (320 mg, 1.5 mmol), and Boc-AMA **4** (60mg, 0.25 mmol) were dissolved in mixed solvent of DMF: isopropanol (1: 1, 10 mL). PMDETA (3.5 mg, 20 μmol) was added to the solution. Then three cycles of freeze-pump-thaw were performed to remove oxygen. CuBr (2.9 mg, 20 μmol) was added under N_2 and the reaction mixture was kept under 60 □ for 6 h. The reaction was quenched by diluting with equal volume of THF (10 mL) and the mixture was passed through a short basic Al_2O_3 column. The solution was collected then concentrated under vacuum followed by dialysis (MWCO 3,500 Da) against pure water for 48 h. The solution in dialysis tubing was collected and lyophilized to give white solid compound mPEG-PDPAMA-PAMA-Boc (380 mg). ^{1}H NMR (500 MHz, $CDCl_3$, ppm) δ 4.12 – 3.77 (m, 142H), 3.65 (s, 454H), 3.38 (s, 3H), 2.99 (s, 120H), 2.63 (s, 120H), 2.08 – 1.70 (m, 142H), 1.53 – 1.39 (m, 99H), 1.15 – 0.80 (m, 933H).

The purified mPEG-PDPAMA-PAMA-Boc polymer (380 mg) was dissolved with pure TFA (3 mL) and stirred for 1 h for Boc deprotection. TFA was removed by a rotavapor and the residue was dissolved in THF (~ 3 mL) and dialyzed against pure water (MWCO 3,500 Da) for 24h followed by lyophilization to yield white powdered mPEG-PDPAMA-PAMA **5** (322 mg, yield = 92%). $_1$H NMR (500 MHz, $CDCl_3$, ppm) δ 4.70 – 4.00 (m, 142H), 3.85 – 3.59 (m, 574H), 3.48 – 3.15 (m, 120H), 2.43 – 1.77 (m, 355H), 1.72 – 0.51 (s, 720H).

3.4.10 Synthesis of carboxy-dimethylmaleic anhydride (CDM)[41]

Triethyl 2-phosphonopropionate (1.8g, 7.5 mmol) was dissolved in THF (5 mL) and added to a suspension of NaH (60% dispersion in mineral oil, 250 mg, 6.25 mmol) in THF (30 mL) on ice. The mixture was stirred for 0.5 h on ice, followed by addition of a solution of diethyl ketoglutarate (1 g, 5 mmol) in THF (5 mL). The stirring was continued for 30 min. The reaction was quenched by pouring the solution into saturated aq. NH_4Cl (100 mL) and then extracted with diethylether. The organic phase was dried over Na_2SO_4 and concentrated. The crude product was then purified with silica gel column chromatography using ether: hexanes = 2: 1 as the eluant. The resulting clear oil-like triester product was then dissolved in a mixture of 2 N aq. KOH (12.5 mL) and ethanol (50 mL) and heated to reflux for 1 h. The solution was diluted with water and ethanol was removed by a rotavapor. The resulting aqueous solution was acidified by HCl to pH 2 and extracted with ethyl acetate. The organic phase was dried and concentrated to give the desired product without further purification (460 mg, yield = 50% for two steps). ^{1}H NMR (500 MHz, $CDCl_3$, ppm) δ 2.77 (s, 4H), 2.13 (s, 3H). ^{13}C NMR (126 MHz, $CDCl_3$, ppm) δ 177.11, 165.72, 165.49, 142.42, 141.76, 30.70, 19.59, 9.69. MS: (ESI^+): $C_8H_8O_5$ $[M+MeOH+Na]^+$ calculated mass: 239.0526, observed mass: 239.0552.

3.4.11 Synthesis of mPEG-PDPAMA-PAMA-CDM 6 conjugate[42]

The CDM linker **11** was synthesized right before conjugation with mPEG-PDPAMA-PAMA **5**. CDM (20 mg, 108 μmol) was dissolved in anhydrous DCM (1 mL) and cooled on ice for 10

min. Oxalyl chloride (20 μL, 233 μmol) was added followed by a catalytic amount of DMF (20 μL). The reaction was stirred on ice for 15 min then allowed to reach room temperature and stirred for another 1 h. The reaction mixture was dried under vacuum to yield CDM linker **11** without purification.

To conjugate CDM linker **11** with mPEG-PDPAMA-PAMA **5**, mPEG-PDPAMA-PAMA **5** (100 mg, ~5 μmol) was dissolved in anhydrous DCM (5 mL) and added to CDM linker **11**. Small amount of pyridine (30 μL) was added to the reaction mixture as catalyst. The reaction was stirred for 24h under room temperature. Then DCM was removed by a rotavapor. The residue was dissolved in THF (~ 3 mL) and dialyzed against pure water (MWCO 3,500 Da) for 24 h. The solution in dialysis tubing was lyophilized to yield orange color solid product (94 mg, yield = 86%). ^{1}H NMR (500 MHz, $CDCl_3$, ppm) δ 4.29 (s, 142H), 3.76 – 3.42 (m, 574H), 3.38 (s, 3H), 3.35 – 2.94 (s, 120H), 2.80 – 2.69 (m, 20H), 2.36 (s, 30H), 2.17 – 2.08 (m, 20H), 1.95 – 0.75 (m, 1174H).

3.4.12 Synthesis of P-CDM-OVA 8 and P-CDM-IMQ 10

With mPEG-PDPAMA-PAMA-CDM **6** in hand, we covalently conjugated antigen OVA peptide and TLR 7 agonist IMQ with the polymer respectively. Briefly, OVA peptide or IMQ (2.2 mg, 11 wt% of polymer) and mPEG-PDPAMA-PAMA-CDM **6** (20 mg) were dissolved in DMSO (0.5 mL) followed by addition of solid K_2CO_3 (50 mg). The reaction mixture was stirred under room temperature for 24 h. Solid K_2CO_3 was filtered out and DMSO phase was collected and diluted in 10x water with triethylamine (TEA, pH = 9). The resulting cloudy mixture was filtered

by centrifuge filtration tube (MWCO = 10 KDa) and washed twice with 5% DMSO in water with TEA (pH = 9) and twice with water with TEA (pH = 9). The polymer product was collected and lyophilized to give P-CDM-OVA **8** (20.3 mg) or P-CDM-IMQ **10** (19.8 mg). Yield >90%. All washing elution was collected for HPLC (for OVA) or UV (for IMQ) analysis to determine the wt% of OVA or IMQ conjugated to polymer. For P-CDM-OVA **8**, the final loading was 10.4 wt%. For P-CDM-IMQ 10, the loading was 9.7 wt%.

3.4.13 Synthesis of P-ADA-OVA 9

Adipic acid di-NHS ester linker **12** was prepared according to literature reports3. mPEG-PDPAMA-PAMA **5** (20 mg, ~ 2.5 μmol) was dissolved in DMSO (1 mL) with adipic acid-di-NHS ester linker **12** (85 mg, 0.25 mmol). The mixture was stirred under room temperature overnight. 0.1 N HCl (20 mL) was added to the reaction mixture in order to precipitate out the unreacted linker. The supernatant was collected, and centrifuge filtration (MWCO 10 KDa) was performed to concentrate mPEG-PDPAMA-PAMA-ADA **7**. The mPEG-PDPAMA-PAMA-ADA **7** solution was lyophilized and re-dissolved in DMSO (1 mL), then OVA peptide (2.2 mg) was added. The reaction was carried out for 24h at room temperature. The reaction mixture was then diluted in 10x water and filtered by 30 K cut-off centrifuge filtration tube and washed twice with 5% DMSO in water and twice with water. The polymer product was collected and lyophilized to give P-ADA-OVA **9**. All washing elution was collected for HPLC analysis to determine the wt% of OVA conjugated to polymer. The loading level of P-ADA-OVA **9** was 9.1 wt%.

3.4.14 Release profile of small molecule cargoes

P-CDM-OVA **8** or P-CDM-IMQ **10** (1 mg) was dissolved in THF (50 μL) and diluted in 1 mL buffer with different pH values. At various time points, centrifuge filtration with 10K cut-off filter was performed to collect buffer with released small molecules. 0.5 mL of the elution was used for HPLC or UV analysis to quantify the amount of released small molecules.

3.4.15 General procedure of nanoparticle preparation

mPEG-PDPAMA **3** or antigen/adjuvant-polymer conjugates (P-CDM-OVA **8**, P-ADA-OVA **9** or P-CDM-IMQ **10**, 2 mg) was dissolved in THF (0.1 mL), then the polymer solution was slowly dropped into PBS buffer (1 mL) under sonication through a 25 G needle over 5 minutes. The mixture was sonicated for another 2 min upon completion of polymer addition. The resulting particles were washed with PBS buffer 3 times by centrifuge filtration (MWCO = 100 KDa). The washed particles were then collected and adjusted to 1 mL final volume with PBS buffer (2 mg polymer/mL, containing 200 μg OVA or IMQ/mL). These particles were used for cellular and *in vivo* immunization directly.

For P-CDM-OVA **8**/P-CDM-IMQ **10** hybrid particles, 1 mg of P-CDM-OVA **8** and 1 mg of P-CDM-IMQ **10** were combined and dissolved in THF (0.1 mL) followed by the same procedure as described above.

3.4.16 Antigen presentation on cell surface MHC I molecules

EL4 cells ($3x10^5$ in 1 mL media) were cultured with 100 ng/mL OVA peptide, P-CDM-OVA **8** or P-ADA-OVA **9** respectively in FACS tubes for different time period (2, 12, 24, 48, 72 h). Cells are collected and washed with FACS buffer (1% FBS, 0.5% NaN_3 in PBS), then stained with a monoclonal antibody (anti-SIINFEKL bound to H2Kb , clone 25-D1.16) or anti-mouse IgG1K (isotype control) for 30 min on ice in dark. Cells are washed twice with FACS buffer followed by FACS analysis.

3.4.17 B3Z assay

2 x 10^4 BMDCs were cultured overnight in a 96 well plate and subsequently incubated with free OVA, free OVA + IMQ, free OVA + empty particle (1 mg/mL mPEG-PDPAMA **3**), P-CDM-OVA **8**, P-CDM-OVA **8** + IMQ, P-CDM-OVA **8** +P-CDM-IMQ **10** (mixture of two types of particles) or P-CDM-OVA **8**/P-CDM-IMQ **10**(hybrid particles) at increasing concentrations (0.1 – 1000 ng OVA/mL). After 12 hours, the cells were washed and 1 x 10^5 B3Z cells were added to the BMDCs and co-cultured for an additional 24 hours. The culture media was removed and 100 µL of chlorophenol red-β-D-galactopyranoside (CPRG) buffer (9.1 mg of CPRG, 90 mg $MgCl_2$ and 0.1% Triton-X-100 in 100 mL of PBS) was added to each well. After 4 hours, the absorbance at 595 nm was measured using a microplate reader. The results were presented as a mean of triplicate.

3.4.18 Quanti-Blue assay

Solutions of various stimulators (free IMQ or P-CDM-IMQ **10** at various IMQ concentrations, 100 ng/mL LPS, 1mg/mL PEG-PDPAMA **3**) were added to 96-well plate respectively (adjusted to 20 μL total volume), each as a triplicate. 1 x 10^5 RAW-Blue cells in cell culture media (180 μL) were then seeded to the wells with the stimulators and cultured for 24 h. After the 24 h incubation, 20 μL/well of cell supernatant was transferred to a new 96 well plate. Then 180 μL/well Quanti-BlueTM solution (pre-warmed to 37 □) was added to the cell supernatant in the new 96 well plate. The mixture was incubated under 37 °C for 2 h then the absorbance values were read under 655 nm by a plate reader. The results were presented as a mean of triplicate.

3.4.19 BMDC activation study

BMDCs (3 x 10^5 cells per sample) were incubated with culture medium only, PEG-PDPAMA **3** (1 mg/mL) or LPS (100ng/mL) for 48 h at 37 °C. The cells were washed twice after incubation followed by staining with APC-anti-mouse CD11c mAb (clone N418), PE-anti-mouse CD80 mAb (clone 16-10A1), APC/Cy7-anti-mouse CD86 mAb (clone GL-1), and FITC-anti-mouse CD40 mAb (clone 3/23) on ice in dark for 30 min. The stained cells were washed for 3 times with FACS buffer followed by FACS analysis. Non-stained cells (cell only) were used as a negative control. The $CD11c^+$ cells were gated and the mean fluorescence intensity (MFI) of PE channel (for CD80), APC/Cy7 channel (for CD86) and FITC channel (for CD40) were reported. The results were presented as a mean of triplicate.

3.4.20 *In vivo* CTL assay

P-CDM-OVA **8**, P-CDM-IMQ **10** and P-CDM-OVA **8**/P-CDM-IMQ **10** hybrid nanoparticles were prepared as described above. OVA encapsulated Ac-Dex MPs were prepared as previously reported[43]. These particles were used for vaccine immunization.

8-week-old C57BL/6 female mice were immunized with different vaccine formulations once a week for a total of 3 injections. For comparing the CTL activation effect of P-CDM-OVA **8** and Ac-Dex-OVA, P-CDM-OVA **8** or Ac-Dex-OVA was used for subcutaneous or intravenous immunization (20 μg OVA per dose) without any additional adjuvants. For evaluating the adjuvant efficiency, free OVA/P-CDM-OVA **8** and free IMQ/P-CDM-IMQ **10** were used for subcutaneous immunization at a dose of 20 μg OVA and 20 μg IMQ per mouse.

On day 3 after the final immunization, a mixture of non-treated $CFSE^{lo}$ and OVA pulsed $CFSE^{hi}$ splenic cells (0.2 mL, 4 million cells) was injected through the tail vein to the immunized mice. The excess cell mixture was stored in culture media under 37 °C as a "before injection" sample. Mice were sacrificed after 24 hours. Spleen cells were collected, washed with PBS twice and then fixed in 10 mL 10% formalin in PBS. 3-4 lymph nodes were collected from each mouse. Lymph nodes were set in same Petri dish, smashed and filtered to create lymph node cell samples. Cells were washed twice with PBS buffer and fixed in 4 mL 10% formalin in PBS. The spleen and lymph node samples were analyzed by FACS. The changes of ratio of $CFSE^{hi}$: $CFSE^{lo}$ before and after injection were achieved from FITC-SSC plot to calculate target cell viability.

3.4.21 Tumor challenge

Eight week old C57BL/6 mice were subcutaneously injected 1 million EG7 cells on the right flank and divided into 5 groups (PBS, free OVA + IMQ + empty NP, aPD-1, P-CDM-OVA **8** + P-CDM-IMQ **10** and P-CDM-OVA **8** + P-CDM-IMQ **10**+aPD-1) with 10 mice in each group. On days 5, 7, 9, 11 and 13, mice received the treatments intratumorally (the doses correspond to 25 μg OVA and 25 μg IMQ). On days 6, 9, and 12, the aPD-1 and P-CDM-OVA **8** +P-CDM-IMQ **10** +aPD-1 group received 100 μg aPD-1 treatment intraperitoneally. Tumor growth was monitored every other day and tumor sizes were calculated using the formula: 1/2(L x W x H). Data was recorded before first animal's tumor size reached 1600mm3.

3.4.22 The influence of BSA protein on P-CDM-OVA cleavage

P-CDM-OVA **8** (1 mg/ml final concentration, 0.5 ml volume) in pH = 6.4 or 7.4 citric buffer were incubated at room temperature with or without the addition of BSA protein in the buffer (0.5 mg/ml final concentration) for 4h, 24h and 1 week. Cold ethanol (10 ml) was added to each sample to precipitate out most part of the BSA protein and salts in the buffer. The mixture was centrifuged, and the supernatant was collected and dried for LC-MS analysis. For quantification standard, different amounts of OVA peptide were dissolved in citric buffer with or without the addition of BSA protein (0.5 mg/ml), followed by ethanol precipitation and centrifuge. The supernatants were collected and dried for LC-MS analysis standards. The OVA release from samples with and without BSA addition were quantified with the corelated OVA standard curve.

3.4.23 Serum TNF-α detection

Eight-week-old C57BL/6 mice were subcutaneously injected with PBS, free IMQ (20 μg/dose), empty NPs (200 μg/dose) or P-CDM-OVA **8** +P-CDM-IMQ **10** (20 μg OVA and 20 μg IMQ/dose). Two mice from each group were euthanized 24 h after injection for sera collection. Another two mice from each group were euthanized on day 7 after received 3 injections on day 0, 3 and 6 for sera collection. Sera samples were analyzed with TNF-α ELISA kit without dilution. TNF-α level in each sample was quantified with the standard curve of TNF-α protein.

APPENDICES

APPENDIX A: TEM image of particles

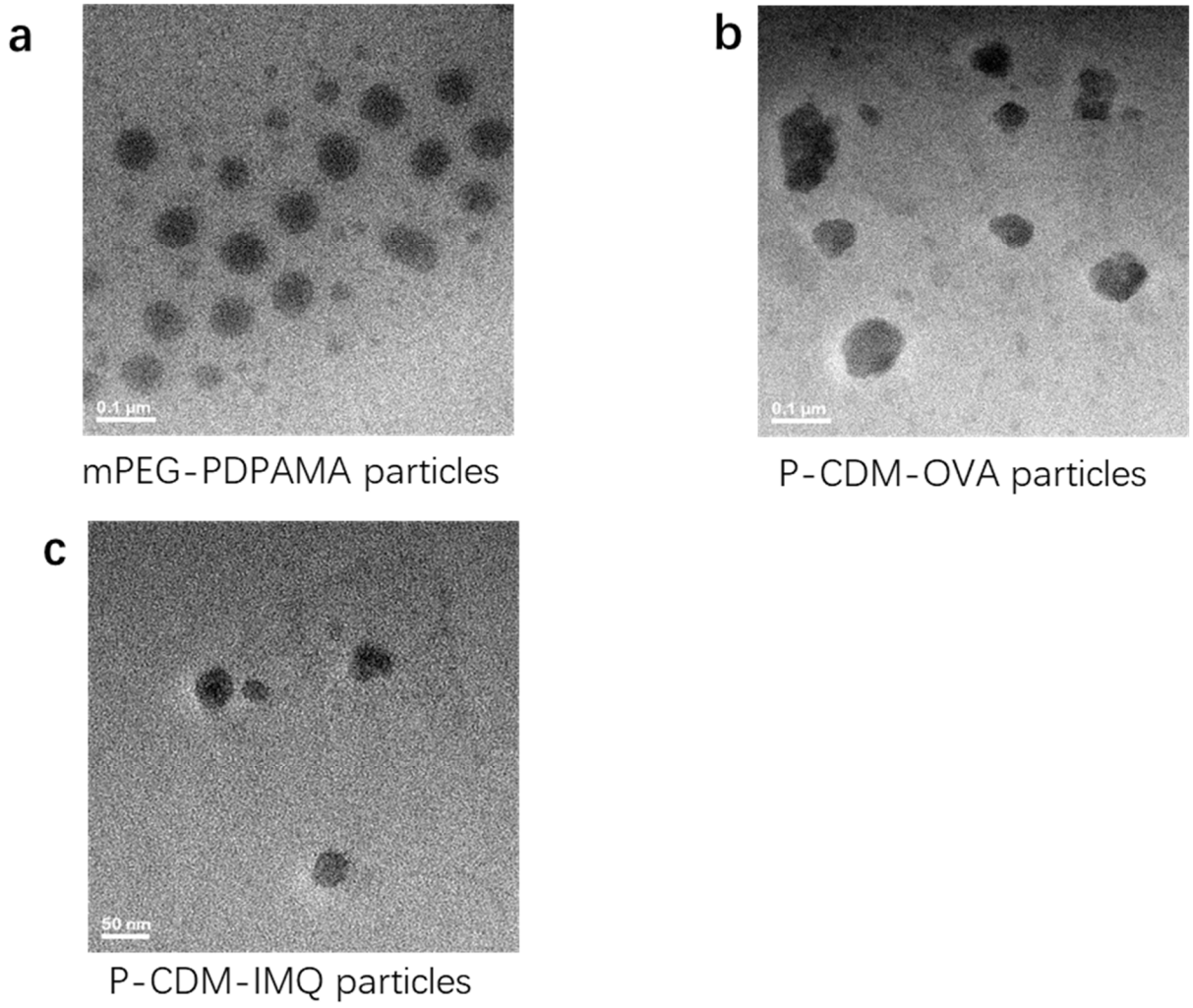

Figure 3.14 TEM images of nanoparticles formed by **a.** mPEG-PDPAMA, **b.** P-CDM-OVA, and **c.** P-CDM-IMQ

APPENDIX B: Quantification standard curves

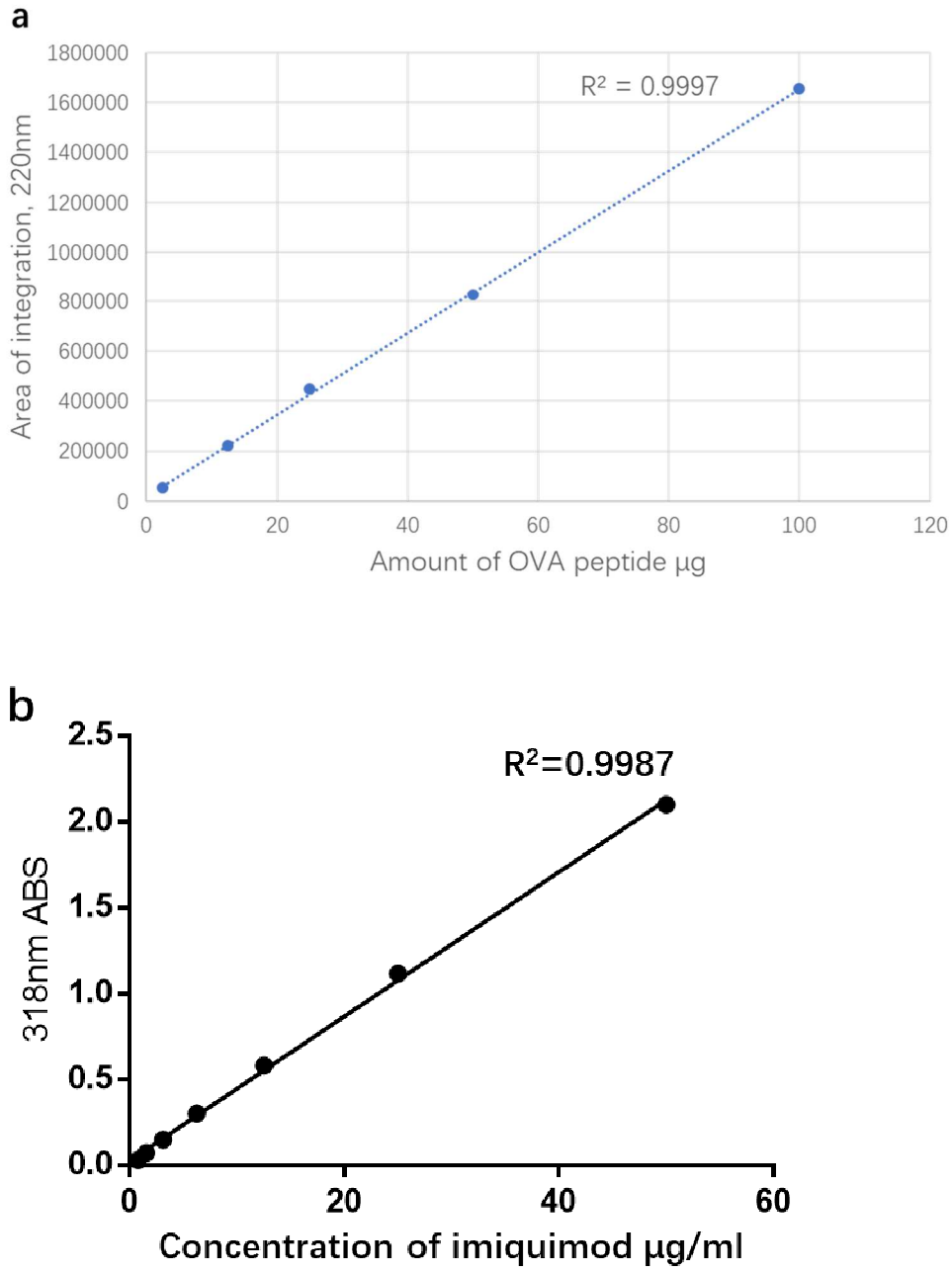

Figure 3.15 Standard curve for quantification of free OVA peptide and imiquimod. **a.** Standard curve between the amounts of OVA peptide and areas of integration from HPLC chromatograms. **b.** Standard curve for correlation between the concentration of imiquimod and UV absorbance value at 318nm.

APPENDIX C: NMR spectra

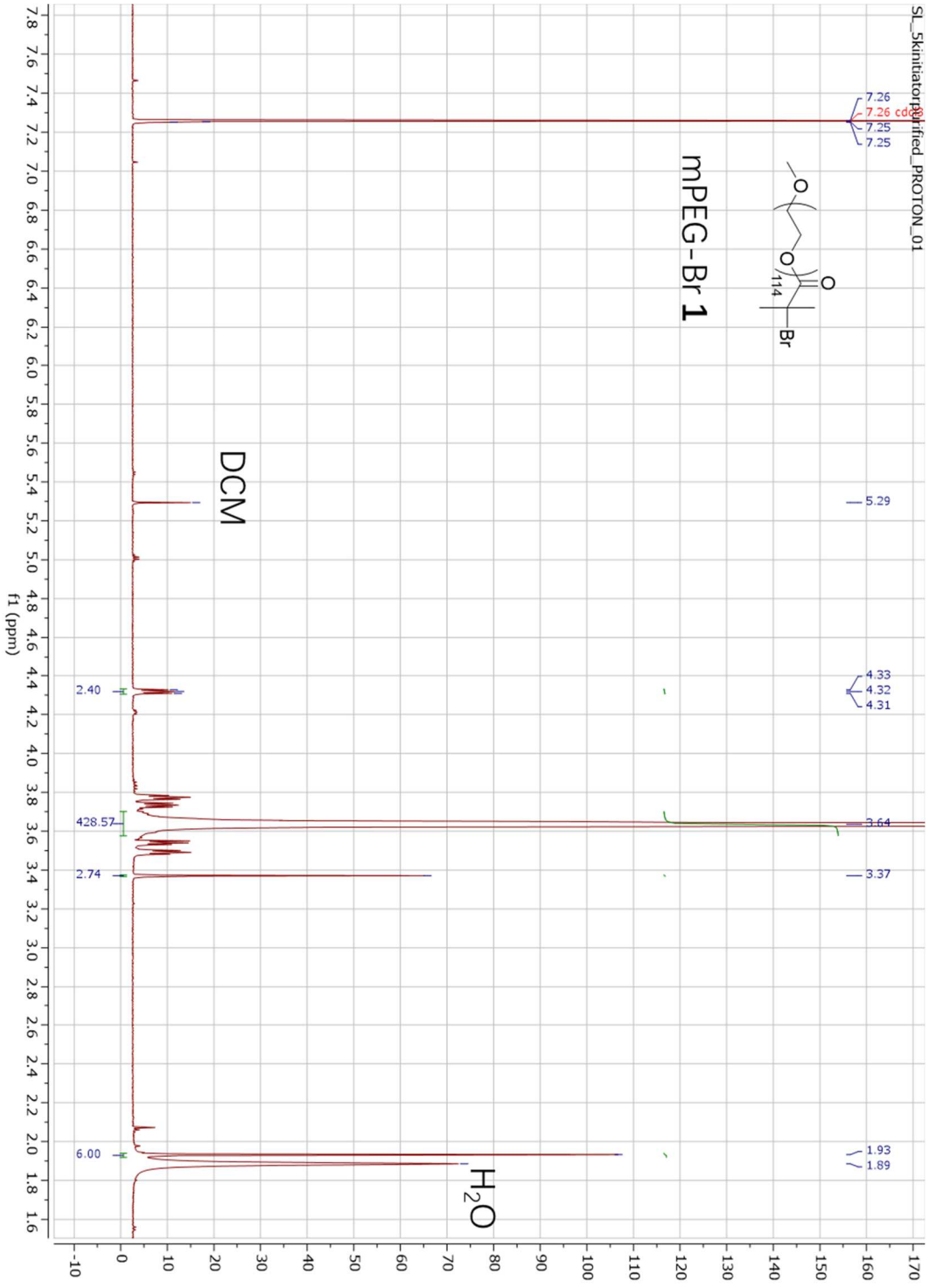

Figure 3.16 ^{1}H NMR spectrum of mPEG-Br **1** (500 MHz, $CDCl_3$)

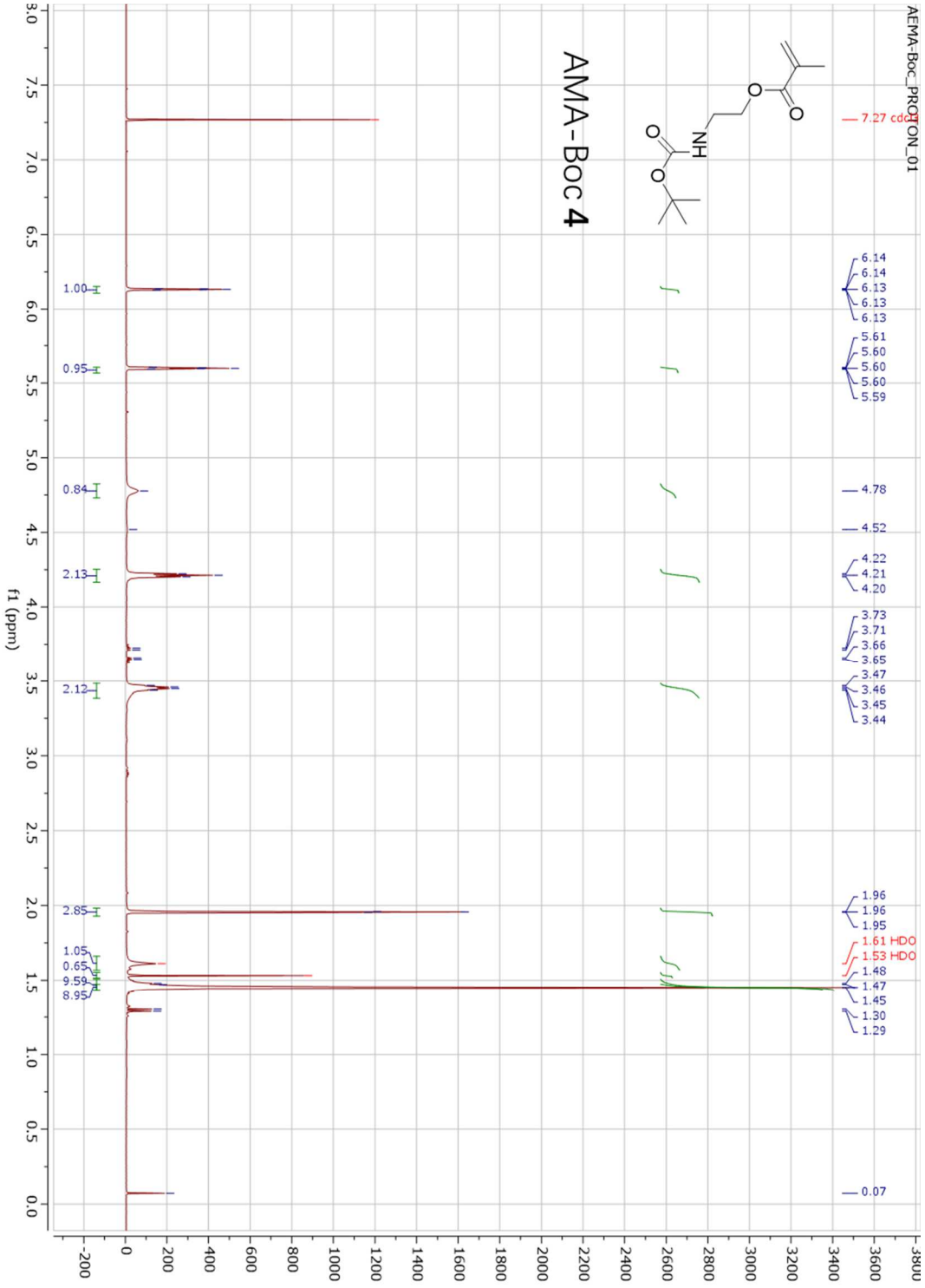

Figure 3.17 ^{1}H NMR spectrum of AMA-Boc **4** (500 MHz, $CDCl_3$)

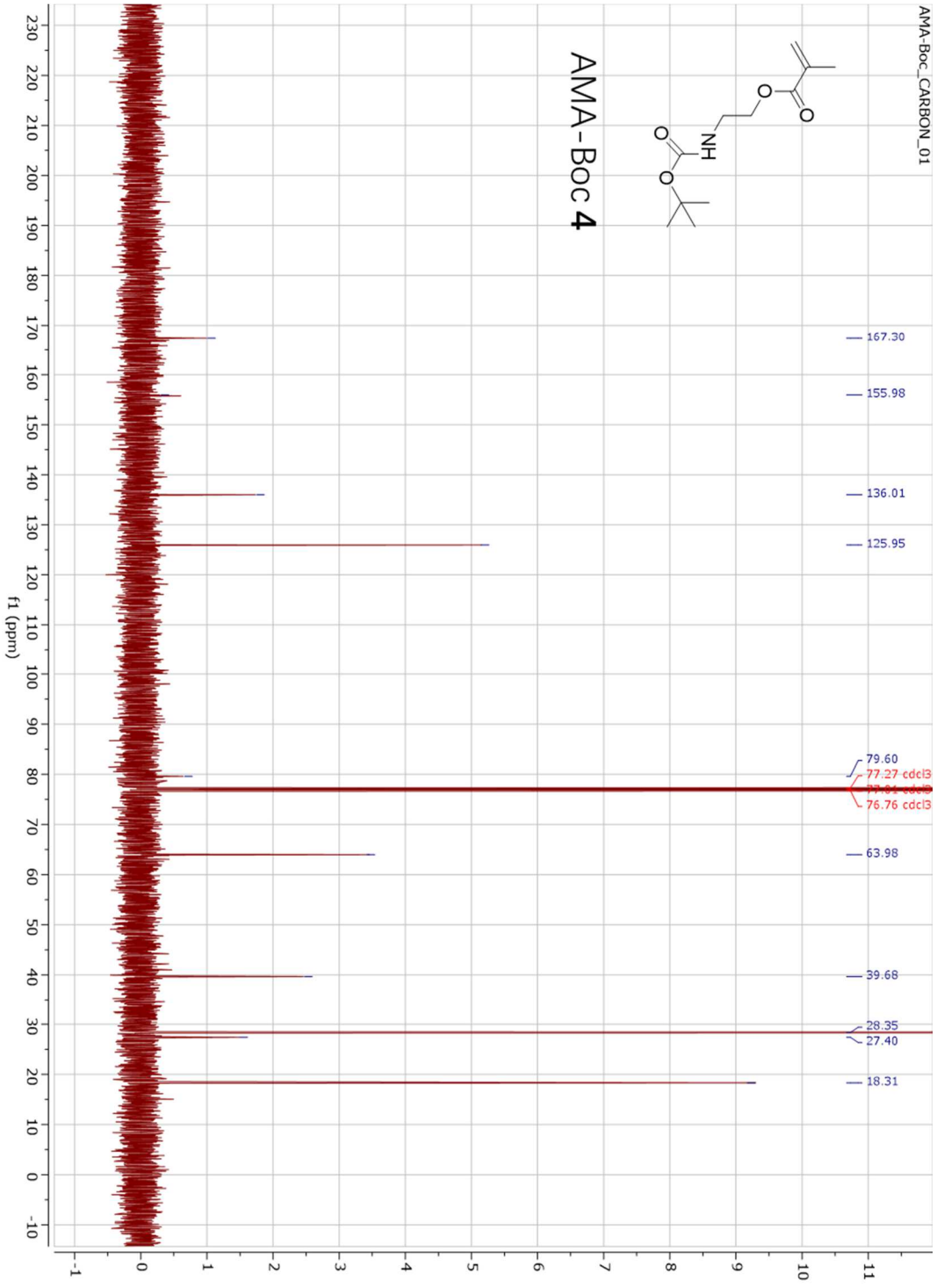

Figure 3.18 ^{13}C NMR spectrum of AMA-Boc **4** (125 MHz, $CDCl_3$)

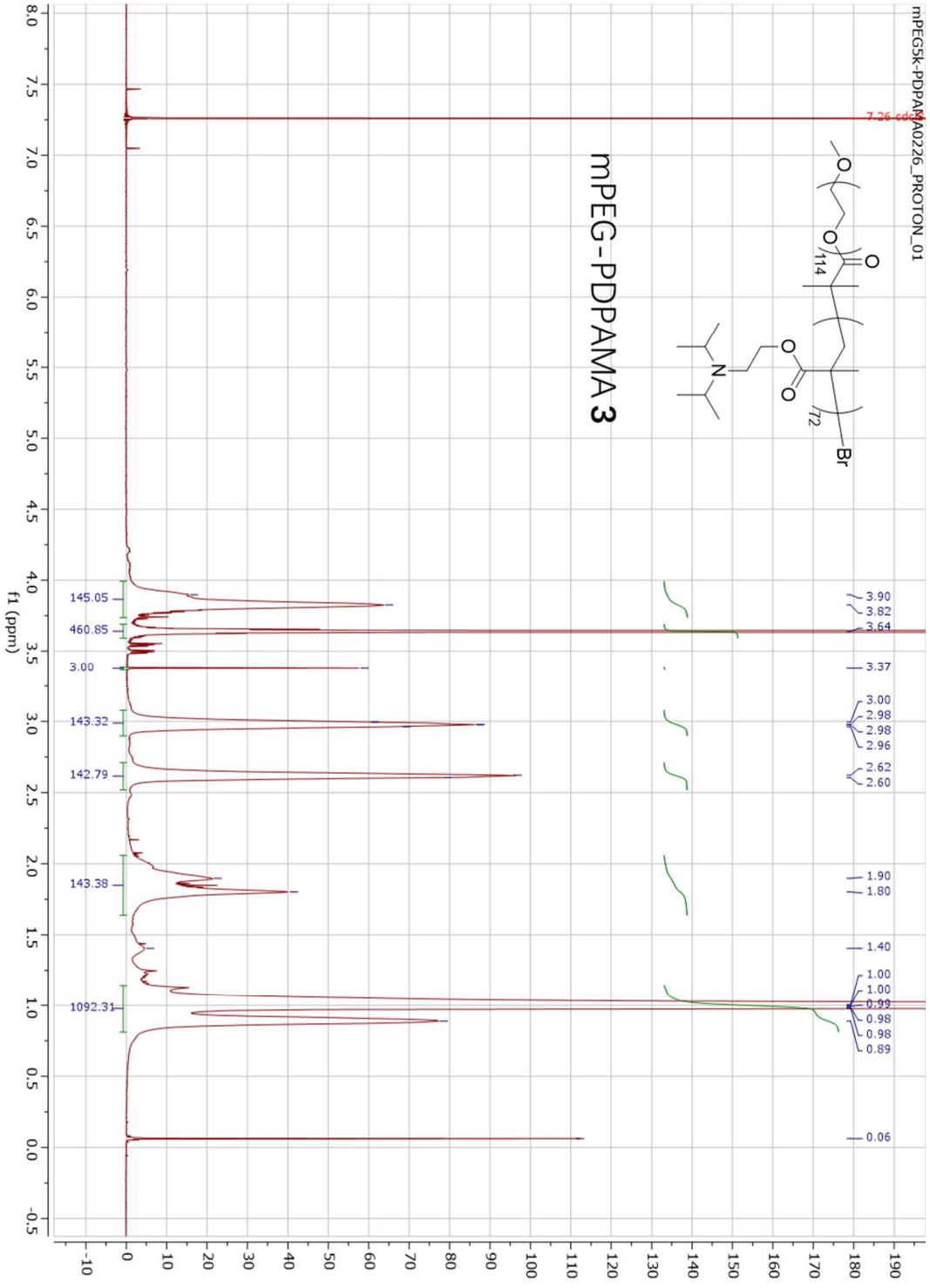

Figure 3.19 ^{1}H NMR spectrum of mPEG-PDPAMA **3** (500 MHz, $CDCl_3$)

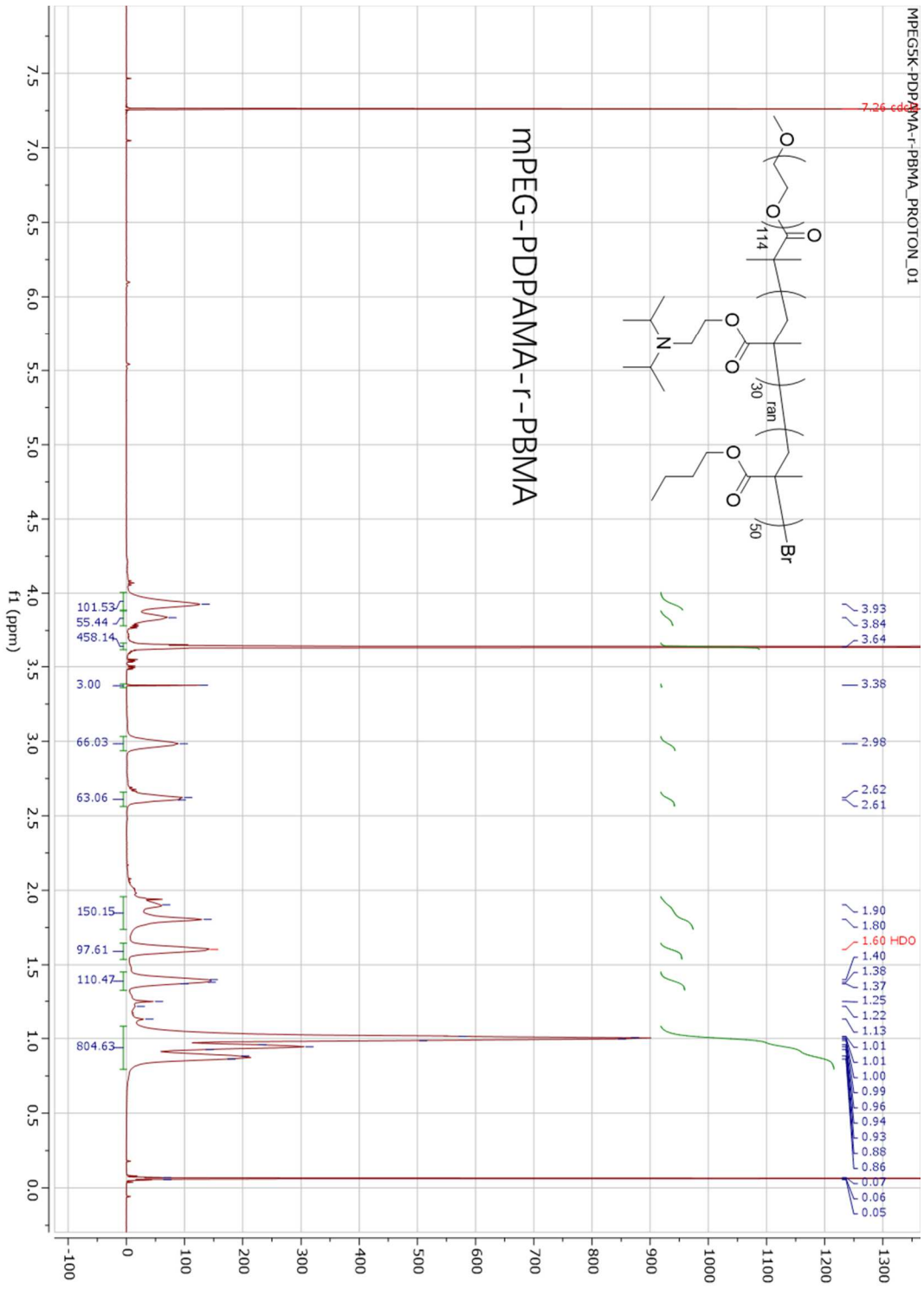

Figure 3.20 ^{1}H NMR spectrum of mPEG-PDPAMA-r-PBMA (500 MHz, $CDCl_3$)

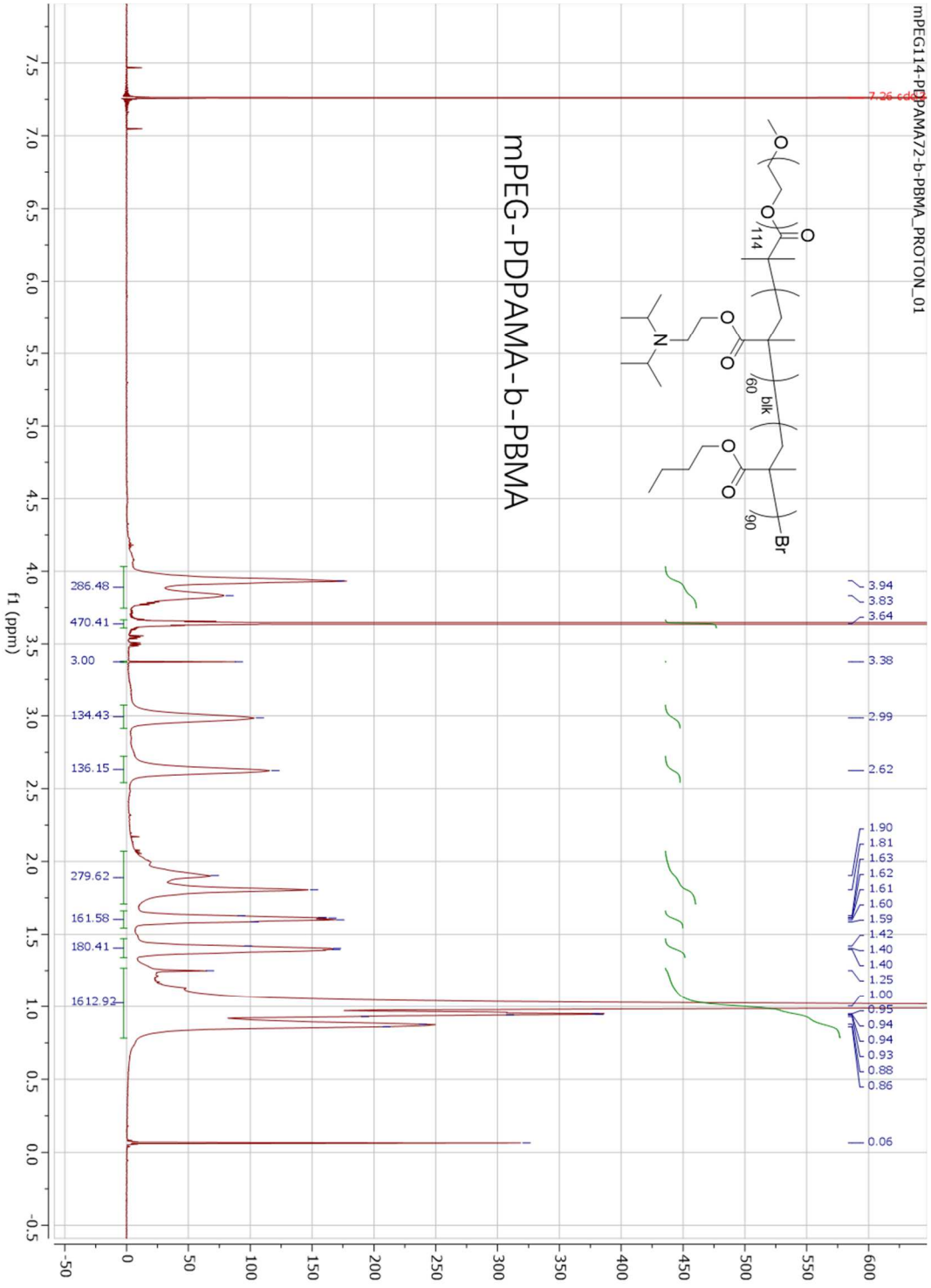

Figure 3.21 ^{1}H NMR spectrum of mPEG-PDPAMA-b-PBMA (500 MHz, $CDCl_3$)

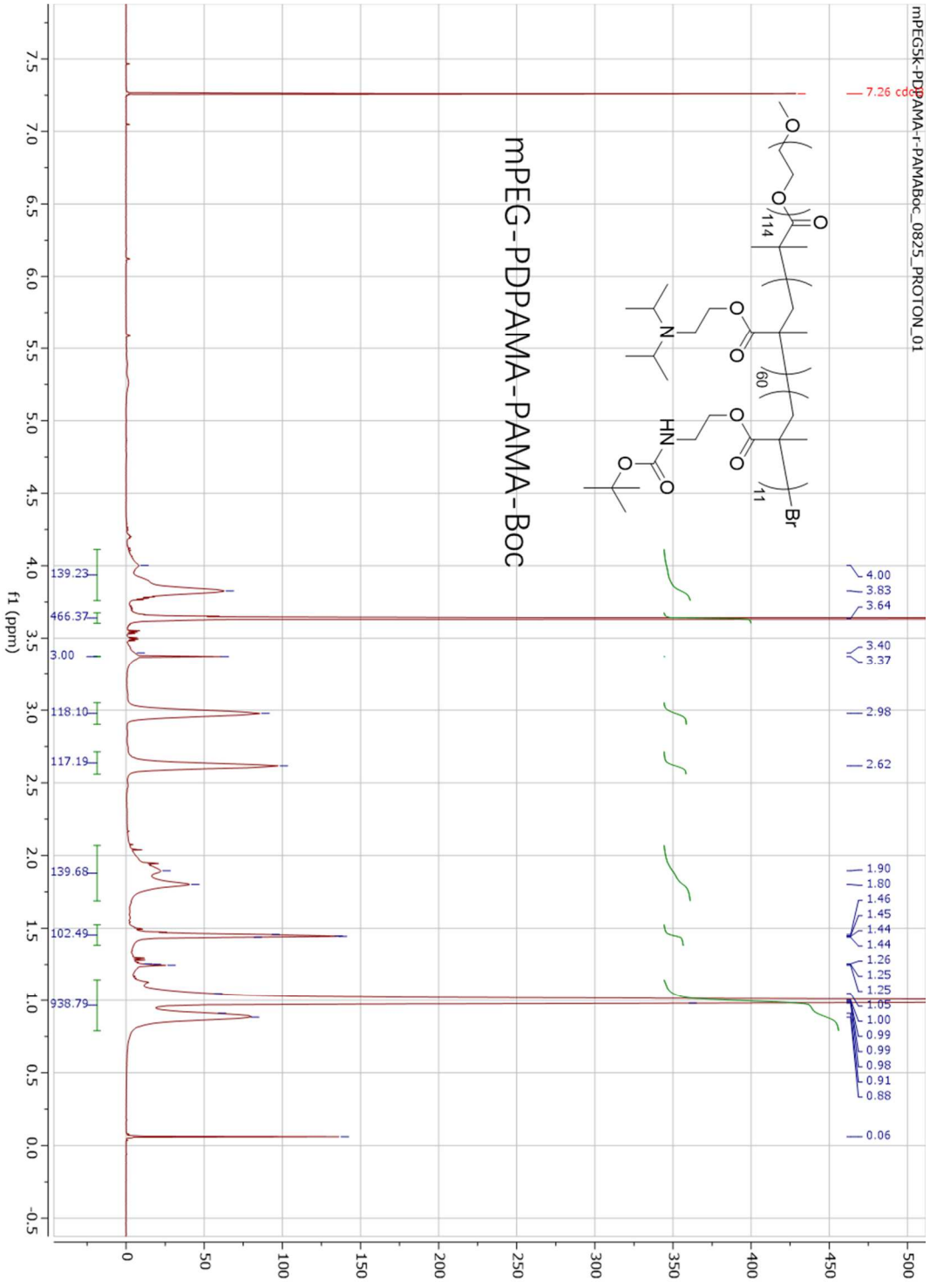

Figure 3.22 ^{1}H NMR spectrum of mPEG-PDPAMA-PAMA-Boc (500 MHz, $CDCl_3$)

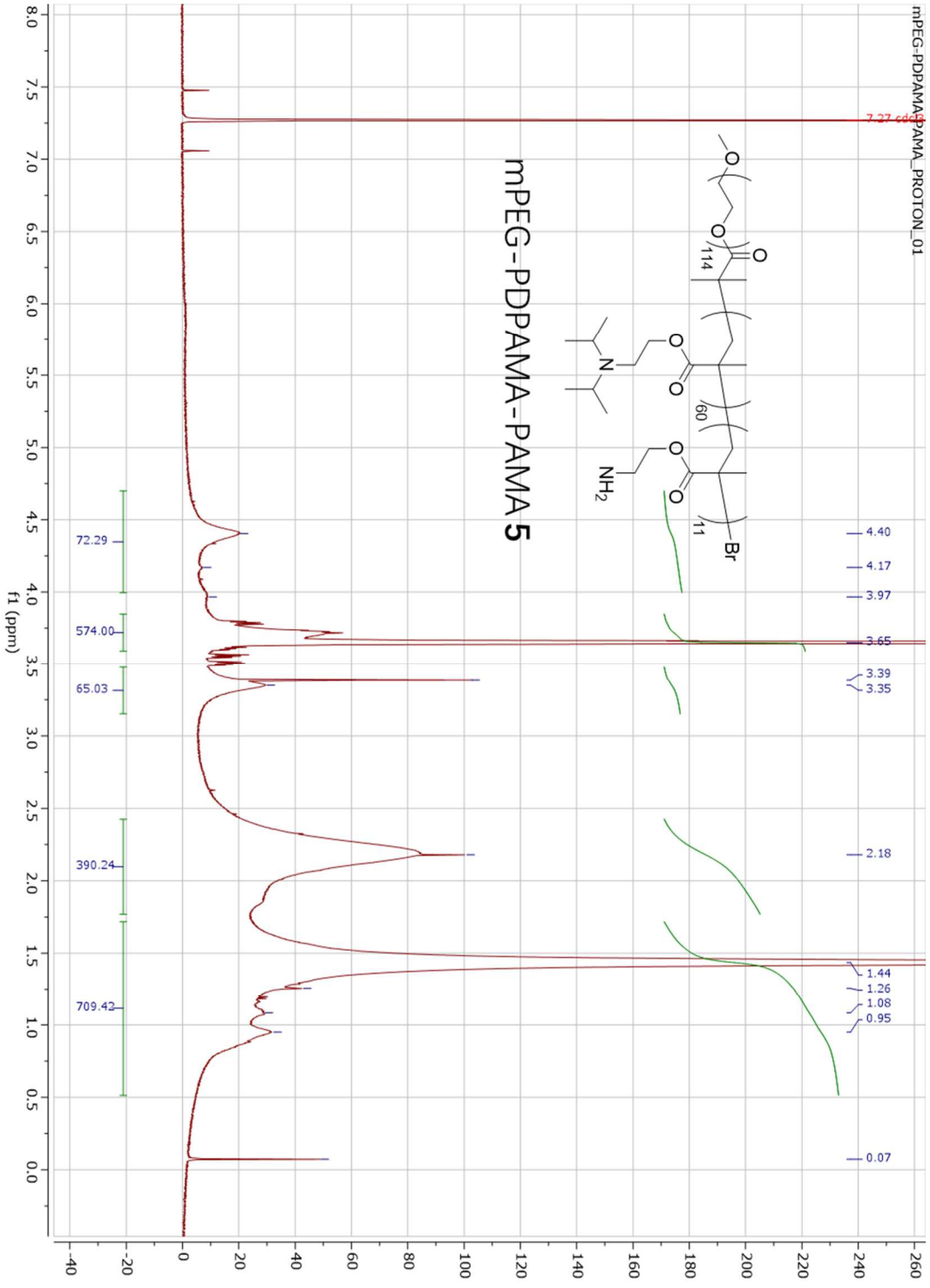

Figure 3.23 ^{1}H NMR spectrum of mPEG-PDPAMA-PAMA **5** (500 MHz, $CDCl_3$)

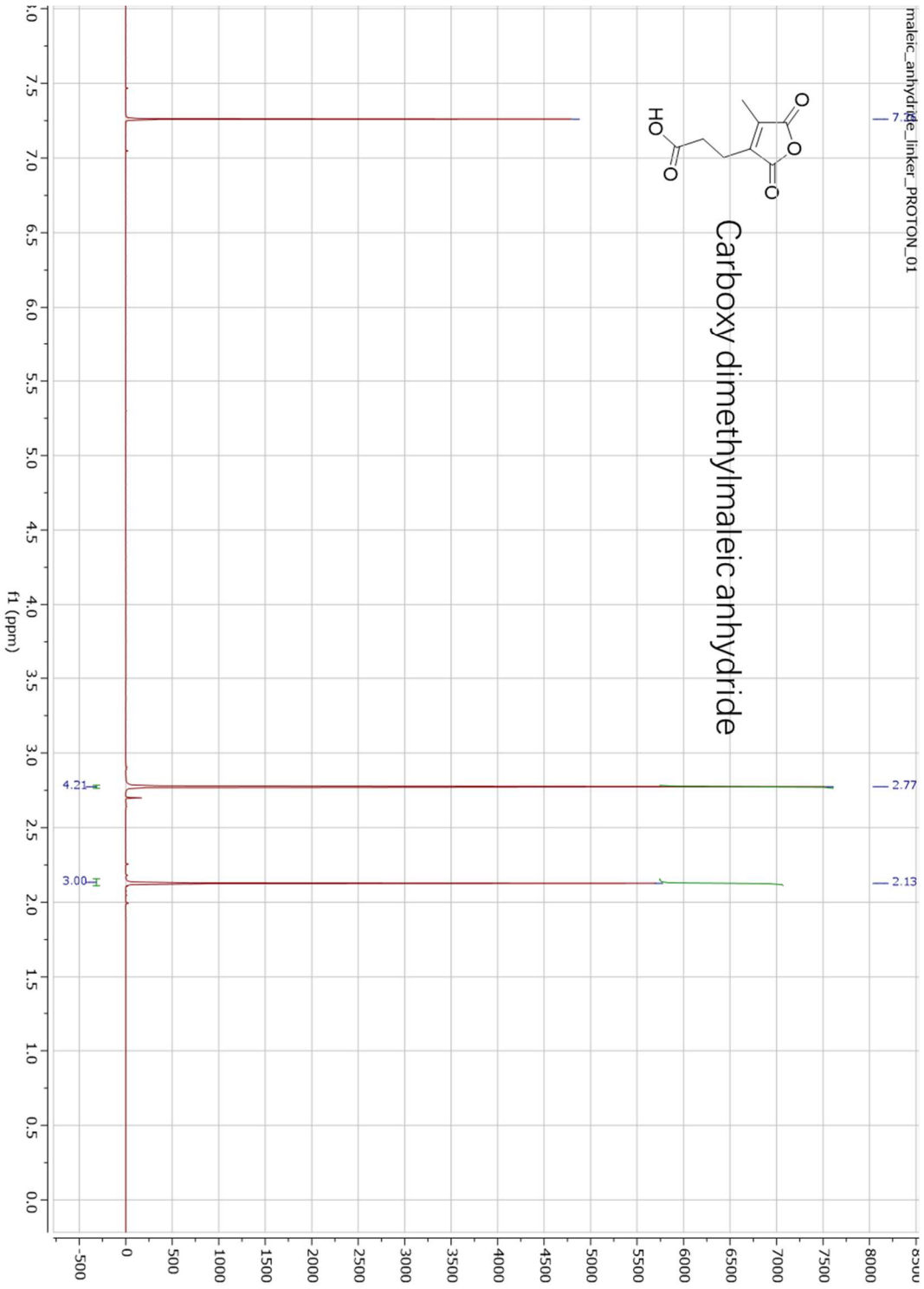

Figure 3.24 ^{1}H NMR spectrum of CDM (500 MHz, $CDCl_3$)

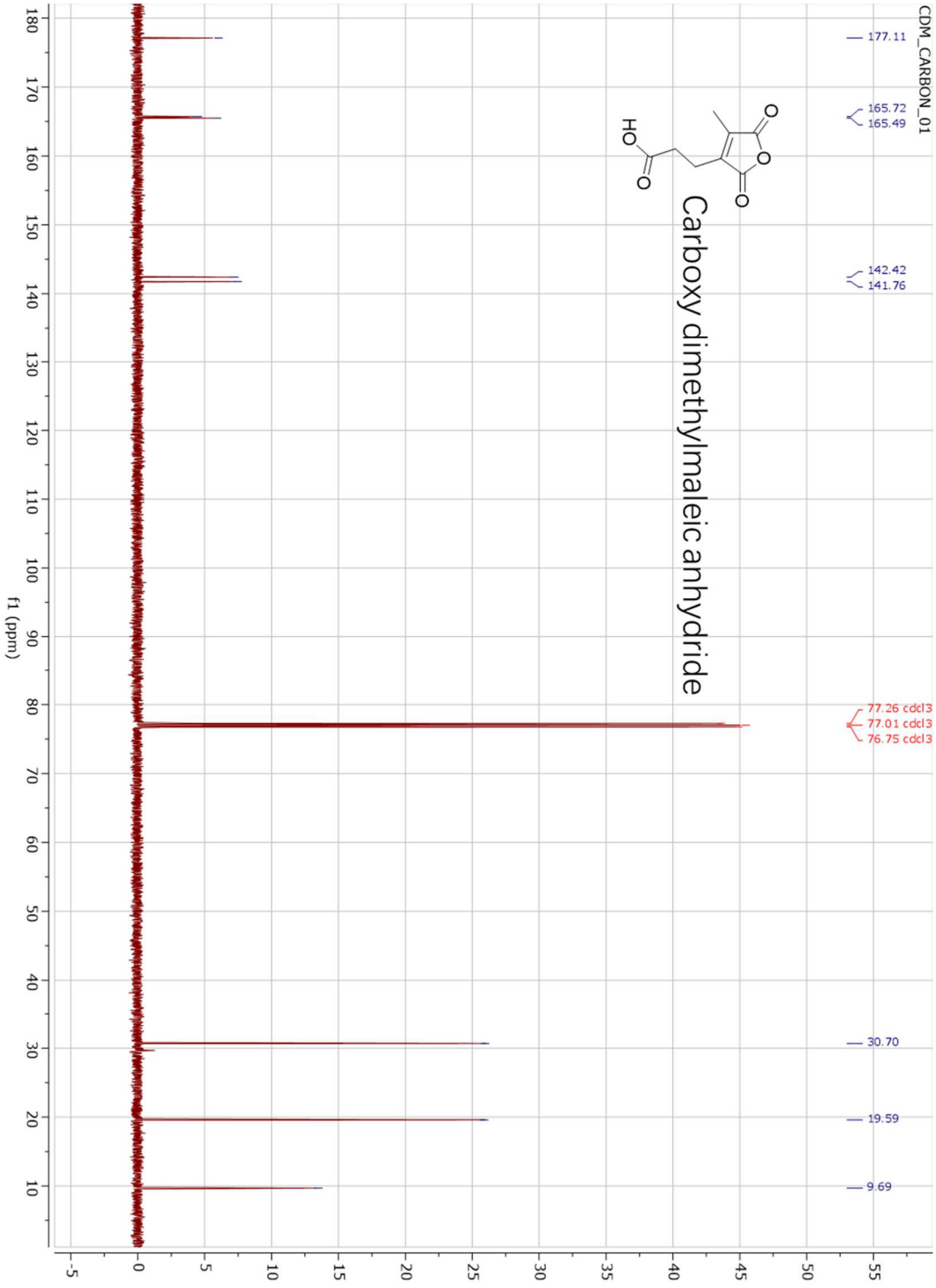

Figure 3.25 ^{13}C NMR spectrum of CDM (125MHz, $CDCl_3$)

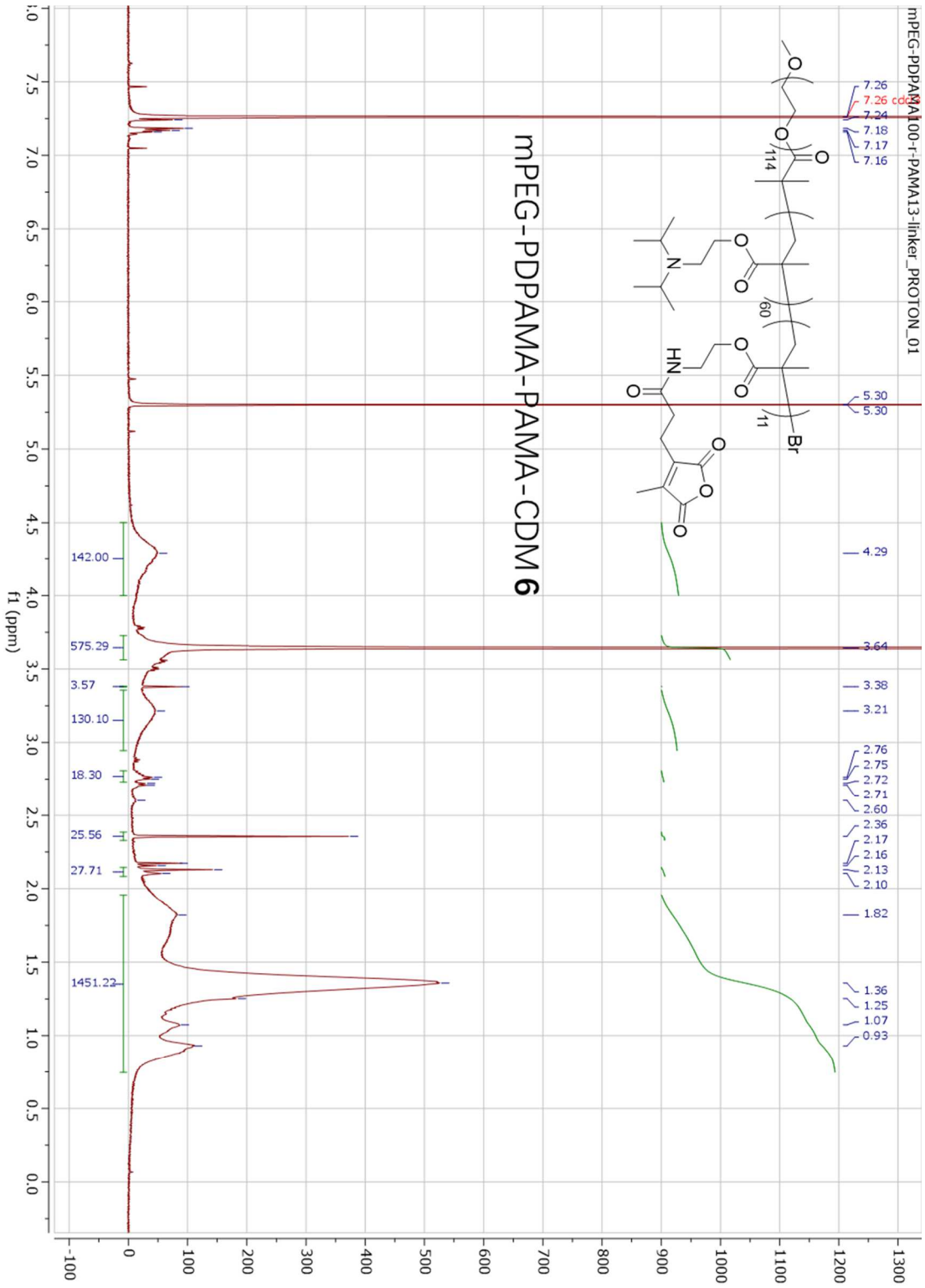

Figure 3.26 ^{1}H NMR spectrum of mPEG-PDPAMA-PAMA-CDM **6** (500 MHz, $CDCl_3$)

APPENDIX D: GPC and HPLC traces

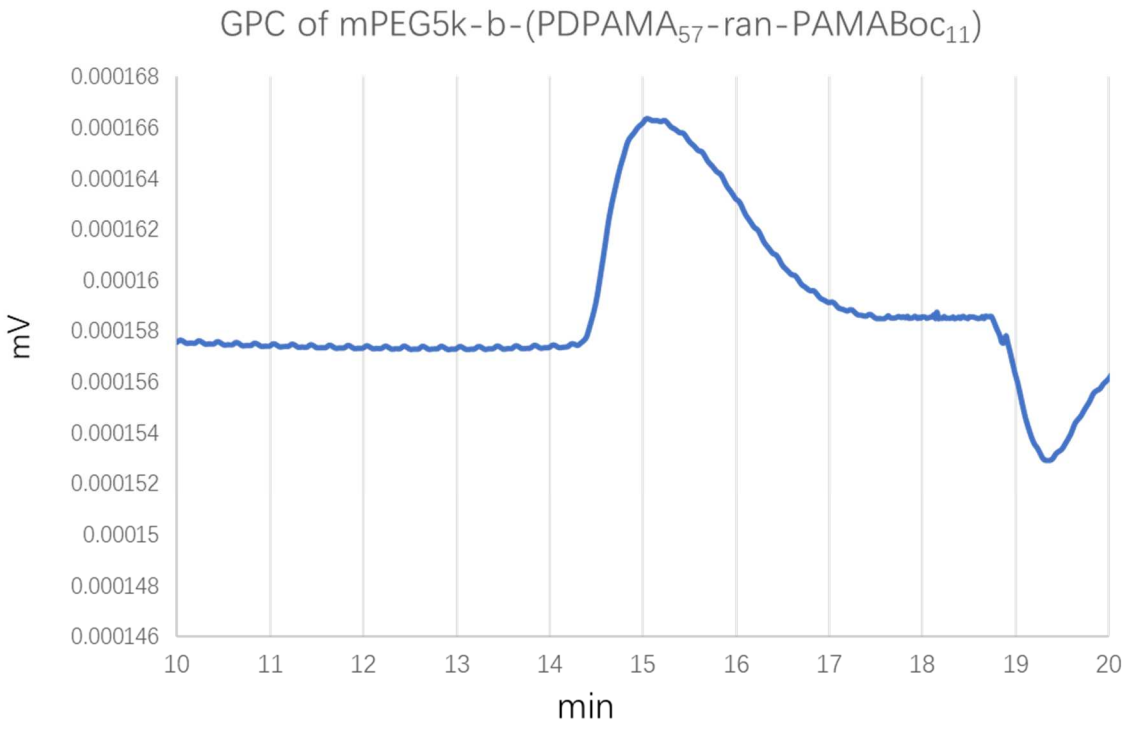

Figure 3.27 GPC trace of mPEG-PDPAMA-PAMABoc

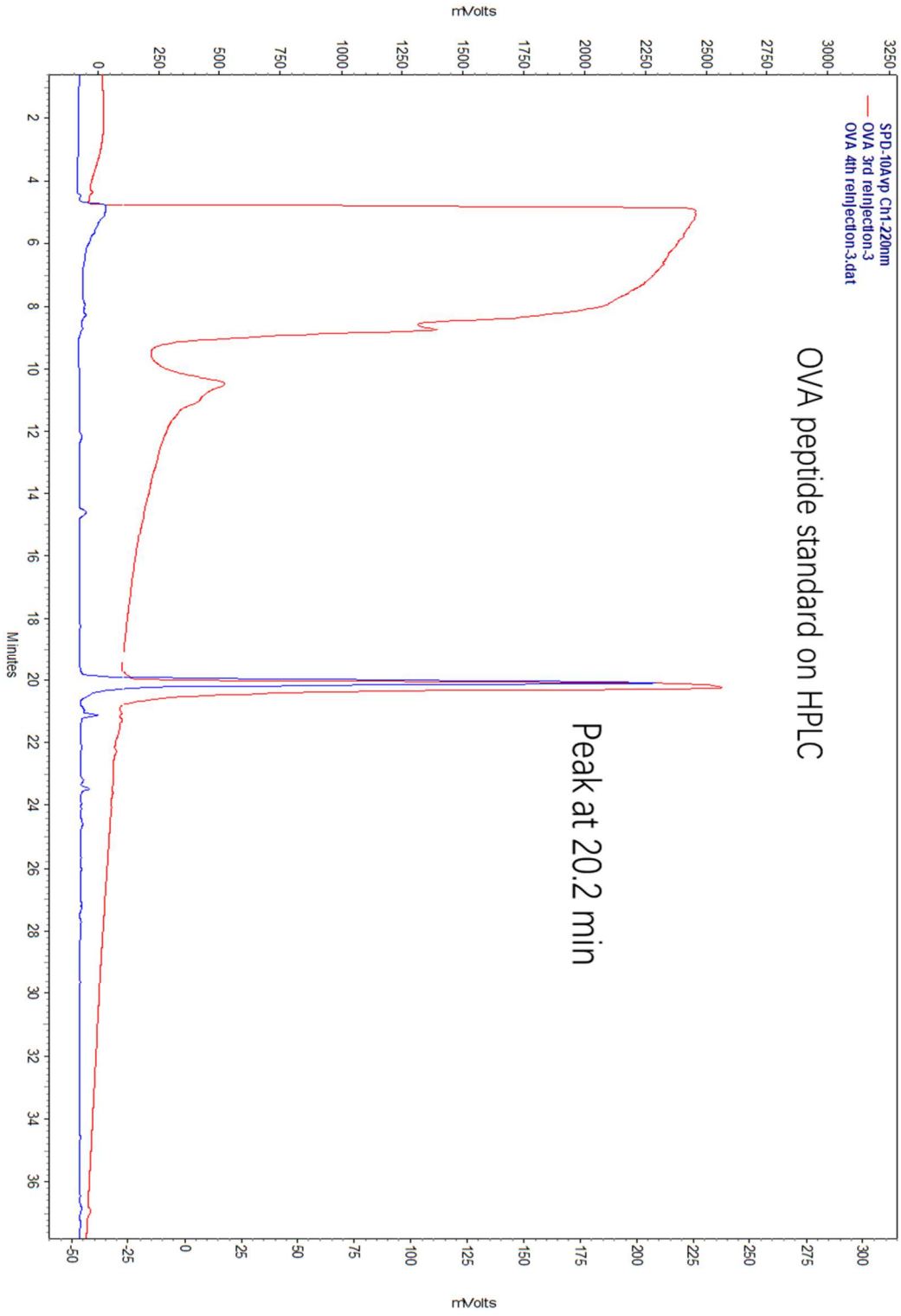

Figure 3.28 OVA peptide standard on HPLC

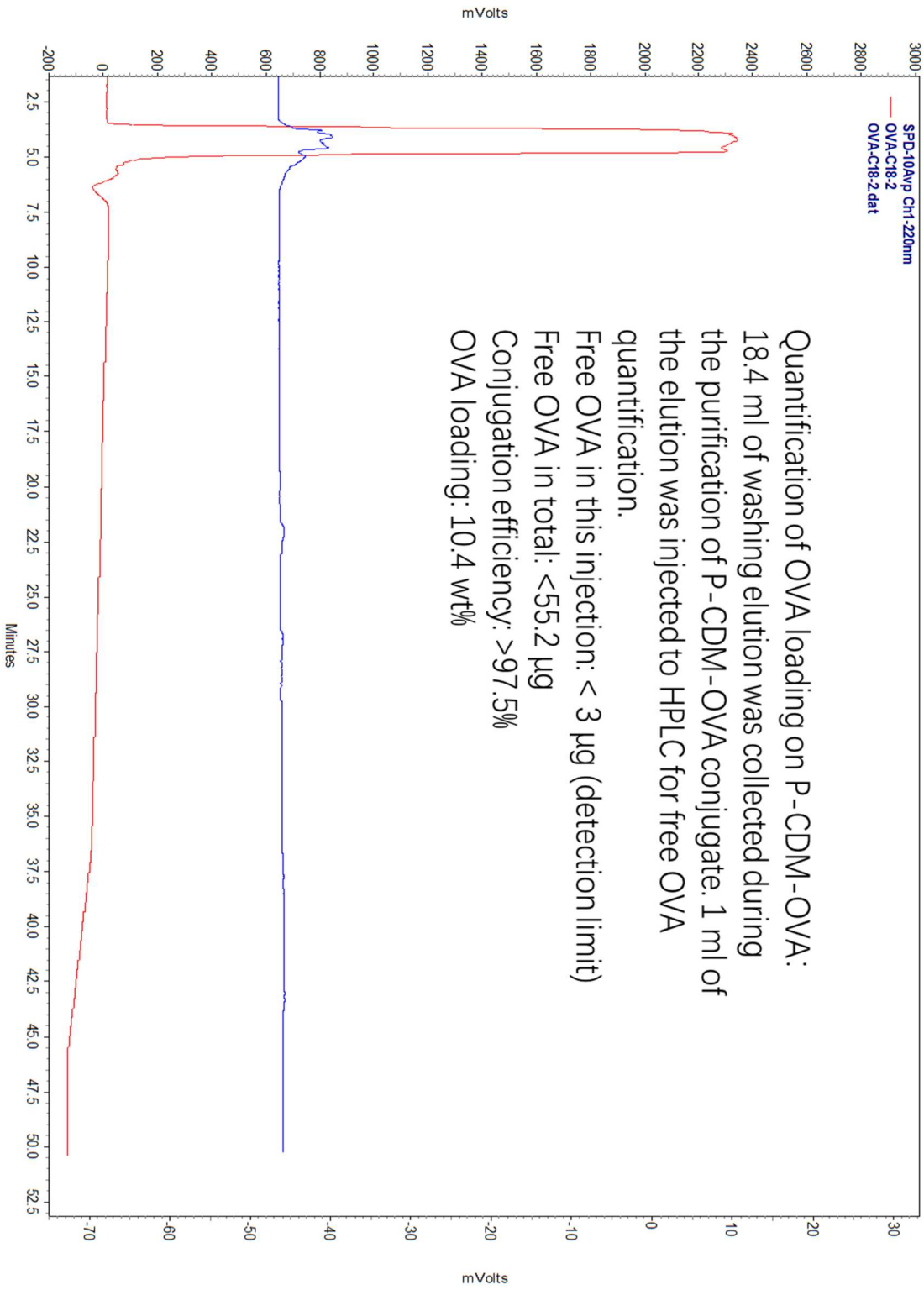

Figure 3.29 Quantification of OVA loading on P-CDM-OVA **8**

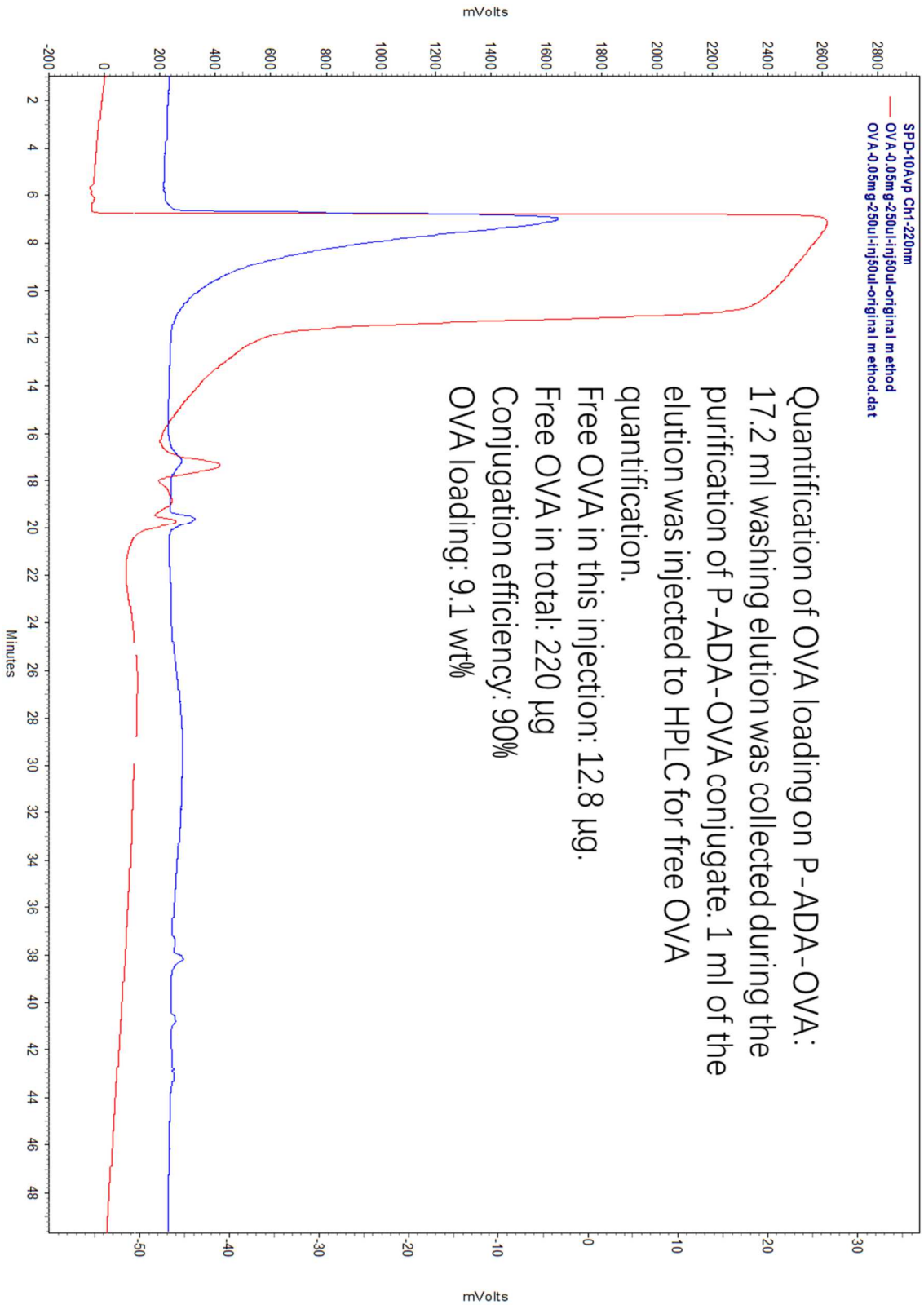

Figure 3.30 Quantification of OVA loading on P-ADA-OVA **9**

REFERENCES

REFERENCES

1. Lang, S.; Tan, Z.; Wu, X.; Huang, X., Synthesis of Carboxy-Dimethylmaleic Amide Linked Polymer Conjugate Based Ultra-pH-sensitive Nanoparticles for Enhanced Antitumor Immunotherapy. *ACS Macro Letters* **2020,** *9*, 1693-1699.

2. Romero, P.; Banchereau, J.; Bhardwaj, N.; Cockett, M.; Disis, M. L.; Dranoff, G.; Gilboa, E.; Hammond, S. A.; Hershberg, R.; Korman, A. J.; Kvistborg, P.; Melief, C.; Mellman, I.; Palucka, A. K.; Redchenko, I.; Robins, H.; Sallusto, F.; Schenkelberg, T.; Schoenberger, S.; Sosman, J.; Türeci, Ö.; Van den Eynde, B.; Koff, W.; Coukos, G., The Human Vaccines Project: A roadmap for cancer vaccine development. *Sci. Transl. Med.* **2016,** *8*, 334PS9.

3. Van der Burg, S. H.; Arens, R.; Ossendorp, F.; Van Hall, T.; Melief, C. J. M., Vaccines for Established Cancer: Overcoming the Challenges Posed by Immune Evasion. *Nat. Rev. Cancer* **2016,** *16*, 219-233.

4. Pamer, E.; Cresswell, P., Mechanisms of MHC Class I–Restricted Antigen Processing. *Annu. Rev. Immunol.* **1998,** *16*, 323-358.

5. Liu, J.; Miao, L.; Sui, J.; Hao, Y.; Huang, G., Nanoparticle Cancer Vaccines: Design Considerations and Recent Advances. *Asian J. Pharm. Sci.* **2020,** *15*, 576-590.

6. Lung, P.; Yang, J.; Li, Q., Nanoparticle Formulated Vaccines: Opportunities and Challenges. *Nanoscale* **2020,** *12*, 5746-5763.

7. Fan, Y.; Moon, J. J., Nanoparticle Drug Delivery Systems Designed to Improve Cancer Vaccines and Immunotherapy. *Vaccines (Basel)* **2015,** *3*, 662-685.

8. Li, L.; Yang, Z.; Chen, X., Recent Advances in Stimuli-Responsive Platforms for Cancer Immunotherapy. *Acc. Chem. Res.* **2020,** *53*, 2044-2054.

9. Alsuraifi, A.; Curtis, A.; Lamprou, D. A.; Hoskins, C., Stimuli Responsive Polymeric Systems for Cancer Therapy. *Pharmaceutics* **2018,** *10*, 136.

10. Pacifici, N.; Bolandparvaz, A.; Lewis, J. S., Stimuli-Responsive Biomaterials for Vaccines and Immunotherapeutic Applications. *Advanced Therapeutics* **2020,** *3*, 2000129.

11. Du, J.-Z.; Mao, C.-Q.; Yuan, Y.-Y.; Yang, X.-Z.; Wang, J., Tumor Extracellular Acidity-activated Nanoparticles as Drug Delivery Systems for Enhanced Cancer Therapy. *Biotechnol. Adv.* **2014,** *32*, 789-803.

12. Muraoka, D.; Seo, N.; Hayashi, T.; Tahara, Y.; Fujii, K.; Tawara, I.; Miyahara, Y.; Okamori, K.; Yagita, H.; Imoto, S.; Yamaguchi, R.; Komura, M.; Miyano, S.; Goto, M.; Sawada, S.-i.; Asai, A.; Ikeda, H.; Akiyoshi, K.; Harada, N.; Shiku, H., Antigen Delivery Targeted to Tumor-associated Macrophages Overcomes Tumor Immune Resistance. *J. Clin. Invest.* **2019,** *129*, 1278-1294.

13. Hammerich, L.; Binder, A.; Brody, J. D., *In situ* Vaccination: Cancer Immunotherapy both Personalized and Off-the-shelf. *Molecular Oncology* **2015,** *9*, 1966-1981.

14. Montealegre, S.; van Endert, P. M., Endocytic Recycling of MHC Class I Molecules in Non-professional Antigen Presenting and Dendritic Cells. *Front. Immunol.* **2019,** *9*, 3098.

15. Basha, G.; Lizée, G.; Reinicke, A. T.; Seipp, R. P.; Omilusik, K. D.; Jefferies, W. A., MHC Class I Endosomal and Lysosomal Trafficking Coincides with Exogenous Antigen Loading in Dendritic Cells. *PLoS One* **2008,** *3*, e3247.

16. Ma, X.; Wang, Y.; Zhao, T.; Li, Y.; Su, L.-C.; Wang, Z.; Huang, G.; Sumer, B. D.; Gao, J., Ultra-pH-Sensitive Nanoprobe Library with Broad pH Tunability and Fluorescence Emissions. *J. Am. Chem. Soc.* **2014,** *136*, 11085-11092.

17. Wang, Y.; Zhou, K.; Huang, G.; Hensley, C.; Huang, X.; Ma, X.; Zhao, T.; Sumer, B. D.; DeBerardinis, R. J.; Gao, J., A Nanoparticle-based Strategy for the Imaging of a Broad Range of Tumours by Nonlinear Amplification of Microenvironment Signals. *Nat. Mater.* **2013,** *13*, 204-212.

18. Zhou, K.; Wang, Y.; Huang, X.; Luby-Phelps, K.; Sumer, B. D.; Gao, J., Tunable, Ultrasensitive pH-Responsive Nanoparticles Targeting Specific Endocytic Organelles in Living Cells. *Angew. Chem., Int. Ed.* **2011,** *50*, 6109-6114.

19. Zhou, K.; Liu, H.; Zhang, S.; Huang, X.; Wang, Y.; Huang, G.; Sumer, B. D.; Gao, J., Multicolored pH-Tunable and Activatable Fluorescence Nanoplatform Responsive to Physiologic pH Stimuli. *J. Am. Chem. Soc.* **2012,** *134*, 7803-7811.

20. Luo, M.; Wang, H.; Wang, Z.; Cai, H.; Lu, Z.; Li, Y.; Du, M.; Huang, G.; Wang, C.; Chen, X.; Porembka, M. R.; Lea, J.; Frankel, A. E.; Fu, Y.-X.; Chen, Z. J.; Gao, J., A STING-activating Nanovaccine for Cancer Immunotherapy. *Nat. Nanotechnol.* **2017,** *12*, 648-654.

21. Du, J.-Z.; Li, H.-J.; Wang, J., Tumor-Acidity-Cleavable Maleic Acid Amide (TACMAA): A Powerful Tool for Designing Smart Nanoparticles To Overcome Delivery Barriers in Cancer Nanomedicine. *Acc. Chem. Res.* **2018,** *51*, 2848-2856.

22. Clemente, T.; Dominguez, M. R.; Vieira, N. J.; Rodrigues, M. M.; Amarante-Mendes, G. P., *In vivo* Assessment of Specific Cytotoxic T Lymphocyte Killing. *Methods* **2013,** *61*, 105-109.

23. Kavunja, H. W.; Lang, S.; Sungsuwan, S.; Yin, Z.; Huang, X., Delivery of Foreign Cytotoxic T Lymphocyte Epitopes to Tumor Tissues for Effective Antitumor Immunotherapy Against Pre-established Solid Tumors in Mice. *Cancer Immunol. Immunother.* **2017,** *66*, 451-460.

24. Lynn, G. M.; Laga, R.; Darrah, P. A.; Ishizuka, A. S.; Balaci, A. J.; Dulcey, A. E.; Pechar, M.; Pola, R.; Gerner, M. Y.; Yamamoto, A.; Buechler, C. R.; Quinn, K. M.; Smelkinson, M. G.; Vanek, O.; Cawood, R.; Hills, T.; Vasalatiy, O.; Kastenmüller, K.; Francica, J. R.; Stutts, L.; Tom, J. K.; Ryu, K. A.; Esser-Kahn, A. P.; Etrych, T.; Fisher, K. D.; Seymour, L. W.; Seder, R. A., *In vivo* Characterization of the Physicochemical Properties of Polymer-linked TLR Agonists that Enhance Vaccine Immunogenicity. *Nat. Biotechnol.* **2015,** *33*, 1201-1210.

25. Moyer, T. J.; Zmolek, A. C.; Irvine, D. J., Beyond Antigens and Adjuvants: Formulating Future Vaccines. *J. Clin. Invest.* **2016,** *126*, 799-808.

26. Liu, J.; Liu, X.; Han, Y.; Zhang, J.; Liu, D.; Ma, G.; Li, C.; Liu, L.; Kong, D., Nanovaccine Incorporated with Hydroxychloroquine Enhances Antigen Cross-Presentation and Promotes Antitumor Immune Responses. *ACS Appl. Mater. Interfaces* **2018,** *10*, 30983-30993.

27. Bal, S. M.; Hortensius, S.; Ding, Z.; Jiskoot, W.; Bouwstra, J. A., Co-encapsulation of Antigen and Toll-like Receptor Ligand in Cationic Liposomes Affects the Quality of the Immune Response in Mice After Intradermal Caccination. *Vaccine* **2011,** *29*, 1045-1052.

28. Dölen, Y.; Kreutz, M.; Gileadi, U.; Tel, J.; Vasaturo, A.; van Dinther, E. A. W.; van Hout-Kuijer, M. A.; Cerundolo, V.; Figdor, C. G., Co-delivery of PLGA Encapsulated Invariant NKT Cell Agonist with Antigenic Protein Induce Strong T Cell-mediated Antitumor Immune Responses. *Oncoimmunology* **2016,** *5*, e1068493.

29. Fischer, N. O.; Rasley, A.; Corzett, M.; Hwang, M. H.; Hoeprich, P. D.; Blanchette, C. D., Colocalized Delivery of Adjuvant and Antigen Using Nanolipoprotein Particles Enhances the Immune Response to Recombinant Antigens. *J. Am. Chem. Soc.* **2013,** *135*, 2044-2047.

30. Ilyinskii, P. O.; Roy, C. J.; O'Neil, C. P.; Browning, E. A.; Pittet, L. A.; Altreuter, D. H.; Alexis, F.; Tonti, E.; Shi, J.; Basto, P. A.; Iannacone, M.; Radovic-Moreno, A. F.; Langer, R. S.; Farokhzad, O. C.; von Andrian, U. H.; Johnston, L. P. M.; Kishimoto, T. K., Adjuvant-carrying Synthetic Vaccine Particles Augment the Immune Response to Encapsulated Antigen and Exhibit Strong Local Immune Activation without Inducing Systemic Cytokine Release. *Vaccine* **2014,** *32*, 2882-2895.

31. Mohsen, M. O.; Gomes, A. C.; Cabral-Miranda, G.; Krueger, C. C.; Leoratti, F. M. S.; Stein, J. V.; Bachmann, M. F., Delivering Adjuvants and Antigens in Separate Nanoparticles Eliminates the Need of Physical Linkage for Effective Vaccination. *J. Controlled Release* **2017,** *251*, 92-100.

32. Kasturi, S. P.; Skountzou, I.; Albrecht, R. A.; Koutsonanos, D.; Hua, T.; Nakaya, H. I.; Ravindran, R.; Stewart, S.; Alam, M.; Kwissa, M.; Villinger, F.; Murthy, N.; Steel, J.; Jacob, J.; Hogan, R. J.; García-Sastre, A.; Compans, R.; Pulendran, B., Programming the Magnitude and Persistence of Antibody Responses with Innate Immunity. *Nature* **2011,** *470*, 543-547.

33. Hanson, M. C.; Crespo, M. P.; Abraham, W.; Moynihan, K. D.; Szeto, G. L.; Chen, S. H.; Melo, M. B.; Mueller, S.; Irvine, D. J., Nanoparticulate STING Agonists are Potent Lymph Node-Targeted Vaccine Adjuvants. *J. Clin. Invest.* **2015,** *125*, 2532-2546.

34. Chen, N.; Johnson, M. M.; Collier, M. A.; Gallovic, M. D.; Bachelder, E. M.; Ainslie, K. M., Tunable Degradation of Acetalated Dextran Microparticles Enables Controlled Vaccine Adjuvant and Antigen Delivery to Modulate Adaptive Immune Responses. *J. Controlled Release* **2018,** *273*, 147-159.

35. Whiteside, T. L., Immune Suppression in Cancer: Effects on Immune Cells, Mechanisms and Future Therapeutic Intervention. *Semin. Cancer Biol.* **2006,** *16*, 3-15.

36. Stewart, T. J.; Smyth, M. J., Improving Cancer Immunotherapy by Targeting Tumor-induced Immune Suppression. *Cancer Metastasis Rev.* **2011,** *30*, 125-140.

37. Munn, D. H.; Bronte, V., Immune Suppressive Mechanisms in the Tumor Microenvironment. *Curr. Opin. Immunol.* **2016,** *39*, 1-6.

38. Meng, X.; Huang, Z.; Teng, F.; Xing, L.; Yu, J., Predictive Biomarkers in PD-1/PD-L1 Checkpoint Blockade Immunotherapy. *Cancer Treat. Rev.* **2015,** *41*, 868-876.

39. Ribas, A.; Wolchok, J. D., Cancer Immunotherapy Using Checkpoint Blockade. *Science* **2018,** *359*, 1350-1355.

40. Pardoll, D. M., The Blockade of Immune Checkpoints in Cancer Immunotherapy. *Nat. Rev. Cancer* **2012,** *12*, 252-264.

41. Naganawa, A.; Ichikawa, Y.; Isobe, M., Synthetic Studies on Tautomycin: Synthesis of 2,3-Disubstituted Maleic Anhydride Segment. *Tetrahedron* **1994,** *50*, 8969-8982.

42. Sun, C.-Y.; Shen, S.; Xu, C.-F.; Li, H.-J.; Liu, Y.; Cao, Z.-T.; Yang, X.-Z.; Xia, J.-X.; Wang, J., Tumor Acidity-Sensitive Polymeric Vector for Active Targeted siRNA Delivery. *J. Am. Chem. Soc.* **2015,** *137*, 15217-15224.

43. Bachelder, E. M.; Beaudette, T. T.; Broaders, K. E.; Dashe, J.; Fréchet, J. M. J., Acetal-derivatized Dextran: An Acid-responsive Biodegradable Material for Therapeutic Applications. *J. Am. Chem. Soc.* **2008,** *130*, 10494-10495.

CHAPTER 4 Glycoengineering of Natural Killer Cells with CD22 Ligands for Enhanced Anticancer Immunotherapy[1]

4.1 Introduction

The chimeric antigen receptor T cells (CAR-T) are breakthrough anticancer therapies with two types of CAR-T cells approved by the FDA for cancer treatment.[2-3] However, despite great promise, CAR-T therapies have several limitations.[4] Because of the potential immune responses by the host against the foreign major histocompatibility complex (MHC) molecules expressed on the surface of nonautologous T cells,[5] the patient's own T cells need to be extracted, genetically engineered with a chimeric antigen receptor for tumor recognition, expanded into a larger number, and reinfused back to the patient. Such a process is time and resource intensive, which is reflected by the high costs of CAR-T therapy ($475,000).[6] In addition, for patients who have been heavily pretreated with chemotherapy and/or radiation, it can be difficult to acquire sufficient numbers of

autologous T cells for CAR-T generation. CAR-T may not be produced in time for patients with rapidly developing diseases.

Natural killer (NK) cells are another type of cytotoxic immune cells that are capable of killing tumor cells, providing an attractive alternative to T cell-based therapy.[4] NK cells do not express MHC class I molecules on the cell surface. As a result, they can be potentially used as an off-the-shelf cellular therapy with clinical evidence showing that adoptive transfer of allogeneic NK cells is safe to patients.[7-9] NK cells can be prepared in a large scale and readily available to patients. On the other hand, NK cells do not have inherent targeting abilities toward cancer cells. To overcome this drawback, NK cells have been genetically engineered with chimeric antigen receptors (CAR-NK).[4, 10] However, NK cells are known to be notoriously adverse to endogenous gene uptake, resulting in low transgene expression.[11] Therefore, new methods need to be developed to enhance the abilities of NK cells to recognize tumor cells.

We have begun to investigate strategies to engineer NK cells and bestow *de novo* abilities for NK cells to recognize cancer, such as B cell lymphoma. Each year, approximately 70,000 people are diagnosed with B-cell lymphoma in the United States alone. While the anti-CD20 antibody rituximab can be effective,[12-13] it does not provide a cure, especially for the indolent lymphoma with annual deaths reaching 20,000.[13-16] As native NK cells lack intrinsic affinities toward B cell lymphoma, we envision that if NK cells can be engineered to better recognize lymphoma cells, better therapeutic efficacy may be achieved.

Herein, we report for the first time that glycoengineering of NK cells with 9-*O* modified sialic acid-based CD22 ligands can significantly improve their abilities to bind and kill $CD22^+$ lymphoma cells. CD22, also known as siglec-2, is a B-cell restricted antigen, which can serve as a selective target for B cell lymphoma.[17-20] The natural ligand on the cell for CD22 is the trisaccharide Neu-5Acα-2-6-Galβ1-4GlcNAc that terminates glycans on the cell surface.[21-23] Ground-breaking studies[18, 22-24] by the Paulson and Nitschke groups showed that the installation of a modified benzoate amide at the C-9 position of sialic acid in CD22 ligands can significantly enhance the binding affinity toward CD22. Furthermore, these compounds are highly selective toward CD22 with little crossreactivities to other siglecs, such as siglec-7, which is an inhibitory receptor on NK cells.[22] Glycan engineering of NK cells with CD22 ligands is an exciting new strategy for anticancer immunotherapy.

*The work in this chapter was in collaboration with Dr. Xianwu Wang. For a clear demonstration of this work, Dr. Wang's data has been included.

4.2 Results and discussions

4.2.1 Constructing NK Cells with CD22 Ligands through Glycoengineering

As a proof-of-concept, we selected NK-92 cells, which are a well-established NK cell line[25-27] readily expandable to reach clinically useful doses. Furthermore, NK-92 cells have been tested in phase I clinical trials for cancer treatment, exhibiting good safety profiles.[28-29]

Two glycoengineering approaches to introduce CD22 ligands onto NK-92 cells have been tested. In the first method, the possibilities of cells to take up exogenous sialic acids and metabolically incorporate the sialic acid into endogenous glycoproteins on the surface of cells. While glycan metabolic engineering has been applied to cells such as cancer,[30-31] it is unclear whether NK cells can uptake modified sialic acid (sia) derivatives such as MPB-sia **1** and BPC-sia **2** as precursors and transform them into CD22 ligands through the cellular biosynthesis machinery (**Figure 4.1, Method A**). In the second approach, we synthesized an amphiphilic polymer bearing multiple CD22 ligand trisaccharide **3** (**Figure 4.2**). This glyco-polymer may directly insert into NK-92 membrane, bestowing CD22 targeting abilities to NK-92 cells (**Figure 4.1**, **Method B**).

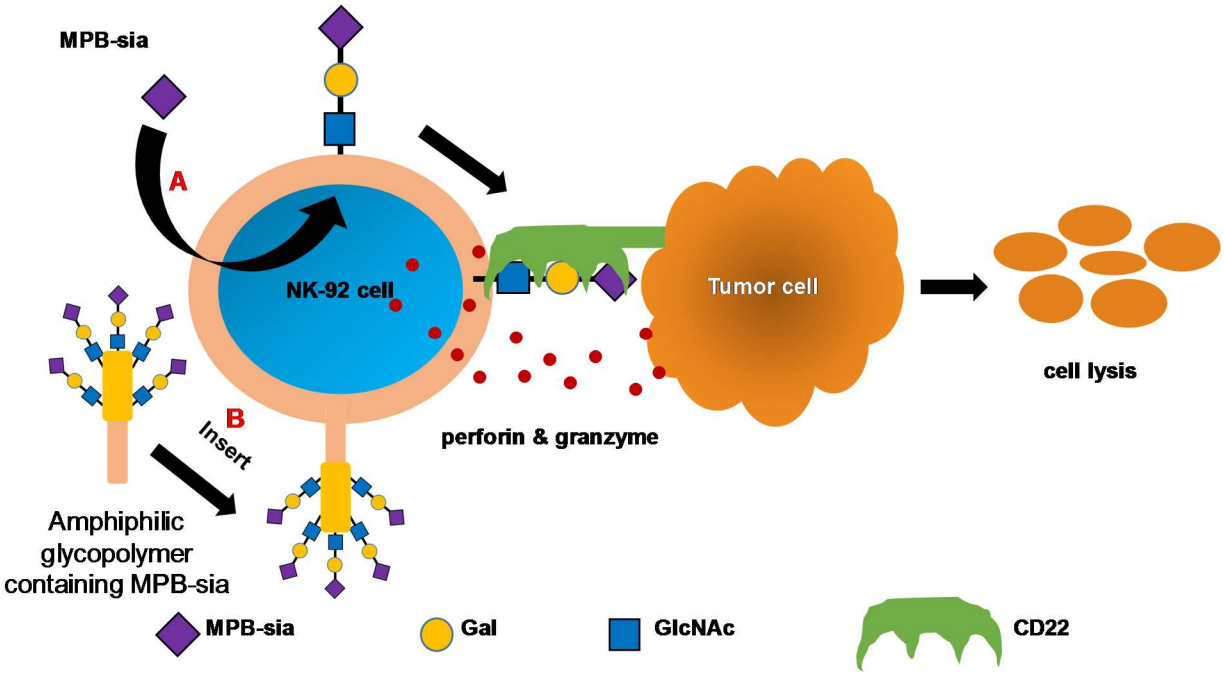

Figure 4.1 Modification of NK-92 with CD22 ligands through glyco-engineering. Two methods have been developed. **Method A** is metabolic glycoengineering using a sialic acid derivative, e.g., MPB-sia 1, which could be metabolized onto the surface of NK-92 cell through the sialic acid biosynthetic pathway. **Method B** uses a glyco-polymer containing MPB-sia, which could insert into the NK-92 cell membrane presumably due to its amphiphilicity. Both approaches could

Figure 4.1 (cont'd) enhance the ability of targeting and binding of NK-92 cells towards CD22 positive cells resulting in more effective lysis of target cancer cells.

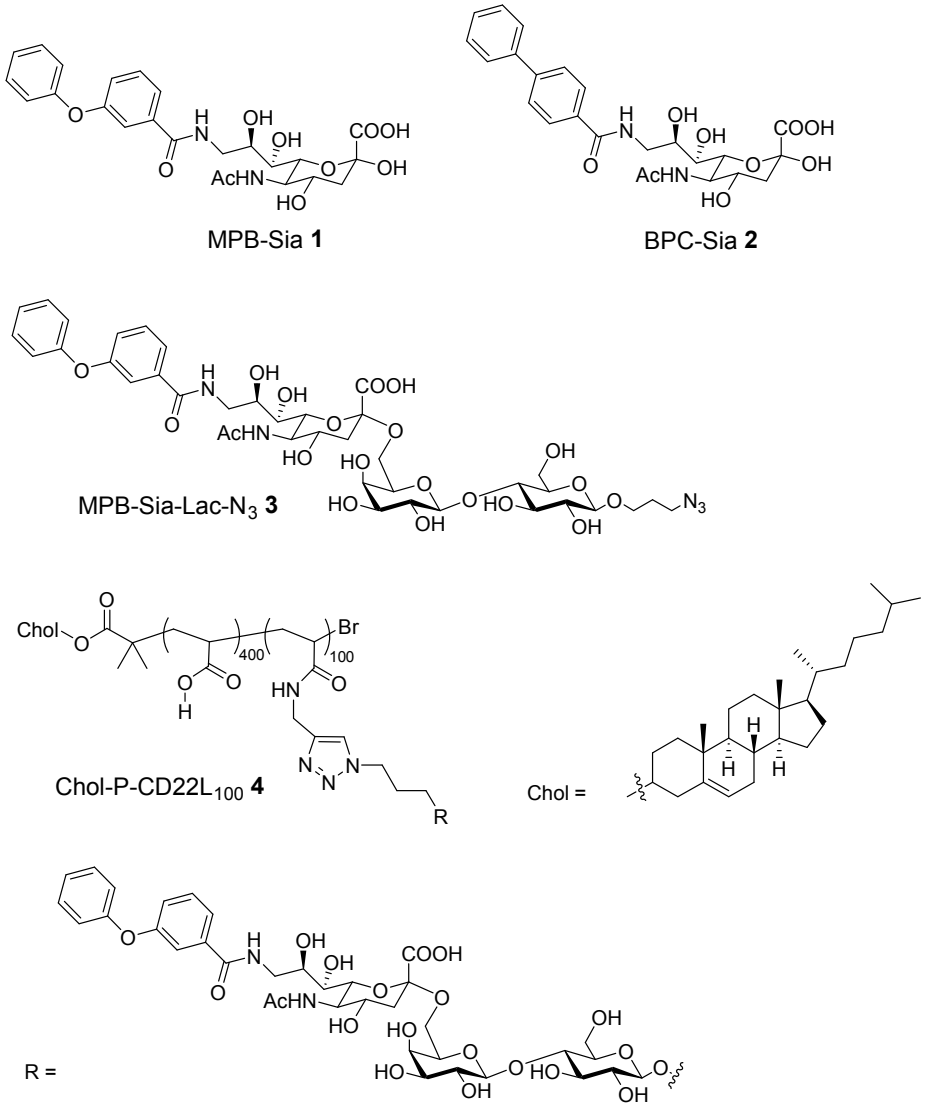

Figure 4.2 Structures of sialic acid derivatives and glyco-polymer used in this study.

MPB-Sia **1** was synthesized from Neu5Ac (**Figure 4.8a**). The carboxylic acid group was first protected by methyl ester, followed by activation of 9-OH for azide substitution. After reducing 9-N_3 to amino group with H_2, MPB-NHS **10** was used for introducing the MPB moiety to 9 position

of Neu5Ac. Final produce MPB-Sia **1** was achieved after deprotection of methyl ester by LiOH. To test metabolic glycoengineering, NK-92 cells were incubated with MPB-sia **1** or BPC-sia **2** supplemented medium as well as that with equal amount of unmodified free sialic acid as a control. Upon removing all free sialic acid or derivatives by thorough washing, the cells were treated with an α2-3,6,8 neuraminidase that can cleave α2-3, α2-6, and α2-8 sialyl linkages. The amounts of free sialic acid and derivatives released were functionalized with 1,2-diamino-4,5-methylenedioxybenzene (DMB)[32-33] and quantified by mass spectrometry through comparison with standard compounds. As shown in **Table 4.1**, while no MPB-sia **1** was detected in parent cells, incubation of NK-92 cells with MPB-sia **1** led to the detection of significant amounts of MPB-sia (5.2×10^6 molecules/cell) from cells. DMB functionalized BPC-sia was also detected from BPC-sia **2** treated cells. However, the amount of BPC-sia **2** was too small to be accurately quantified, suggesting MPB-sia **1** was more efficiently incorporated into cells.

	Sialic acid amount (ng) /10^7 cells	Number of sialic acid molecules (x10^6) per cell	MPB-sia amount (ng) /10^7 cells	Number of MPB-sia molecules (x10^6) per cell	BPC-sia amount (ng) /10^7 cells	Number of BPC-sia molecules (x10^6) per cell
cell only	4.2	0.8	N/A	N/A	N/A	N/A
cell+ Sia	16	3.1	N/A	N/A	N/A	N/A
cell+ MPB-sia	5.2	1.0	44	5.2	N/A	N/A
cell+ BPC-sia	5.9	1.1	N/A	N/A	peak detected	peak detected

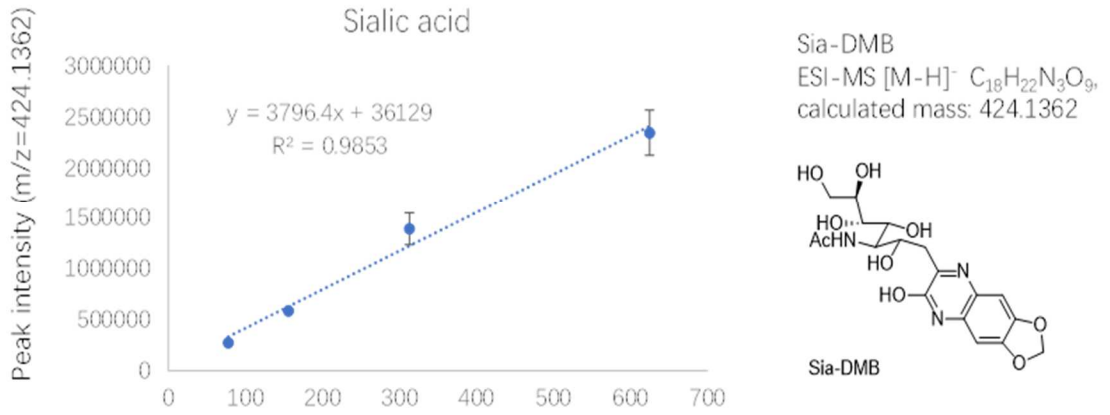

Table 4.1 Quantification of sialic acid and derivatives from engineered NK-92 cells. Following incubation with sialic acid, MPB-sia, and BPC-sia respectively, the corresponding NK-92 cells (cell + Sia, cell + MPB-sia, cell + BPC-sia) were thoroughly washed and then treated with an α2-3,6,8 neuraminidase. The supernatant was incubated with 1,2-diamino-4,5-methylenedioxybenzene (DMB). The amounts of sialic acid, MPB-sia, BPC-sia were quantified by comparing the MS intensities of the corresponding DMB adducts with the standard samples. N/A indicates no significant peaks in MS. For cell + BPC-sia group, while BPC-sia-DMB adduct was detected by MS, its amount was too small to be accurately quantified. The calibration curves and the structures of the DMB adducts are shown below the table.

Dr. Xianwu Wang tested the function of engineered CD22 ligands on the cell surface. Glycoengineered NK-92 cells were treated with CD22 protein followed by PE labeled anti-CD22 monoclonal antibody (mAb, clone HIB22). Both flow cytometry analysis (**Figure 4.3a**, **b**) and confocal imaging (**Figure 4.3c**) observed strong CD22 binding from the surface of MPB-sia **1**

treated cells (MsNK-92) but not native NK-92 or free sialic acid treated NK-92 (sNK-92), which suggest that NK-92 cells could be metabolically glycoengineered with sialic acid derivatives such as MPB-sia **1** to install CD22 ligands on the cell surface. These results can be explained by the higher affinity of MPB functionalized CD22 ligand with CD22[22] and/or the more ready incorporation of MPB-sia **1** onto the cells (**Table 4.1**).

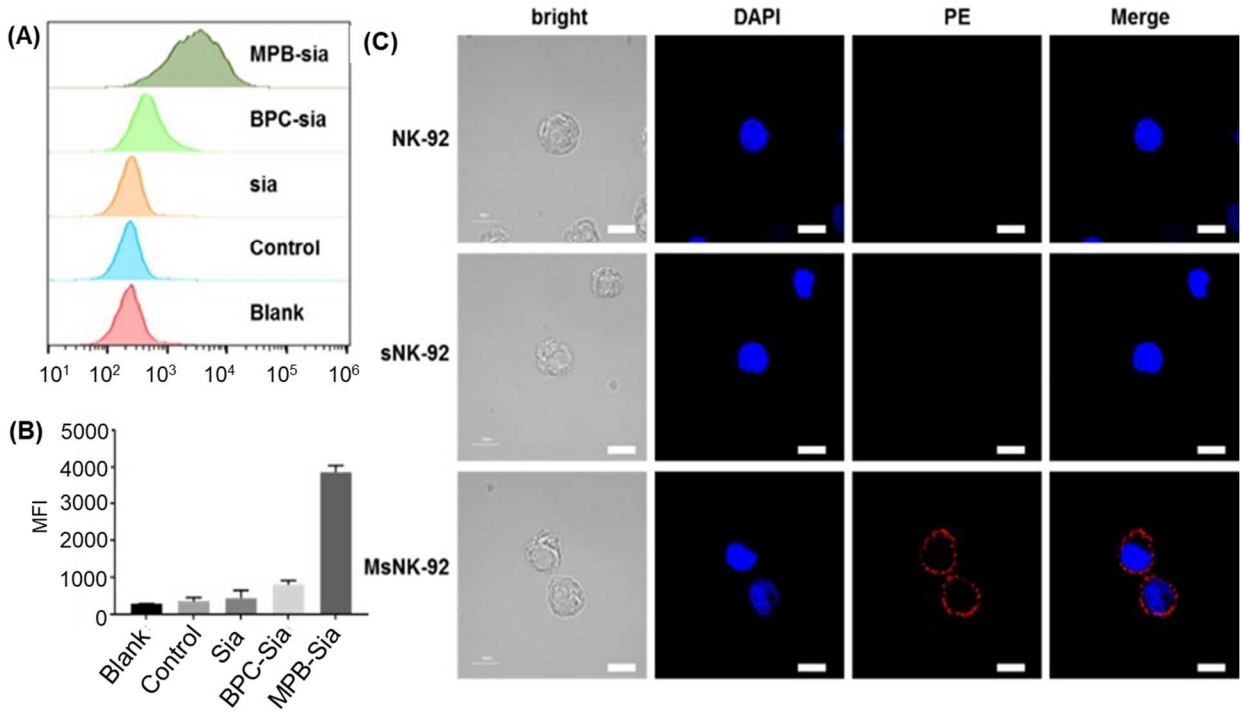

Figure 4.3 MPB-sia can be metabolically engineered onto the surface of NK-92 cell to enhance the binding ability to CD22 protein. **a.** Metabolic incorporation of various sialic acid derivatives onto NK-92 cells as measured by flow cytometry. Control represents *non-engineered* NK-92 cells treated with CD22-Fc and PE-mouse anti human CD22 mAb (Clone HIB22). **b.** Quantification of the mean fluorescence intensities upon cells upon incubation with various sialic acid derivatives. Mean with SD are presented for n = 3. **c.** Confocal microscopy images of NK-92 cells engineered with sialic acid (sNK-92) or MPB-sia **1** (MsNK-92), followed by human CD22-Fc incubation and PE-mouse anti human CD22 mAb staining. Cells were fixed and nuclei were stained with DAPI. Scale bar, 10 μm. (Data collected by Dr. Xianwu Wang)

Dr. Wang also investigated the kinetic of metabolic engineering. A dose- and time-dependent manner of CD22 ligand level on NK-92 was detected (**Figure 4.4**). Cell viability studies showed slight decreases of cell viability when concentrations of MPB-sia **1** were over 4 mM (**Figure 4.5**). Thus, 2 mM MPB-sia **1** was selected for further study. Upon removal of MPB-sia **1** from cell culture medium, 50% of CD22 binding remained on NK-92 cells after 48 h (**Figure 4.6**). Little influence on the overall amounts of α2-6-sia linkages by MPB-sia **1** incubation was detected when staining NK-92 with FITC-labeled α2-6-sia binding plant lectin Sambucus nigra lectin (SNA) before and after metabolic engineering (**Figure 4.7**).

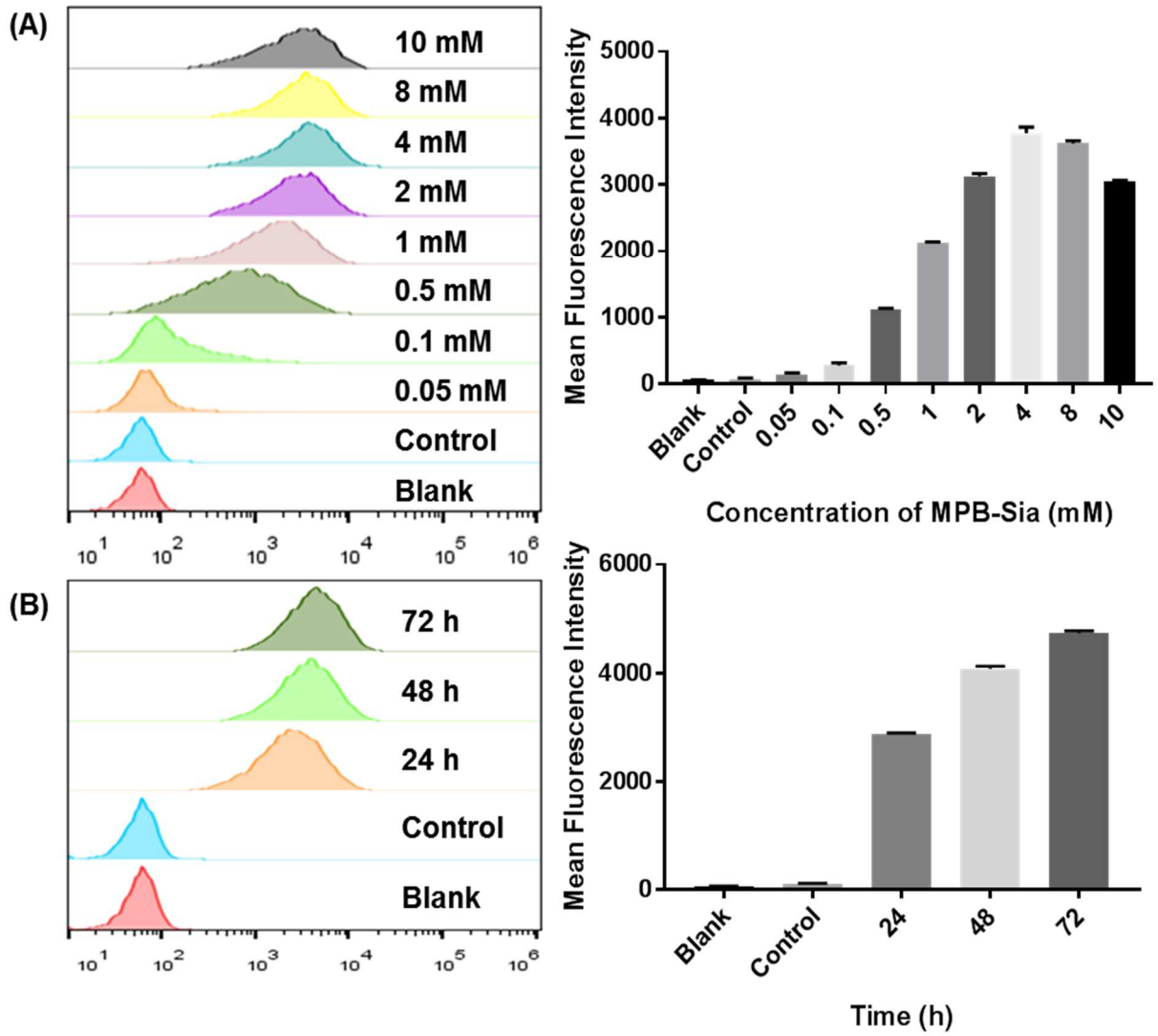

Figure 4.4 Metabolic incorporation of MPB-sia **1** onto NK-92 cells. **a.** Dose-dependence of metabolic incorporation of MPB-sia **1**. NK-92 cells (5×10^5 per sample) were incubated with different concentration of MPB-sia **1** (0.05 mM, 0.1 mM, 0.5 mM, 1 mM, 2 mM, 4 mM, 8 mM or 10 mM) for 48 h. The cells were then incubated with human CD22-Fc protein followed by PE-anti-human CD22 antibody staining for FACS analysis. **b.** Time-dependence of metabolic incorporation of MPB-sia **1**. NK-92 cells (5×10^5 per sample) were incubated with 2 mM MPB-sia **1** for different time periods (24 h, 48 h or 72 h). The cells were then incubated with human CD22-Fc protein followed by PE-anti-human CD22 antibody staining for FACS analysis. Mean with SD are presented for n = 3. (Data collected by Dr. Wang)

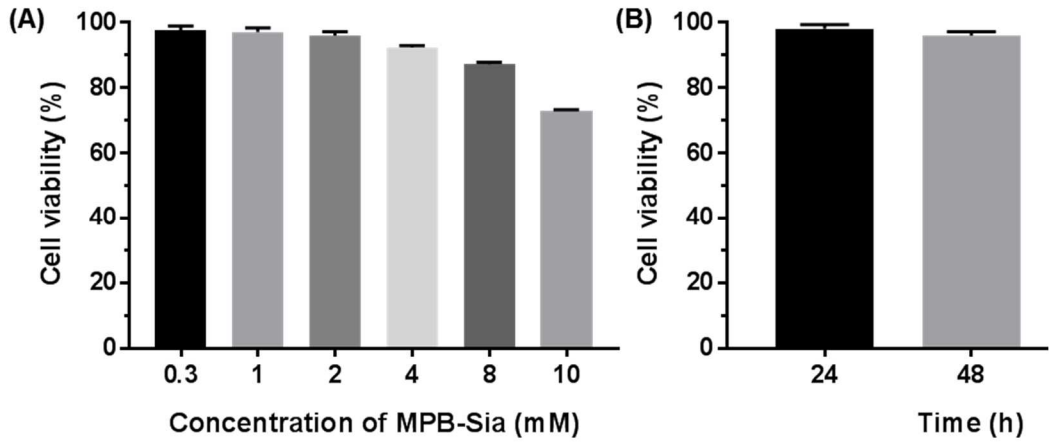

Figure 4.5 The effect of MPB-sia **1** on NK-92 cell viability. **a.** NK-92 cells (5×10^5 per sample) were incubated with different concentrations of MPB-sia **1** (0.3 mM, 1 mM, 2 mM, 4 mM, 8 mM or 10 mM) for 48 h. Cells were then stained with Calcein AM and the cell viability was analyzed by FACS. **b.** NK-92 cells (5×10^5 per sample) were incubated with 2 mM of MPB-sia **1** for 24 h or 48 h. Cells were then stained with Calcein AM and the cell viability was analyzed by FACS. Mean with SD are presented for n = 3. (Data collected by Dr. Wang)

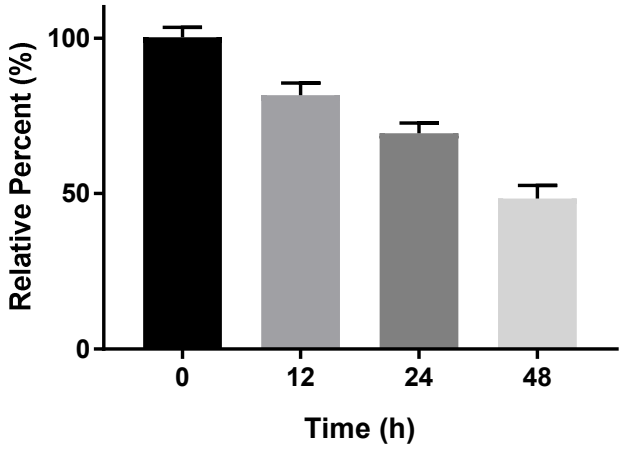

Figure 4.6 Persistence of cell surface CD22 ligands after metabolic engineering. NK-92 cells were first incubated with 2 mM MPB-sia **1** for 48 h, followed by washing and incubating with fresh culture medium without MPB-sia **1** for various time periods (0 h, 12 h, 24 h or 48 h). The cells were further incubated with human CD22-Fc protein followed by PE-anti-human CD22 antibody staining for FACS quantification of surface CD22 ligand level. Mean with SD are presented for n = 3. (Data collected by Dr. Wang)

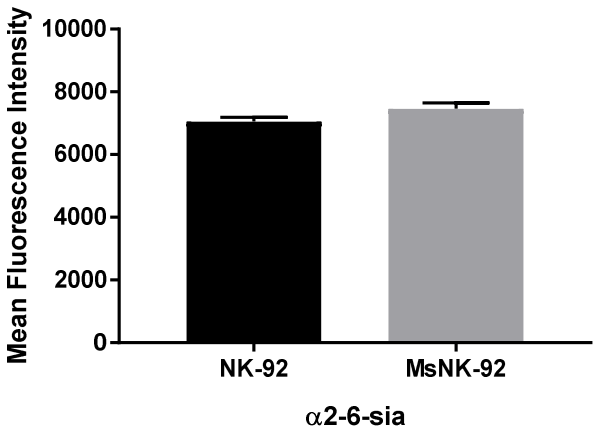

Figure 4.7 The level of α2-6-sia linkage on NK-92 cell surface before and after metabolic engineering. Unmodified NK-92 cells and metabolic engineered NK-92 (MsNK-92) cells (5×10^5 per sample) stained by FITC-labeled α2-6-sia binding plant lectin Sambucus *nigra* lectin (SNA) followed by FACS analysis. Mean with SD are presented for n = 3. (Data collected by Dr. Wang)

As an alternative to metabolic glycoengineering, I investigated the possibility of directly inserting CD22 ligands onto the surface of NK-92 cells (**Figure 4.1**, **Method B**). In order to accomplish this, a cholesterol-terminated poly(acrylic acid) polymer was synthesized by atom-transfer radical-polymerization (ATRP) from a cholesterol initiator with an average molecular weight of 30 kDa (**Figure 4.8b**). The carboxylic acid side chain of the polymer was partially modified with alkynes. The trisaccharide CD22 ligand with an azide handle, MPB-sia-α2-6-Lac-N_3 **3**, was synthesized by enzymatic glycosylation between MPB-Sia **1** and Lac-N_3 **11**. The polymer and trisaccharide CD22 ligands were conjugated through the copper catalyzed azide−alkyne cycloaddition reaction with an average of 100 trisaccharides per polymer chain producing glyco-polymer Chol-P-$CD22L_{100}$ **4** (**Figure 4.2**). Upon incubation of NK-92 cells with

the Chol-P-CD22L$_{100}$ **4**, the cholesterol end of the polymer could insert into the cellular membrane through hydrophobic−hydrophobic interactions, anchoring the polymer onto the cell surface. After 1 h of incubation, the cells were washed followed by treatment with human CD22 and the PE-labeled anti-CD22 mAb. Strong CD22 binding was detected with 2.5 μM polymer (equivalent to 250 μM MPB-sia **1**) (**Figure 4.9a**). A dose dependent manner of hydrophobic insertion engineering was observed and with higher polymer concentration (5 μM and 10 μM, equivalent to 500 μM and 1mM MPB-Sia **1** respectively), a stronger CD 22 binding can be detected (**Figure 4.9a**). The success of surface modification was confirmed by confocal imaging as well (**Figure 4.9b**). With the glycopolymer, while the surface CD22 ligand level decreased rapidly (~85% loss) during the first 24 h after removal of polymer-containing medium, CD22 binding remained detectable for at least 72 h by FACS analysis (**Figure 4.10**). No significant cytotoxicities were noticed when NK-92 cells were co-incubated with Chol-P-CD22L$_{100}$ **4** for up to 48 h at concentrations lower than 12.5 μM (**Figure 4.11**). Compared to metabolically engineered NK cells (**Figure 4.6**), the polymer approach was associated with much faster drops in surface CD22 ligand levels. This may be because through metabolic glycoengineering, MPB-sia **1** taken up inside the cells could be continuously modified into CD22 ligands over time.

I also studied whether a polymer containing multiple copies of cholesterol can help prolong the retention of polymer on NK-92 surface. Multiple attempts for synthesizing cholesterol grafted polymers have been made (Appendix **Scheme 4.1**). Direct polymerization of cholesterol

monomers via either ATRP or RAFT failed to produce reasonable monomer conversion and only short oligomers containing no more than 4 cholesterols were obtained. Besides, the product typically suffering from poor solubility in both water and organic solvents, which made the following reactions extremely difficult. Instead, by first synthesizing a hydrophilic di-block polymer via ATRP, followed by post-polymerization modification of cholesterol and the CD22 ligand, MPB-Sia-Lac-N_3 **3**, a polymer containing 8 copies of cholesterol on one block and 25 copies of CD22 ligand on the other block can be obtained. However, the 8 cholesterol molecules did not help prolong the retention of polymer on NK-92 surfaces (**Figure 4.12**).

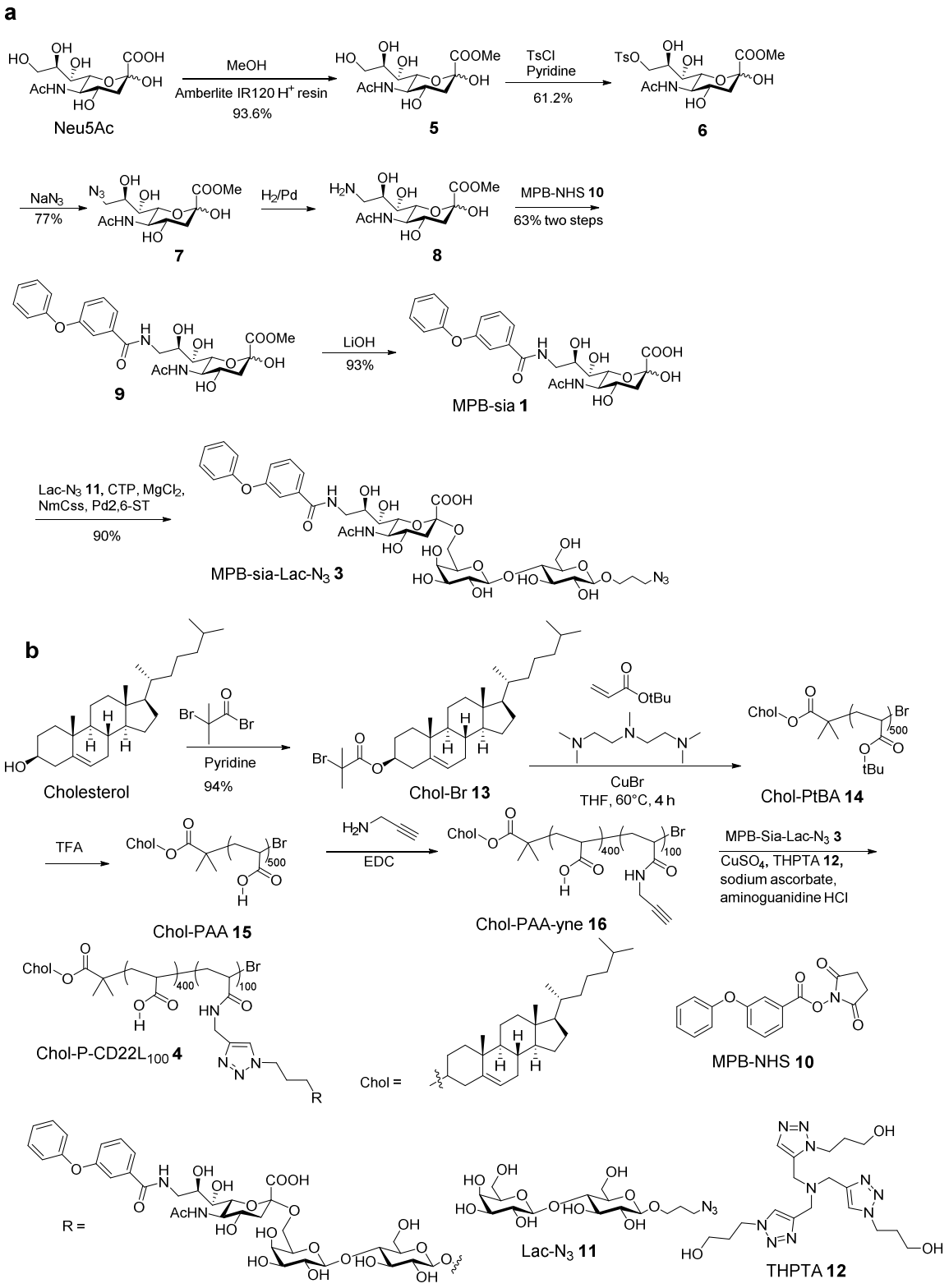

Figure 4.8 a. Synthesis of MPB-sia **1** and MPB-sia-α2-6-Lac-N_3 **3**; **b.** synthesis of Chol-P-$CD22L_{100}$ **4**.

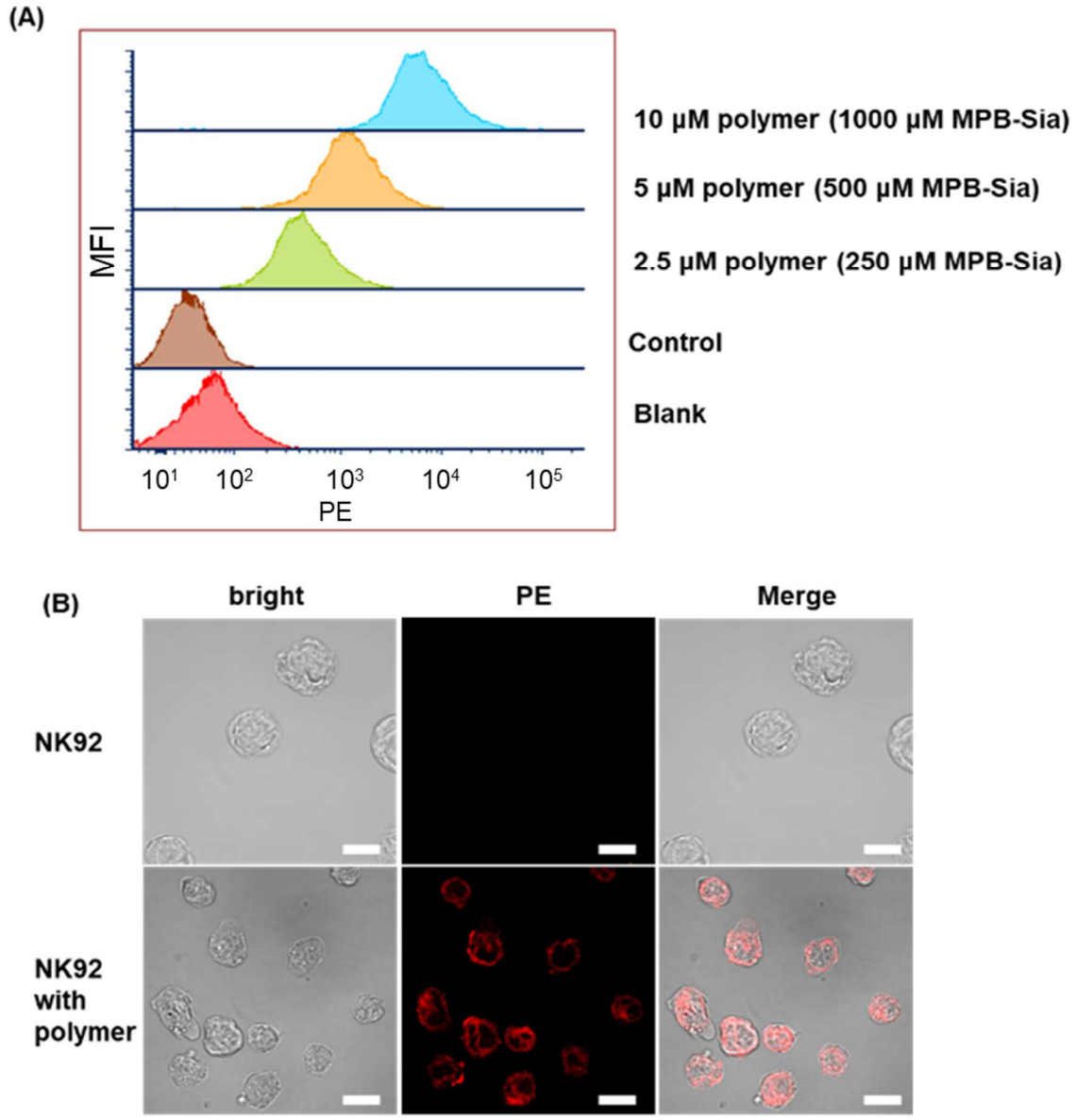

Figure 4.9 Incubation of Chol-P-CD22L$_{100}$ **4** with NK-92 cells significantly enhanced the levels of CD22 ligands on cell surface. **a.** FACS analysis of Chol-P-CD22L$_{100}$ **4** incubated NK-92 cells. NK-92 cells (5×10^5 per sample) were incubated with various concentrations of Chol-P-CD22L$_{100}$ **4** (2.5 μM, 5 μM or 10 μM) for 1 h in PBS buffer at room temperature. After washing, the cells were then incubated with human CD22-Fc protein followed by PE-anti-human CD22 antibody staining for FACS analysis. **b.** Confocal image of Chol-P-CD22L$_{100}$ **4** treated NK-92 cells after incubated with 10 μM Chol-P-CD22L$_{100}$ **4** for 1 h in PBS buffer at room temperature.

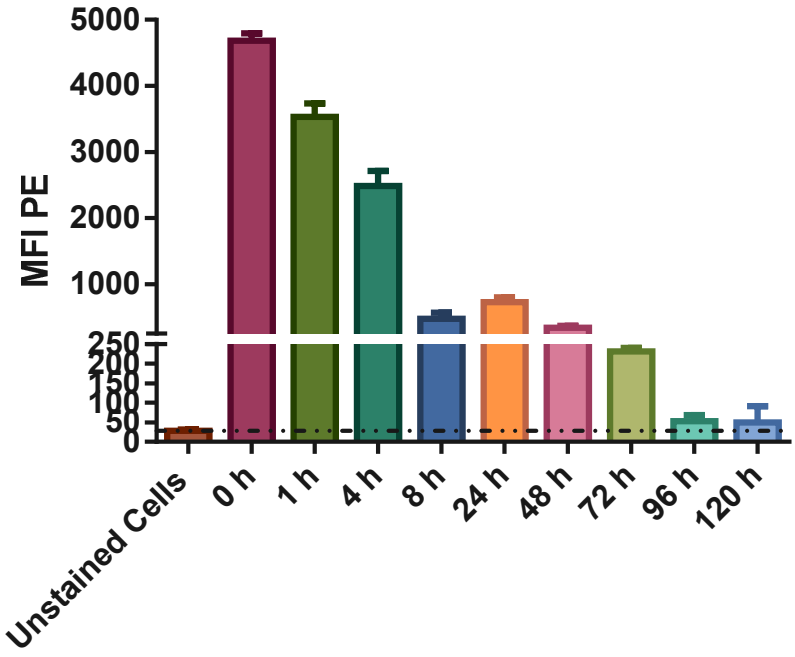

Figure 4.10 Time-dependent persistence of CD22 ligands on cell surface after incubation with Chol-P-CD22L$_{100}$ **4**. NK92 cells were incubated with 10μM Chol-P-CD22L$_{100}$ **4** for 1h in PBS under room temperature. Cells were washed and cultured in fresh medium. An aliquot of cells was collected from the cell culture at different time points (0, 4, 8, 12, 24, 48, 72, 96 and 120 h) and incubated with human CD22-Fc protein followed by PE-anti-human CD22 antibody staining. FACS was used for detecting CD22 binding level. Polymer can last on cell surface for ~72h.

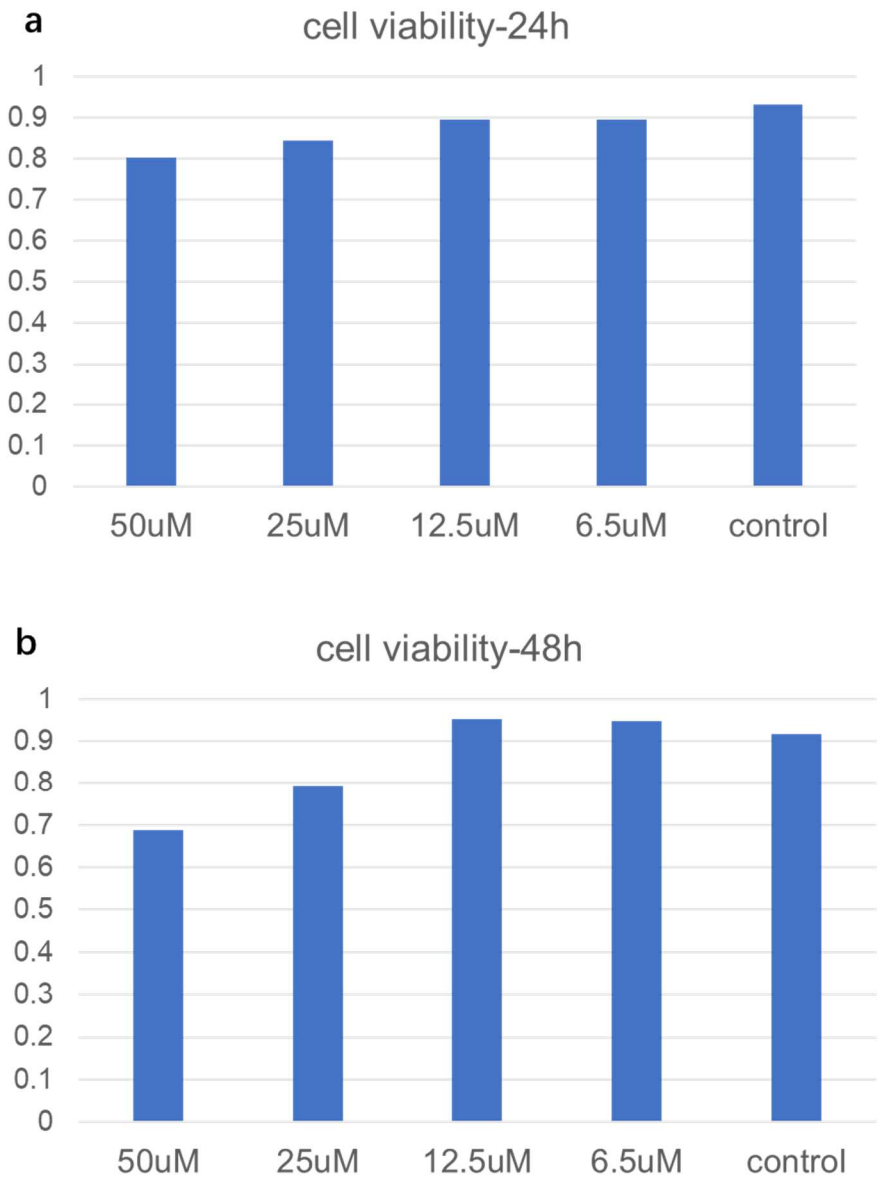

Figure 4.11 The effect of Chol-P-CD22L$_{100}$ **4** on NK-92 cell viability. NK-92 cells (5×10^5 per sample) were incubated with different concentrations of Chol-P-CD22L$_{100}$ **4** (6.5 μM, 12.5 μM, 25 μM or 50 μM) for **a.** 24 h and **b.** 48 h. Untreated NK-92 cells were used as control. Cell viability was analyzed by trypan blue staining.

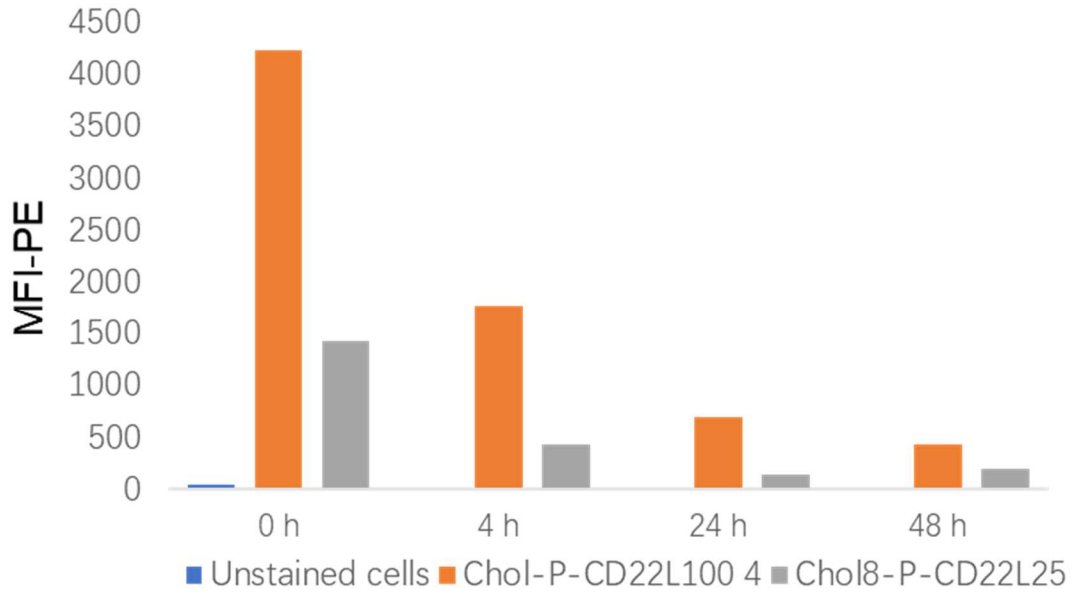

Figure 4.12 Time-dependent persistence of CD22 ligands on cell surface after incubation with polymers containing different copies of cholesterol. NK92 cells were incubated with 10μM Chol-P-CD22L_{100} **4** (1 cholesterol per chain) or 40μM $Chol_8$-P-CD22L_{25} (8 cholesterols per chain) for 1h in PBS under room temperature. Cells were washed and cultured in fresh medium. An aliquot of cells was collected from the cell culture at different time points (0, 4, 24 and 48 h) and incubated with human CD22-Fc protein followed by PE-anti-human CD22 antibody staining. FACS was used for detecting CD22 binding level. Increasing cholesterol copies on polymer did not prolonged the presence of CD22 ligand significantly.

4.2.2 Enhanced Killing of CD22 Positive Cells by Glycoengineered NK-92 Cells

With the increased affinity of glycoengineered NK-92 cells for CD22, their cytotoxicities toward $CD22^+$ cancer cells were evaluated. Dr. Wang observed that the metabolic glycoengineered NK-92 cells significantly enhanced lysis of $CD22^+$ Raji compared to unmodified NK-92 at effector/target cell ratio 1 or greater (**Figure 4.13a**). The killing of Raji cells is CD22 dependent, as the addition of free CD22 to Raji-engineered NK-92 mixture decreased Raji lysis significantly (**Figure 4.13b**). The reduced cytotoxicities in the presence of free CD22 are presumably due to

competitive binding of free CD22 protein to engineered NK-92 cells, suggesting CD22 plays an important role in cytotoxicities of engineered NK-92 cells toward $CD22^+$ cancer cells.

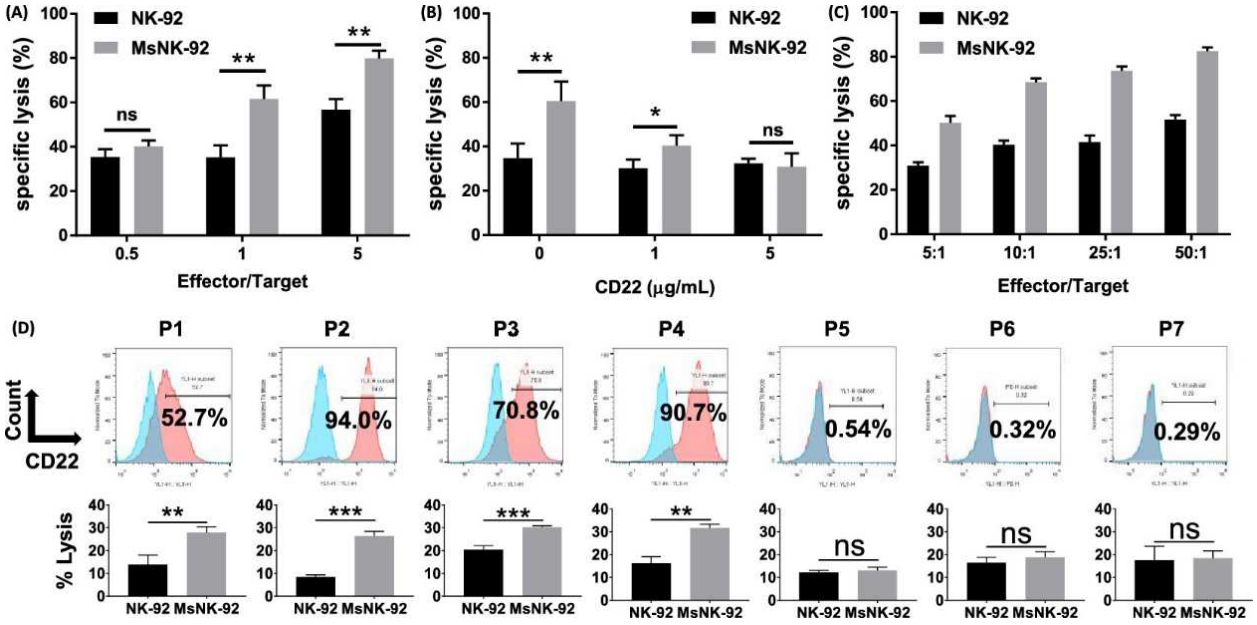

Figure 4.13 Glycoengineered NK-92 cells could enhance killing of CD22 positive cells. **a.** Lysis of Raji-luc cells by NK-92 and MsNK-92. Different effector-to-target cell ratios; P = 0.0049 (E/T = 1) and P = 0.0026 (E/T = 5). **b.** Increasing concentration of CD22 reduced the killing activities of engineered MsNK-92 cells, while impacting little the activities of NK-92 cells without glycoengineering; E/T = 1:1, P = 0.0154 (0 μg/mL free CD22 protein), P = 0.0442 (1 μg/mL). **c.** Relative killing activities of glycoengineered NK-92 cells against CD22 positive CHO cells as detected by flow cytometry. **d.** Significantly enhanced cytotoxicities were bestowed by glycoengineered NK-92 cells toward CD22 high patient-derived leukemic cells (P1−P4) versus those expressing CD22 in low levels (P5−P7). Top row: surface expression of CD22 on patient-derived leukemic samples as determined by flow cytometry. Bottom row: lysis of patient-derived leukemic samples by NK-92 and MsNK-92. p = 0.0077 (P1), p =0.0002 (P2), p = 0.0009 (P3), p = 0.0014 (P4), p = 0.4439 (P5), p = 0.2907 (P6), and p = 0.8473 (P7). Mean with SD are presented for n = 3. Statistical significances were assessed using Student's t test. In all figures, ns, $p > 0.05$; *, $p < 0.05$; **, $p < 0.01$; ***, $p < 0.001$. (Data collected by Dr. Wang)

To further confirm the role of CD22 in cytotoxicities of glycoengineered NK-92 cell, Chinese Hamster Ovarian (CHO) cells were genetically engineered to express human CD22 on the cell

surface (CHO-hCD22), which were subjected to cytotoxicity assay by glycoengineered NK-92 cells[34-35] with wild-type CHO cells (CHO-WT) as the control. Both metabolic glycoengineered and glycopolymer-modified NK-92 cells showed enhanced cytotoxicity toward CHO-hCD22 cells compared to CHO-WT cells (**Figure 4.13c** and **Figure 4.14**), confirming the importance of CD22 in cytotoxicities of engineered NK-92. As the killing activities of both types of NK cells were similar and metabolic engineering requires only the monosaccharide MPB-sia **1** without the need to synthesize trisaccharide **3** and the polymer **4**, further investigation was focused on the metabolic glycoengineering approach.

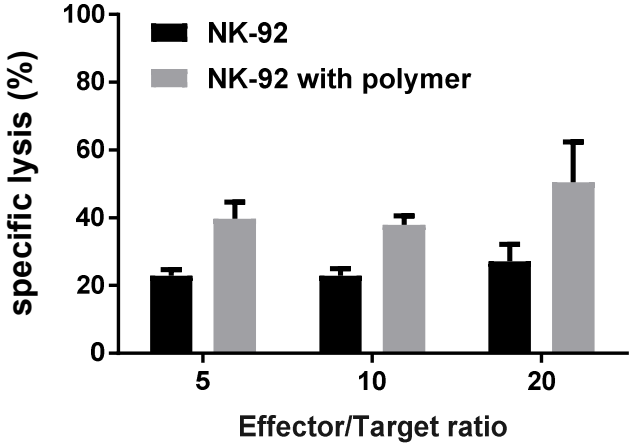

Figure 4.14 Cell lysis of CHO-CD22 after incubation with Chol-P-CD22L$_{100}$ **4**. CFSE^{hi} labeled CHO-CD22 and CFSE^{lo} labeled CHO-WT cells were mixed at 1:1 ratio and co-cultured with NK92 or NK92+Chol-P-CD22L$_{100}$ **4** for 6h followed by FACS analysis. The specific lysis of CD22 was calculated based on the CFSE^{hi}/CFSE^{lo} cell ratio change before and after co-culture with NK cells. Mean with SD are presented for n = 3.

To establish the potential translatability of the glycoengineering strategy, Dr. Wang analyzed the lysing ability of NK-92 cells toward primary lymphoma cells obtained from lymphoma patients

(**Figure 4.13d**). Significantly enhanced cytotoxicities by glycoengineered NK-92 compared to unmodified NK-92 were observed in patient-derived lymphoma cells expressing high levels of CD22 (P1−P4 in **Figure 4.13d**), but not in cells with low levels of CD22 expression (P5−P7 in **Figure 4.13d**). These results suggested glycoengineering of NK-92 cells with MPB-sia **1** can be a promising strategy to treat patients with CD22 positive B cell lymphoma.

4.2.3 Enhanced Killing Mechanism of Glycoengineered NK-92 Cells against Raji Cells

Dr. Wang observed significantly higher percentages of glycoengineered NK-92 cells were found clustered with Raji cells compared with native NK-92 cells and Raji cells (**Figure 4.15**), which could be attributed to the CD22 ligands on the glycoengineered NK-92 increasing the binding affinity with Raji. When bound with Raji cells, increased number of cytotoxic granules (**Figure 4.16**), as well as increased secretion of pro-inflammatory cytokine IFN-γ (**Figure 4.17**), were observed in metabolic glycoengineered NK-92 cells.

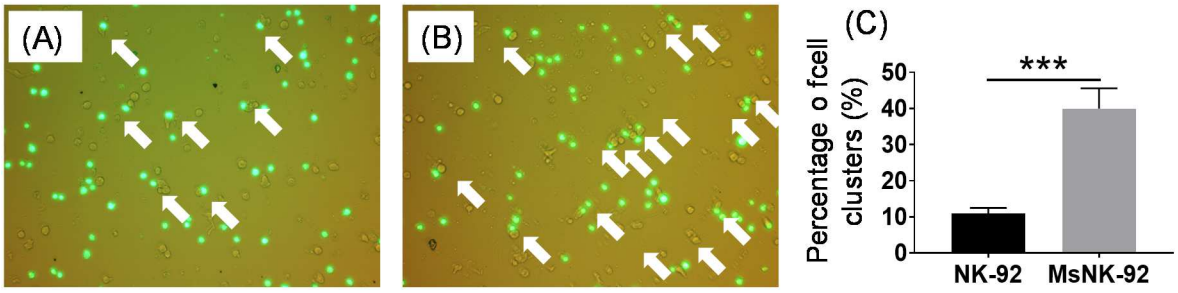

Figure 4.15 Glyco-engineered NK-92 binding with $CD22^+$ cells. Fluorescence microscopy image of cell clusters between Raji cells stained with Calcein-AM and **a.** NK-92 or **b.** MsNK-92. **c.** Percentage of cell clusters, P=0.0010. Mean with SD are presented for n = 3. Statistical significance was assessed using Student`s t-test. In all figures, ns, $p > 0.05$; *$p < 0.05$; **$p < 0.01$; ***$p < 0.001$. (Data collected by Dr. Wang)

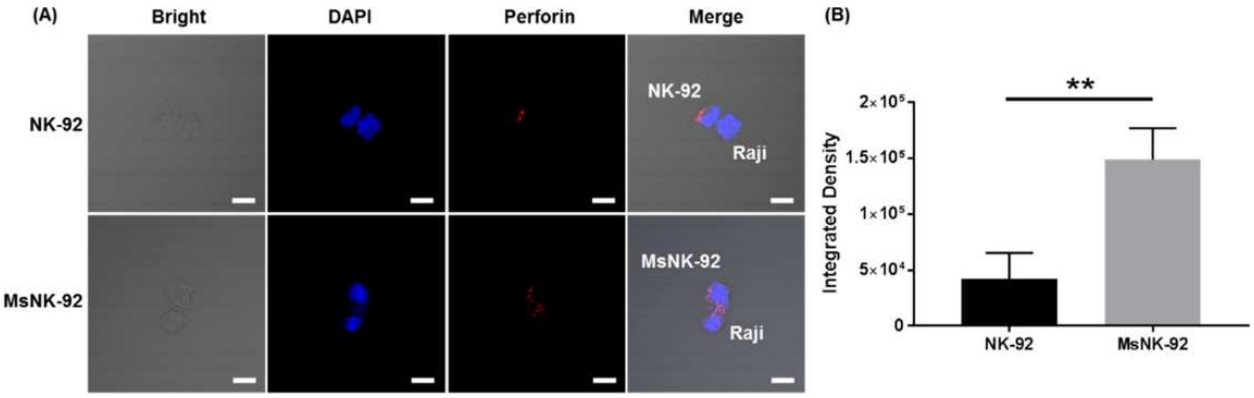

Figure 4.16 Complex formation between NK-92 cells and Raji cells investigated by confocal microscopy. Raji cells and NK-92 cells were co-incubated for 1 h, fixed, permeabilized, and stained for perforin (red) to identify cytotoxic granules. Cell nuclei were labeled with DAPI (blue). Scale bar: 10 μm. **a.** Representative images of cell−cell complex formation. **b.** Perforin (red) fluorescence quantification. P = 0.0071. Mean with SD are presented for n = 3. Statistical significance was assessed using Student's t test. In all figures, ns, $p > 0.05$; *, $p < 0.05$; **, $p < 0.01$; ***, $p < 0.001$. (Data collected by Dr. Wang)

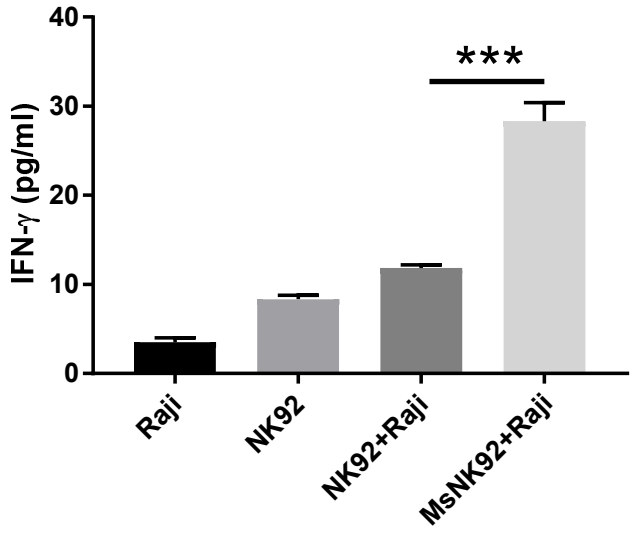

Figure 4.17 IFN-γ production by glycoengineered NK-92 cells when stimulated with $CD22^+$ Raji cells. P=0.0002. Mean with SD are presented for n = 3. Statistical significance was assessed using Student`s t-test. In all figures, ns, $p > 0.05$; *$p < 0.05$; **$p < 0.01$; ***$p < 0.001$. (Data collected by Dr. Wang)

4.2.4 Evaluation of Antitumor Effect of Glycoengineered NK-92 Cells *In Vivo*.

With the promising *in vitro* results, we analyzed the antitumor effect of glycoengineering *in vivo*. Dr. Wang has observed the metabolic glycoengineered MsNK-92 cells significantly slowed down the growth of subcutaneously implanted luciferase engineered Raji (Raji-luc) tumor compared to PBS or unmodified Nk-92 treated group (**Figure 4.18**).

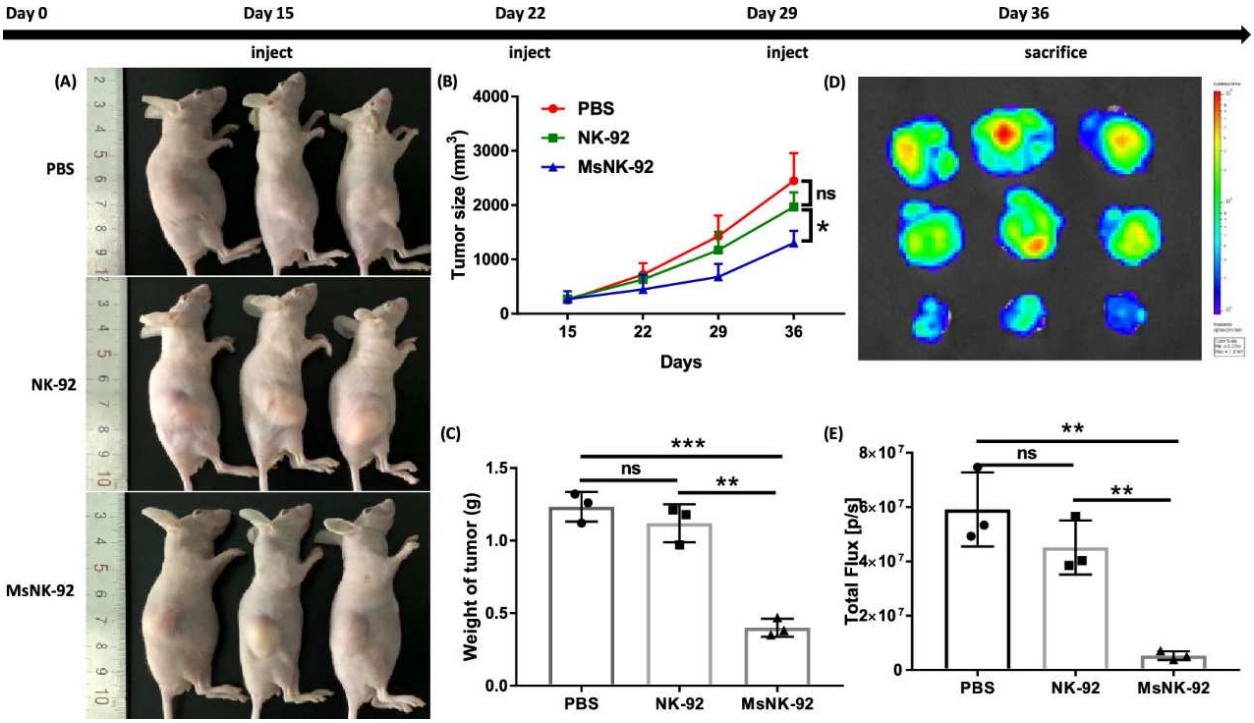

Figure 4.18 *In vivo* antitumor activity of glycoengineered NK-92 cells against Raji-luc xenograft model. 10^7 Raji-luc cells were injected subcutaneously into the flanks of Balb/c nude mice. Fifteen days later, the mice were treated with an intratumoral injection of 10^7 glycoengineered NK-92 cells (MsNK-92 in 50 µL PBS), unengineered NK-92 (NK-92), or PBS buffer (50 µL) once a week. Bioluminescence images (BLI) were acquired with an IVIS Lumina II imaging system. **a.** Images of mice with tumor at day 36. **b.** Tumor growth curve. **c.** Tumor weight measurements. **d.** BLI images of the tumor after surgical removal from mice. **e.** Quantitative BLI signals of the tumor after surgical removal from mice. Mean with SD are presented. Statistical significance was assessed using Student's t test. In all figures, ns, $p > 0.05$; *, $p < 0.05$; **, $p < 0.01$; ***, $p < 0.001$. $p = 0.0294$ (panel B), $p = 0.0003$ (MsNK-92 vs PBS), $p = 0.0010$ (MsNK-92 vs NK-92) (panel C), $p = 0.0025$ (MsNK-92 vs PBS), $p = 0.0024$ (MsNK-92 vs NK-92) (panel E). (Data collected by Dr. Wang)

To better mimic the clinical condition, Dr. Wang further evaluated the efficacy of our strategy in a B cell lymphoma model. Raji-luc cells were injected intravenously on day 0, which were followed by intravenous administration of PBS, unmodified NK-92 cells, or MsNK-92 cells on days 2, 5, 8, 12, and 15. The mice receiving MsNK-92 cells did not lose weight (**Figure 4.19a**), suggesting little toxicities due to systemic administration of cells. The survival of mice was continuously monitored (**Figure 4.19b**). While NK-92 cells provided significant protection to mice compared to the PBS group, all mice eventually died by day 62. Excitingly, all mice in the group receiving MsNK-92 cells survived, highlighting the power of the glycoengineering approach.

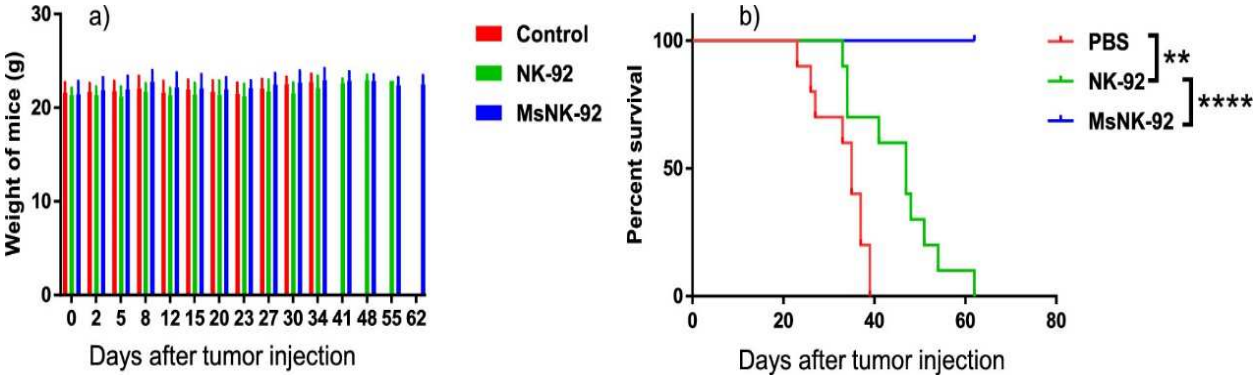

Figure 4.19 *In vivo* antitumor activity of glycoengineered NK-92 cells against Raji-luc B cell lymphoma. 10^6 Raji-luc cells were injected intravenously into NOD SCID mice. On days 2, 5, 8, 12, and 15, mice received intravenous injections of 10^7 glycoengineered NK-92 cells (MsNK-92 in 100 μL PBS), unengineered parent NK-92 (NK-92), or PBS buffer control (100 μL) (n = 10 for each group). (a) The body weights of all mice were continuously monitored. No significant changes in body weight were observed, suggesting little toxicities due to administration of cells. (b) Kaplan−Meier survival curves of mice receiving PBS, NK-92, and MsNK-92 cells. All mice receiving PBS or NK-92 cells died by day 62, while 100% of the mice treated with MsNK-92 survived. Statistical significance was assessed using Student's t test. **, $p < 0.01$; ***, $p < 0.001$. (Data collected by Dr. Wang)

4.3 Conclusion

While NK cells can potentially be cytotoxic against cancer cells, their lack of inherent affinity toward cancer cells is a significant drawback for NK-based therapy. To overcome this, we chemically engineered NK cells to gain novel targeting abilities. Among various strategies and reagents examined, the metabolic glycoengineering with MPB-sia monosaccharide successfully introduced CD22 ligand on NK-92 cells through the sialic acid biosynthetic pathway for B cell lymphoma targeting. The introduced MPB group greatly enhanced the binding ability and killing activity of NK-92 cells against CD22 positive cells in vitro and in mouse tumor models. Moreover, the glycoengineered NK-92 cells exhibited CD22-dependent cytotoxicity against primary lymphoma cells isolated from patients, which highlights its translational potential. The NK cell metabolic glycoengineering approach is simple and effective and can complement well the genetic engineering strategy of chimeric antigen receptors. Although the CD22 ligands on the NK cell surface would eventually become undetectable, the patients can be infused with multiple rounds of engineered NK cells to treat cancer. Studies are underway to further develop the glycoengineering method to enhance the efficacy of NK cell-based immunotherapy.

4.4 Experimental methods

4.4.1 Materials

Sialic acid, Amberlite IR 120 H^+ resin, m-phenoxybenzoic acid (MPB), cytidine-5'-triphosphate (CTP), propargyl amine, tris(3-hydroxypropyltriazolylmethyl)amine (THPTA), 4%

paraformaldehyde were purchased from Millipore-Sigma. Toluenesulfonyl chloride, sodium azide, $Pd(OH)_2/C$ (10-15% loading), 1-ethyl-3-(3-dimethylaminopropyl)carbodiimide hydrochloride (EDC•HCl), *N*-hydroxysuccinimide (NHS), lithium hydroxide, α-bromoisobutyryl bromide, t-butylacrylate (tBA), *N,N,N′,N″,N″*-pentamethyldiethylenetriamine (PMDETA), CuBr, sodium ascorbate, amino guanidine were purchased from Acros Organics. Cholesterol, 4-dimethylaminopyridine (DMAP) were purchased from Alfa Aesar. Anhydrous methanol, anhydrous ethanol, diethyl ether, dichloromethane (DCM), anhydrous pyridine, acetic acid, dimethylformamide (DMF), diisopropylethylamine (DIPEA), magnesium chloride, triethylamine (TEA), sodium chloride, sodium sulfate, tetrahydrofuran (THF), trifluoroacetic acid (TFA) were purchased from Fisher Scientific. E. coli Recombinant CMP-Sialic acid synthetase from Neisseria meningitides (NmCss), Photobacterium damselae α2−6-sialyltransferase (Pd2,6ST) were purchased from Chemily Glycoscience. Human CD22-Fc Chimera protein was purchased from R&D Systems. PE-mouse anti-human CD22 monoclonal antibody (Clone HIB22) was purchased from BD Pharmingen™. FITC-labeled α2,3-sialic acid binding plant lectin Maackia Amurensis Lectin I (FITC-MAL I) and FITC-labeled α2,6-sialic acid binding plant lectin Sambucus Nigra Lectin (FITC-SNA) were purchased from Vector Laboratories. Firefly luciferase reporter gene assay kit, Immunostaining permeabilization buffer with Triton X-100, DAPI were purchased from Beyotime Biotechnology. BPC-Sia **2** was purchased from Xiamen Nuokangde Biological Technology Co. Ltd. Perforin-specific antibody δG9 was purchased from Santa Cruz

Biotechnology. Alexa Fluor 594-coupled anti-mouse antibody was purchased from Life Technologies.

No unexpected or unusually high safety hazards were encountered.

4.4.2 Mice

Pathogen free female NSG mice age 6 - 10 weeks were obtained from Charles River. BALB/c nude mice and NOD SCID mcie (female, 6-8 weeks) were purchased from model animal research center of Nanjing university (Nanjing, China) and all animal experiments were conducted under the animal use and care regulations approved by Institutional Animal Care and Use Committee at Michigan State University and Xiamen University.

4.4.3 Synthesis of compound 5

Sialic acid (20 g, 64.7 mmol) and Amberlite IR 120 H^+ resin (15 g) were suspended in anhydrous methanol (300 ml). The reaction mixture was stirred under room temperature for 72 h. After filtering off the resin, the solvent was concentrated by rotavapor to around 30 ml. Then diethyl ether (300 ml) was added to precipitate out the product. The resulting solid product **5** (19.63 g, yield = 93.6 %) was collected by filtration and dried under nitrogen gas overnight. The product was used without further purification. ^{1}H NMR (500 MHz, Methanol-d_4) δ 4.08 – 3.96 (m, 2H), 3.86 – 3.76 (m, 2H), 3.77 (s, 3H), 3.70 (ddd, J = 9.3, 5.7, 2.9 Hz, 1H), 3.61 (dd, J = 11.4, 5.7 Hz, 1H), 3.47 (dd, J = 9.3, 1.5 Hz, 1H), 2.21 (dd, J = 12.9, 4.9 Hz, 1H), 2.01 (s, 3H), 1.89 (dd, J = 12.9, 11.4 Hz, 1H). ^{13}C NMR (126 MHz, Methanol-d_4) δ 175.29, 171.94, 96.82, 72.20, 71.78, 70.31,

68.00, 64.97, 54.45, 53.34, 40.84, 22.83. ESI-MS: $[M+Na]^+$ $C_{12}H_{21}NaNO_9$ calculated 346.1109; observed: 346.1120. The NMR data matched previously reported data[36].

4.4.4 Synthesis of compound 7

The synthesis of compound **7** followed literature report with modifications[37]. Compound **5** (3.23 g, 10 mmol) was dissolved in anhydrous pyridine (20 ml) and cooled on ice for 10 min. Tosyl chloride (2.5 g, 13 mmol) was dissolved in anhydrous pyridine (10 ml) and added to the solution of compound **5** dropwise. The reaction mixture was allowed to reach room temperature after addition of tosyl chloride was completed followed by stirring overnight. After reaction, the solvent was removed by rotavapor and the residue was collected and purified by silica gel column with DCM: MeOH = 10: 1 elution to obtain product **6** (2.92 g, yield = 61.2 %). ^{1}H NMR (500 MHz, Chloroform-d) δ 7.75 (d, J = 8.3 Hz, 2H), 7.33 (d, J = 8.3 Hz, 2H), 7.17 – 6.98 (m, 1H), 4.38 – 4.18 (m, 1H), 4.18 – 4.04 (m, 3H), 4.03 – 3.91 (m, 1H), 3.89 – 3.79 (m, 1H), 3.76 (s, 3H), 3.48 (s, 1H), 2.42 (s, 3H), 2.31 – 2.16 (m, 1H), 2.04 (s, 3H), 2.00 – 1.92 (m, 1H).

Compound **6** (2.92 g. 6.1 mmol) was dissolved in methanol (50 ml). NaN_3 (2 g, 30.8 mmol) was added to the reaction. Then the reaction mixture was heated to reflux and stirred until compound 6 was completely consumed (monitored by TLC, DCM: MeOH = 10: 1). After the reaction mixture was cooled down to room temperature, the unreacted NaN_3 was carefully filtered off. The filtrate was collected and concentrated by rotavapor followed by silica gel column purification (DCM: MeOH = 10: 1) to yield pure compound **7** (1.64 g, yield = 77%).^{1}H NMR (500

MHz, Methanol-d_4) δ 3.92 (ddd, J = 11.4, 10.1, 4.9 Hz, 1H), 3.87 – 3.79 (m, 2H), 3.73 (s, 3H), 3.73 – 3.65 (m, 1H), 3.51 (dd, J = 12.8, 2.8 Hz, 1H), 3.38 – 3.29 (m, 2H), 2.21 (dd, J = 13.0, 4.9 Hz, 1H), 1.98 (s, 3H), 1.90 (dd, J = 13.0, 11.4 Hz, 1H). ^{13}C NMR (126 MHz, Methanol-d_4) δ 178.11, 174.36, 99.29, 74.42, 73.23, 72.95, 70.34, 58.24, 57.14, 56.63, 43.01, 26.11. ESI-MS: $[M+Na]^+$ $C_{12}H_{10}NaN_4O_8$ calculated: 371.1179, observed: 371.1178.

4.4.5 Synthesis of MPB-Sia 1

Compound **7** (1.5 g, 4.3 mmol) was dissolved in methanol (20 ml), $Pd(OH)_2/C$ (10-15% loading, 200 mg) and acetic acid (1 ml) were added to the flask. The reaction mixture was then stirred under H_2 atmosphere until the compound **7** was completely consumed (monitored by TLC, DCM: MeOH = 10: 1). The reaction mixture was then filtered to remove the $Pd(OH)_2/C$. The resulting filtrate was collected and concentrated to yield compound **8** (1.26 g, 91.3 %). The product was used without further purification. ^{1}H NMR (500 MHz, Methanol-d_4) δ 4.06 (ddd, J = 11.4, 10.1, 5.0 Hz, 1H), 3.97 – 3.89 (m, 2H), 3.84 – 3.73 (m, 4H), 3.55 – 3.47 (m, 1H), 3.25 (dd, J = 12.8, 3.9 Hz, 1H), 3.03 (dd, J = 12.8, 7.5 Hz, 1H), 2.27 (dd, J = 13.0, 5.0 Hz, 1H), 2.03 (s, 3H), 1.88 (dd, J = 13.0, 11.3 Hz, 1H).

MPB-NHS **10** was synthesized by the following procedure: MPB (2.14 g, 10 mmol) was dissolved in DMF (20 ml), followed by adding EDC•HCl (2 g, 10.5 mmol) and NHS (1.2 g, 10.5 mmol). The reaction mixture was stirred under room temperature overnight. After the reaction, the solvent was removed by rotavapor and the residue was purified by silica gel column (hexane: ethyl

acetate =3: 1 to 2: 1) to yield MPB-NHS 10 (2.56 g, 82.3 %).^{1}H NMR (500 MHz, Chloroform-d) δ 7.88 (ddd, J = 8.0, 1.5, 0.9 Hz, 1H), 7.73 (dd, J = 2.5, 1.5 Hz, 1H), 7.48 (t, J = 8.0 Hz, 1H), 7.41 – 7.36 (m, 2H), 7.32 (ddd, J = 8.0, 2.5, 0.9 Hz, 1H), 7.19 – 7.13 (m, 1H), 7.06 – 7.00 (m, 2H), 2.89 (s, 4H). ^{13}C NMR (126 MHz, Chloroform-d) δ 169.18, 161.41, 157.92, 156.13, 130.34, 130.11, 130.09, 126.66, 125.09, 124.22, 120.01, 119.42, 25.68.

Compound **8** (1.26 g, 3.9 mmol) was dissolved in DMF (20 ml) followed by the addition of DIPEA (1.1 ml, 0.81 g, 6.3 mmol) and MPB-NHS **10** (1.8 g, 5.8 mmol). The reaction mixture was stirred overnight under room temperature. After removal of solvent by rotavapor, the residue was purified by silica gel column (DCM: MeOH= 10: 1 to 2: 1) to yield compound **9** (1.40 g, yield = 69.5 %). ^{1}H NMR (500 MHz, Methanol-d4) δ 7.56 (ddd, J = 7.7, 1.7, 0.9 Hz, 1H), 7.50 – 7.41 (m, 2H), 7.41 – 7.34 (m, 2H), 7.18 – 7.11 (m, 2H), 7.04 – 6.98 (m, 2H), 4.07 – 3.96 (m, 2H), 3.89 – 3.77 (m, 3H), 3.76 (s, 3H), 3.57 – 3.36 (m, 2H), 2.20 (dd, J = 12.9, 4.9 Hz, 1H), 1.97 (s, 3H), 1.91 – 1.81 (dd, J = 12.9, 11.5 Hz, 1H).

An aqueous solution of LiOH (324 mg, 13.5 mmol in 20 ml DI water) was added to the flask containing compound **9** (1.40 g, 2.7 mmol). The reaction was stirred under room temperature for 2 h. The reaction mixture was neutralized with Amberlite IR 120 H^{+} resin to pH 5. After removal of resin by filtration, the solution was collected and lyophilized to yield MPB-Sia 1 without further purification (1.26 g, yield = 93 %). ^{1}H NMR (500 MHz, Deuterium Oxide) δ 7.54 – 7.46 (m, 2H), 7.46 – 7.39 (t, J = 8.5 Hz, 2H), 7.42 – 7.30 (m, 1H), 7.27 – 7.18 (m, 2H), 7.11 – 7.05 (d, J = 8.5

Hz, 2H), 4.07 – 3.95 (m, 2H), 3.95 – 3.78 (m, 2H) 3.72 (dd, J = 14.2, 3.1 Hz, 1H), 3.53 – 3.38 (m, 2H), 2.25 (dd, J = 12.9, 4.9 Hz, 1H), 1.97 (s, 3H), 1.81 (dd, J = 12.9, 11.6 Hz, 1H). ^{13}C NMR (126 MHz, Deuterium Oxide) δ 174.62, 173.91, 170.48, 156.96, 156.19, 135.42, 130.34, 130.08, 124.11, 122.07, 119.00, 117.11, 95.40, 70.10, 69.42, 68.73, 66.69, 53.73, 52.01, 43.19, 38.84, 21.93. ESI-MS: $[M-H]^-$ $C_{24}H_{27}N_2O_{10}$ Calculated: 503.1671 Found: 503.1671. The NMR data matched previously reported data.[23]

4.4.6 Synthesis of MPB-Sia-Lac-N_3 3

Lac-N_3 **11**[38] (1.06 mg, 2.5 μmol), MPB-Sia **1** (5.0 mg, 10 μmol), CTP (7.25 mg, 15 μmol), $MgCl_2$ (3.5 mg, 37.5 μmol), Tris buffer (pH = 8.8, 150 μl of 1.5 M stock solution), E. coli Recombinant CMP-Sialic acid synthetase from Neisseria meningitides (NmCss, 0.2 U) and Photobacterium damselae α2−6-sialyltransferase (Pd2,6ST, 0.08 U) were mixed in a vial and Milli Q water was added to a total volume of 750 μl. The reaction mixture was kept under 37 □ for 1 h. Then ice-cold ethanol (750 μl) was added to the reaction mixture, followed by centrifuge at 5000 rpm for 5 min to remove enzyme precipitates. The supernatant was collected and passed through Bio-gel P2 column to obtain the product MPB-Sia-Lac-N_3 **3** in 90% yield. ^{1}H NMR (500 MHz, Deuterium Oxide) δ 7.47 – 7.33 (m, 2H), 7.32 – 7.22 (m, 3H), 7.15 – 7.05 (m, 2H), 7.00 – 6.88 (m, 2H), 4.25 (dd, J = 12.9, 7.9 Hz, 2H), 3.88 (ddd, J = 8.9, 7.3, 3.3 Hz, 1H), 3.84 – 3.75 (m, 4H), 3.72 – 3.67 (m, 1H), 3.66 – 3.55 (m, 5H), 3.52 – 3.33 (m, 9H), 3.29 (t, J = 6.7 Hz, 2H), 3.16 – 3.11 (m, 1H), 2.54 (dd, J = 12.4, 4.7 Hz, 1H), 1.82 (s, 3H), 1.79 – 1.70 (m, 2H), 1.57 (t, J = 12.2 Hz,

1H). ^{13}C NMR (126 MHz, Deuterium Oxide) δ 174.74, 173.36, 170.26, 156.99, 156.24, 135.56, 130.36, 130.12, 124.13, 122.17, 122.04, 119.05, 117.26, 103.09, 101.88, 100.25, 79.54, 74.53, 73.60, 72.59, 72.31, 72.26, 70.66, 70.08, 69.96, 68.43, 68.21, 67.18, 63.58, 60.19, 51.67, 47.76, 42.79, 39.99, 29.48, 28.14, 21.92. ESI-MS: $[M-H]^-$ $C_{39}H_{52}N_5O_{20}$ calculated: 910.3211, observed: 910.3220.

4.4.7 Synthesis of Chol-Br 13

Cholesterol (1 g, 2.6 mmol), DMAP (0.93 g, 7.6 mmol) and trimethylamine (0.73 ml, 0.53 g, 5.3 mmol) were dissolved in DCM (20 ml) and cooled on ice for 15 min. α-Bromoisobutyryl bromide (1.6 ml, 2.98 g, 12.9 mmol) in DCM (5 ml) was then added dropwise. Subsequently, the reaction was stirred on ice for 1 h under room temperature for another 12 h. The reaction mixture was diluted with DCM (50 ml) and washed 3 times with saturated NaCl aqueous solution. The organic phase was collected and dried with Na_2SO_4, then concentrated by rotavapor to ~ 3 ml. Ethanol (50 ml) was used to precipitate out the desired product Chol-Br 13. The product was collected by filtration and dried under N_2 overnight (1.02 g, yield = 74 %).^{1}H NMR (500 MHz, Chloroform-d) δ 5.45 – 5.32 (m, 1H), 4.73 – 4.60 (m, 1H), 2.44 – 2.32 (m, 2H), 2.05 – 1.80 (m, 11H), 1.73 – 1.28 (m, 12H), 1.22 – 0.94 (m, 12H), 0.93 – 0.84 (m, 9H), 0.69 (s, 3H). ^{13}C NMR (126 MHz, Chloroform-d) δ 171.04, 139.34, 122.91, 75.59, 56.66, 56.32, 56.11, 49.97, 42.30, 39.70, 39.51, 37.55, 36.86, 36.59, 36.17, 35.79, 31.91, 31.83, 30.70, 28.23, 28.01, 27.27, 24.28, 23.82, 22.83, 22.57, 21.03, 19.35, 18.71, 11.85.

4.4.8 Synthesis of Chol-PAA 15

Chol-Br **13** (5 mg, 9.4 μmol) and tbutyl acrylate (0.75 g, 5.86 mmol) were dissolved in THF (5 ml). PMDETA (2 μl, 1.6 μg, 9.4 μmol) was added, followed by three freeze-pump-thaw cycles to remove oxygen. CuBr (1.4 mg, 9.4 μmol) was then added under N_2 protection. The reaction was kept under 60 □ for 3 h. After polymerization, 50 μl of the reaction mixture was taken for NMR analysis (Monomer conversion= 95% based on NMR analysis). The remaining solvent was concentrated to ~2 ml by rotavapor after the reaction and H_2O: MeOH = 1: 1 (20 ml) was added. The precipitate was collected and re-dissolved in THF (2 ml). The precipitation process was repeated 3 times to yield crude Chol-PtBA **14** (0.58 g).

Chol-PtBA **14** (0.58 g) was dissolved in TFA: DCM = 1: 1 (2 ml) and stirred under room temperature for 1 h. The solvent was then removed by rotavapor and the residue was re-dissolved in water and dialyzed against pure water (MWCO = 3500 Da) for 24 h followed by lyophilization to yield Chol-PAA **15** (0.29 g, yield = 68% (two steps)). ^{1}H NMR (500 MHz, Deuterium Oxide) δ 4.98 – 4.96 (m, 1H), 2.42 – 2.11 (m, 500H), 1.88 – 1.37 (m, 1000H), 0.95 – 0.94 (m, 3H), 0.73 – 0.69 (m, 3H).

4.4.9 Synthesis of Chol-PAA-yne 16

Chol-PAA **15** (0.1 g, ~2.8 μmol) was dissolved in water (5 ml) followed by the addition of EDC•HCl (100 mg, 0.52 mmol) and propargyl amine (18 mg, 0.33 mmol). The reaction was stirred under room temperature for 24 h. The reaction mixture was then collected and dialyzed against

0.1x PBS buffer for 48 h then in pure water for another 24 h (MWCO = 3500). The solution in dialysis tubing was collected and lyophilized to yield Chol-PAA-yne **16** (87 mg, yield= 74%). ^{1}H NMR (500 MHz, Deuterium Oxide) δ 4.03 – 3.82 (m, 200H), 2.71 – 2.49 (m, 100H), 2.35 – 1.15 (m, 1500H), 0.67 (s, 3H).

4.4.10 Synthesis of Chol-P-CD22L$_{100}$ 4

MPB-Sia-Lac-N_3 **3** (6 mg, 6.5 μmol), CuSO4 (0.5 mg, 3.25 μmol), THPTA 12 (5 mg, 13 μmol), sodium ascorbate (11 mg, 52 μmol), amino guanidine (6 mg, 52 μmol), Chol-PAA-yne **16** (2 mg, containing 6.5 μmol alkyne) were dissolved in water (1 ml) in a sealed vial and stirred under room temperature for 24 h. The reaction mixture was passed through G25 column to yield purified **4**. ^{1}H NMR (500 MHz, Deuterium Oxide) δ 7.31 (s, 900H), 4.41 – 4.09 (m, 100H), 4.09 – 3.20 (m, 2300H), 3.11 – 2.87 (m, 100H), 2.80 – 0.63 (m, 2000H).

4.4.11 General procedure of metabolic glyco-engineering of NK-92 cells

NK-92 cells (5×10^5 cells/mL) were incubated with culture medium supplemented with MPB-sia **1**, BPC-sia **2** or free sialic acid at different final concentrations for various time periods. In this study, "MsNK-92" refers the NK-92 cells incubated with 2 mM MPB-sia **1** for 48 h if not specified. After incubation, the cells were washed three times with PBS buffer. These cells were collected and used in this study. The binding ability of these engineered NK-92 cells toward human CD22 protein was studied by FACS and confocal imaging. 5×10^5 of cells were suspended in 0.1 ml PBS buffer and incubated with 0.5 μg human CD22-Fc on ice for 30 min. The cells were washed twice

with PBS buffer after incubation followed by PE mouse anti-human CD22 mAb (clone HIB22) staining on ice in dark for another 30 min. The cells were washed twice with PBS buffer and analyzed by FACS directly. For confocal imaging study, the cells were fixed by 4% paraformaldehyde after mAb staining and washing, then stained by DAPI before imaging.

4.4.12 Mass spectrum analysis of surface sialic acid and derivatives on NK92 cells after metabolic glycoengineering

NK92 cells (1 x 10^7 cells) were incubated with medium only (10 mL), or medium (10 mL) containing 2 mM sialic acid, 2 mM MPB-sia **1**, 2 mM BPC-sia **2** respectively for 24 h followed by thorough washing with PBS buffer for 3 times to remove all free ligands. 1x10^7 of NK92 cells from each group were collected and resuspended in 200 µl PBS buffer.

1 µl enzyme stock solution containing 50 units of α-2-3,6,8 neuraminidase (New England Biolabs) was added to each group and the resulting cell-enzyme mixtures were kept under 37□ on a shaker for 1 h. After the incubation, the enzyme was deactivated by heating to 65 □ for 15 min. The samples were centrifuged at 5,000 rpm for 5 min and the supernatants were collected and lyophilized. On the same day of mass spectrum analysis, the lyophilized samples were dissolved in 50 µl DI water followed by addition of 50 µl of DMB reagent stock (3.5 mg DMB hydrochloride, 172 µl acetic acid, 112 µl 2-mercaptoethanol and 4.9 mg sodium hydrosulfite dissolved in 1.5 ml DI water, prepared right before use). For standard curve measurement, 50 µl of sialic acid, MPB-sia **1** and BPC-sia **2** (1 mg/ml in DI water) were mixed with 50 µl of the DMB reagent stock. All reaction mixtures were kept in dark in 60 □ water bath for 2 h. The samples were then cooled on

ice and diluted with acetonitrile : water (1:1) for mass spectrum analysis. For standard curves and sialic acid quantification results, see **Table 4.1**.

4.4.13 Insertion of Chol-P-CD22L$_{100}$ 4 onto NK-92 cells

NK-92 cells (1×10^7 cells/ml) were incubated with Chol-P-CD22L$_{100}$ **4** in PBS buffer at various final concentrations (2.5 μM, 5 μM or 10 μM) for 1 h under room temperature. After incubation, the cells were washed three times with PBS buffer. These cells were collected and used for further study.

4.4.14 Dose and time dependent metabolic incorporation of MPB-Sia 1 on NK-92 cells

To study the dose dependence of MPB-Sia **1** metabolic incorporation, NK-92 cells (5×10^5 per sample) were incubated with NK-92 medium (1 ml) supplemented with different concentrations of MPB-sia **1** for 48 h. After incubation, the cells were collected and washed three times with PBS buffer. The cells were then incubated with human CD22-Fc followed by PE-mouse anti-human CD22 mAb staining and FACS analysis as described above. The data represent the mean of triplicate samples.

To study the metabolic incorporation of MPB-Sia 1 during different time periods, NK-92 cells (5×10^5 per sample) were incubated with NK-92 medium (1 ml) supplemented with 2 mM MPB-sia **1** for 24 h, 48 h or 72 h. After incubation, the cells were collected and washed three times with PBS buffer. The cells were then incubated with human CD22-Fc followed by PE-mouse anti-

human CD22 mAb staining and FACS analysis as described above. The data represent the mean of triplicate samples.

4.4.15 The level of α2-6-sia linkage on NK-92 cell surface before and after metabolic engineering

NK-92 cells (5×10^5 per sample) were suspended in 100 μl Hanks buffer containing 4% BSA and 0.1% NaN_3. 1 μg FITC-labeled α2,6-SA binding plant lectin Sambucus Nigra Lectin (SNA) was added to each sample. After incubation on ice in dark for 30 min, the cells were collected and washed 3 times with Hanks buffer. Unmodified NK-92 cells were stained by the same procedure. An unstained NK-92 sample was included as the negative control for analysis. The samples were analyzed by FACS. The data represent the mean of triplicate samples.

4.4.16 The influence of MPB-sia 1 on NK-92 cell viability

NK-92 cells (5×10^5 per sample) were incubated with different concentrations of MPB-Sia **1** for 48 h, or with 2 mM MPB-Sia **1** for different time periods (24 h, 48 h or 72 h). After incubation, the cells were collected and washed twice with PBS buffer. The cells were resuspended in 1 ml of PBS buffer containing 1μM Calcein AM and were incubated under 37□ for 15 min. The samples were analyzed by FACS and the cell viability was calculated based on fluorescent cell counts per 100 μl sample.

4.4.17 Time dependent decrease of CD22 binding after metabolic glyco-engineering

Metabolic engineered or polymer engineered NK-92 cells (5×10^5 cells per sample) were collected and washed 3 times with PBS buffer to remove free MPB-Sia **1** or Chol-P-$CD22L_{100}$ **4**.

The CD22 binding at 0 h was obtained by incubating 5 x 10^5 cells with human CD22-Fc followed by PE-mouse anti-human CD22 mAb staining and FACS analysis immediately after the removal of MPB-Sia **1** or Chol-P-CD22L_{100} **4**. Other cells were re-suspended in fresh culture medium without MPB-Sia **1** or Chol-P-CD22L_{100} **4** and incubated at 37 ºC for another 12 h, 24 h or 48 h. At each time point, 5×10^5 cells were collected, stained and analyzed by FACS. An unmodified NK-92 sample was incubated with CD22 protein and stained with PE-mouse anti-human CD22 mAb as the negative control. The mean fluorescence intensities of PE were normalized to 0 h (100%).

4.4.18 Measurement of surface CD22 expression level on different cell lines

Raji or Hela cells (1×10^6 cells per sample) were collected and washed with PBS for three times. The cells were re-suspended in 100 μl PBS buffer and stained with PE mouse anti-human CD22 on ice in dark for 30 min, followed by FACS analysis. An unstained cell sample was included as the negative control.

4.4.19 Imaging analysis of NK-92 cell and Raji cell binding

Raji cells (1×10^6/ml) were incubated with 1μM Calcein AM for 15 min at 37□ and then washed three times with 1640 medium containing FBS, followed by incubation with NK-92 cells or MsNK-92 cells at a 1: 1 ratio. Two hours later, the cells mixture was imaged by fluorescent microscope. The percentages of cell complexes were calculated as the proportion of the Raji cells

attached to the NK-92 cells over the total number of Raji cells. The data represent the mean of triplicate samples.

4.4.20 *In vitro* NK cytotoxicity assay against Raji cells

Raji cells stably transfected with firefly luciferase (Raji-luc, 1×10^4 per well) were co-incubated with unmodified NK-92 or MsNK-92 at different effector to target cell ratios (E/T = 0.5, 1, 5) at 37 ºC in 200 μL of mixture medium (RPMI-1640 : NK-92 medium = 1: 1). After 5 h incubation, the cells were centrifuged, and the supernatant was discarded. The cells were lysed, and bioluminescence was detected by firefly luciferase reporter gene assay kit according to manufacturer's instruction. The luminescence intensity of Raji-luc cells was recorded. The cell lysis of each sample was normalized to the luminescence intensity of Raji-luc only (100 %) and buffer only (0 %) samples. The data represent the mean of triplicate samples. To study the influence of CD22 binding on specific killing against Raji, a competition experiment was performed. NK-92 or MsNK-92 (1×10^4 per well) were first incubated with various amounts of human CD22-Fc (0 μg/mL, 1 μg/mL, 5 μg/mL) on ice for 30 min. Then Raji-luc cells (1×10^4 per well) were added to NK-92 or MsNK-92 to reach E/T = 1: 1. After 5 h incubation under 37 ºC, the cells were centrifuged, and the supernatant was discarded. The cells were lysed, and bioluminescence was detected by firefly luciferase reporter gene assay kit according to manufacturer's instruction. The luminescence intensity of Raji-luc cells was recorded. The cell

lysis of each sample was normalized to the luminescence intensity of Raji-luc only (100 %) and buffer only (0 %) samples. The data represent the mean of triplicate samples.

4.4.21 CD22 specific *in vitro* killing assay on CHO-WT and CHO-hCD22 cells

CHO WT cells and CHO hCD22 cells were incubated with 0.5 μM and 5 μM CFSE respectively in 1 mL of PBS buffer containing 0.1% BSA under 37 ºC for 10 min. After incubation, 10 mL of complete culture medium were added to each tube respectively and the cells were incubated under room temperature for another 10 min. The cells were collected respectively and washed once with complete culture medium. The cell densities of both $CFSE^{lo}$-CHO WT cells and $CFSE^{hi}$-CHO hCD22 cells were adjusted to 1×10^5/mL. The two type of cells were mixed at a 1:1 ratio, and co-incubated with NK-92 or MsNK-92 cells at different effector to target ratios (E/T = 5: 1, 10: 1, 25: 1, and 50: 1) under 37 ºC for 5 h. The cell mixtures were analyzed by FACS after co-incubation. The percentages of lysis of CHO-hCD22 cells were calculated based on the $CFSE^{hi}/CFSE^{lo}$ cell ratio changes before and after incubating with NK-92 or MsNK-92.

4.4.22 *In vitro* NK cytotoxicity assay against patient-derived leukemic samples

Patient-derived leukemic samples were from to be discarded samples following routine diagnostic procedures. The white blood cells were enriched by density gradient centrifugation and then treated with red blood cell lysis buffer. The purified cells were treated with 5 μL PE mouse anti-human CD22 in 0.1 mL volume on ice for 30 min to identify the CD22 expression levels. For the cell-mediated cytotoxicity assay, the purified cells were labeled with 1 μM Calcein AM and

incubated with NK-92 cells or MsNK-92 cells for 5h at E/T=5:1 under 37 ºC. The samples were analyzed by FACS and the cell viability was calculated based on fluorescent cell counts per 100 μL sample.

4.4.23 Perforin imaging

Cell-cell complex formation and redistribution of cytotoxic granules containing perforin were analyzed by confocal microscopy. NK (5×10^5) cells and Raji cells (5×10^5) were co-incubated at a 1: 1 ratio for 1 h at 37 ºC, then fixed for 10 min with 4% polyformaldehyde solution. Immunostaining permeabilization buffer with Triton X-100 was added for cell permeabilization. Cells were washed and blocked for 30 min with 10% FBS in PBS to avoid unspecific binding. The cells were incubated for 75 min at room temperature with perforin-specific antibody δG9, followed by Alexa Fluor 594-coupled anti-mouse antibody. Cell nuclei were counterstained with DAPI. Cells were wash twice with PBS, then dropped onto the slide to make microscopic slides and analyzed with Olympus FV1000MPE-B.

4.4.24 IFN-γ release assay

IFN-γ release by NK-92 cells was determined by using BD Cytometric Bead Array Flex Set for Human IFN-γ according to the manufacturer`s protocol. Briefly, 2×10^4 Raji cells were incubated with equal numbers of NK-92 cells in the wells of 96-well V-bottom plates for 5 h at 37 ºC. IFN-γ concentrations in supernatants were measured using BD Cytometric Bead Array Flex Set for Human IFN-γ.

4.4.25 Tumor challenge

For intratumoral administration of NK cells

BALB/c nude mice (female, 6-8 weeks) were purchased from model animal research center of Nanjing University (Nanjing, China). Prior to tumor implantation, mice received cyclophosphamide (2 mg in 0.1 mL PBS) intraperitoneally for three days. 1×10^7 Raji-luc cells in 0.2 mL were injected subcutaneously in the right flank of the mice on day 0. Mice were treated on day 15, 22 and 29 with intratumoral injections of 1×10^7 NK-92 cells or MsNK-92 cells (n =3 per group) in 50 μL PBS. The tumor size was measured before intratumoral injections with Vernier caliper and the tumor volumes were calculated by the formula length×width×width×0.5. Animals were sacrificed at day 36 and xenografts were surgically excised and weighed. For *in vivo* imaging, the mice were injected with 100 μL D-luciferin (30 mg/mL) intraperitoneally and the bioluminescence signal in mice was measured using IVIS® Lumina II system. For ex vivo imaging, the excised tumor was immersed in 10 mL D-luciferin (3 mg/mL) for about 5 min, then the bioluminescence signal was measured using IVIS® Lumina II system. These experiments were repeated with n=5 mice per group. The results from the repeat experiments were similar to those in **Figure 4.17**.

For intravenous administration of NK cells

NOD SCID mice (female, 6-10 weeks) were purchased from model animal research center of Nanjing University (Nanjing, China). 1×10^6 Raji-luc cells were injected intravenously on day 0.

At days 2, 5, 8, 12, 15, animals were administrated with 1×10^7 NK-92 cells or MsNK-92 cells via the tail vein (each group n = 10). The control group received PBS only. The body weight and survival of the mice were continuously monitored. Mice that developed hind-limb paralysis in the course of the experiments were euthanized. Kaplain-Meier curves were constructed.

APPENDICES

APPENDIX A: Cell surface CD22 expression

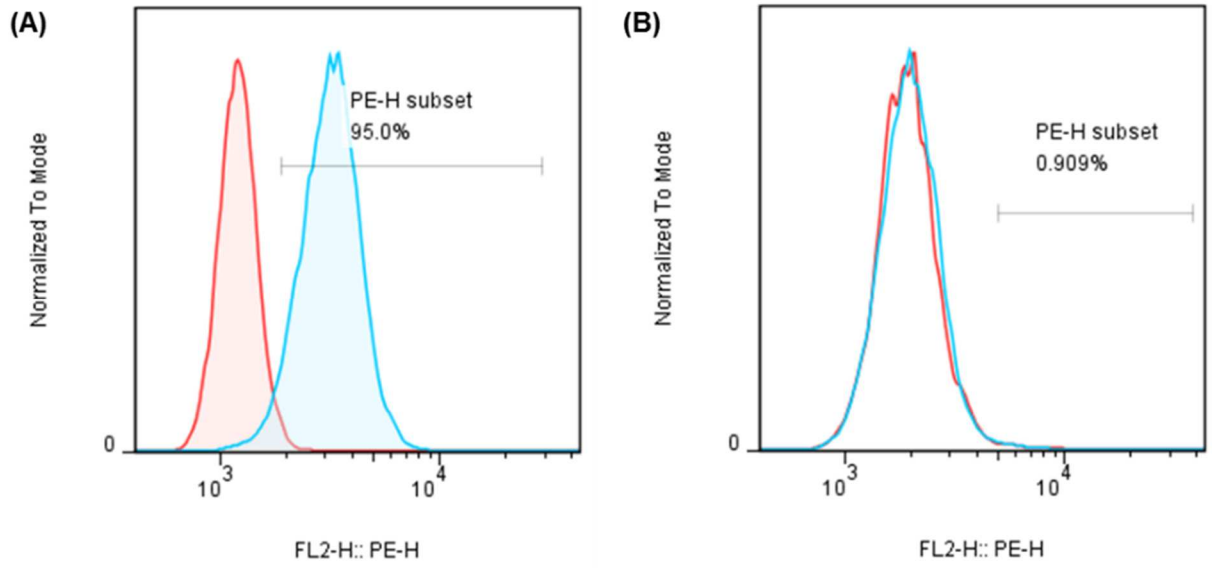

Figure 4.20 Surface expression levels of CD22 on **a.** Raji-luc vs **b.** Hela cells as detected by flow cytometry. Raji-luc cells have much higher expression of CD22 compared to Hela cells.

APPENDIX B: Attempts for synthesizing polymers with multiple cholesterol copies

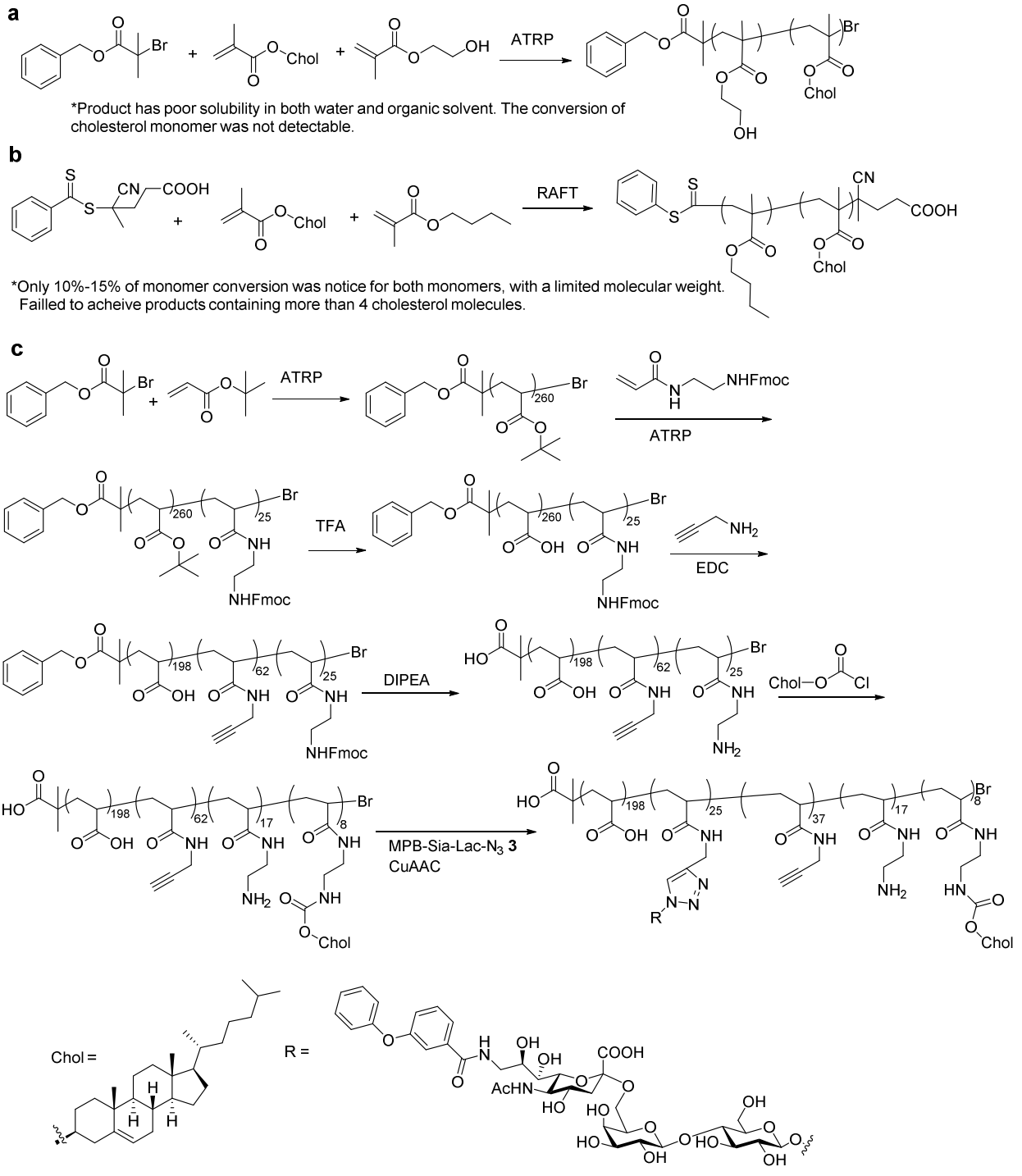

Scheme 4.1 Synthesis of polymers with multiple cholesterol copies. **a.** Polymerizing cholesterol monomers *via* ATRP. **b.** Polymerizing cholesterol monomers *via* RAFT. **c.** Polymerization of block polymer with different functional groups, followed by post-polymerization modification of cholesterol and MPB-Sia-Lac-N_3 **3**.

APPENDIX C: NMR Spectra

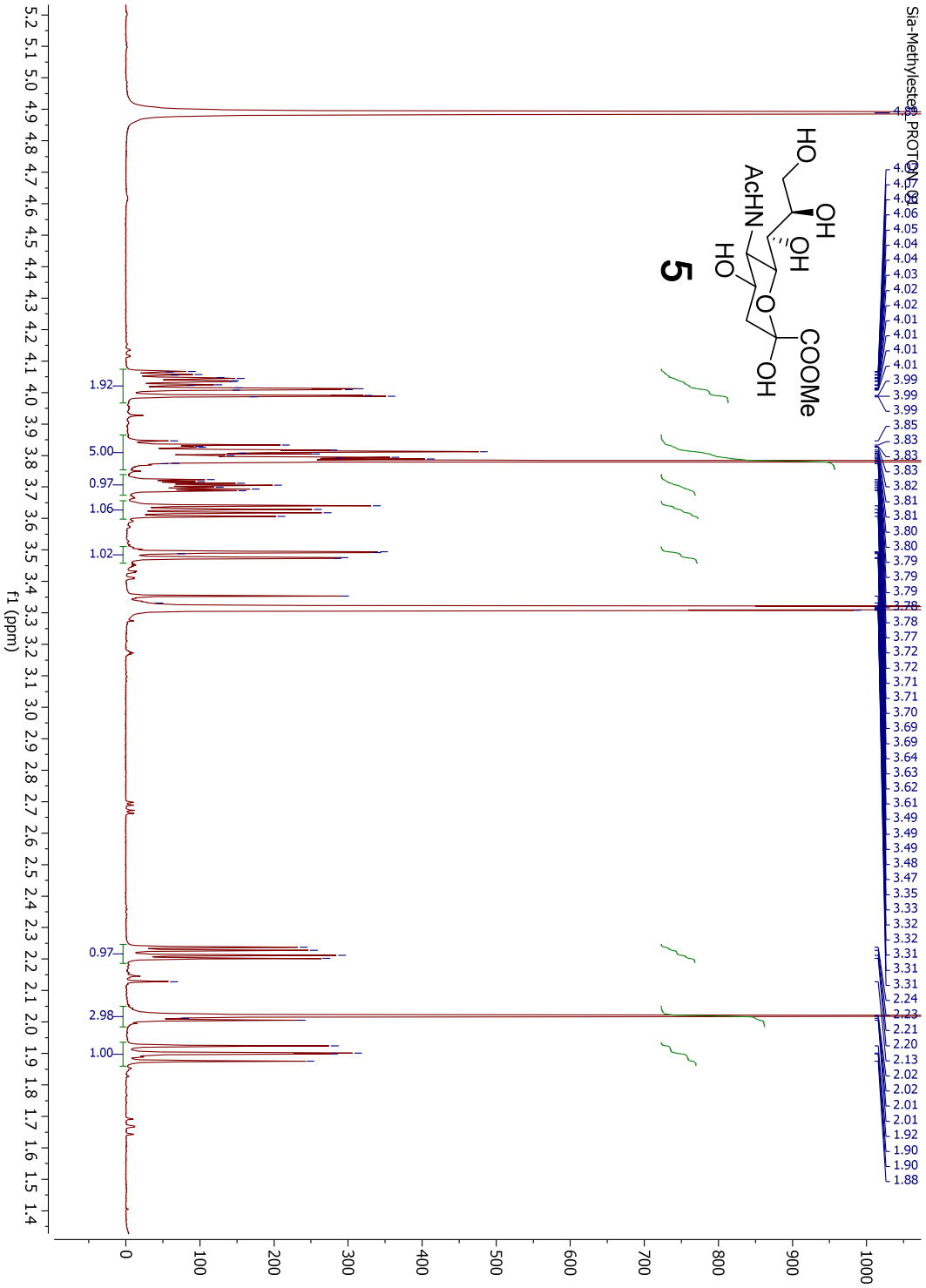

Figure 4.21 ^{1}H NMR of **5** (500MHz, D_2O)

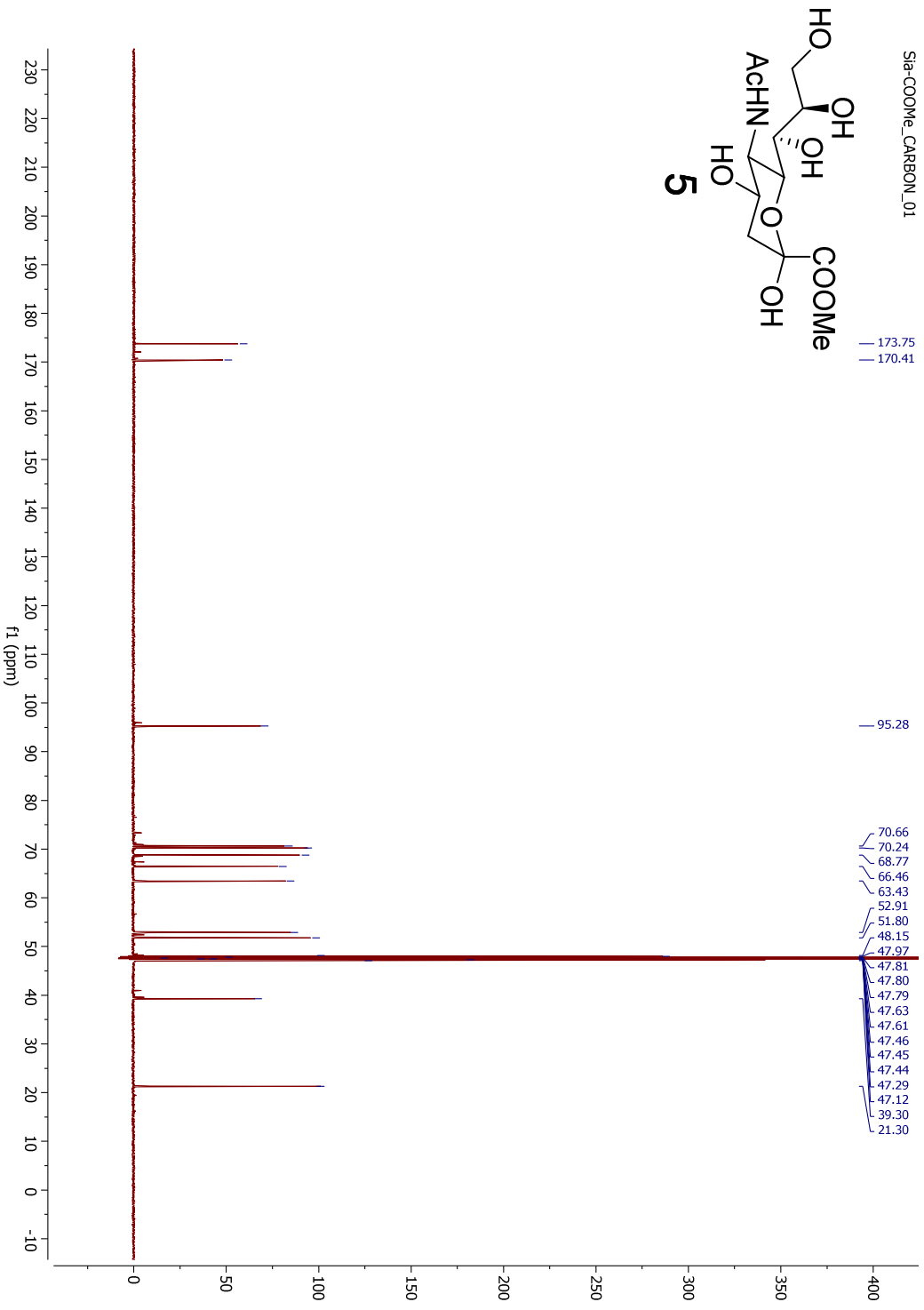

Figure 4.22 ^{13}C NMR of **5** (500MHz, D_2O)

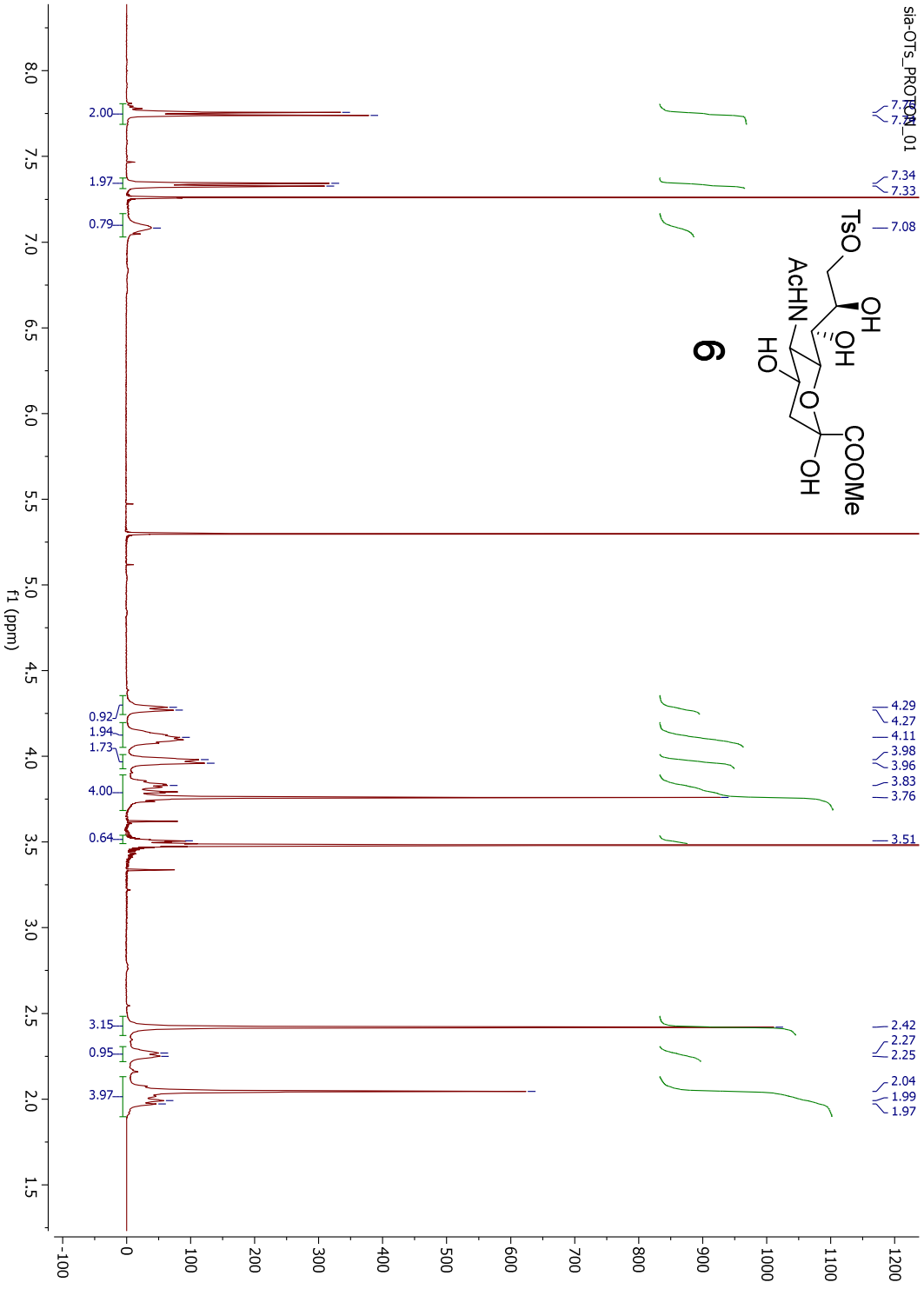

Figure 4.23 ^{1}H NMR of **6** (500MHz, $CDCl_3$)

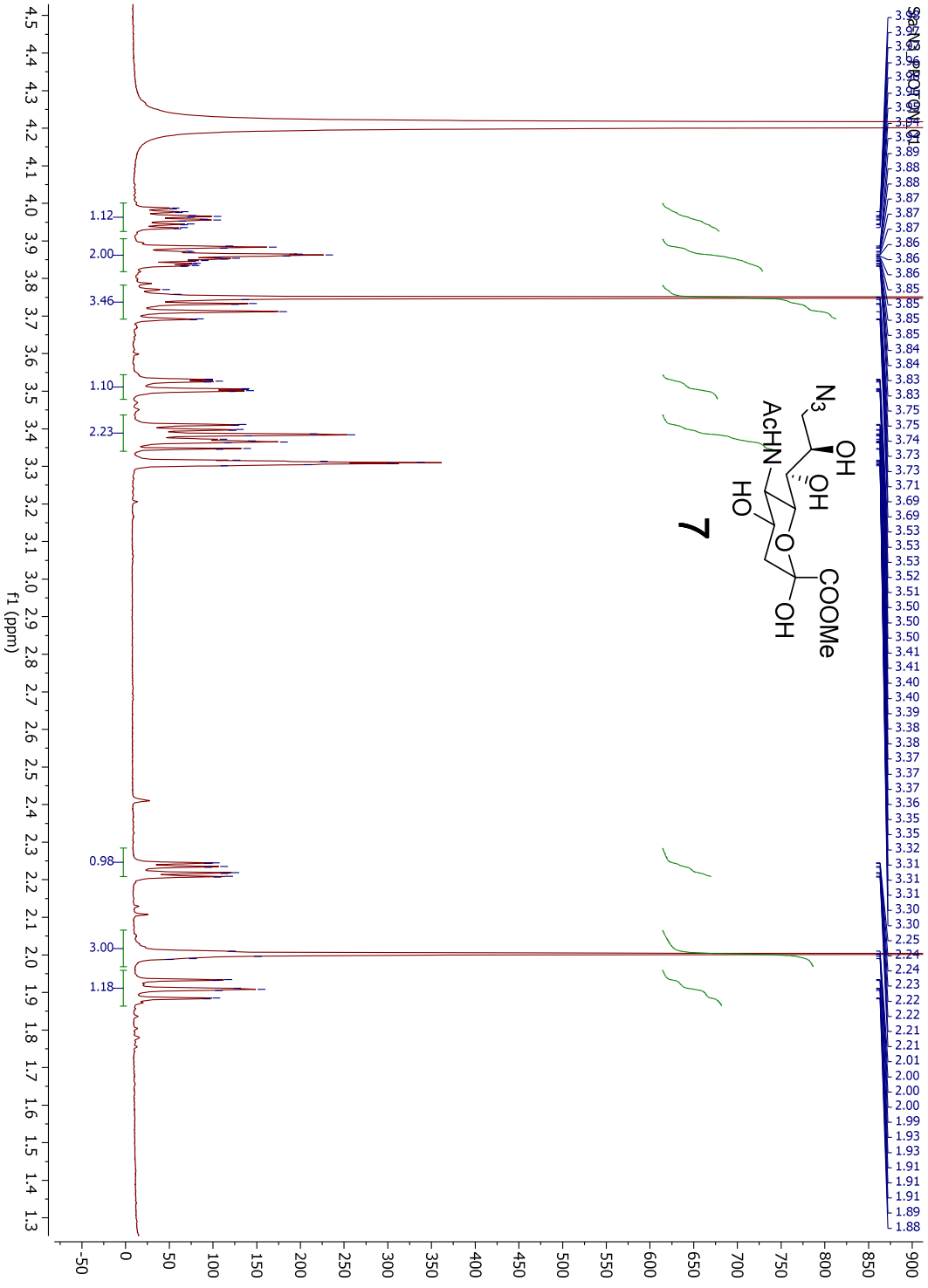

Figure 4.24 ^{1}H NMR of **7** (500MHz, D_2O)

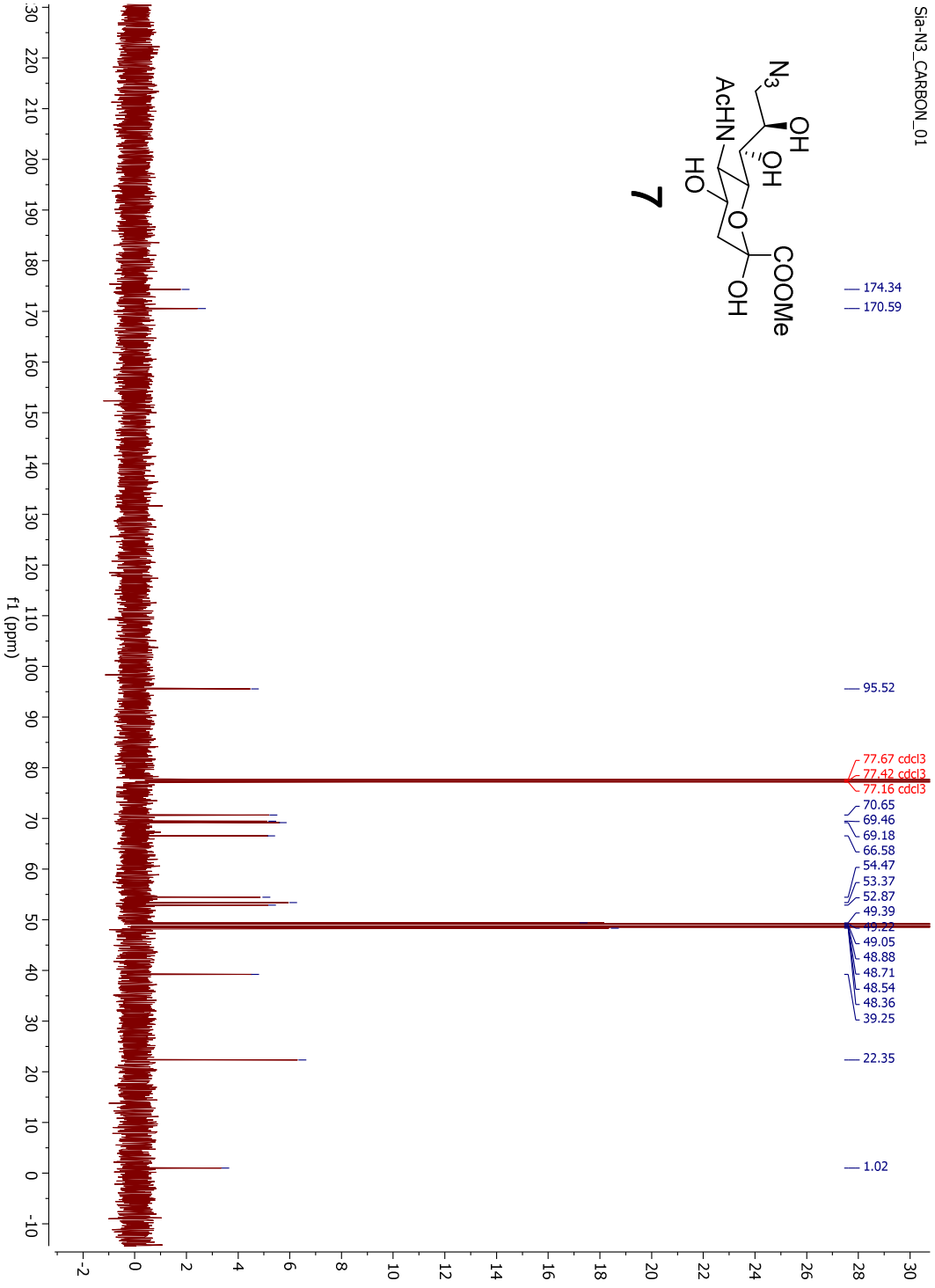

Figure 4.25 ^{13}C NMR of **7** (500MHz, D_2O)

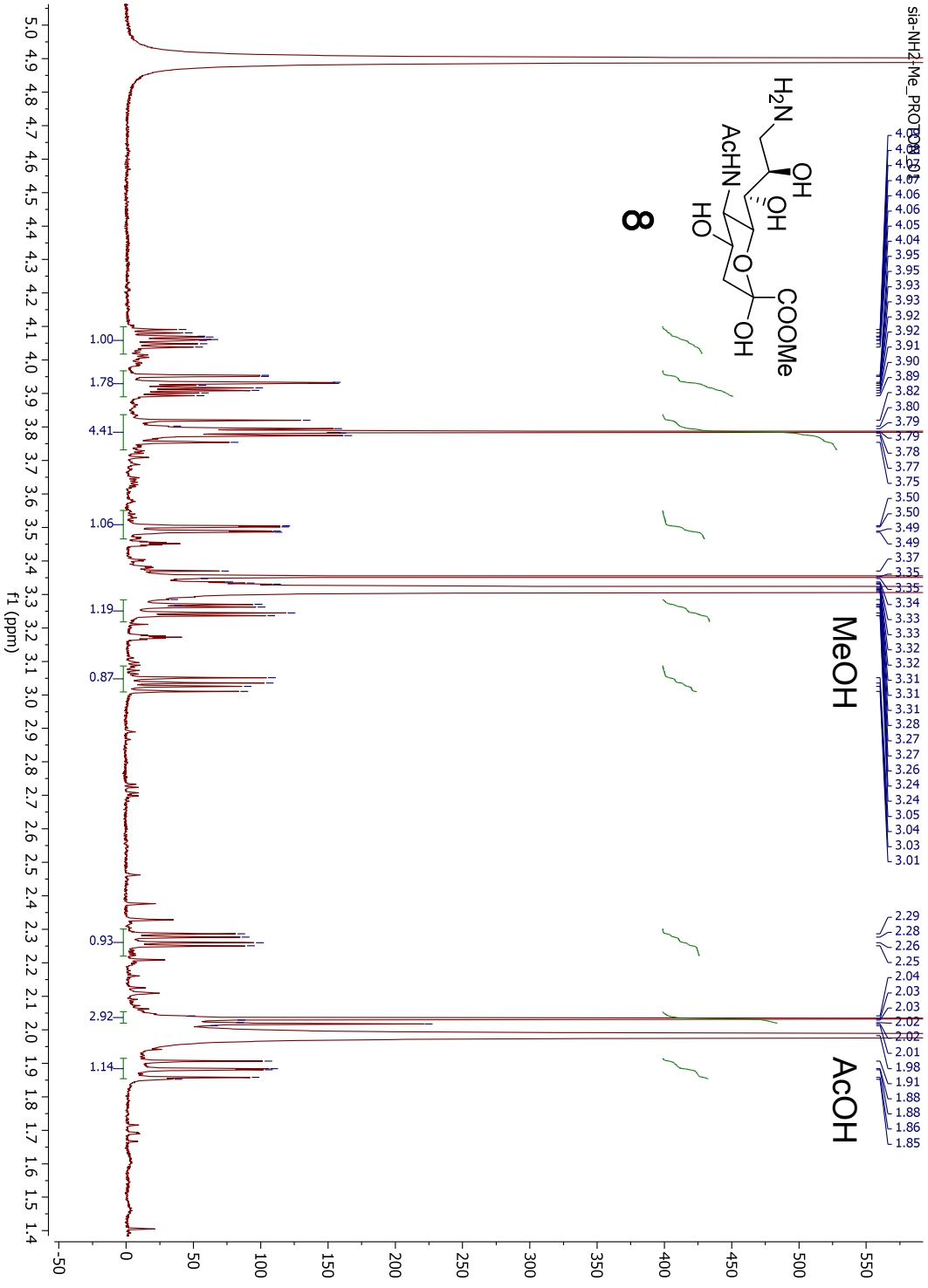

Figure 4.26 ^{1}H NMR of **8** (unpurified, 500MHz, D_2O)

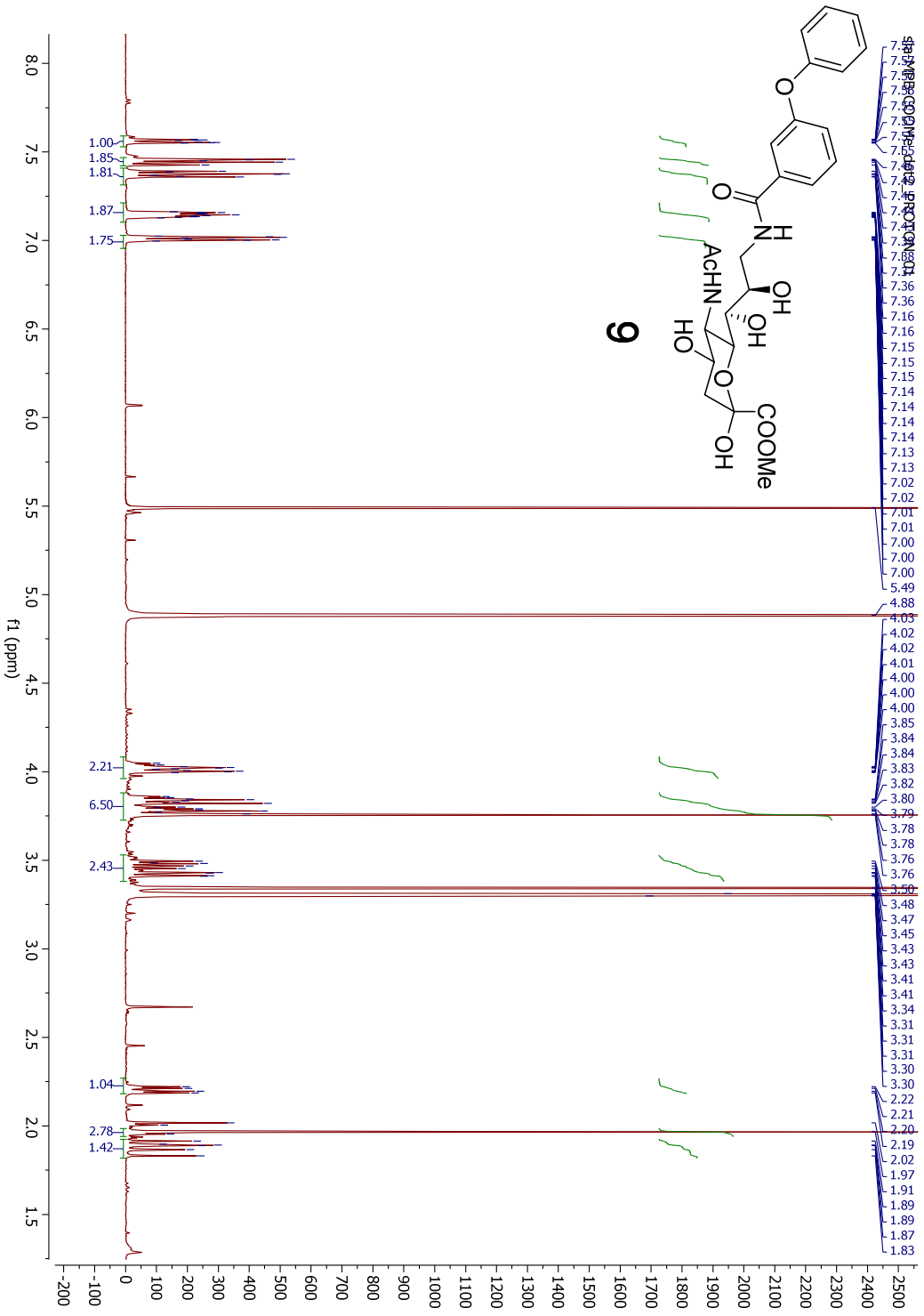

Figure 4.27 ^{1}H NMR of **9** (unpurified, 500MHz, D_2O)

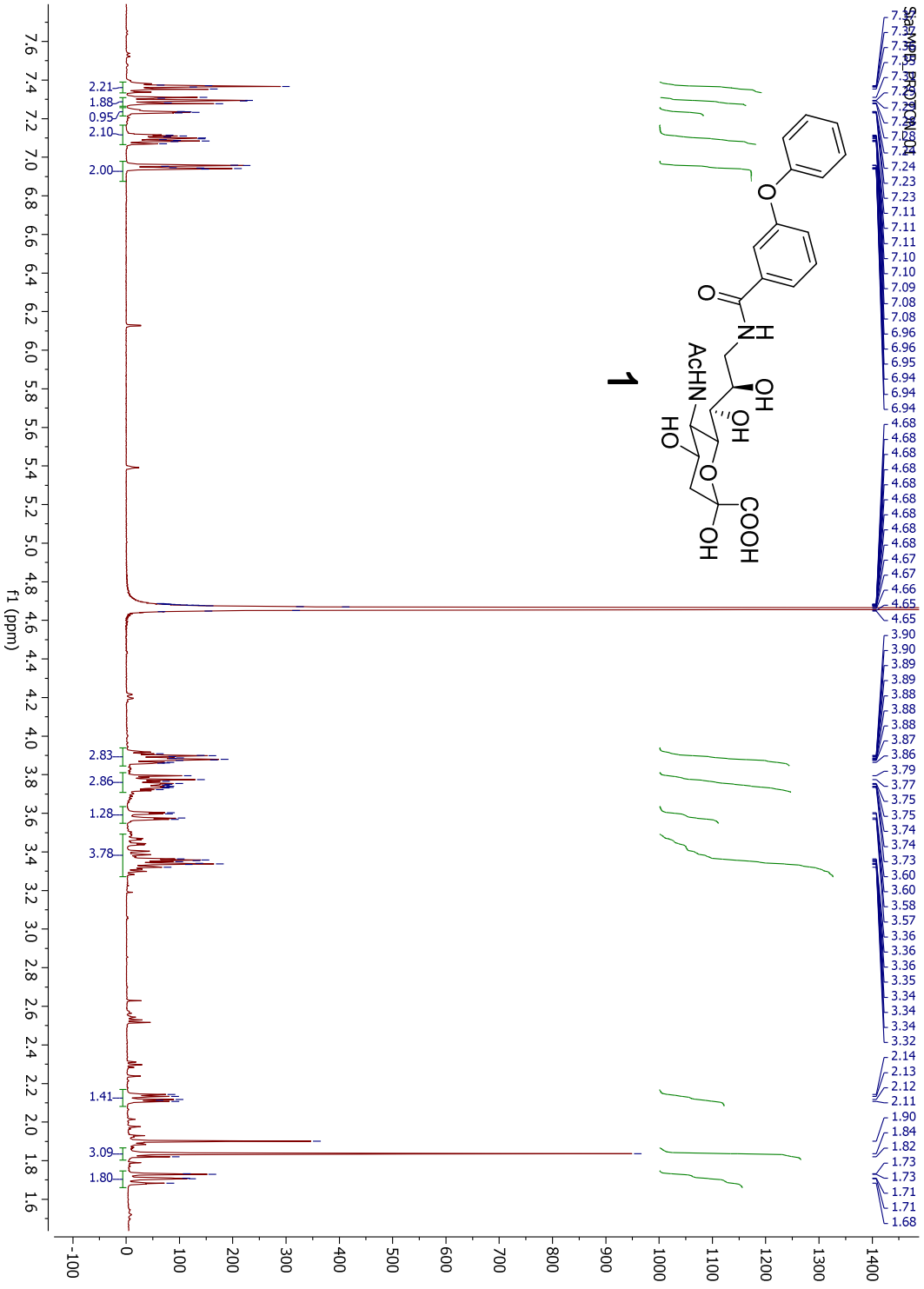

Figure 4.28 ^{1}H NMR of **1** (500MHz, D_2O)

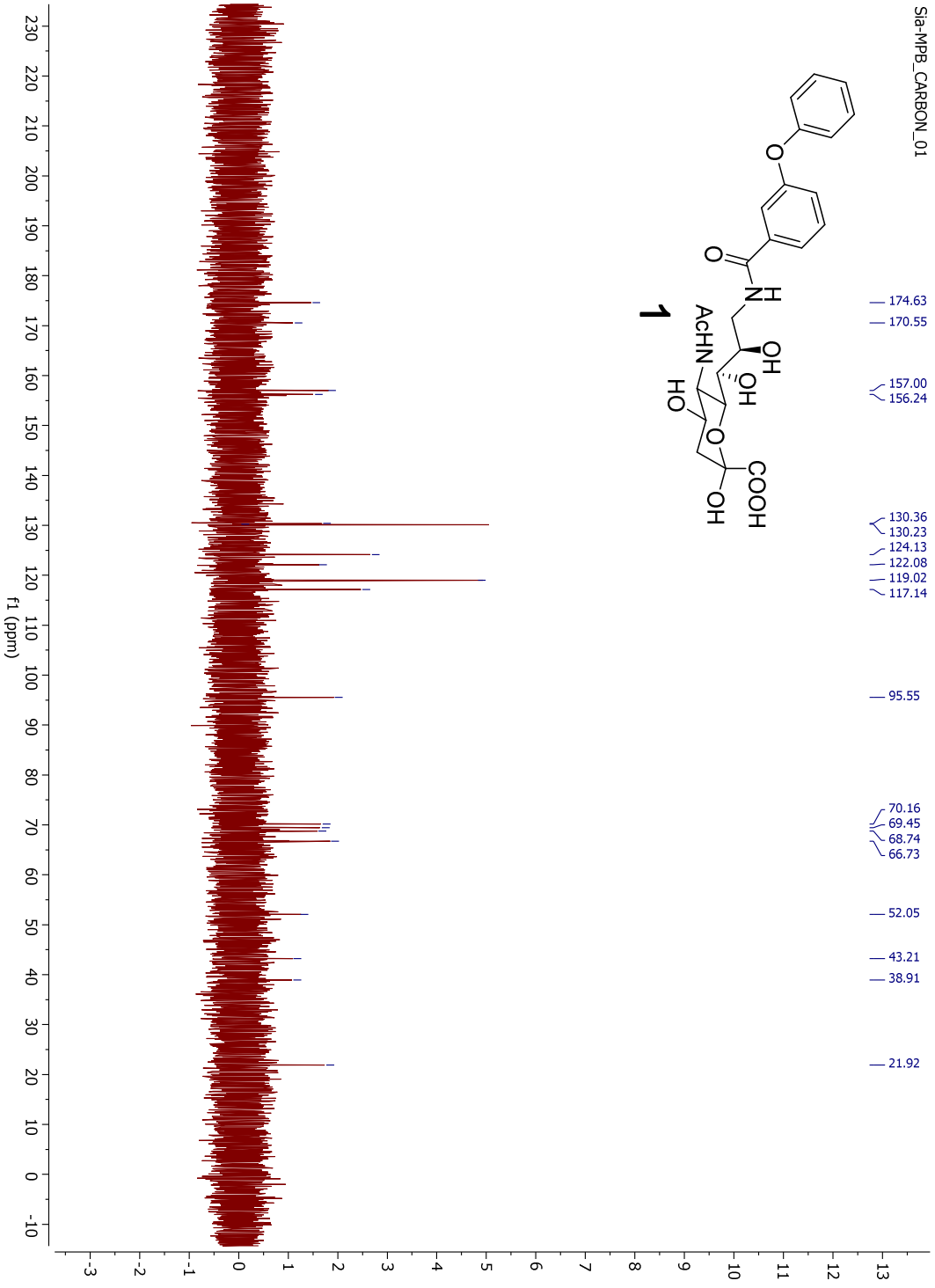

Figure 4.29 ^{13}C NMR of **1** (500MHz, D_2O)

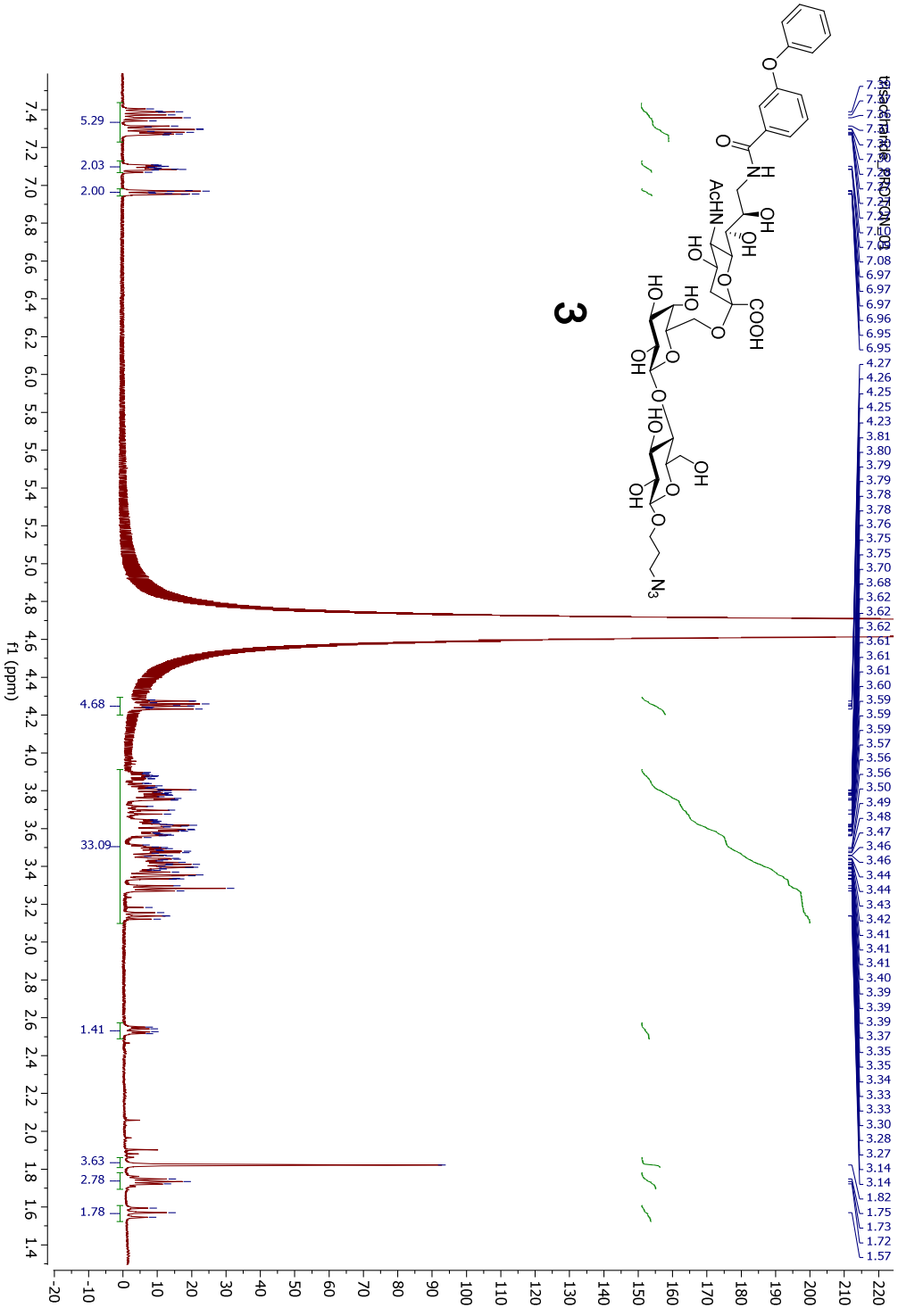

Figure 4.30 ^{1}H NMR of **3** (500MHz, D_2O)

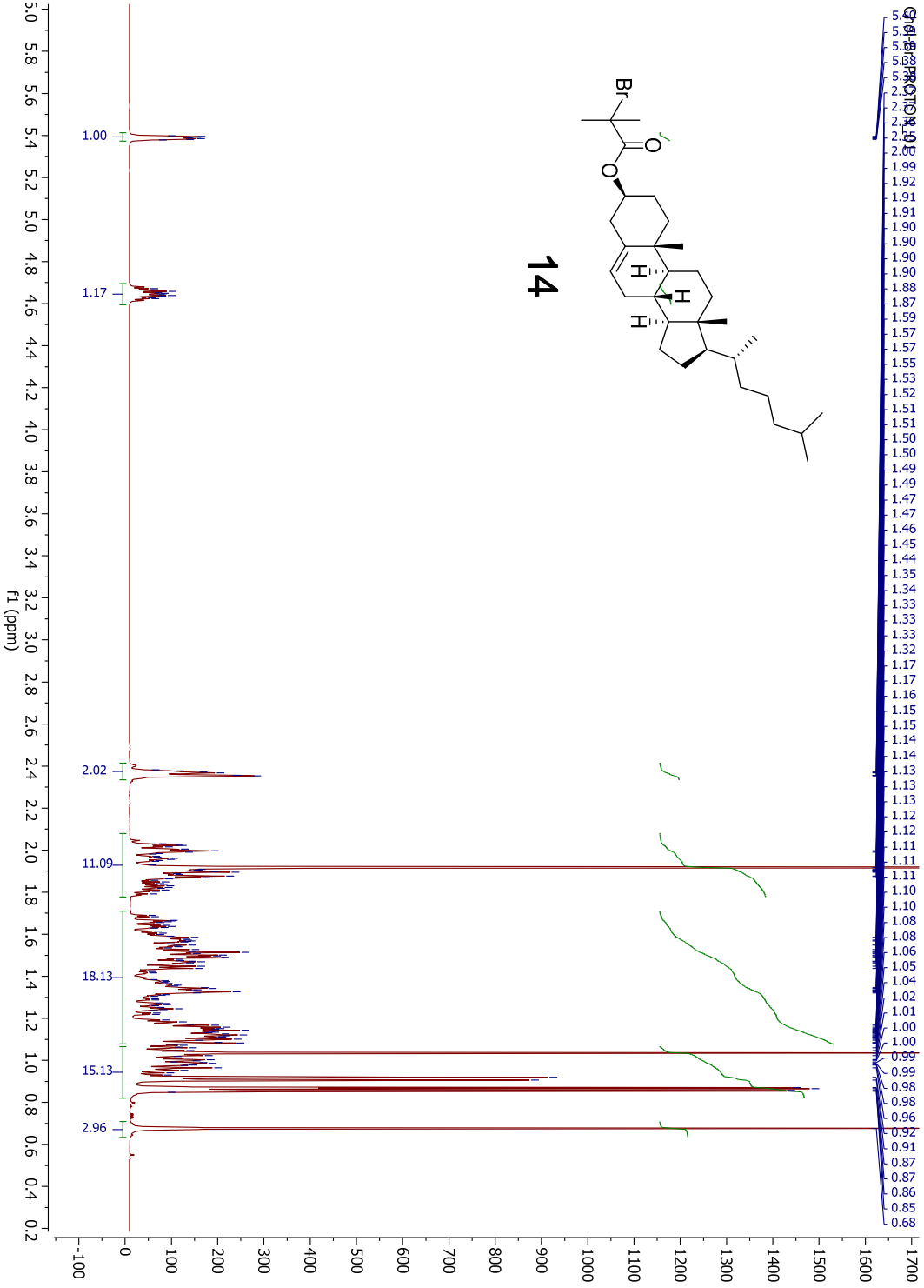

Figure 4.31 ^{1}H NMR of **14** (500MHz, $CDCl_3$)

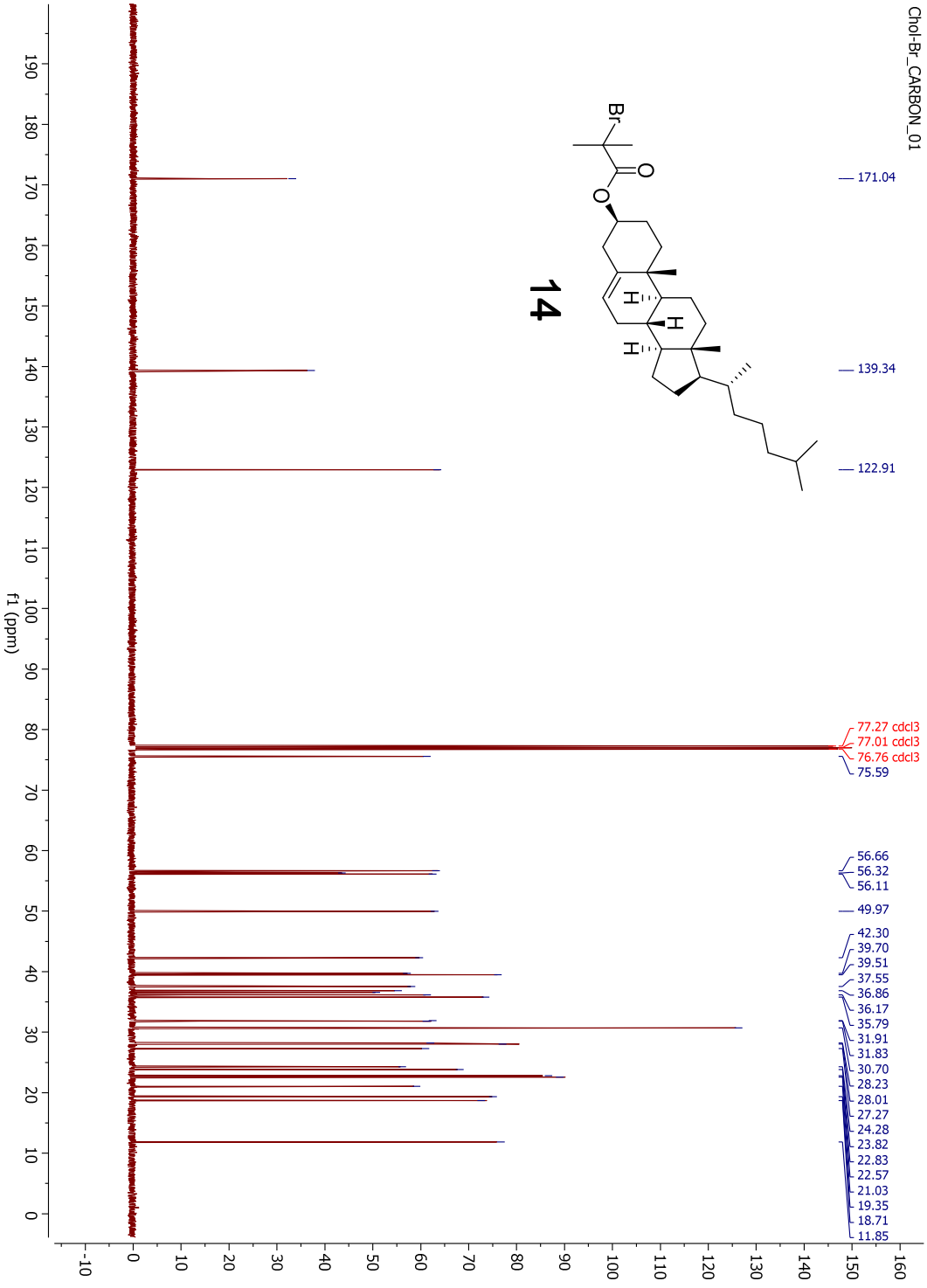

Figure 4.32 ^{13}C NMR of **14** (125MHz, $CDCl_3$)

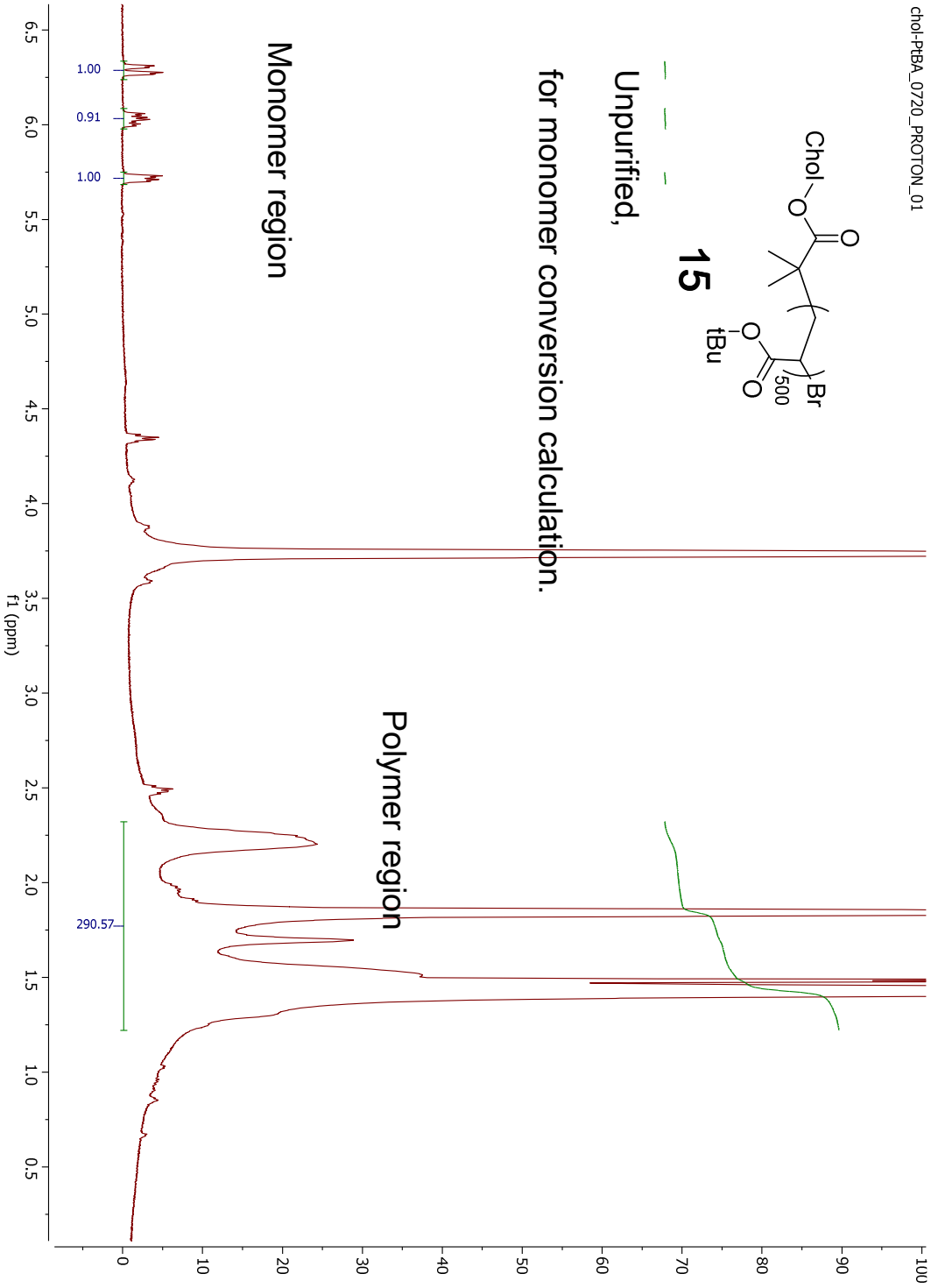

Figure 4.33 ^{1}H NMR of **15** (500MHz, D_2O)

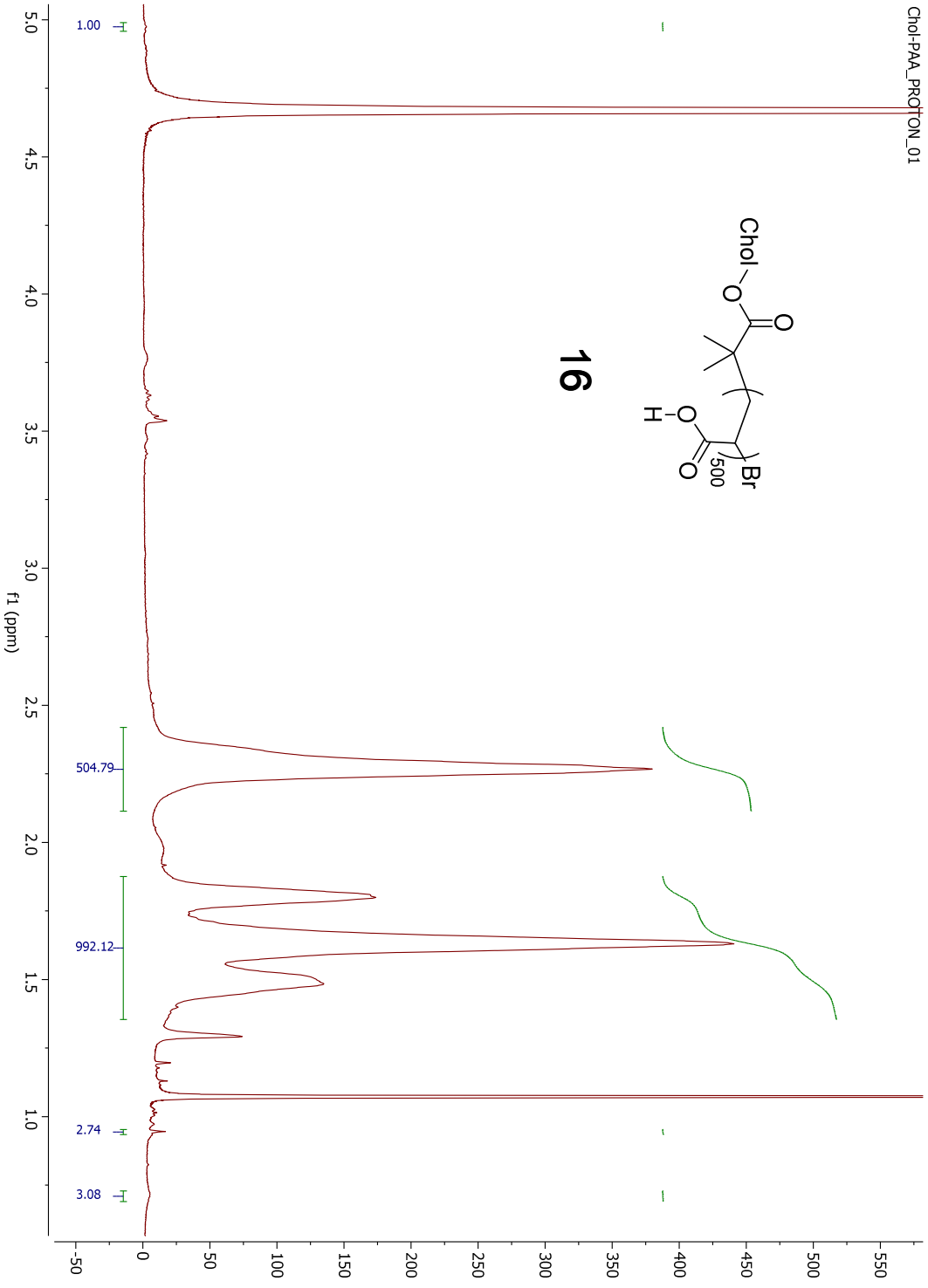

Figure 4.34 ^{1}H NMR of **16** (500MHz, D_2O)

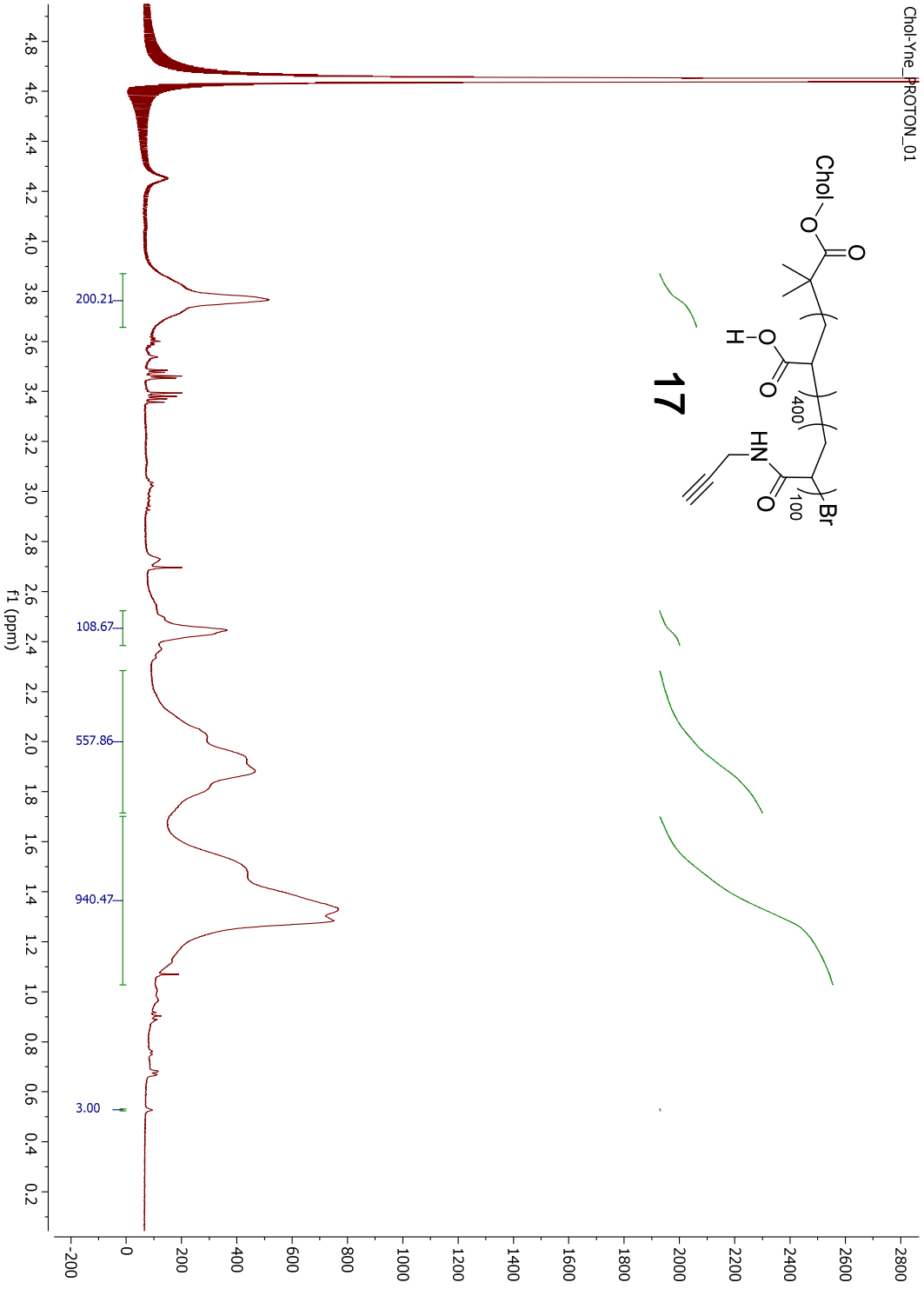

Figure 4.35 ^{1}H NMR of **17** (500MHz, D_2O)

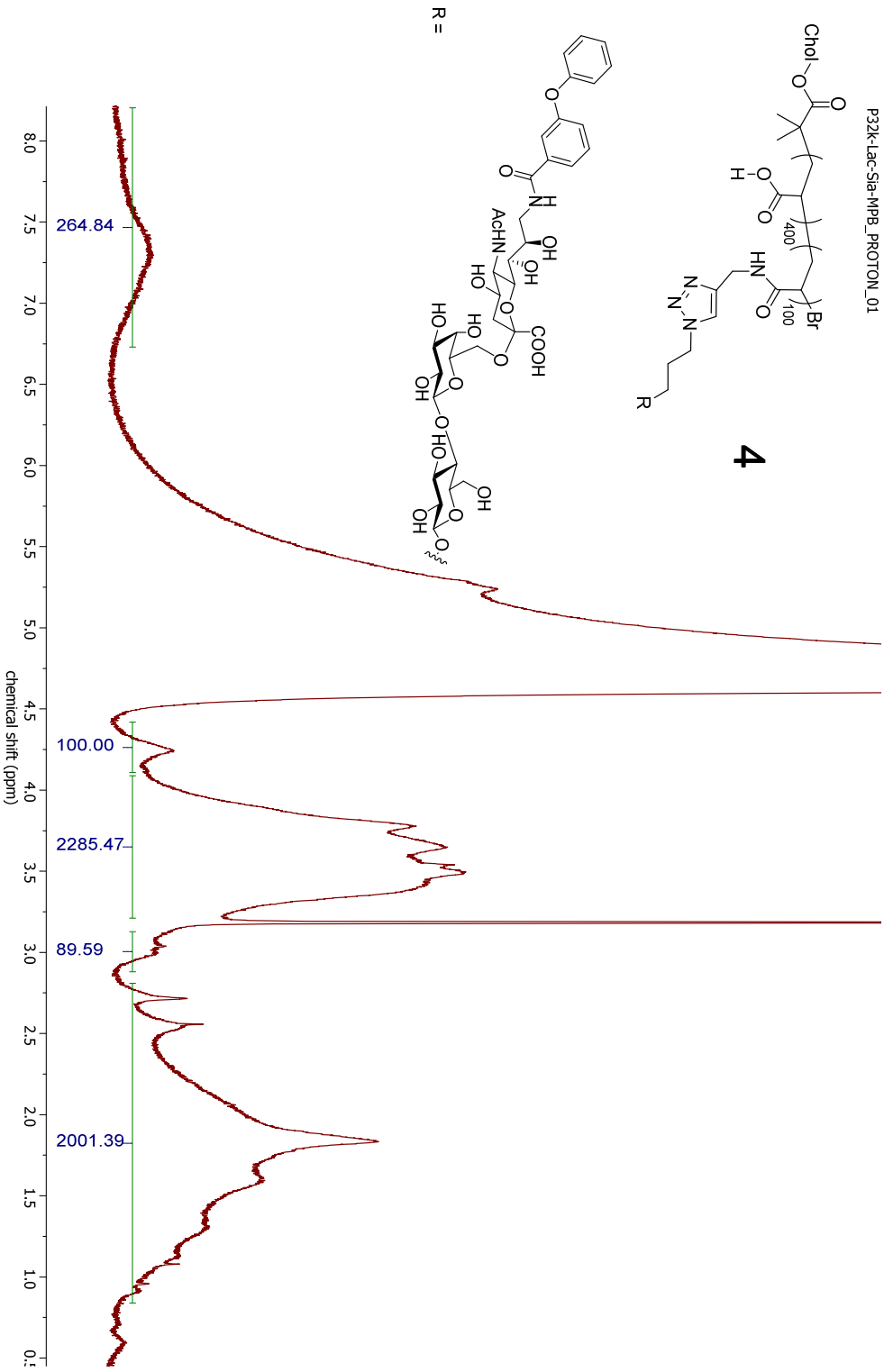

Figure 4.36 ^{1}H NMR of **4** (500MHz, D_2O)

REFERENCES

REFERENCES

1. Wang, X.; Lang, S.; Tian, Y.; Zhang, J.; Yan, X.; Fang, Z.; Weng, J.; Lu, N.; Wu, X.; Li, T.; Cao, H.; Li, Z.; Huang, X., Glycoengineering of Natural Killer Cells with CD22 Ligands for Enhanced Anticancer Immunotherapy. *ACS Cent. Sci.* **2020,** *6*, 382-389.

2. Fesnak, A. D.; June, C. H.; Levine, B. L., Engineered T cells: The Promise and Challenges of Cancer Immunotherapy. *Nat. Rev. Cancer* **2016,** *16*, 566-581.

3. June, C. H.; O'Connor, R. S.; Kawalekar, O. U.; Ghassemi, S.; Milone, M. C., CAR T Cell Immunotherapy for Human Cancer. *Science* **2018,** *359*, 1361-1365.

4. Mehta, R. S.; Rezvani, K., Chimeric Antigen Receptor Expressing Natural Killer Cells for the Immunotherapy of Cancer. *Front. Immunol.* **2018,** *9*, 283.

5. Zeiser, R.; Blazar, B. R., Acute Graft-versus-Host Disease — Biologic Process, Prevention, and Therapy. *N. Engl. J. Med.* **2017,** *377*, 2167-2179.

6. Hay, A. E.; Cheung, M. C., CAR T-cells: Costs, Comparisons, and Commentary. *J. Med. Econ.* **2019,** *22*, 613-615.

7. Olson, J. A.; Leveson-Gower, D. B.; Gill, S.; Baker, J.; Beilhack, A.; Negrin, R. S., NK Cells Mediate Reduction of GVHD by Inhibiting Activated, Alloreactive T Cells While Retaining GVT Effects. *Blood* **2010,** *115*, 4293-4301.

8. Miller, J. S.; Soignier, Y.; Panoskaltsis-Mortari, A.; McNearney, S. A.; Yun, G. H.; Fautsch, S. K.; McKenna, D.; Le, C.; Defor, T. E.; Burns, L. J.; Orchard, P. J.; Blazar, B. R.; Wagner, J. E.; Slungaard, A.; Weisdorf, D. J.; Okazaki, I. J.; McGlave, P. B., Successful Adoptive Transfer and *in vivo* Expansion of Human Haploidentical NK Cells in Patients with Cancer. *Blood* **2005,** *105*, 3051-3057.

9. Curti, A.; Ruggeri, L.; Addio, A.; Bontadini, A.; Dan, E.; Motta, M. R.; Trabanelli, S.; Giudice, V.; Urbani, E.; Martinelli, G.; Paolini, S.; Fruet, F.; Isidori, A.; Parisi, S.; Bandini, G.; Baccarani, M.; Velardi, A.; Lemoli, R. M., Successful Transfer of Alloreactive Haploidentical KIR Ligand-Mismatched Natural Killer Cells After Infusion in Elderly High Risk Acute Myeloid Leukemia Patients. *Blood* **2011,** *118*, 3273-3279.

10. Tang, X.; Yang, L.; Li, Z.; Nalin, A. P.; Dai, H.; Xu, T.; Yin, J.; You, F.; Zhu, M.; Shen, W.; Chen, G.; Zhu, X.; Wu, D.; Yu, J., First-in-man Clinical Trial of CAR NK-92 Cells: Safety Test of CD33-CAR NK-92 Cells in Patients with Relapsed and Refractory Acute Myeloid Leukemia. *Am. J. Cancer. Res.* **2018,** *8*, 1083-1089.

11. Matosevic, S., Viral and Nonviral Engineering of Natural Killer Cells as Emerging Adoptive Cancer Immunotherapies. *J Immunol Res* **2018,** *2018*, 4054815.

12. Dotan, E.; Aggarwal, C.; Smith, M. R., Impact of Rituximab (Rituxan) on the Treatment of B-Cell Non-Hodgkin's Lymphoma. *Pharm. Ther.* **2010,** *35*, 148-157.

13. Bello, C.; Sotomayor, E. M., Monoclonal Antibodies for B-Cell Lymphomas: Rituximab and Beyond. *Hematology Am Soc Hematol Educ Program* **2007,** *1*, 233-242.

14. Castillo, J.; Winer, E.; Quesenberry, P., Newer Monoclonal Antibodies for hematological Malignancies. *Exp. Hematol.* **2008,** *36*, 755-768.

15. Molina, A., A Decade of Rituximab: Improving Survival Outcomes in Non-Hodgkin's Lymphoma. *Annu. Rev. Med.* **2008,** *59*, 237-250.

16. Evans, L. S.; Hancock, B. W., Non-Hodgkin Lymphoma. *Lancet* **2003,** *362*, 139-146.

17. Ereño-Orbea, J.; Sicard, T.; Cui, H.; Mazhab-Jafari, M. T.; Benlekbir, S.; Guarné, A.; Rubinstein, J. L.; Julien, J.-P., Molecular Basis of Human CD22 Function and Therapeutic Targeting. *Nat. Commun.* **2017,** *8*, 764.

18. Chen, W. C.; Completo, G. C.; Sigal, D. S.; Crocker, P. R.; Saven, A.; Paulson, J. C., *In vivo* Targeting of B-cell Lymphoma with Glycan Ligands of CD22. *Blood* **2010,** *115*, 4778-4786.

19. Haso, W.; Lee, D. W.; Shah, N. N.; Stetler-Stevenson, M.; Yuan, C. M.; Pastan, I. H.; Dimitrov, D. S.; Morgan, R. A.; FitzGerald, D. J.; Barrett, D. M., Anti-CD22–chimeric Antigen Receptors Targeting B-cell Precursor Acute Lymphoblastic Leukemia. *Blood* **2013,** *121*, 1165-1174.

20. Fry, T. J.; Shah, N. N.; Orentas, R. J.; Stetler-Stevenson, M.; Yuan, C. M.; Ramakrishna, S.; Wolters, P.; Martin, S.; Delbrook, C.; Yates, B., CD22-targeted CAR T Cells Induce Remission in B-ALL that is Naive or Resistant to CD19-targeted CAR Immunotherapy. *Nat. Med.* **2018,** *24*, 20-28.

21. Powell, L. D.; Sgroi, D.; Sjoberg, E. R.; Stamenkovic, I.; Varki, A., Natural Ligands of the B Cell Adhesion Molecule CD22 Beta Carry *N*-linked Oligosaccharides with Alpha-2,6-linked Sialic Acids that are Required for Recognition. *J. Biol. Chem.* **1993,** *268*, 7019-7027.

22. Rillahan, C. D.; Macauley, M. S.; Schwartz, E.; He, Y.; McBride, R.; Arlian, B. M.; Rangarajan, J.; Fokin, V. V.; Paulson, J. C., Disubstituted Sialic Acid Ligands Targeting Siglecs CD33 and CD22 Associated with Myeloid Leukaemias and B Cell Lymphomas. *Chem. Sci.* **2014,** *5*, 2398-2406.

23. Peng, W.; Paulson, J. C., CD22 Ligands on a Natural N-Glycan Scaffold Efficiently Deliver Toxins to B-Lymphoma Cells. *J. Am. Chem. Soc.* **2017,** *139*, 12450-12458.

24. Kelm, S.; Gerlach, J.; Brossmer, R.; Danzer, C.-P.; Nitschke, L., The Ligand-binding Domain of CD22 is Needed for Inhibition of the B Cell Receptor Signal, as Demonstrated by a Novel Human CD22-Specific Inhibitor Compound. *J. Exp. Med.* **2002,** *195*, 1207-1213.

25. Zhang, C.; Oberoi, P.; Oelsner, S.; Waldmann, A.; Lindner, A.; Tonn, T., Chimeric Antigen Receptor-engineered NK-92 Cells: An Off-the-shelf Cellular Therapeutic for Targeted Elimination of Cancer Cells and Induction of Protective Antitumor Immunity. *Front. Immunol.* **2017,** *8*, 533.

26. Klingemann, H.; Boissel, L.; Toneguzzo, F., Natural Killer Cells for Immunotherapy-Advantages of the NK-92 Cell Line over Blood NK Cells. *Front. Immunol.* **2016,** *7*, 91.

27. Suck, G.; Odendahl, M.; Nowakowska, P.; Seidl, C.; Wels, W. S.; Klingemann, H. G.; Tonn, T., NK-92: An 'Off-the-shelf Therapeutic'for Adoptive Natural Killer Cell-based Cancer Immunotherapy. *Cancer Immunol. Immunother.* **2016,** *65*, 485-492.

28. Arai, S.; Meagher, R.; Swearingen, M.; Myint, H.; Rich, E.; Martinson, J.; Klingemann, H., Infusion of the Allogeneic Cell line NK-92 in Patients with Advanced Renal Cell Cancer or Melanoma: a Phase I Trial. *Cytotherapy* **2008,** *10*, 625-632.

29. Tonn, T.; Schwabe, D.; Klingemann, H. G.; Becker, S.; Esser, R.; Koehl, U.; Suttorp, M.; Seifried, E.; Ottmann, O. G.; Bug, G., Treatment of Patients with Advanced Cancer with the Natural Killer Cell Line NK-92. *Cytotherapy* **2013,** *15*, 1563-1570.

30. Du, J.; Meledeo, M. A.; Wang, Z.; Khanna, H. S.; Paruchuri, V. D. P.; Yarema, K. J., Metabolic Glycoengineering: Sialic Acid and Beyond. *Glycobiology* **2009,** *19*, 1382-1401.

31. Feng, L.; Hong, S.; Rong, J.; You, Q.; Dai, P.; Huang, R.; Tan, Y.; Hong, W.; Xie, C.; Zhao, J., Bifunctional Unatural Sialic Acids for Dual Metabolic Labeling of Cell-surface Sialylated Glycans. *J. Am. Chem. Soc.* **2013,** *135*, 9244-9247.

32. Lewis, A. L.; Nizet, V.; Varki, A., Discovery and characterization of sialic acid O-acetylation in group B Streptococcus. *Proc. Natl. Acad. Sci. U. S. A.* **2004,** *101*, 11123-11128.

33. Cavdarli, S.; Yamakawa, N.; Clarisse, C.; Aoki, K.; Brysbaert, G.; Le Doussal, J.-M.; Delannoy, P.; Guérardel, Y.; Groux-Degroote, S., Profiling of O-acetylated Gangliosides Expressed in Neuroectoderm Derived Cells. *Int. J. Mol. Sci.* **2020,** *21*, 370.

34. Durward, M.; Harms, J.; Splitter, G., Antigen Specific *in vivo* Killing Assay using CFSE Labeled Target Cells. *J. Vis. Exp.* **2010**, e2250.

35. Smith, L. K.; Boukhaled, G. M.; Condotta, S. A.; Mazouz, S.; Guthmiller, J. J.; Vijay, R.; Butler, N. S.; Bruneau, J.; Shoukry, N. H.; Krawczyk, C. M., Interleukin-10 Directly Inhibits $CD8^+$ T Cell Function by Enhancing *N*-glycan Branching to Decrease Antigen Sensitivity. *Immunity* **2018,** *48*, 299-312.

36. Buchini, S.; Buschiazzo, A.; Withers, S. G., A New Generation of Specific Trypanosoma Cruzi trans-Sialidase Inhibitors. *Angew. Chem., Int. Ed.* **2008,** *47*, 2700-2703.

37. Han, S.; Collins, B. E.; Bengtson, P.; Paulson, J. C., Homomultimeric Complexes of CD22 in B Cells Revealed by Protein-glycan Cross-linking. *Nat. Chem. Biol.* **2005,** *1*, 93-97.

38. Wang, Z.; Zhou, L.; El-Boubbou, K.; Ye, X.-s.; Huang, X., Multi-Component One-Pot Synthesis of the Tumor-Associated Carbohydrate Antigen Globo-H Based on Preactivation of Thioglycosyl Donors. *J. Org. Chem.* **2007,** *72*, 6409-6420.